

**TISSUE ENGINEERING OF A HUMAN PERIODONTAL
LIGAMENT FIBROBLAST MEMBRANE – ALVEOLAR
OSTEOBLAST SCAFFOLD DOUBLE CONSTRUCT**

CHOU AI MEI

(B. Sc. (Hons), NUS)

A THESIS SUBMITTED

FOR THE DEGREE OF DOCTOR OF PHILOSOPHY

DEPARTMENT OF BIOLOGICAL SCIENCES

NATIONAL UNIVERSITY OF SINGAPORE

2007

ACKNOWLEDGEMENTS

I would like to express my most sincere gratitude to my supervisors: Prof. Hew Choy Leong, A/P. Lim Tit Meng, A/P. Varawan Sae-Lim, and A/P. Dietmar Werner Hutmacher for their supervision and support during this dissertation.

My deepest appreciation goes to A/P. Martha Somerman for her guidance in establishing explant culture, and A/P. Michael Raghunath for his council in my pursuit of collagen.

I would like to extend my gratitude to Prof. Teoh Swee Hin for his provision of membrane fabrication facilities, and Dr Gregory Lunstrum for his generous gift of anti-collagen XII and XIV antibodies.

My heartfelt thanks to Mr. Yan Tie, Soh Jim Kim Unice, Zhou Yefang and Li Zhimei, as well as fellow members of the Tissue Engineering Laboratory, Developmental Biology Laboratory, and the Centre for Biomedical Materials Applications and Technology (BIOMAT), for their constructive suggestions and friendship.

I would also like to thank National University Hospital staff for their kind assistance with tissue collection; Dr. Thorsten Schantz for his guidance on surgical procedures; Ms. Patricia Netto and Ms. Tan Phay Shing Eunice for their technical instruction in the use of Scanning Electron Microscopy and Atomic Force Microscopy, respectively.

This work would not have been possible without the support from the Faculty Research Grant (R-224-000-011-112) of the Faculty of Dentistry, as well as Graduate Research Scholarships from the National University of Singapore, and the Agency for Science, Technology and Research (A*STAR).

Last but not the least, I am grateful to God who called me to this journey of scientific- and self-discovery, as well as to my family and loved ones for their encouragement and patient understanding.

TABLE OF CONTENTS

Acknowledgements	i
Table of Contents	iii
Summary	x
List of Publications Related to This Thesis	xi
List of Tables	xiii
List of Figures	xiv
List of Abbreviations	xvii

CHAPTER 1 INTRODUCTION

1.1. Introduction to periodontal regeneration	1
1.2. Limitations of current therapeutic procedures	2
1.3. Tissue engineering as a potential regenerative strategy	3
1.4. Research aim	4

CHAPTER 2 LITERATURE REVIEW

2.1. Anatomy of the periodontal ligament (PDL)	6
2.2. Connective tissue matrix of the PDL	7
2.2.1. Collagens	8
2.2.2. Noncollagenous proteins	12
2.2.3. Proteoglycans	13
2.3. Cells of the PDL	14
2.3.1. Development of the PDL	14
2.3.2. Cell populations and phenotype	17
2.4. Biology of periodontal regeneration	18
2.4.1. Molecules in periodontal regeneration	18
2.4.2. Cell populations in periodontal regeneration	19
2.5. Choice of scaffolds for periodontal tissue engineering	21
2.5.1. Scaffold morphology	21
2.5.2. Biodegradability	22
2.6. Surface properties of the biomaterial	23
2.6.1. Biocompatibility	23
2.6.2. Cell-substratum interactions	25
2.6.3. Surface wettability and protein adsorption	27

2.6.4. Surface topography, and cell growth and differentiation	30
2.7. Biodegradable synthetic polymers	32
2.7.1. Overview of polyesters	32
2.7.2. Poly(ϵ -caprolactone) (PCL)	34
CHAPTER 3 COMMON MATERIALS AND METHODS	
3.1. Fabrication of PCL membranes	38
3.1.1. Solvent casting	38
3.1.2. Heat press and biaxial stretching	38
3.1.3. Perforation	39
3.1.4. Alkaline hydrolysis treatment	39
3.2. Collagen induction	40
3.3. Cell proliferation assay	40
3.4. Cell viability assay	41
3.5. Alkaline phosphatase (ALP) assays	41
3.5.1. ALP stain	41
3.5.2. ALP enzyme substrate assay	42
3.6. Collagen extraction by limited pepsin digestion	42
3.7. Sodium dodecyl sulphate-polyacrylamide gel electrophoresis (SDS-PAGE)	43
3.7.1. Tris-acetate gels	43
3.7.2. Tris-glycine gels	44
3.8. Protein gel stain	44
3.8.1. Coomassie Blue stain	44
3.8.2. PageBlue™ stain	44
3.8.3. Silver stain	45

3.9. Western blot analysis	45
3.9.1. Protein transfer	45
3.9.2. Immunoblotting	46
3.10. Semi-quantitative densitometry	47
3.11. Double-labelling immunofluorescence	47
3.12. Phalloidin stain	48
3.13. Von Kossa stain	48
3.14. Confocal laser scanning microscopy	49
3.15. Scanning electron microscopy	49
3.16. Statistical analysis	50

CHAPTER 4 ESTABLISHMENT OF PRIMARY hPDLF CELL LINE *IN*

VITRO

4.1. Background	51
4.2. Materials and methods	52
4.2.1. Isolation of explants	52
4.2.2. Cell expansion and cryopreservation	54
4.2.3. Osteogenic induction	55
4.3. Results	55
4.3.1. Establishment of hPDLF and hAO cell lines	55
4.3.2. hPDLF cell line demonstrated ALP induction	56
4.3.3. hPDLF cell line demonstrated matrix maturation	58
4.3.4. hPDLF cell line demonstrated mineral-like tissue formation	59
4.5. Discussion	61
4.5.1. Characterization of hPDLF and hAO cell lines	61

4.5.2. Analysis of ALP activity and mineralization potential	64
4.5.3. Patient-to-patient variation	66
CHAPTER 5 COLLAGEN SYNTHESIS DURING EXPANSION OF	
PRIMARY hPDLF <i>IN VITRO</i>	
5.1. Background	77
5.2. Materials and methods	79
5.2.1. Collagen induction	79
5.2.2. Reverse transcription polymerase chain reaction (RT-PCR)	80
5.2.3. Collagen I assay	81
5.2.4. SDS-PAGE	81
5.2.5. Immunofluorescence	82
5.3. Results	83
5.3.1. Asc supplementation led to increased collagen synthesis	83
5.3.2. Serum modulated collagen III and V, as well as fibre morphology	85
5.3.3. hPDLF produced the large isoforms of collagen XII and XIV	88
5.4. Discussion	89
5.4.1. Collagen synthesis and ALP activity	89
5.4.2. Collagen deposition and fibre morphology	90
5.4.3. hPDLF exhibited a dedifferentiated phenotype during expansion <i>in vitro</i> that was partially reversed by serum deprivation	91
CHAPTER 6 DEVELOPMENT OF hPDLF-MEMBRANE CONSTRUCTS	
6.1. Background	102
6.2. Material and methods	104

6.2.1. Preparation of PCL membranes	104
6.2.2. Atomic force microscopy	104
6.2.3. Water contact angle measurements	104
6.2.4. Toluidine blue assay	105
6.2.5. Fibronectin adsorption	106
6.2.6. Seeding of hPDLF onto PCL membranes	106
6.2.7. Cell adhesion efficiency	107
6.2.8. Focal contact formation	108
6.3. Results	109
6.3.1. Alkali-treatment and perforation increased surface roughness and area	109
6.3.2. Alkali-treatment increased wettability and accessibility of HFN7.1	110
6.3.3. Alkali-treatment increased cell adhesion and formation of focal contacts	111
6.3.4. hPDLF-membrane constructs demonstrated FN and collagenous matrix formation in the process of maturation	114
6.4. Discussion	117
6.4.1. Cytocompatibility of alkali-treated PCL membranes	117
6.4.2. Evaluation of hPDLF-membrane constructs	119

CHAPTER 7 TISSUE ENGINEERING OF A hPDLF MEMBRANE-hAO SCAFFOLD DOUBLE CONSTRUCT

7.1. Background	133
7.2. Material and methods	134
7.2.1. Preparation of membranes and scaffolds	134

7.2.2. Seeding and culture of hPDLF and hAO	135
7.2.3. Cell metabolic assay	136
7.2.4. Implantation	137
7.2.5. Histology	137
7.2.6. Immunohistochemical analysis	138
7.3. Results	138
7.3.1. Adhesion and proliferation of hPDLF and hAO <i>in vitro</i>	138
7.3.2. Tissue formation of hPDLF-hAO double construct <i>in vivo</i>	139
7.4. Discussion	141
7.4.1. Membranes and scaffolds supported cell adhesion and proliferation <i>in vitro</i>	141
7.4.2. Membrane-scaffold double construct facilitated tissue growth and vascularization <i>in vivo</i>	143
CHAPTER 8 GENERAL CONCLUSIONS AND FUTURE WORK	
8.1. General conclusions	153
8.2. Future work	154
REFERENCE	156
APPENDIX	188

SUMMARY

This study aimed to develop a human periodontal ligament fibroblast (hPDLF)-alveolar osteoblast (hAO) cell-scaffold double construct. Ten hPDLF and three hAO primary cell lines were established by explant culture up to passage 3-5. hPDLF and hAO produced varying levels of alkaline phosphatase and mineral-like tissue upon osteogenic induction by day 28. Three selected hPDLF cell lines demonstrated a preservation of collagen-synthetic capability as seen from the synthesis of type I, III, V, XII and XIV, and a dedifferentiated or embryonic-like collagenous matrix under culture expansion in the presence of ascorbic acid over 21 days. Cell-substratum interactions of three hPDLF cell lines on poly(ϵ -caprolactone) (PCL) membranes were examined. Cytocompatibility of alkali-treated PCL membranes was enhanced via a two-fold increase in cell adhesion rate and total efficiency, attributable to a greater accessibility of fibronectin cell-binding domain. Constructs consisting of perforated PCL membranes provided greater cell anchorage, and cell and matrix alignment than unperforated ones via contact guidance, while retaining hPDLF phenotypic expression and promoting matrix maturation at day 21. hPDLF proliferated on alkali-treated, perforated PCL membranes, while hAO produced mineral-like tissue on alkali-treated PCL scaffolds at day 21. Vascularized, well-integrated hPDLF-hAO double construct was observed at day 28 of subcutaneous implantation in athymic mice, but no further osteogenesis in the earlier-mineralized matrix was seen.

LIST OF PUBLICATIONS RELATED TO THIS THESIS

This thesis is submitted for the degree of Doctorate of Philosophy in the Department of Biological Sciences at the National University of Singapore. No part of this thesis has been submitted for any other degree or equivalent to another university or institution. All the work in this thesis is original unless references are made to other works. Parts of this thesis have been published or presented in the following:

International Journal Publications

Chou A.M., Sae-Lim V., Hutmacher D.W., Lim T.M. Tissue Engineering of a Periodontal Ligament-Alveolar Bone Graft Construct. *The International Journal of Oral & Maxillofacial Implants*, 21: 526–534, 2006.

Chou A.M., Sae-Lim V., Lim T. M., Schantz J.T., Teoh S.H., Chew C.L., Hutmacher D.W. Culturing and Characterization of Human Periodontal Ligament Fibroblasts – A Preliminary Study, *Materials Science and Engineering C*, 20: 77–83, 2002.

Presentations and Awards

Chou A.M., Sae-Lim V., Hutmacher D.W., Lim T.M. Effects of Ascorbic Acid 2-Phosphate on Human Periodontal Ligament Fibroblasts under Low and High Serum Conditions *in vitro*. 8th Annual Meeting of Tissue Engineering Society International, China (2005); Merit winner award (Dental poster), Combined Scientific Meeting, Singapore (2005)

Chou A.M., Sae-Lim V., Hutmacher D.W., Lim T.M. Characterization of Human Periodontal Ligament Cell Sheets on Ultra-Thin and Cell-Permeable Bioresorbable

Membrane. 6th Annual Meeting of Tissue Engineering Society International, USA (2003); 7th NUS-NUH Annual Scientific Meeting, Singapore (2003)

Chou A.M., Sae-Lim V., Zhou Y.F., Hutmacher D.W., Lim T.M. Preliminary studies on human periodontal ligament fibroblasts and alveolar osteoblasts cultured on foil-scaffold constructs. Young Investigator Award, 1st NHG Scientific Congress, Singapore (2002); Best Clinical Science Poster Award, 6th NUS-NUH Annual Scientific Meeting (2002)

LIST OF TABLES

2.1	Summary of reported collagens in the PDL (Adapted from Kirkham and Robinson, 1995; Kielty and Grant, 2002).	11
2.2	Summary of selected polyesters (Gunatillake and Adhikari, 2003).	34
4.1	Summary of western blot results (Fig. 4.5) of ON, OPN and BSP synthesis by paired hPDLF and hAO, derived from three individuals, under normal and mineralizing culture.	73
4.2	Biodata of donors, categorized by the pattern of mineral-like nodule formation at day 28 in hPDLF and hAO.	75
5.1	List of primer sequences and expected size of PCR products.	94
7.1	Summary of immunostaining results.	151

LIST OF FIGURES

1.1	Schematic representation of periodontal regeneration using an autologous cell-scaffold construct.	5
2.1	Stages in collagen synthesis (adapted from Gage <i>et al.</i> , 1989).	10
2.2	Schematic representation of a developing tooth bud at the cap stage (adapted from Cho and Garant, 2000).	16
2.3	The contact angle of a liquid with a solid.	28
2.4	Illustration of events at the biomaterial surface (adapted from Kasemo and Gold, 1999).	29
4.1	Representative images of cellular outgrowth and morphology of hPDLF and hAO.	68
4.2	Effects of dexamethasone (Dex) on the alkaline phosphatase (ALP) activities of hPDLF and hAO.	69
4.3	ALP activities of hPDLF and hAO cultured in the absence and presence of 100 nM Dex.	70
4.4	Representative images of (A-B) hPDLF and (C-D) hAO after staining for ALP under normal and mineralizing cultures, respectively.	71
4.5	Western blot analysis of (A) osteonectin (ON), (B) osteopontin (OPN) and (C) bone sialoprotein (BSP) in whole cell lysates of paired hPDLF and hAO, derived from three individuals, under normal and mineralizing culture.	72
4.6	Representative morphology of hPDLF (A-C) and hAO (D-F) at stage I, II and III of nodule formation, respectively.	74
4.7	Mineral-like tissue formation in hPDLF and hAO under mineralizing culture, as observed (A-C) before and (D-F) after von Kossa staining at day 28.	74
4.8	Correlation between ALP activity and mineral-like nodule formation in hPDLF and hAO.	76
4.9	Schematic diagram showing the metabolism of ATP and AMP, and the role of ALP on mineralization.	76
5.1	Synthesis of (A) DNA and (B) proteins over time.	94
5.2	Gene expression of three representative collagens in the PDL, namely types I, III and XII, as represented by their respective $\alpha 1$ chains using RT-PCR.	95

5.3	Synthesis of (A) collagen I and (B) alkaline phosphatase (ALP), normalized to dsDNA.	95
5.4	Three-day window of collagen synthesis.	96
5.5	Accumulative collagen deposition.	96
5.6	Silver-stained non-reducing SDS-PAGE of cell layer fractions in 3-8% Tris-acetate gel, as compared to that in 5% Tris-glycine gels.	97
5.7	Ratio of collagenous peptides obtained by limited pepsin digestion of medium and cell layer fractions under 0.2% and 10% FBS over time, as determined by densitometry.	98
5.8	Phase contrast light (PCLM) and fluorescence light microscopy images of hPDLF cultures stained with anti-collagen I-FITC antibody at day 21 (200x magnification).	99
5.9	Confocal laser microscopy images of hPDLF cultures double immunolabeled for collagen I/XII and I/XIV, and singly labeled for collagen III at day 21. Cells were counter-stained with Hoechst (scale bar = 50 μ m).	100
5.10	Western blot analysis of undigested medium.	101
6.1	Modulation of cell behaviour through substrate-dependent changes in FN conformation (adapted from Garcia <i>et al.</i> , 1999).	121
6.2	Manufacturing procedure and classification of PCL membranes.	121
6.3	Representative surface morphologies of UP/UT, UP/T, P/UT, P/T membranes obtained by scanning electron (SEM) and atomic force (AFM) microscopy.	122
6.4	(A) Root-mean-square (RMS) surface roughness and (B) surface area of membranes obtained by AFM at a scan size of 5 μ m x 5 μ m.	123
6.5	Optical density of ELISA of antibody binding to FN adsorbed from 2 μ g/ml by (A) anti-FN polyclonal antibody and (B) HFN7.1 monoclonal antibody in the absence and presence of a 100-fold excess of BSA.	123
6.6	Representative PCLM images of hPDLF attached onto UP/UT, UP/T, P/UT, and P/T membranes at 1, 2, 6 and 18 h after seeding in culture medium containing 10% serum (magnification 600X).	124
6.7	Adhesion efficiency of hPDLF, expressed as the percentage of double-stranded DNA (dsDNA) harvested from attached cells from initial cell suspension, at 1, 2, 6 and 18 h after seeding on membranes.	125
6.8	Immunofluorescence of <i>f</i> -actin (green) and vinculin (red) in hPDLF at 6, 12 and 24 h after seeding on membranes (scale bar = 50 μ m).	127

6.9	Close-up images of Fig. 6.8 (numbered boxes) of vinculin (red) at 24 h after seeding on membranes (scale bar = 10 μ m).	127
6.10	Representative images of hPDLF cell sheet on UP/T and P/T membranes (magnification 100X, unless stated otherwise).	128
6.11	Cell sheet coverage on membranes as deduced from FDA/PI staining at 100X magnification after image analysis by Micro-Image® over 21 days.	129
6.12	Cell proliferation in terms of dsDNA harvested from attached hPDLF over 21 days.	129
6.13	Western blot and densitometric analysis of reducing SDS-PAGE containing whole cell lysates of hPDLF cultured on UP/T, P/T membranes and TCP at day 21.	130
6.14	Representative images of non-reducing SDS-PAGE in 3-8% gradient Tris-acetate gel of (A) medium and (B) cell layer fractions after limited pepsin digestion at day 21.	130
6.15	Representative confocal laser microscopy images of hPDLF immunolabeled for FN and type I collagen on UP/T membrane, P/T membrane and TCP at day 21 (scale bar = 50 μ m).	131
6.16	Level of alkaline phosphatase (ALP) of hPDLF at day 7, 14 and 21.	132
7.1	Attachment, growth and viability of hPDLF on PCL membranes.	146
7.2	Attachment, morphology and viability of hAO on PCL scaffolds.	147
7.3	Metabolic activities of hPDLF on membranes and of hAO on scaffolds, with their respective wells at weekly intervals.	148
7.4	Implantation and excision of membrane-scaffold constructs.	149
7.5	Histological analysis of constructs after 4-weeks <i>in vivo</i> .	150
7.6	Immunohistochemical analysis of constructs after 4-weeks <i>in vivo</i> .	152

LIST OF ABBREVIATIONS

5'NT	5' nucleotidase
AFM	atomic force microscopy
AMP	adenosine monophosphate
AO	alveolar osteoblast
Arg	arginine
Asc	ascorbic acid
Asp	aspartate
ATP	adenosine 5'-triphosphate
β-GP	beta-glycerophosphate
BMP	bone morphogenetic protein
BSA	bovine serum albumin
BSP	bone sialoprotein
cDNA	complementary DNA
DAB	3,3'-diaminobenzidine
Dex	dexamethasone
DMEM	Dulbecco's Modified Eagle Medium
DMSO	dimethyl sulphoxide
DNA	deoxyribonucleic acid
DTT	dithiothreitol
ECL	enhanced chemiluminescence
ECM	extracellular matrix
EDTA	ethylenediaminetetraacetic acid
ELISA	enzyme-linked immunosorbent assay

EtBR	ethidium bromide
FBS	fetal bovine serum
FDA	fluorescein diacetate
FDM	fused deposition modeling
FITC	fluorescein isothiocyanate
FN	fibronectin
FRET	fluorescence resonance energy transfer
g	gram
Gly	glycine
h	human
HRP	horseradish peroxidase
Kb	kilo base
kDa	kilo Dalton
LDS	lithium dodecyl sulfate
M	molar
MAPK	mitogen-activated protein kinase
min	minute
MTS	3-(4,5-dimethylthiazol-2-yl)-5-(3-carboxy-methoxyphenyl)-2-(4-sulfophenyl)-2H-tetrazolium
NADP	nicotinamide adenine dinucleotide phosphate
NaOH	sodium hydroxide
NTPPPH	nucleoside triphosphate pyrophosphohydrolase
OD	optical density
ON	osteonectin
OPN	osteopontin

PBS	phosphate buffered saline
PCL	poly(ϵ -caprolactone)
PCLM	phase contrast light microscopy
PCR	polymerase chain reaction
PDL	periodontal ligament
PDLF	periodontal ligament fibroblast
PHSRN	Pro-His-Ser-Arg-Asn
Pi	inorganic phosphate
PI	propidium iodide
PPi	inorganic pyrophosphate
RGD	Arg-Gly-Asp
RNA	ribonucleic acid
SD	standard deviation
SDS	sodium dedocyl sulphate
SEM	scanning electron microscopy
sec	second
Tris	trishydroxyaminomethane
TRITC	tetramethylrhodamine isothiocyanate
IU	international unit
UV	ultra-violet
VN	vitronectin
v/v	volume by volume
w/v	weight by volume

1. INTRODUCTION

1.1. Introduction to periodontal regeneration

Periodontal regeneration aims to achieve reconstitution of soft (gingival and periodontal ligament) and mineralized (bone and cementum) tissues lost due to periodontal disease or trauma, as well as congenital defects. Ideally, four criteria must be met in order for regeneration to have occurred. These include the restoration of (i) a functional epithelial seal, (ii) new connective tissue fibres (Sharpey's fibres) on the root surface to reproduce both the periodontal ligament (PDL) and the dentogingival fibre complex, (iii) new acellular, extrinsic fibre cementum on the root surface, and (iv) alveolar bone height (Bartold *et al.*, 2000). In essence, all the features of the normal dentogingival complex have to be restored to their original form, function and consistency.

Regeneration of the alveolar bone and other periodontal structures does not usually occur on a clinically predictable basis (Melcher, 1976). Instead, healing takes place, consisting of inflammation, granulation tissue formation and tissue remodelling (Clark, 1996). Periodontal healing following mechanical or surgical therapy leads to one of the following outcomes: a control of inflammation, formation of long junctional epithelium, connective tissue re-attachment to the root surface, new bone formation, root resorption and/or ankylosis, or formation of new functional attachment apparatus (reviewed in Bartold and Narayanan, 1998).

The outcome of healing by regeneration or repair by scar tissue depends upon at least three factors that are not mutually exclusive: (i) availability of the appropriate cell type(s), (ii) soluble mediators of cell function that activate these cells, and (iii) a developing extracellular matrix (ECM) (Bartold *et al.*, 2000).

1.2. Limitations of current therapeutic procedures

Conventional periodontal surgical procedures, such as surgical debridement and resective procedures, have been established as effective treatment regimes (Hill *et al.*, 1981; Lindhe *et al.*, 1982; Pihlstrom *et al.*, 1983; Ramfjord *et al.*, 1987; Becker *et al.*, 1988; Kaldahl *et al.*, 1996). This may be accomplished by the excision of tissues, or by the attempted replacement and attachment of tissues to the root surface. Despite this, healing typically takes place by repair. The failure to obtain a new connective tissue attachment after conventional periodontal therapy has been attributed to the formation of long junctional epithelium, as a result of an ability of oral epithelium to migrate apically along the root surface (Caton and Nyman, 1980; Caton *et al.*, 1980). Hence, the formation of new epithelial attachment is classified as repair and not regeneration.

A regenerative therapeutic approach called “guided tissue regeneration” (GTR) was thus developed based on the exclusion of gingival connective tissue cells from the wound and the prevention of apical migration of epithelium, thus favouring healing primarily from the PDL space and adjacent alveolar bone (reviewed in American Academy of Periodontology, 2005). This procedure consists of the placement of a barrier membrane between the periodontal defect and the gingival tissues (GTR), or between the bone defect and the gingival tissues (guided bone regeneration, GBR). First introduced by Nyman *et al.* (1982), these barriers allow controlled repopulation by cells with regenerative potential, such as PDL cells, bone cells and possibly cementoblasts, space maintenance and clot stabilization at the wound site (Nyman *et al.*, 1982; Caton *et al.*, 1987; Nyman *et al.*, 1987). The use of bone allografts consisting of tricalcium phosphate and/or decalcified freeze-dried

bone in addition to barrier membrane further augmented bone fill (Schallhorn and McClain, 1988; Anderegge *et al.*, 1991).

Despite the fact that guided tissue regeneration (GTR) and osseous grafting are the two techniques with the most histological documentation of periodontal regeneration (reviewed in Academy Report, 2005), clinical outcome was still less than optimal for a number of reasons (Bartold *et al.*, 2000), including: (i) preferential regeneration of bone over that of cementum and fibrous connective tissues, (ii) inability to control the formation of a long junctional epithelium, and (iii) inability to adequately seal the healing site from the oral environment and prevent infection.

Therefore, current difficulties associated with achieving predictable periodontal regeneration point to the need for novel techniques in order to regenerate the critically lost or damaged soft and hard tissues. As mentioned previously, the outcome of healing depends upon an availability of appropriate cell type(s), biological mediators, and a developing ECM (Bartold *et al.*, 2000). This could be realized by developing tissue engineering strategies, as detailed in the next section.

1.3. Tissue engineering as a potential regenerative strategy

Tissue engineering is the application of principles and methods of engineering and life sciences toward fundamental understanding of structure-function relationships in normal and pathological mammalian tissues, and the development of biological substitutes to restore, maintain, or improve tissue function (Langer and Vacanti, 1993). It involves the use of a combination of cells, scaffolds and suitable biochemical factors, as opposed to inert implants, in developing biological substitutes. Tissue engineering efforts in dentistry are aimed at replacing the supporting structures

of the dentition as well as the surrounding soft tissue for restoration of function (Buckley *et al.*, 1999).

The application of cell-based scaffold constructs is postulated to be a potential regenerative strategy in reconstituting normal periodontal tissue architecture (Bartold *et al.*, 2000). Due to the juxtaposition of the PDL between the alveolar bone and the root, it is hypothesized that optimal and sustained availability of viable PDL cells on the damaged denuded root surface would facilitate periodontal tissue regeneration (Hasegawa *et al.*, 2005). Cell sheets of selective phenotype (Okuda *et al.*, 2004) theoretically provide the critical cell mass allowing for competitive wound healing favouring desirable tissue regeneration (Gottlow *et al.*, 1984, Sae-Lim *et al.*, 2004). In this way, the need for recruitment of cells to the site is negated and the predictability of the outcome may be enhanced. Moreover, the periodontium is under constant mechanical loading. A cell-supportive scaffold would hypothetically maintain the integrity of the engineered tissue during and after implantation.

The most likely source of cells for periodontal tissue engineering is the PDL and alveolar bone, whose progenitor cells could be isolated and propagated in culture for seeding into scaffolds. Preliminary studies have indicated that cells from the PDL (Van Dijk *et al.*, 1991; Lang *et al.*, 1998) and bone (Malekzadeh *et al.*, 1998) can be transplanted into periodontal sites with no adverse immunologic or inflammatory consequences, giving rise to new connective tissue attachment and bone.

1.4. Research aim

It is envisioned that tissue-engineered cell-scaffold constructs could be obtained by a stimulation of autologous periodontal cells into the desired cell lineages within scaffolds of biocompatible material, and that the subsequent implantation of

such a construct could lead to autologous cell-based therapy (Fig. 1.1). The aim of this thesis was therefore to tissue engineer a hPDLF membrane-hAO scaffold double construct for the purpose of periodontal regeneration.

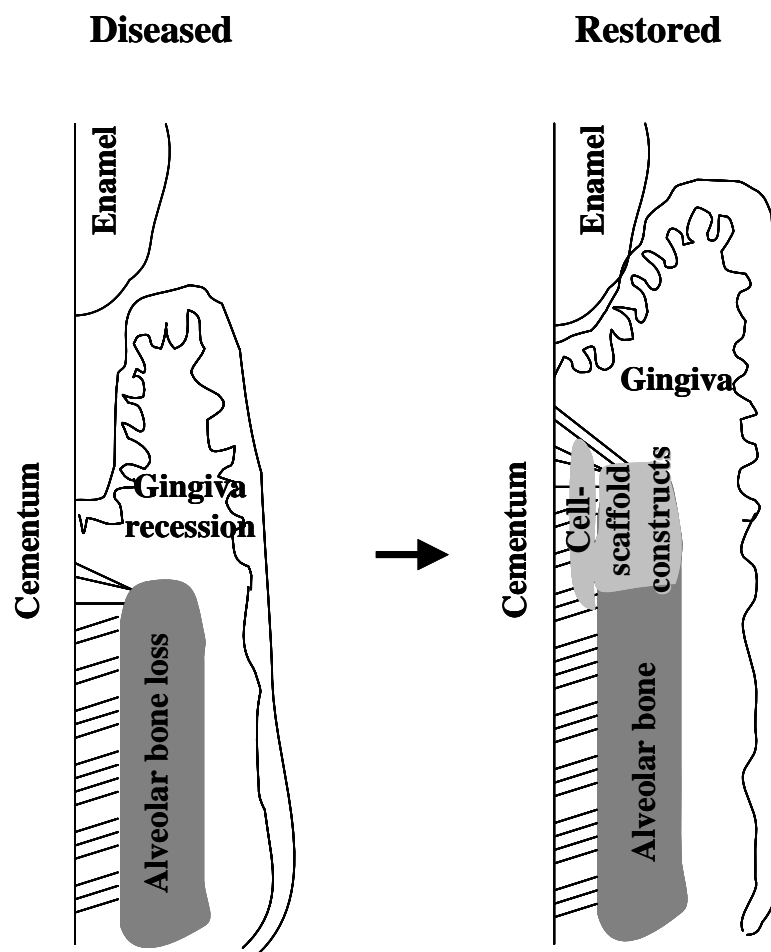


Figure 1.1. Schematic representation of periodontal regeneration using an autologous cell-scaffold construct.

2. LITERATURE REVIEW

2.1. Anatomy of the periodontal ligament (PDL)

The periodontium comprises the connective tissues around the teeth and consists of gingiva, periodontal ligament (PDL), cementum, and alveolar bone (Berkovitz and Shore, 1995). The PDL, varying between 0.1 to 0.25 mm in width (Coolidge, 1937), is the dense connective tissue located between the alveolar bone and the root surface. It extends from the apex to the cemento-enamel junction of the healthy tooth, with the coronal part continuous with the subepithelial connective tissue of the gingiva. The ligament is widest near the cemento-enamel junction and the apex, and narrowest near the middle of the root. The width is dependent on age and functionality of the tooth, being thinner in aged tooth, and greatest for heavily loaded tooth (reviewed by Holmstrup, 2003).

The main function of the PDL is anchorage of the tooth, by resisting displacement forces during occlusal loading, and maintaining the tooth in a functional position during tooth eruption. This is achieved by collagen, arranged into bundles called principal fibre groups, in an extracellular matrix (ECM) through which vessels and nerves innervate. These collagen bundles traverse the space between the root and the alveolar wall, conferring elasticity to the PDL and compensating for minute movements of the tooth during mastication. Furthermore, the proprioceptor nerve endings of the PDL form part of the extremely refined neurological control of mastication, and the mechano-receptors monitor changes in pressure within the ligament space (reviewed in Berkovitz and Shore, 1995).

The collagen bundles, about 5 µm in diameter, are inserted as Sharpey's fibres into the cementum at one end, and into the compact bone plate of the alveolus at the other (Cohn, 1972; Raspanti *et al.*, 2000). The principal fibres of the PDL can be

divided into six groups, with presumed functions based on location and insertion (Hassell, 1993): (i) alveolar crest fibres which retain tooth in the socket, oppose lateral forces, and protect deeper PDL structures, (ii) oblique fibres which oppose axially directed forces, (iii) transseptal fibres which maintain contact between teeth, (iv) horizontal fibres which oppose lateral forces, (v) interradicular fibres which maintain tooth in socket, and (vi) apical fibres which prevent tooth extrusion, protect vessel and nerve supply.

The remaining fibres consist of secondary collagen fibres, oxytalan and reticulin fibres, which are randomly oriented and often associated with vessels and nerves. It has been hypothesized that oxytalan fibres, which resemble immature elastic fibres, function in a supportive, developmental and/or sensory role in the PDL (Mariotti, 1993). Their fibres are thicker and more numerous in teeth that carry heavy loads and that moved by orthodontic treatment.

2.2. Connective tissue matrix of the PDL

The ECM provides a controlled environment for the exchange of substances for survival, strength and shape for tissues, and protection from external physical stress. The two main components of the connective tissue ECM are firstly, the insoluble fibres that resist tensile forces, and secondly, the soluble interfibrillar macromolecules that inflate the fibrous network, providing resistance to compressive forces. The former consists mainly of collagen, whereas the latter consists of carbohydrate-protein complexes occurring primarily as proteoglycans. The remaining non-collagenous proteins, such as fibronectin (FN), laminin, tenascin, provide a bridge between the ECM and the cells embedded within.

Matrix-matrix interactions between modular motifs within the ECM molecules regulate fibril or lamina formation, hence giving rise to diverse structures that determine tissue architecture. The relative proportions of collagenous and proteoglycan components determine the unique mechanical properties of tissues, influencing connective tissue structure and function. Taken altogether, these ECM components provide cells with a mechanical scaffold optimal for adhesion, migration and differentiation of a specific cell type.

2.2.1. Collagens

Collagens are the major constituent of the periodontal structures. In addition to their structural role, collagens have also been shown to be involved in promoting cell attachment and differentiation, either directly or indirectly, and as a chemotactic agent for both fibroblasts and macrophages (Linsenmayer, 1991).

More than 19 different collagen types have been described (reviewed in Kiely and Grant, 2002). Each collagen is a homotrimer or a heterotrimer of three polypeptide alpha chains (α chains) that fold to form triple-helical domains (Piez, 1976). A repeating gly-X-Y amino acid sequence within the polypeptide is responsible for the triple helix, where X is often proline and Y is often hydroxyproline.

Collagen synthesis involves the production of a precursor called procollagen at the ribosomes on the rough endoplasmic reticulum (RER), triple-helix formation in the cytosol and the secretion of the fully associated trimeric procollagen out of the cell (reviewed by Kirkham and Robinson, 1995). The synthesis of procollagen involves extensive co-translational and post-translational modifications such as hydroxylation, signal peptide cleavage, and glycosylation. In particular, hydroxylation of pre-pro peptide chains at proline and lysine is responsible for helix stability and

intermolecular cross-linkage. Triple-helix formation is initiated by peptide alignment via non-covalent interactions at the C-terminal propeptide, and subsequently stabilized by interchain disulphide bond formation in the propeptide domain. After secretion, collagen fibrils are formed via the removal of the propeptides at the N- and C-termini by endopeptidases, and aggregation at the ECM (Fig. 2.1). Further assembly of collagen fibrils into bundles is believed to occur at cytoplasmic recesses and convoluted surface folds of secreting cells (Birk and Trelstad, 1984; 1986). Lastly, supramolecular aggregates of collagen are formed through lysine-derived intra-chain and inter-chain crosslinks in the extracellular space (Bornstein and Traub, 1979).

Collagen types present within the PDL are summarized in Table 2.1. Type I collagen is the predominant protein of most connective tissues including PDL. Type I collagen, which consists of two identical α_1 chains and a chemically different α_2 chain, accounts for about 80% of PDL collagen. Type III collagen, consisting of three α_1 III chains and constituting approximately 20% of PDL collagen, is the next abundant collagen. Both type I and III collagens belong to the fibrillar or fibril-forming collagens, in which the triple-helical domain contains an uninterrupted stretch of 338 to 343 gly-X-Y triplets in each chain (Bartold and Narayanan, 2003). Type III collagen is more fibrillar and extensible than type I, and may be important in maintaining the integrity of the PDL during vertical and horizontal movements during mastication. Moreover, the relatively high level of type III collagen, in similar proportions in embryonic tissues, is believed to reflect the high turnover rate within the ligament (Butler *et al.*, 1975). Small amounts of other collagens are also present. Type IV is localized to basement membranes (Gage *et al.*, 1989), whereas type V is distributed in the matrix of the lamina propria, in close association with cells. Type VI

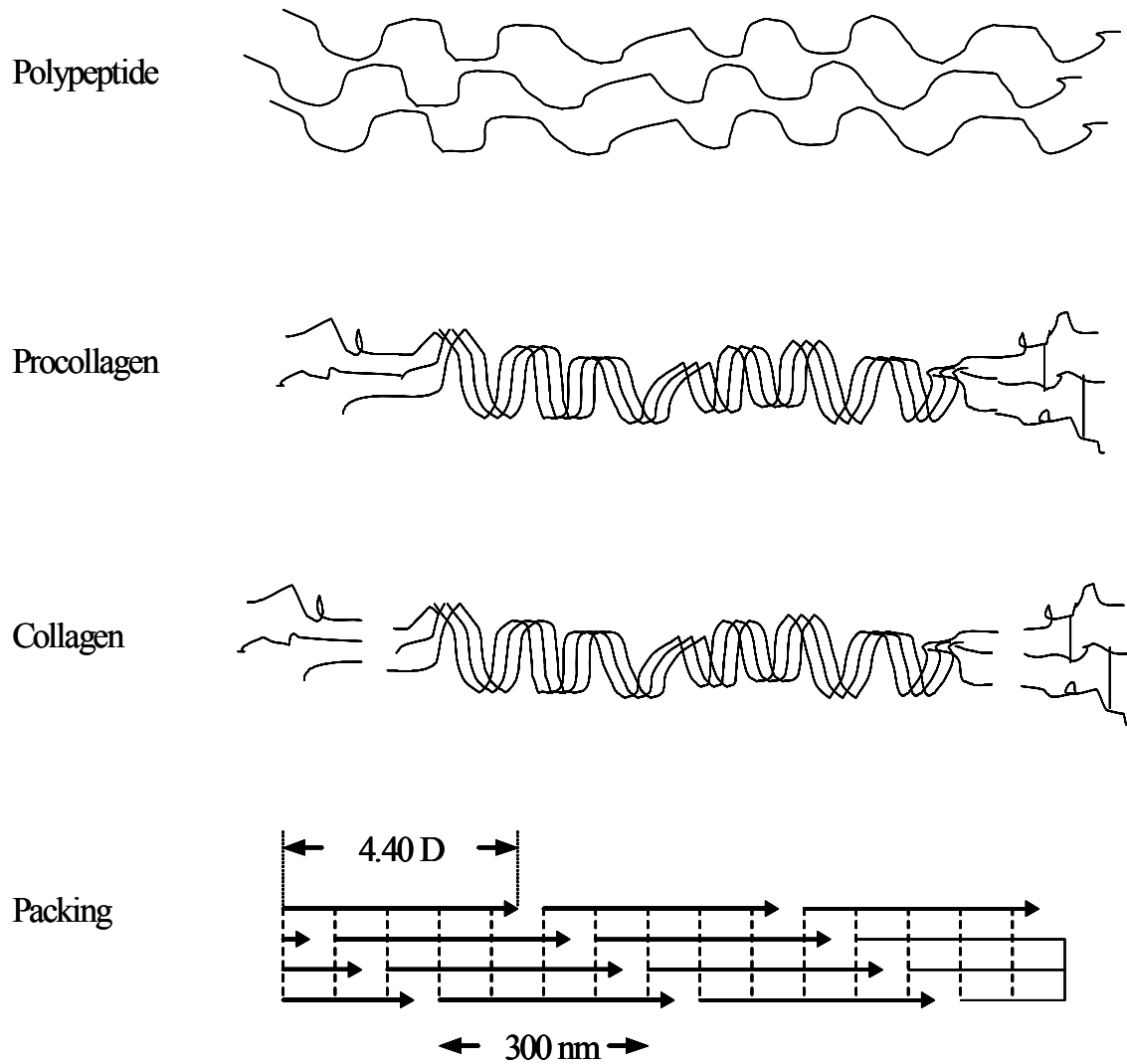


Fig. 2.1. Stages in collagen synthesis showing (from top) collagen α -chain polypeptides, the procollagen molecule, collagen, and the packing of individual collagen molecules into a fibril (adapted from Gage *et al.*, 1989). Each molecule of 300 nm length is displaced laterally by the distance, D , of 67 nm.

Type	Chains	Mr (10 ³) of chains	Macromolecular structure	Special characteristics
I	[$\alpha 1(I)$] ₂ [$\alpha 2(I)$] [$\alpha 1(I)$] ₃	95	Quarter-staggered array, forming large-diameter, banded fibrils	Uninterrupted helix
III	[$\alpha 1(III)$] ₃	95	Quarter-staggered array, forming small-diameter banded fibrils	Uninterrupted helix; co-expressed with type I
IV	[$\alpha 1(IV)$] ₂ [$\alpha 2(IV)$]; also $\alpha 3(IV)$, $\alpha 4(IV)$, $\alpha 5(IV)$, $\alpha 6(IV)$	170-180	End-to-end association, forming reticular, non-fibrillar network	Interrupted helix
V	[$\alpha 1(V)$] ₂ [$\alpha 2(V)$] [$\alpha 1(V)$][$\alpha 2(V)$][$\alpha 3(V)$] [$\alpha 1(V)$] ₃	120-145	Quarter-staggered array, forming fine banded fibrils	Uninterrupted helix; co-expressed with type I and II
VI	[$\alpha 1(VI)$][$\alpha 2(VI)$][$\alpha 3(VI)$]	$\alpha 1$ 140 $\alpha 2$ 140 $\alpha 3$ 340	End-to-end association into tetramers, forming microfibrillar network	Short helix
VIII ^a	[$\alpha 1(VIII)$] ₂ [$\alpha 2(VIII)$]	61	Hexagonal non-fibrillar lattice network ^a	Short helix with interruptions
XII	[$\alpha 1(XII)$] ₃	220, 340	Association with surface of banded fibrils	Two short helices
XIV ^b	[$\alpha 1(XIV)$] ₃	220	Association with surface of banded fibrils	Two short helices

Table 2.1. Summary of reported collagens in the PDL (Adapted from Kirkham and Robinson, 1995; Kielty and Grant, 2002). ^a, Sawada and Konomi, 1991; ^b, Zhang *et al.*, 1993.

collagen has a microfibrillar distribution (Romanos *et al.*, 1993). Types V, XII and XIV are co-distributed with type III surrounding type I collagen in Sharpey's fibres (Bartold, 1995). Types XII and XIV, homotrimers of three α_1 XII and α_1 XIV chains respectively, belong to the fibril-associated collagens with interrupted triple helices (FACITs).

2.2.2. Noncollagenous proteins

Fibronectin (FN), a high molecular weight, insoluble, fibre-forming glycoprotein, is present both intra- and extracellularly (Yamada and Olden, 1978). It contains an Arg-Gly-Asp (RGD) sequence that binds to cells as well as other sites that bind to collagen, heparin and fibrin (Mariotti, 1993). During granulation tissue formation, fibronectin provides a temporary substratum for migration and proliferation of cells, and acts as a template for collagen deposition. Therefore, cells preferentially adhere to FN, which is involved in cell migration and orientation (reviewed in Embery *et al.*, 1995). FN may have considerable biological significance within the PDL with its high rate of turnover. Immunochemical techniques showed that FN is uniformly distributed throughout the PDL both during eruption and in fully erupted teeth. It is also found in the endosseal spaces, periosteum and bone lining cells at their interface with alveolar bone (Steffensen *et al.*, 1992). However, it is expressed particularly strongly along attachment sites of the PDL collagen fibres to cementum but not to alveolar bone (Lukinmaa *et al.*, 1991). Moreover, its expression is weaker in cementum than in PDL (Zhang *et al.*, 1993). A loss of FN has been observed during the terminal maturation of many connective tissue matrices, its continued presence within the PDL may be indicative of its immature characteristics or its high turnover.

Tenascin, a glycoprotein characteristic of immature connective tissue, has also been found in the PDL. In contrast to other major ECM proteins, tenascin is expressed during wound healing (Mackie *et al.*, 1988) and in a few adult tissues including bone marrow and the PDL. Unlike FN, it is not uniformly distributed in the PDL. It is found between less densely packed collagen fibrils of the PDL (Zhang *et al.*, 1993) and accumulated towards the alveolar bone and cementum (Lukinmaa *et al.*, 1991; Steffensen *et al.*, 1992), with only weak expression throughout the alveolar bone matrix and cementum.

Laminin is found exclusively in the basement membrane, and is located in the basal lamina of blood vessels and the oral, sulcus and junction epithelium in the periodontium (Steffensen *et al.*, 1992). Vitronectin (VN), a protein that promotes the attachment and spreading of cells, has been found on lining cells of the alveolar bone and cementum (Steffensen *et al.*, 1992). It is also associated with the connective tissue fibres of the gingival and PDL (Matsuura *et al.*, 1995).

2.2.3. Proteoglycans

The ligament ECM is an amorphous matrix of glycosaminoglycans (GAGs), proteoglycans and glycoproteins, and plays an important role in the absorption of functional stresses. The GAGs are represented by several species, including chondroitin sulphate, dermatan sulphate, keratan sulphate and hyaluronan (Mariotti, 1993). The PDL and gingival ground substance compositions are similar, and contains, in addition to the above, versican, decorin, biglycan and syndecan (Purvis *et al.*, 1984; Pearson and Pringle, 1986; Larjava *et al.*, 1992). These molecules, secreted by fibroblasts, have important functions, including ion and water binding and exchange, control of collagen fibrillogenesis and fibre orientation. Proteoglycans also regulate

cell adhesion and growth, and have capacity to bind and regulate growth factor activity (Bartold and Narayanan, 1998).

Many aspects of cell function are influenced by the ECM. Cell-matrix interactions regulate tissue remodelling during growth, differentiation, morphogenesis, and wound healing, as illustrated below.

2.3. Cells of the PDL

Mature PDL is a highly vascularized cellular tissue. Fibroblasts are the most abundant cell type in the PDL. They are spindle shaped, with their long axes parallel to the principal fibres. The functions of the PDL fibroblasts (PDLF) includes the synthesis and degradation of collagen and ground substance components (Limeback *et al.*, 1983), playing an important role in the maintenance and repair of the PDL. Hence, the fibres and the ground substance of the PDL have a relatively high turnover rate compared to that of the cells (Crumley, 1964; Minkoff and Engstrom, 1979; McCulloch and Melcher, 1983a). Defence cells may also be present in the PDL, including macrophages, mast cells and eosinophils as in other connective tissues, and play an important role in immunity. Groups of epithelial cells, the ‘epithelial rests of Malassez’, which are remnants of the Hertwig root sheath, are found close to the cementum (reviewed in Berkovitz and Shore, 1995).

The major cell populations in the PDL are discussed below, in light of their origin during development to their subsequent differentiation.

2.3.1. Development of the PDL

The majority of periodontal tissues have an origin from the dental follicle that is derived from neural crest. Following the development of the neural tube by

invagination of the overlying ectoderm, migratory pluripotent neuroepithelial cells, also known as neural crest cells, lose their epithelioid nature and acquired a mesenchymal phenotype, and formed dental ectomesenchyme. This is followed by tooth development via an aggregation of neural crest ectomesenchymal cells (reviewed in Cho and Garant, 2000).

Tooth development is generally divided into the following stages: the bud stage, the cap stage, the bell stage and finally, maturation stage (reviewed in Nanci and Ten Cate, 2003). The tooth bud is divided into the enamel organ, the dental papilla and the dental follicle (Fig. 2.2). The enamel organ gives rise to ameloblasts, which produce enamel and the reduced enamel epithelium. The dental papilla consists of cells that develop into odontoblasts which form dentin. Mesenchymal cells within the dental papilla forms the tooth pulp. The dental follicle gives rise to cementoblasts, osteoblasts, and PDLF which form cementum, alveolar bone and the PDL, respectively (reviewed in Ross *et al.*, 2002).

During the development of the periodontal tissues, cells of the dental follicle are separated from the newly formed root dentin by the cells of Hertwig's epithelial root sheath, which secrete a fine layer of enamel-like proteins onto the dentin surface, known as the hyaline layer (Lindskog, 1982; Slavkin *et al.*, 1989). Subsequently, the Hertwig's epithelial root sheath fragments, possibly by apoptosis, permitting direct contact of the dental follicle onto the newly formed hyaline layer on the root surface. Cementoblasts appear, presumably differentiated from the cells of the dental follicle, and cementogenesis proceeds. This hypothesis, in which cells derived from oral epithelium participate in formation of cementum, is based on the established principle that epithelial-mesenchymal interactions are critical for development of tissues such as heart, hair follicles, limb buds, dentin and enamel of teeth (MacNeil and Somerman,

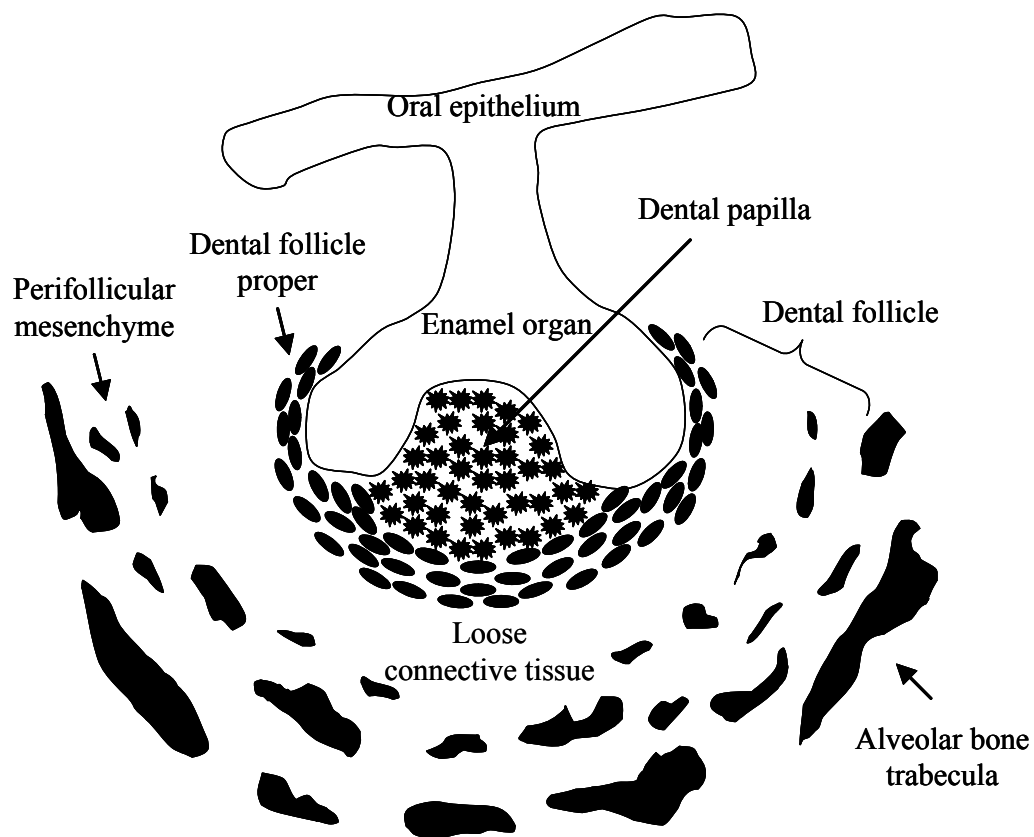


Figure. 2.2. Schematic representation of a developing tooth bud at the cap stage (adapted from Cho and Garant, 2000).

1999). Specifically, the differentiation factors may be dentin-associated or secreted by epithelial root sheath cells (reviewed in Ten Cate, 1996; 1997). Enamel proteins from this matrix, such as amelogenin, may act as a reservoir of biologic factors in stimulating the migration, adhesion and differentiation of cells (Harrison and Roda, 1995; Hammarström *et al.*, 1996; Ten Cate, 1996), rendering it conducive for connective tissue attachment. Following the coordinated formation of PDL fibres and alveolar bone, root development occurs in an apical direction till the attachment apparatus becomes complete (reviewed in Bartold and Narayanan, 1998).

2.3.2. Cell populations and phenotype

In light of tooth development, PDLF near the cementum are thought to be derivatives of the ectomesenchymal cells of the investing layer, whereas PDLF near the alveolar bone are derivatives of perivascular mesenchyme. In agreement to this hypothesis, reports have shown that the mitotic activity and collagen turnover rates within the PDL at the tooth surface are different from those near the alveolar bone, particularly during trauma from occlusal imbalances (Beertsen, 1975). However, identities of the specific cell types and the required stimuli for differentiation of dental follicle cells have not been established.

In addition, studies indicate that phenotypically distinct and functional sub-population of cells of both fibroblast and osteoblast/cementoblast lineage exists in the PDL (McCulloch and Bordin, 1991; Pitaru *et al.*, 1994). These cells probably consist of other mesenchymal cells, including progenitor cells, important in repair and regeneration (Lekic and McCulloch, 1996). In support of this theory, PDL cells have been shown to possess osteoblast-like characteristics, including the production of osteonectin (Somerman *et al.*, 1990; Nohutcu *et al.*, 1996; Yamada *et al.*, 2001), alkaline phosphatase (ALP) (Kawase *et al.*, 1988; Groeneveld *et al.*, 1995), and cyclic adenosine monophosphate (cAMP) and bone *gla* protein in response to parathyroid hormone (PTH) and 1,25-dihydroxyvitamin D₃, respectively (Cho *et al.*, 1992). Indeed, PDL cells consist of two fibroblast types, one existing as soft tissue fibroblasts and the other possessing high ALP levels similar to osteoblasts. The latter form bone- and cementum-like structures *in vitro*, and appears capable of differentiating into cementoblasts that synthesize Sharpey's fibres of the cementum (Schroeder, 1992; Cho *et al.*, 1995). Hence, PDLF appears to play a role in periodontal regeneration.

2.4. Biology of periodontal regeneration

Periodontal regeneration refers to the reproduction or reconstitution of a lost or injured tissue which entails the full restoration of its architecture or function (American Academy of Periodontology, 2005). Periodontal regeneration therefore involves both soft (gingival and PDL) and mineralized (bone and cementum) connective tissues, as detailed in section 1.1. In order to elaborate on the mechanism of periodontal regeneration, the roles of signalling molecules and cells in regeneration are detailed below.

2.4.1. Molecules in periodontal regeneration

Many molecules and cell types participate in periodontal regeneration. The associated events include an initial inflammatory reaction, recruitment of connective tissue cell populations by chemotaxis, their proliferation and differentiation, and synthesis of ECM (Bartold and Narayanan, 1998).

Soluble mediators bind to cell surface receptors to activate intracellular signalling molecules and mechanisms which lead to cell responses such as cell migration, changes in cell shape and synthesis of ECM macromolecules. Soluble mediators involved in periodontal regeneration include (i) growth factors and other inflammatory mediators, including cytokines, lymphokines, and chemokines, (ii) adhesion proteins like FN and laminin, and (iii) matrix components such as collagens, proteoglycans, and hyaluronan (reviewed in Bartold *et al.*, 2000).

Firstly, growth factors and cytokines regulate cell migration, proliferation, and differentiation during inflammation and wound repair (Nakae *et al.*, 1991; MacNeil and Somerman, 1993; Pitaru *et al.*, 1994; Narayanan and Bartold, 1996). Their effects are pleiotropic, and depend upon many factors, such as healing stage, target cell type,

and the nature of the ECM (Bartold *et al.*, 2000). Secondly, adhesion proteins localize cells at required sites and hence regulate cell recruitment and healing. They may exhibit cell-specificity. Lastly, ECM components such as collagens and proteoglycans are necessary for the structural and physiological integrity of the new tissue, as well as for subsequent cell differentiation.

The origins of these molecules may be from the circulation, or produced locally by cells residing in the ECM. The former are secreted by inflammatory cells and resident connective tissue cells during inflammation and wound healing. For example, growth factors such as insulin-like growth factor-1 and adhesion molecules such as VN are derived from the blood plasma, while platelet-derived growth factor, transforming growth factor- β , interleukin-1 and interferon- γ are secreted by fibroblasts and inflammatory cells. The latter, normally sequestered by the ECM, are released (Hauschka *et al.*, 1988; Clark, 1996). These include growth factors such as insulin-like growth factor-1, fibroblast growth factor-1 and -2, transforming growth factor- β , and bone morphogenetic proteins, and adhesion proteins such as osteopontin (OPN), bone sialoprotein (BSP) and FN from cementum and alveolar bone (Nakae *et al.*, 1991; MacNeil and Somerman, 1993; Narayanan and Bartold, 1996). The mechanism of action of these soluble factors is considered to be via cell surface receptors which leads to an induction of downstream transcription factors and gene expression cascades (Maniatis *et al.*, 1987; Vellanoweth *et al.*, 1994).

2.4.2. Cell populations in periodontal regeneration

Progenitor cells within the PDL and alveolar bone marrow of the periodontium are considered to be the parent cells for synthetic cells such as osteoblasts and cementoblasts. Progenitor cells have the capacity to undergo

continuous cell division to maintain their progeny, and to give rise to specialized cell types in a process called tissue homeostasis. It has been demonstrated that such progenitor cells are located close to the blood vessels in PDL (Gould *et al.*, 1980; McCulloch and Melcher, 1983b). These progenitor cells divide slowly but continually in paravascular zones, from which daughter cells migrate toward the root surface, alveolar bone, or into the body of the PDL (McCulloch and Melcher, 1983b; McCulloch *et al.*, 1987). Due to the numerous interconnections of vascular channels in the PDL and the stromal compartment in alveolar bone, progenitor cells may originate from the bone stromal compartment. This was supported by *in vitro* observations that cells cultured from bone have the capacity to form cementum-like material (Melcher *et al.*, 1986). In addition, progenitor cells located in paravascular zones undergo rapid cell division in periodontal wounding models and presumably supply the healing site with synthetic cell types that deposit ECM (Gould *et al.*, 1980; Iglhaut *et al.*, 1987).

Similar to embryonic development, PDL fibroblasts (Gould *et al.*, 1980; Roberts *et al.*, 1987; Lin *et al.*, 1994; Nohutcu *et al.*, 1996) as well as paravascular and endosteal fibroblasts (McCulloch *et al.*, 1987) when properly induced, were demonstrated to have the capacity to synthesize PDL, cementum and alveolar bone during regeneration of the periodontium. However, the exact identity of cells responsible for periodontal regeneration are not established. Yet, while populations of cells exist within the PDL having the capacity to function as cementoblast or osteoblast-like cells, there are others within the PDL, both during development and regeneration, secret factors that inhibit mineralization (Melcher, 1970; Saito *et al.*, 1990; Ogiso *et al.*, 1991; Lang *et al.*, 1995), thus preventing ankylosis, the fusion of tooth root with surrounding alveolar bone.

An accumulation of recently published data demonstrates that epithelial cells derived from the epithelial rests of Malassez (ERM) in the PDL express high amounts of OPN, as well as other proteins usually associated with mesenchymal cells (Mouri *et al.*, 2003; Mizuno *et al.*, 2005; Rincon *et al.*, 2005). The ERM, which are remnants of the Hertwig root sheath, are found close to the cementum (Berkovitz and Shore, 1995), and are postulated to play a role in cementum repair and regeneration (reviewed in Rincon *et al.*, 2006).

2.5. Choice of scaffolds for periodontal tissue engineering

As discussed in Chapter 1, limitations in current therapeutic procedures open up new revenues for tissue engineering. The term “tissue engineering” was first coined at a scientific workshop in 1987 (Heineken and Skalak, 1991), depicting the multi-disciplinary technologies in the controlling of cell behaviour and in the implantation of cells with non-biological scaffolds, in place of traditional synthetic prostheses, to achieve tissue repair and reconstruction. It is hoped that by utilizing the regenerative capacity of cells, functional tissue analogues having the desired dimensions, mechanical properties and biological function could be deployed that overcome existing limitations. Having highlighted the roles of PDLF in periodontal regeneration, the physical and chemical properties of scaffolds, as well as their roles in influencing cell-substratum interactions and the biological outcome, will be reviewed.

2.5.1. Scaffold morphology

Many large or non-space-containing defects often require grafting materials in the form of scaffolds to assist in space maintenance and enhance tissue formation.

This is particularly relevant for bone defects of critical size, as in Class III furcation defects described in section 1.2.2. Hence, the requirements for successful tissue engineering of the periodontium can be divided into (i) the biomechanical properties of scaffold, such as architectural geometry and space maintaining properties, and (ii) the biological functions of the engineered matrix, including cell recruitment, permission of neovascularization and delivery of the requisite morphogenetic, regulatory and growth factors for tissue regeneration (reviewed in Bartold *et al.*, 2000).

Design features to obtain satisfactory space maintenance would include an ability to be fashioned into a desired shape and be of a consistency compatible with easy handling (reviewed in Brekke and Toth, 1998). The scaffold material should also be of sufficient form to allow placement into a defect and to withstand soft tissue collapse (reviewed in Scantlebury, 1993). The internal architecture of the scaffold should allow rapid colonization by cells of the desired phenotype and ingrowth of tissue compatible with that at the site of regeneration (Whang *et al.*, 1999). At the same time, the scaffold should ideally function as a barrier to the ingrowth of unwanted tissues, such as gingival epithelium and connective tissue, yet permit selective ingrowth of regenerative tissues, consistent with the principles of guided tissue regeneration (GTR) (reviewed in Bartold *et al.*, 2000). Consequently, a sufficient wound space and a suitable environment will act synergistically to permit regeneration as required.

2.5.2. Biodegradability

For therapeutic tissue engineering, one of the most desirable material properties is degradation or resorption (reviewed in Griffith, 2000). “Degradable”

polymers undergo extensive chain scission to form small soluble oligomers or monomers in the presence of body fluids. This degradation may proceed by a biologically active process, such as enzymatic digestion, or by passive hydrolytic cleavage. “Bioresorbable” polymers, on the other hand, can be completely degraded *in vivo*, and their degradation by-products can be totally eliminated via natural metabolic pathways. A bioresorbable biomaterial is favourable over non-resorbable ones to support gradual tissue ingrowth and to achieve complete replacement by a regenerated matrix for two major reasons. Firstly, permanent implants almost always elicit a chronic inflammatory reaction or a foreign body response, characterized by formation of a poorly vascularised fibrous layer analogous to a scar at the material-tissue interface, which likely affects tissue function. Secondly, mechanical properties of hybrid tissues may be compromised compared to native ones (reviewed in Griffith, 2000).

2.6. Surface properties of the biomaterial

2.6.1. Biocompatibility

Biocompatibility can be defined as the acceptance (or rejection) of an artificial material by the surrounding tissues and by the body as a whole (Park, 2000). Biocompatibility encompasses many different aspects, including (i) cell adhesion, (ii) cytotoxicity, (iii) tissue compatibility, (iv) hemocompatibility and (v) biofunctionality (Kirkpatrick *et al.*, 1998; Rhodes, 2004; Stieglitz, 2004; Owen *et al.*, 2005; Tang and Hu, 2005).

Two important aspects of material screening refer to *in vitro* cytotoxicity and tissue- or hemocompatibility behaviour (Sgouras and Duncan, 1990). In the former, cell injury is indicated by a reduction in metabolic activity as measured by cellular

ATP levels or mitochondrial activity, and a loss of membrane integrity. This is followed by morphological change and subsequent cell death. Cytotoxicity comes about due to unfavourable interactions of the material components with cell membranes, leading to cell damage (reviewed in Wang *et al.*, 2004). In the latter, tissue compatibility is defined by the degree of material-mediated foreign body reactions, manifested as inflammation, fibrosis, infection and thrombosis. Molecular interactions between the phagocyte integrin Mac-1 (CD11b/CD18) and P1 sequence within the fibrinogen D domain is responsible for inflammatory response via phagocyte accumulation on the material, due to the exposure of P1 in surface-mediate denaturation of fibrinogen and thrombin-mediated conversion of fibrinogen to fibrin (Hu *et al.*, 2001). Further contact with blood results in rapid adsorption of plasma proteins onto its surface, an interaction of which results in complement cascade activation and subsequent cell lysis (reviewed in Rihova, 1996). Moreover, platelet adhesion and activation initiates the coagulation process, leading to thrombosis (reviewed in Andrade, 1985).

Despite the importance of the above in determining cell acceptance or rejection, the first and foremost requirement for biocompatibility is the ability of the scaffold material in supporting cell adhesion. Cell adhesion triggers integrin-dependent pathways involving focal adhesion kinase (FAK) and the Src-family kinases. This in turn activates downstream mitogen-activated protein kinase (MAPK) pathway, resulting in transcriptional regulation of genes responsible for growth and differentiation (reviewed in Owen *et al.*, 2005a). Furthermore, the MAPK pathway has the potential in modulating the extent of attachment depending on the signals it receives by the “inside-out, outside-in” paradigm (reviewed in Boudreau and Jones, 1999). Therefore, initial cell adhesion, critical to these processes, is a major

determinant of cytocompatibility *in vitro*, and a possible determinant of biocompatibility *in vivo*.

Biomaterials used for tissue engineering can be broadly divided into categories of synthetic or naturally derived. Synthetic polymers are widely used as graft materials because (i) they offer a wide range of physical, chemical and mechanical properties that are easily altered by chemical means, and (ii) they are more readily fabricated into various shapes and forms (Thomson *et al.*, 1997). In light of the importance of cell adhesion, the following section will examine cell-substratum interactions at the liquid-solid interface, as well as the influence of two most extensively studied aspects of surface properties, namely surface wettability and topography, with special focus on synthetic polymers.

2.6.2. Cell-substratum interactions

The first studies investigating cell-substratum adhesion were performed with surface contact microscopy (Ambrose, 1961) and transmission electron microscopy (Abercrombie *et al.*, 1971), in which cell adhesion was found to occur at regions marked by an increased electron density in the cytoplasm beneath the cell membrane and an association with microfilament bundles known as 'plaques'. At the same time, Curtis (1964) examined cell-substratum contacts on living specimens with the interference reflection microscope, which exploits a phase shift in illumination when it is moved from the cell-medium boundary between a cell and a substrate. The closest contacts appeared darkest, whereas the less close appear progressively lighter in monochromatic light, up to a separation of about 100 nm. Subsequently, 'focal adhesions' with 10-20 nm separation between the cell membrane and substratum, and 'close contacts' (30-50 nm separation), were identified (Izzard and Lochner, 1976).

Focal adhesions or contacts are comprised of a complex assembly of intra- and extracellular proteins, connecting cytoskeletal actin fibres with the ECM via transmembrane glycoproteins known as integrins (reviewed in Burridge *et al.*, 1988). The integrins are heterodimer receptors, consisting of non-covalently linked α - and β -subunits (Hynes, 1987; Ruoslahti and Pierschbacher, 1987), involved in cell-cell and cell-substratum interactions (Albelda and Buck, 1990; Lampugnani *et al.*, 1991). Intracellular proteins involved in focal adhesions are α -actinin, talin, vinculin (Burridge *et al.*, 1988), and paxillin (Turner *et al.*, 1990). α -actinin crosslinks actin microfilaments and is responsible for cell shape maintenance (Dubreuil, 1991), whereas talin and vinculin act as the structural link between *f*-actin and integrins. The remaining focal adhesion proteins such as focal adhesion kinase (FAK), Cas, and paxillin interact with both α -actinin and the intracellular domain of integrins, thereby participating in integrin-mediated signalling (Burridge and Chrzanowska-Wodnicka 1996), leading to the regulation of cytoarchitecture, cell proliferation and differentiation (Giancotti and Ruoslahti, 1999).

Components of focal contacts, anchored to the distal ends of cytoskeletal microfilaments underlying the cytoplasmic membrane (Heath and Dunn, 1978), traverse the cell and allow it to bind to ECM via integrins. Ligand binding occurs at the outer surface of transmembrane integrins through an Arg-Gly-Asp (RGD) sequence (Ruoslahti and Pierschbacher, 1987) as well as other domains (Aota *et al.*, 1991). Signals from the extracellular environment are also relayed to the cell via integrins, leading to changes in gene expression and protein synthesis. For instance, two subfamilies, namely the integrin β_1 -subfamily, including the FN receptor ($\alpha_5\beta_1$), and the β_3 -subfamily, including the VN receptor ($\alpha_v\beta_3$), are implicated in cell-substratum interactions (Akiyama *et al.*, 1989). The former plays an important role in

initial cell adhesion events (Yamada *et al.*, 1992), FN matrix assembly (Akiyama *et al.*, 1989), and migration (Straus *et al.*, 1989).

The occurrence of focal adhesions is determined largely by substrate composition (Burrige and Fath, 1989), which is influenced by the surface properties of the substratum such as surface wettability and topography.

2.6.3. Surface wettability and protein adsorption

The surface properties of polymers that influence their biocompatibility include (i) the interfacial free energy, (ii) a balance between hydrophilicity and hydrophobicity on the surface, also known as wettability, (iii) the chemical structure and functional groups, (iv) the type and density of surface charges, (v) the molecular weight of the polymer, (vi) conformational flexibility of the polymer and (vii) surface topography and roughness. Among these, wettability is one of the most important parameters in the design of biomaterials or implant devices (reviewed in Wang *et al.*, 2004).

It has been demonstrated that cell adhesion follows the principles of thermodynamics; the extent of cell adhesion decreases as a function of increasing substratum surface free energy (γ_{sv}) when the liquid surface tension (γ_{lv}) is higher than the cell surface tension (γ_{cv}), and vice versa (Schakenraad *et al.*, 1988). The thermodynamics of a liquid/solid interaction can be determined by the measurement of contact angles. Contact angle, θ , is a quantitative measure of the wettability of a solid by a liquid. It is defined geometrically as the angle formed by a liquid at the three phase boundary where a liquid, gas and solid intersect (Fig. 2.3).

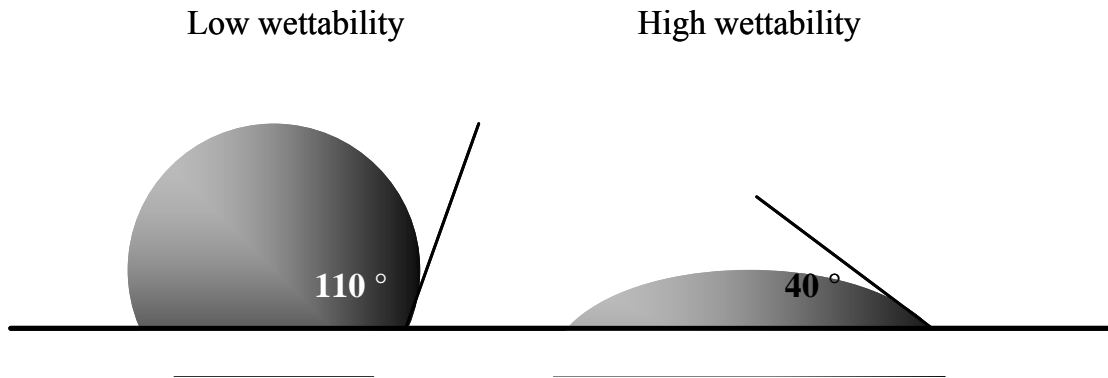


Figure 2.3. The contact angle of a liquid with a solid.

A measurement of surface wettability is warranted by the fact that the first molecule a biomaterial encounters in culture or when implanted is water, whose molecular arrangement varies according to the surface properties of the biomaterial. Natural ions, such as chloride and sodium, are immediately incorporated into the water overlayer as hydrated ions. Subsequently, proteins in the surrounding medium approach the surface (Fig. 2.4), and adsorb via conformation changes or denaturation and/or replacement in a process called the “Vroman effect” (Vroman and Adams, 1969; Horbett, 1984). Proteins bind with their hydrophilic regions and with intact water shells on hydrophilic surfaces, whereas they bind with hydrophobic domains without intervening water shells on hydrophobic surfaces (Israelachvili and Wennerstrom, 1996). As a result, hydrophobic surfaces tend to adsorb larger amounts of proteins that are more tightly bound than hydrophilic ones (reviewed in Elbert and Hubbell, 1996).

The effects of varying surface wettability on cell attachment and proliferation were well documented. A wettability gradient of dichlorodimethylsilane coupled to glass cover slips, with a range of advancing water contact angles between $43 \pm 6^\circ$ to

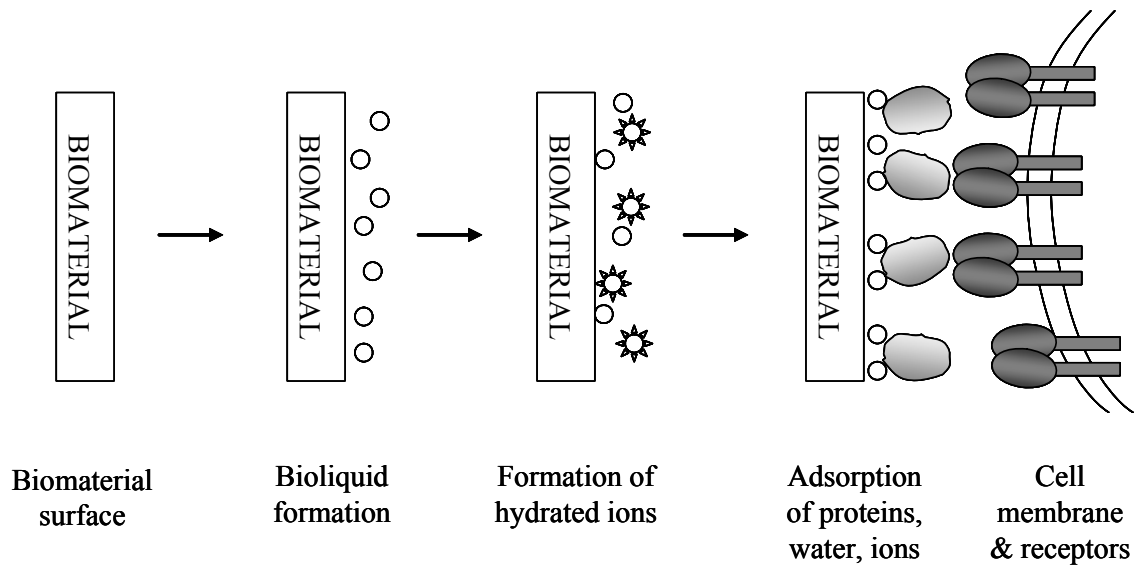


Figure 2.4. Illustration of events at the biomaterial surface (adapted from Kasemo and Gold, 1999).

101 ± 2°, showed that the spread area of fibroblasts at the hydrophilic end was more than twice of that at the hydrophobic end (Ruardy *et al.*, 1995). This is in accordance to previous findings that surfaces with intermediate wettabilities, exhibiting water contact angles between 40° to 60°, provide an optimal substratum for cell adhesion (van Wachem *et al.*, 1985; 1987b; Yanagisawa *et al.*, 1989), and subsequent spreading (Schakenraad *et al.*, 1986) and proliferation (Saltzman, 1997; Lee *et al.*, 1998).

Surface wettability influences cell adhesion and morphology via a modulation of the composition and organization of the protein layer. The deposition of endogenous FN, a major cell adhesion protein (reviewed in Bartold *et al.*, 2000), is possible only on hydrophilic surfaces where FN displaces serum proteins pre-adsorbed onto the substrata (Grinnell and Feld, 1982; Bentley and Klebe, 1985; Van Wachem *et al.*, 1987a). This is because the presence of competing serum lowers the overall densities of adsorbed FN on hydrophobic substratum (Pettit *et al.*, 1992;

McClary *et al.*, 2000), rendering the surface incapable of supporting cell attachment (Grainger *et al.*, 2003). Moreover, surface properties of substratum were found to influence the tightness of FN binding (Pettit *et al.*, 1992) as well as the conformation of its cell binding domain (Iuliano *et al.*, 1993). Accordingly, FN on hydrophobic surfaces is in a conformation that discourages cell-integrin receptor recognition (Grainger *et al.*, 2003). As a result, the focal adhesion complex and the anchorage of cells to the substratum may be compromised, leading to spherical morphology and disorganized cytoskeletal arrangement.

2.6.4. Surface topography, and cell growth and differentiation

Cells are sensitive to the physical characteristics or topography of substrates, with which they interact via focal contacts (Burrige *et al.*, 1988). Topography may be defined as the morphology of a substrate, and can be classified into two different criteria: roughness and texture. Surface roughness is characterized by changes of surface topography including hills and pits with random size and distribution, caused either by natural processes like crystallization, or artificial means such as sand blasting. Surface texture, on the other hand, represents configurations of grooves, ridges or pores designed into a substrate, often with defined dimensions and surface distribution (reviewed in von Recum and van Kooten, 1995).

Surface topography has been identified as an important factor that influences cell attachment and proliferation. Exudates of fibroblasts cultured on controlled surface variations carrying pillar-like filaments in the range of 50 to 150 μm were found to contain factors promoting cell attachment and spreading (Korman *et al.*, 1984). Additionally, fibroblast cell growth was highest on textured surfaces with pillar sizes between 2 and 5 μm , followed by wells and smooth surface (Green *et al.*,

1994). Hence, the physical cues may reside in raised surface elements and possibly in sharp corners or acute discontinuities of the substrate, as deduced from actin condensations at the transitions from ridges to grooves (Brunette, 1986).

On the other hand, the influence on morphogenesis is dependent upon cell type as well as cellular properties such as cytoskeletal organization and cell-cell interactions (reviewed in Boyan *et al.*, 1996). Unlike fibroblasts which showed a preferential growth on textured substrata, osteoblast-like cell adhesion, but not proliferation, was enhanced on polymer surfaces with nano-scale and micro-scale roughness compared to smooth ones (Wan *et al.*, 2005). In fact, MC3T3-E1 osteoblast-like cell proliferation was enhanced on smooth ends of poly(D,L-lactic acid) (PDLLA)-rich roughness gradient than on the rough poly(L-lactic acid) (PLLA)-rich ends configured by polymer blending (Simon *et al.*, 2005). Similarly, the same cells proliferated more on smooth regions of a PLLA polymer crystallinity gradient, with root-mean-square (rms) roughness values ranging from 0.5 to 13 nm (Washburn *et al.*, 2004).

Surface topography can also determine the type of focal adhesion and its configuration in space, thus influencing cell shape and even its phenotypic expression. In terms of cell shape, surface discontinuities representing local changes in surface free energy affect cellular alignment and direction of proliferation via changes in protein adsorption and conformation (reviewed in von Recum and van Kooten, 1995). Meningeal cell and ECM alignment were found to increase with increasing oriented surface roughness, reaching a threshold at 345 nm (Manwaring *et al.*, 2004). Such an induction of cellular locomotion in response to surface topography have been identified and termed as topographic or contact guidance (Brunette and Chehroudi, 1999). In terms of phenotypic expression, MG63 osteoblast-like cells showed

enhanced differentiation on rough compared to smooth alloy surfaces, reflected by decreased proliferation and increased ALP and osteocalcin production (Lincks *et al.*, 1998).

2.7. Biodegradable synthetic polymers

Biodegradable synthetic polymers such as poly(glycolic acid), poly(lactic acid) and their copolymers, poly(p-dioxanone), and copolymers of trimethylene carbonate and glycolide have been used in a number of clinical applications. The major applications include resorbable sutures, drug delivery systems and orthopaedic fixation devices (reviewed in Suggs and Mikos, 1996; Gunatillake and Adhikari, 2003). Among the families of synthetic polymers, polyesters and copolyesters of naturally occurring hydroxyl-acids have been successfully employed as implants for tissue regeneration, and are summarized below.

2.7.1. Overview of polyesters

Aliphatic polyesters with physical and chemical properties suitable as matrix materials (Chaignaud *et al.*, 1997; Hutmacher, 2000b) constitute the most versatile and widely used family of polymers studied to date. The reasons are, firstly, the ester bonds in these polymers are hydrolytically labile (Vert and Li, 1992), rendering the materials easily degradable by nonenzymatic means. Secondly, the initial stages of polymer degradation involves a lowering of molecular weight, but not the mass (Hoffman and Casey, 1985), hence preserving the space maintenance properties of a scaffold. Thirdly, it is possible to alter the degradation kinetics by modifying the structure, and some of the degradation products can be resorbed through natural metabolic pathways. Lastly, these polyesters are thermoplastic and can be formed into

desired shapes by moulding, extrusion and solvent processing (reviewed in Gunatillake and Adhikari, 2003).

The key polymers in this family are poly(glycolic acid), poly(lactic acid), poly(glycolic-co-lactic acid), poly(dioxanone), poly(caprolactone), poly(3-hydroxybutyrate), poly(3-hydroxyvalerate), poly(valerolactone), poly(tartronic acid), poly(β -malonic acid). The prominent members for which biocompatibility and biodegradation studies were documented were listed in Table 2.2. Among polyesters, poly(α -hydroxy acids) such as poly(glycolic acid), poly(lactic acid) and a range of their copolymers have a long history of use as synthetic biodegradable materials in a number of clinical applications including scaffolds for cell transplantation (reviewed in Gunatillake and Adhikari, 2003). Polyesters have also been considered for development of tissue engineering applications (Hubbell, 1995; Wong and Mooney, 1997), particularly for bone tissue engineering (Kohn and Langer, 1996; Burg *et al.*, 2000).

It is therefore envisioned that a biodegradable, biocompatible material with the ease of processability to specified shapes with appropriate porosity from the family of polyesters, that satisfy the basic requirements for tissue engineering (detailed in section 2.5.1), would be used in the regeneration of hard and soft tissues of the periodontium. From the list of clinically tested polyesters, poly(ϵ -caprolactone) (PCL) stands out due to its excellent cyto- and tissue-compatibility and versatility (Pitt, 1990; Ng *et al.*, 2000). Therefore, the physical and chemical properties of PCL are examined in greater detail in the following section.

Polymer	Thermal & mechanical properties			Approx. degradation time (mths)	Degradation products	Biocompatibility and biodegradation
	Melting point (°C)	Glass transition (°C)	Approx. strength			
Poly(glycolic acid)	225-230	35-40	7.0 GPa (Modulus)	6 to 12	Glycolic acid	Generally considered to be biocompatible. Systemic or local reactions due to acidic degradation products in some, which are eliminated by natural pathways <i>in vivo</i> .
Poly(L-lactic acid)	173-178	60-65	2.7 GPa (Modulus)	>24	L-lactic acid	
Poly(D,L-lactic acid)	Amorphous	55 to 60	1.9 GPa (Modulus)	12 to 16	D,L-lactic acid	
Poly(D,L-lactic-co-glycolic acid) (85/15)	Amorphous	50 to 55	2.0 GPa (Modulus)	5 to 6	D,L-lactic acid and glycolic acid	
Poly(caprolactone)	58 to 63	-65 to 60	0.4 GPa (Modulus)	>24	Caproic acid	Generally considered as a non-toxic and tissue compatible polymer
Poly(propylene fumarate)	-	-	2 to 30 MPa (Compressive strength)	Depends on formulation; several months based on <i>in vitro</i> data	Fumaric acid, propylene glycol and poly(acrylic acid-co-fumaric acid)	Mild inflammatory response and no deleterious long-term response

Table 2.2. Summary of selected polyesters (Gunatillake and Adhikari, 2003).

2.7.2. Poly(ϵ -caprolactone) (PCL)

Poly(ϵ -caprolactone) (PCL) is an FDA-approved semi-crystalline, bioresorbable aliphatic polyester belonging to the family of poly(ω -hydroxy esters) (Kimura, 1993). PCL can be prepared by ring opening polymerization of ϵ -caprolactone using a catalyst. The repeating molecular structure of PCL homopolymer consists of five non-polar methylene (-CH₂) groups and a single relatively polar ester (O-C=O) group. Hence, the mechanical properties of PCL are polyolefin-like in terms of elasticity and tensile strength (Pitt, 1990), while its hydrolytic degradability resembles that of polyesters due to the presence of the aliphatic-ester linkage (reviewed in Perrin and English, 1997).

Previous work established that PCL is biocompatible based on the finding that its degradation by-products are non-toxic (Darney *et al.*, 1989; Kweon *et al.*, 2003). The first stage in the biodegradation process involving auto-catalyzed random hydrolytic cleavage of the ester linkage leads to a decrease in molecular weight (Pitt *et al.*, 1981). Intracellular degradation in Sprague-Dawley rats as an animal model demonstrated that PCL became encapsulated by collagen filaments, with occasional giant cells, during this stage of non-enzymatic bulk hydrolysis lasting approximately nine months. A transient initial inflammatory response was observed around the avascular connective tissue capsule, of less than 100 microns, during the first two weeks (Woodward *et al.*, 1985). This is followed by an onset of weight loss and a reduction in the rate of chain scission in the second stage, when the molecular weight is reduced to about 5,000, with the eventual fragmentation of the polymer into a powder. Short chain oligomers produced were rapidly degraded in phagosome of macrophages, giant cells and occasionally in fibroblasts, (Woodward *et al.*, 1985), requiring only 13 days for complete absorption in some cases (reviewed in Perrin and English, 1997). The by-products of auto-catalysed bulk hydrolysis are monomeric acids, which are eliminated from the body by direct renal secretion or metabolized via the Krebs cycle primarily as carbon dioxide and water (Kweon *et al.*, 2003). Moreover, hydroxyl free radicals from extracellular exudate and inflammatory cells have been implicated to be one of the major causes of PCL degradation (Ali *et al.*, 1993; 1994), in addition to enzymatic degradation (Pitt *et al.*, 1984).

Despite its biocompatibility, one major disadvantage of PCL is its slow rate of degradation; homopolymer bulk PCL has a degradation time of the order of two to three years (Holland and Tighe, 1992). This could be overcome by altering the rate of hydrolysis via copolymerization with other lactones (Pitt *et al.*, 1981). Hence, PCL

has been extensively investigated for developing long-term, implantable drug delivery systems (reviewed in Suggs and Mikos, 1996; Gunatillake and Adhikari, 2003).

In comparison to other commercially available bioresorbable polymers, PCL is flexible and versatile. Firstly, PCL has unusual thermal stability, with a decomposition temperature of 350 °C, whereas other tested aliphatic polyesters have decomposition temperatures between 235 °C and 255 °C (Suggs and Mikos, 1996). Secondly, PCL has unique physical properties due to its low melting point (T_m) of 57 °C and a glass transition temperature (T_g) of -62 °C (Engelberg and Kohn, 1991), imparting it with a rubbery state at room temperature (reviewed in Perrin and English, 1997). Consequently, PCL possesses high drawability compared to other aliphatic biodegradable polyesters. This ease of processing facilitates the fabrication of membranes through biaxial drawing method, which improves physical properties such as tensile strength and modulus in both the longitudinal and lateral directions (Ng *et al.*, 2000). Furthermore, three-dimensional porous scaffolds fabricated from PCL demonstrated high elasticity and mechanic strength (Guan *et al.*, 2002; Zein *et al.*, 2002; Jeong *et al.*, 2004).

PCL substrates have been rigorously tested with different cell types for various biomedical applications. For example, alkali-hydrolyzed PCL membranes have been demonstrated to support the attachment and growth of dermal fibroblasts (Ng *et al.*, 2001), keratinocytes (Khor *et al.*, 2002, 2003), bladder smooth muscle cells (Thapa *et al.*, 2003), endothelial and smooth muscle cells (Serrano *et al.*, 2005), and conjunctival epithelial cells (Ang *et al.*, 2006). In addition, PCL scaffolds fabricated by fused deposition modelling (FDM) possessing fully interconnected channel network, and controllable porosity and channel size (Zein *et al.*, 2002; Hutmacher *et al.*, 2001) have been studied as potential matrices for tissue engineering of bone and

cartilage (Hutmacher, 2000; Hutmacher *et al.*, 2001). PCL can be regarded as a soft- and hard-tissue-compatible bioresorbable material, and is therefore a candidate scaffold biomaterial for periodontal regeneration.

3. COMMON MATERIALS AND METHODS

3.1. Fabrication of PCL membranes

3.1.1. Solvent casting

Membranes were prepared by solution-casting, heat press and biaxial stretching, as previously described (Ng *et al.*, 2000). Poly (ϵ -caprolactone) (PCL) pellets ($M_n = 80,000$, density = 1.145 g/cm^3 , Sigma-Aldrich, WI, USA) were checked for purity by differential scanning calorimetry (DSC), after which they were desiccated in a vacuum oven at $40 \text{ }^\circ\text{C}$ for 24 h to remove trapped moisture. A polymer-solution (3% w/w) was prepared by dissolving dried PCL pellets in dichloromethane (JT Baker, NJ, USA) on a platform shaker for 3 h, and cast over custom-designed glass moulds, 16 cm x 16 cm. The solution was swirled gently to ensure uniform coverage in the moulds, and sealed by aluminium foil to allow slow evaporation of the solvent at room temperature in a safety hood cabinet overnight. Solvent-cast PCL films of about $100 \pm 10 \text{ }\mu\text{m}$ thus obtained were dried as before at $40 \text{ }^\circ\text{C}$ for 24 h to remove residual solvent.

3.1.2. Heat press and biaxial stretching

PCL films, 5 cm x 5 cm, were sandwiched between 2 steel plates covered with aluminium foil and heat pressed at $55\text{-}58 \text{ }^\circ\text{C}$ and at 100 bars for 10 min with a Cavar heat press (PH Hydraulics and Engineering, Singapore) to remove surface defects due to solvent evaporation. Films were visually inspected to ensure surface homogeneity and thickness uniformity. Heat-pressed films were mounted onto an in-house biaxial stretch machine (Ng *et al.*, 2000) and pre-heated for 2 h at $55\text{-}58 \text{ }^\circ\text{C}$ to achieve temperature equilibrium. Biaxial stretching of films to a draw ratio of 3 x 3 was performed at $55\text{-}58 \text{ }^\circ\text{C}$ at a uniform speed (Appendix). Biaxially stretched membranes

were maintained in the machine for 6 h for polymer stabilization. Membrane thickness was measured with a digital micrometer screw gauge (Mitutoyo, Singapore). Samples within 20 μm thickness were retained for further processing.

3.1.3. Perforation

Membrane perforation was achieved using a 3-axis desktop robot (Sony Robokids, Model CAST_AU4/B2521E, Tokyo, Japan), a 0.57 mm-diameter needle and customized software (Htay *et al.*, 2004). Biaxially stretched membranes were adhered onto a polystyrene foam stage and an orderly array of perforations, approximately 100 μm in diameter, was obtained by the vertical punching action of the needle. The distance between two hole-centres was set at 0.5 mm and the speed of perforation at 50 mm/s, as described previously (Htay *et al.*, 2004). Perforation diameter and density were determined from PCLM (Olympus IX70, Tokyo, Japan) images using Micro-Image[®] (Media Cybernetics, MD, USA).

3.1.4. Alkaline hydrolysis treatment

Membranes were treated by immersion in 5 M NaOH for 3 h with agitation at 100 rpm at room temperature to increase hydrophilicity, and rinsed several times in distilled water to ensure complete removal of NaOH. Purity and crystallinity of the polymeric membranes before and after treatment were determined by differential scanning calorimetry as described previously (Htay *et al.*, 2004). Membranes were sterilized with 70% ethanol and *uv* irradiation, and stored in a desiccator under vacuum before use.

3.2. Collagen induction

PDLF between passage 3 to 5 were seeded at a density of 10,000 cells/cm², and cultured in Dulbecco's Modified Eagle's Medium (DMEM) (Gibco, Life Technologies, NY, USA) containing 10% (v/v) foetal bovine serum (FBS) (Gibco) and 2% penicillin-streptomycin (Invitrogen, CA, USA). Collagen stimulation was carried out one day after seeding with culture medium supplemented with 200 µM ascorbic acid 2-phosphate magnesium salt (Asc; Sigma), the level present in gingival crevicular fluid (Meyle and Kapitza, 1990), and 350 µM of L-proline (Sigma). Fresh ascorbic acid aliquots (100X stock in DMEM at -20 °C) were added at medium change every 3 to 4 days, and 1 ml of medium was added per well in 12-well tissue culture plates (TPP, MO, USA).

3.3. Cell proliferation assay

Cell proliferation as reflected by the amount of dsDNA was assayed by PicoGreen® dsDNA quantitation kit (Molecular Probes, Invitrogen, CA, USA) as previously described (Ng *et al.*, 2005), with slight modifications. Samples ($n \geq 3$) were rinsed thrice with PBS to remove unattached cells and incubated with 200 µl of 0.1% (w/v) collagenase and 0.1% (w/v) trypsin in PBS at 37 °C for up to 30 min with periodic agitation at 200 rpm to release cells from the extracellular matrix. Whole cell suspensions were pelleted and lysed by two freeze-thaw cycles in autoclaved deionized water. Samples were diluted with appropriate volumes of DNase-free Tris-EDTA (TE) buffer (10 mM Tris-Cl, pH 7.5, 1 mM EDTA), whereas DNA standards (0 ng/ml, 1 ng/ml, 10 ng/ml, 100 ng/ml, 1000 ng/ml) were diluted from 100 µg/ml of λ DNA (Molecular Probes) with the same. Samples and DNA standards in 100 µl aliquots were incubated with equal volumes of PicoGreen reagent, pre-diluted 200-

fold in TE buffer, in triplicates in an opaque 96-well plate (TPP, MO, USA) for 5 min at room temperature in the dark. Fluorescence was measured at 485 nm excitation and 535 nm emission in a microplate reader (GENios, Tecan Group, Switzerland). Calibration curves showed fluorescence measurements to be proportional to cell number. Cell proliferation was presented as the quantity of dsDNA (μg) as determined from λ DNA standard curve, over a 3-week period.

3.4. Cell viability assay

Cell viability assay was performed ($n=3$) with fluorescein diacetate (FDA, Molecular Probes) and propidium iodide (PI, Molecular Probes). Constructs were incubated with 2 $\mu\text{g}/\text{ml}$ of FDA for 15 min at 37 °C and 5% CO_2 , and rinsed thrice with PBS for 3 min each. Then they were incubated with 0.1 mg/ml PI for 3 min at room temperature, and rinsed again with PBS. Viewing was performed with a Confocal laser scanning microscope (CLSM; Olympus FluoViewTM FV500, Japan). Viable cells, having the ability to metabolise FDA and exclude PI, were stained green, whereas non-viable or apoptotic cells were stained red with PI. The areas of green and red colour were calculated in pixels from a confocal image at 100X magnification using Micro-Image[®] (Media Cybernetics, MD, USA) as described (Vidal *et al.*, 2003). Cell viability on membranes after FDA/PI staining were determined as the percentage of green area over the sum of green and red, whereas cell retention as the percentage of green area over the total image area.

3.5. Alkaline phosphatase (ALP) assays

3.5.1. ALP stain

Alkaline phosphatase (ALP) functions as an ectoenzyme attached to the cell membrane (Magnusson *et al.*, 1999). ALP activity was detected in cells by staining using ALP kit 86-R (Sigma) according to the manual. Cell nuclei were counterstained with Haematoxylin.

3.5.2. ALP enzyme substrate assay

Quantitative measurements of ALP activity was determined via colorimetric enzymatic substrate assay, as described previously (Chou *et al.*, 2002). Protein supernatants obtained from whole cell lysates were diluted 10-fold with alkaline substrate buffer (Sigma). Samples in 50 μ l aliquots were incubated with 150 μ l of 0.2% (w/v) para-nitrophenyl phosphate disodium (Sigma) in 1 M diethanolamine HCL at pH 9.83 for 30 min at 37 °C. The reaction was terminated by the addition of 200 μ l of 2 M NaOH/0.2 mM EDTA to each sample. Absorbance of 100 μ l mixtures in a 96-well plate was measured at 405 nm in triplicates with a microplate reader (Magellian, CA, USA). ALP activity was inferred as μ M pNP/ml from a standard curve prepared using known concentrations of para-nitrophenol (pNP) (Sigma) and NaOH / EDTA as blank. ALP activities were presented as international units per mg protein (IU/mg protein) in whole cell lysates, in which the IU of ALP activity was defined as μ moles of pNP substrate liberated per min under optimal conditions (Young, 1977).

3.6. Collagen extraction by limited pepsin digestion

The extraction of collagen by pepsin digestion relies on the resistance of collagen triple helix to enzymatic digestion, but the susceptibility of other proteins to degradation. To extract collagens in the medium, 500 μ l of 3-day conditioned medium

was split into two groups, 250 µl each. The first medium fraction was supplemented with protease inhibitor cocktail with a final concentration of 5 µM AEBSF, 1.5 nM aprotinin, 10 nM E-64, 5 µM EDTA, 10 nM leupeptin (Calbiochem, CA, USA), and loaded immediately for SDS-PAGE (section 3.8) or freeze stored in aliquots at -20 °C. The second medium fraction was digested with 25 µl pepsin (1 mg/ml in 1 N HCl) for 2 h at room temperature with constant agitation at 100 rpm.

To extract collagens in the cell layer, hPDLF were washed twice with HBSS and digested with 250 µl of HBSS containing 25 µl of pepsin (1 mg/ml in 1 N HCl). Pepsin digestion of cell layer fraction was performed separately, but identically to medium fraction, as described above. After 2 h, the reaction was irreversibly terminated by neutralization with 25 µl of 1 N NaOH until the pH was at least 7.0 as indicated by phenol red.

3.7. Sodium dodecyl sulphate-polyacrylamide gel electrophoresis (SDS-PAGE)

3.7.1. Tris-acetate gels

To facilitate the resolution of high M.W. collagens, protein samples were separated on pre-cast 3-8% gradient NuPAGE® Tris-acetate gels (Invitrogen). Pepsin-digests and undigested medium fractions were denatured for 10 min at 70 °C in NuPAGE® lithium dodecyl sulfate (LDS) sample buffer (Invitrogen), with or without dithiothreitol (DTT) as reducing agent, and loaded alongside Precision Plus protein pre-stained standards (Bio-Rad Laboratories). Gel electrophoresis was performed using NuPAGE gel system (Invitrogen) in NuPAGE® Tris-acetate SDS Running Buffer (Invitrogen). Electrophoresis was run at a constant voltage of 120V until the dye front reached the bottom of the gel.

3.7.2. Tris-glycine gels

For the separation of non-collagenous proteins, polyacrylamide gels (6% stacking, 12% resolving) were cast using 30% acrylamide/bis (37:5:1) solutions, N,N,N,N-tetramethyl-ethylenediamine (TEMED) as the accelerator (all from Bio-Rad Laboratories) and 10% (w/v) ammonium persulphate (APS) (Invitrogen) as the polymerization catalyst. Whole-cell-lysates, normalized according to total protein content (Appendix), were denatured for 5 min at 90 °C in 4X SDS-PAGE reducing sample buffer (250 mM Tris-HCl [pH 6.8], 8% (w/v) SDS, 40% (v/v) glycerol, 20% (v/v) β -mercapthoethanol, 0.2% (w/v) bromophenol blue), and loaded alongside BenchMark™ pre-stained protein ladder (Invitrogen), or Precision Plus protein pre-stained standards (Bio-Rad Laboratories). Gel electrophoresis was performed using the Mini-PROTEAN II Electrophoresis System (Bio-Rad Laboratories) in Tris-glycine buffer and run at a constant voltage of 60V and 120V for 6% stacking and 12% resolving gel respectively, until the dye front reached the bottom of the gel.

3.8. Protein gel stain

3.8.1. Coomassie Blue stain

Size-fractionated proteins were visualized by routine Coomassie Blue stain (0.25% (v/w) Coomassie Brilliant Blue R250, 50% methanol, 10% acetic acid) for 4 h at room temperature with gentle agitation, and destained with destain solution (40% methanol and 10% (v/v) acetic acid) overnight.

3.8.2. PageBlue™ stain

Size-fractionated proteins were visualized by PageBlue™ Protein Staining Solution (Fermentas Inc., MD, USA) according to manufacturer's instructions. Since

PageBlue™ is compatible with silver staining, the same gels were visualized subsequently with silver stain, bypassing the fixation step.

3.8.3. Silver stain

Protein gels were fixed in 40% (v/v) methanol and 10% (v/v) acetic acid overnight at room temperature. Fixed gels or PageBlue™-stained gels were immersed in 50% (v/v) methanol for 15 min with gentle agitation, and washed with milliQ water 5 times, 5 min each. Then, the gels were sensitized with 0.02% (w/v) sodium thiosulphate for 1 min, and washed with milliQ water 2 times, 1 min each. Silver staining was performed with 0.2% (w/v) silver nitrate for 25 min at 4 °C in the dark, followed by washing with milliQ water 2 times, 1 min each. Development of silver stain was carried out by immersing the gels in 3% (w/v) sodium carbonate anhydrous and 2.5×10^{-3} % (v/v) formaldehyde with gentle agitation for about 5 min, changing solution when it yellowed. The gels were washed with milliQ water 2 times, 1 min each, to remove undeveloped stain, and staining was terminated by the addition of 5% (v/v) acetic acid and stored in 1% (v/v) acetic acid at room temperature.

3.9. Western blot analysis

3.9.1. Protein transfer

For the immuno-detection of collagens, fresh or frozen conditioned medium separated in 3-8% Tris-acetate NuPAGE gels were transferred onto nitrocellulose membranes (Pall Corp., NY, USA) with NuPAGE® Transfer buffer (Invitrogen) containing 10% (v/v) methanol. For the immuno-detection of non-collagenous proteins, fresh or frozen whole cell lysates separated in 12% polyacrylamide SDS-PAGE were transferred onto nitrocellulose membranes with Tris-glycine transfer

buffer (25 mM Tris-HCl, 192 mM glycine, 20% (v/v) methanol). The gel was sandwiched between one pre-equilibrated membrane and two 3MM Chr papers (Whatman plc., Middlesex, UK), and finally assembled between two sponges in a Trans-Blot cell (Bio-Rad Laboratories). Protein transfer was carried out at 100-120V for 90 min at 4 °C.

3.9.2. Immunoblotting

After protein transfer, nitrocellulose membranes were equilibrated in Tris buffered saline (TBS) (10 mM Tris [pH 7.4], 150 mM NaCl,) and incubated in blocking buffer, TBS-T (TBS, 0.1% (v/v) Tween-20) containing 5% (w/v) non-fat milk, for either 1 h at room temperature or overnight at 4 °C on an orbital shaker. For immunoblotting, membranes were incubated with primary antibodies (Appendix), diluted in incubation buffer, TBS containing 2-5% (w/v) non-fat milk, for either 2 h at room temperature or overnight at 4 °C on an orbital shaker. Primary antibodies were filter-sterilized and stored at 4 °C for re-use, and discarded after the third use. After primary antibody binding, membranes were washed 3 times with TBS-T at room temperature, 10 min each, before incubation with the appropriate horseradish peroxidase-conjugated secondary antibodies (Appendix) for 1 h at room temperature on an orbital shaker. The membranes were then subjected to 3 additional 10 min wash in TBS-T, incubated in chemiluminescence reagents (Supersignal West Pico Kit, Pierce Biotechnology, Inc., IL, USA), according to manufacturer's instructions and placed between transparency sheets. Signal detection was performed by exposure to X-ray film (Kodak, Japan) and developed in a RP X-OMAT Processor (Eastman Kodak Co., NY, USA).

3.10. Semi-quantitative densitometry

The relative concentrations of bands ($n=3$) generated by PageBlueTM or silver stain on SDS-PAGE, or by Chemilluminescence on Western blots, were determined by semi-quantitative densitometry. Signals were digitized into an image by gel scanner (GS-800 calibrated densitometer; Bio-Rad Laboratories). Each pixel was stored in the memory in 12 bits, and the gray level of each pixel was assigned a value. The relative concentrations of the bands of interest were determined with Quantity-One software (Bio-Rad Laboratories) by summing the gray levels of all pixels within the boundaries of each band.

3.11. Double-labelling immunofluorescence

Cells were rinsed with sterile PBS, and fixed with absolute methanol at -20 °C for 10 min. After air-drying and re-equilibration with PBS, blocking was performed with 5% bovine serum albumin (w/v) (Sigma) and 1% goat serum (v/v) (Invitrogen) in PBS for 2 h at room temperature. For double labelling of collagens, cells were incubated with anti-collagen I (1:5000; Sigma) overnight in a humidified chamber at 4 °C, rinsed thrice with PBS-T, followed by anti-mouse FITC (1:100; DAKO, CA, USA) for 2 h at room temperature in the dark. After rinsing thrice with PBS-T, each 10 min, and re-blocking, cells were incubated with either anti-collagen XII or XIV (1:500; kind gifts from Dr Greg Lunstrum) overnight in a humidified chamber at 4 °C, rinsed as above, followed by anti-rabbit Alexa Fluor 555 (1:100; Molecular Probes) for 2 h at room temperature. Cells were counterstained with Hoechst 33258 (1:200; Molecular Probes), and observed under a Confocal laser scanning microscope (CLSM; Olympus FluoViewTM FV500, Japan; Section 3.14).

3.12. Phalloidin stain

For visualization of cytoskeletal microfilaments, fibrillar actin (*f*-actin) were labelled with phalloidin (A12379 Alexa Fluo 488, Molecular Probes). Samples were fixed in 3.7% (w/v) formaldehyde in cytoskeleton buffer, containing 10 mM MES (pH 6.1), 138 mM KCl, 3 mM MgCl₂, 2 mM EGTA and 0.32 M sucrose, for 30 min at room temperature. After rinsing twice with cytoskeleton buffer for 3 min each time, samples were extracted with 0.1% Triton X-100 in cytoskeleton buffer for 5 min, followed by RNA digestion with 200 µg/ml of RNase A (Sigma) in PBS for 30 min at room temperature. After rinsing twice with PBS for 3 min each time, samples were incubated with 1% BSA in PBS for 30 min to reduce non-specific staining. Incubation with 5 U/ml of phalloidin (1:40) (Molecular Probes) was carried out for 30 – 45 min at room temperature in the dark before rinsing thrice with PBS, 5 min each time. For visualization of nuclei, samples were counterstained with 5 µg/ml of PI (Molecular Probes) for 20 min at room temperature in the dark and rinsed thrice with PBS, 5 min each time. Signals were visualized under Confocal laser scanning microscopy (Section 3.14).

3.13. Von Kossa stain

Cells were fixed in 10% neutral buffered formalin for 30 min at room temperature and rinsed thrice with distilled water. Cells were first immersed in 5% silver nitrate solution for 45 min under strong light and rinsed thrice with distilled water, and then immersed in 5% sodium bicarbonate and 25% formalin for 8 min, followed by rinsing once with distilled water for 10 min. Subsequently, cells were fixed with 5% sodium thiosulphate for 5 min, and rinsed with tap water for 15 min.

Mineralized tissues appear gray-black, whereas osteoid appears bright brown under light microscopy.

3.14. Confocal laser scanning microscopy

Stained samples were mounted with liquid mounting media (DAKO, CA, USA) and viewed under a Confocal laser scanning microscope (CLSM; Olympus FluoView™ FV1000, Japan). Omission of primary antibodies and staining with secondary antibodies alone served as negative controls. To increase signal to noise ratio for weak intensity stains, images were acquired under Kalman filter with averaging from two to three scans. To reduce cross emission in double-labelled samples, images were acquired with sequential scanning. Singly-labelled samples were used as internal controls. Double-labelling images were obtained by superimposing green and red fluorescence. Depth projection images from consecutive 0.5- to 1- μ m-thick optical sections were obtained with Fluoview FV1000 Viewer software (Olympus, Japan).

3.15. Scanning electron microscopy

Samples were fixed with 2.5% glutaraldehyde (Merck, Darmstadt, Germany) in PBS (pH 7.4) at 4 °C for 2 h. After washing thrice in PBS, cells were dehydrated in ascending series of ethyl alcohol (30 %, 50 %, 70%, 90 % and absolute), 5 min each, and dried in 37 °C oven. Specimens were gold-coated with a Fine Coater (BAL-TEC SCP005, MA, USA) at 30 mA for 80 sec, and viewed under magnifications between 100x to 5000x with scanning electron microscopy (SEM; Jeol JSM-5600LV, Tokyo, Japan) with an accelerating voltage between 10-15 kV. Three representative SEM images were obtained for each specimen.

3.16. Statistical analysis

All quantitative results were obtained from at least 3 independent experiments, and expressed as the mean \pm standard deviation. Experimental data were analyzed by Student's t-test and two-way Analysis of Variance (ANOVA). Intergroup differences were determined by post-hoc Tukey test. Differences among samples were considered statistically significant when $p < 0.05$.

4. ESTABLISHMENT OF PRIMARY hPDLF CELL LINES IN VITRO

4.1. Background

Periodontal therapy, which aims to restore the damaged tissues to their original form and function, requires regeneration of the destroyed periodontal connective tissues through the formation of new cementum, new bone and attachment of new connective tissue fibres (Minabe, 1991; Schroeder, 1992; Wikesjo *et al.*, 1992; Garrett, 1996).

Periodontal ligament (PDL) cells are thought to play an important role in promoting periodontal regeneration and alveolar bone homeostasis. In animal studies, it was found that when tooth roots were covered with PDL cells grown in culture and then re-implanted *in vivo*, they acted as progenitor cells and gave rise to the formation of new PDL (Boyko *et al.*, 1981; Van Dijk *et al.*, 1991; Lang *et al.*, 1995, 1998). Further experiments on human PDL cells demonstrated that subpopulation of cells exist which possess osteoblastic characteristics including high alkaline phosphatase (ALP) levels, increased cyclic adenosine monophosphate (cAMP) production in response to parathyroid hormone (PTH) stimulation, the capacity to form mineral-like nodules *in vitro*, and increased bone Gla protein production in response to 1,25(OH)₂ vitamin D₃ (Somerman *et al.*, 1988; Arceo *et al.*, 1991; Liu *et al.*, 1997; Hou *et al.*, 2000). Hence, it is established that the PDL consists of heterogeneous subpopulations of cells that can differentiate into the osteoblastic or cementoblastic lineage, hence taking part in periodontal repair and regeneration.

The sequence of osteoblastic differentiation is believed to comprise three steps: i) proliferation, ii) matrix synthesis and maturation, and iii) mineralization (Lian and Stein, 1992). Procollagen I and osteonectin (ON) are maximally expressed

during proliferation (Stein and Lian, 1993), whereas ALP expression peaks during the post-proliferative period of matrix maturation (Owen *et al.*, 1990; Sodek and Cheifitz, 2000). During skeletal development, osteopontin (OPN) is deposited into the matrix by immature and mature osteoblasts, whereas bone sialoprotein (BSP) level peaks just prior to mineralization (Cowles *et al.*, 1998). These Ca²⁺-binding bone-matrix proteins have proven to be particularly useful osteogenic markers (Sodek and Cheifitz, 2000).

In order for hPDLF to be used for periodontal regeneration, the most important requirement is that the osteogenic potential of PDLF must be retained *in vitro*. Therefore, it was hypothesized that primary hPDLF cell line established by explant culture up to passage 3-5 retained sufficient progenitor cells with osteogenic potential. To establish a reliable source of hPDLF cell line as a first step in tissue engineering of the PDL, we investigated the synthesis of ON which indicates that the cells are at the proliferation phase, of ALP and OPN which indicates the matrix maturation phase, and of BSP which indicates an initiation of matrix mineralization *in vitro*.

4.2. Materials and methods

4.2.1. Isolation of explants

Periodontal ligament and alveolar bone tissues were harvested (Chou *et al.*, 2002) from clinically healthy premolar or upper third molar of human patients undergoing orthodontic or routine extraction after informed consent was obtained according to the ethical guidelines of the Helsinki II declaration (52nd World Medical Association General Assembly, 2000) and approved by the National University of Singapore Institutional Review Board (NUS-IRB No. 036). Impacted, non-functional or broken teeth were excluded in the selection criteria. Explant database was

established according to guidelines stated (Freshney, 2000). Information such as tooth number, age, gender, reason for extraction, were documented strictly for research purposes and kept confidential, according to ethical guidelines.

Extracted teeth were rinsed extensively with sterile Dulbecco's Phosphate Buffered Saline (PBS) (137 mM NaCl, 3 mM KCl, 10 mM Na₂HPO₄, 2 mM KH₂PO₄ [pH 7.4]) containing 2% penicillin-streptomycin solution (100 IU/ml and 100 µg/ml) to wash off blood. Next, they were rinsed extensively in biopsy media: Dulbecco's Modified Eagle's Medium (DMEM; Gibco, Life Technologies, NY, USA) with glucose (4,500 mg/l), 2% penicillin-streptomycin (Invitrogen Corp., CA, USA), 250 µg/ml gentamicin sulfate (Sigma, WI, USA) and 2.5µg/ml amphotericin B (Gibco, Life Technologies, NY, USA).

PDL explants were obtained by scraping the middle third of the root surface using a sterile surgical blade as reported previously. Care was exercised to avoid contamination from gingival or periapical granulation tissues. PDL explants were teased into 1-2 mm³ fragments in 100-mm tissue culture dishes (TPP, MO, USA), wetted by several drops of culture medium, and weighed down by sterilised glass slides. They were then cultured in PDL biopsy culture medium: DMEM (Gibco, Life Technologies, NY, USA) with glucose (4,500 mg/l), 10% (v/v) foetal bovine serum (FBS; Gibco, Life Technologies, NY, USA), 2% penicillin-streptomycin (Invitrogen Corp., CA, USA) and 2.5µg/ml amphotericin B (Invitrogen Corp., CA, USA) at 37 °C and 5% CO₂ in a humidified environment, as previously described (Somerman *et al.*, 1988).

Alveolar bone explants attached to the root surface were removed by a sterile surgical blade and isolated as positive control. The resulting bone chips were fully scraped to remove any attached connective tissue and briefly sterilized by immersion

in 70% ethanol. They were then diced into small cubes of 1-2 mm³ and cultured in T-75 flasks (TPP, MO, USA) in bone biopsy culture medium: Medium-199 (Gibco, Life Technologies, NY, USA) containing 10% (v/v) FBS, 2% penicillin-streptomycin and 2.5 µg/ml amphotericin B at 37 °C and 5% CO₂ in a humidified environment.

4.2.2. Cell expansion and cryopreservation

Explants were monitored regularly for cell outgrowth under phase contrast light microscope (PCLM; Olympus, IX70, Tokyo, Japan). When cell confluency was reached, explants and cells were lifted from tissue culture dishes or flasks by 0.25% (v/w) trypsin and 0.2 g/L EDTA in Hank's Balanced Salt Buffer (HBSS; HyClone, UT, USA), centrifuged at 1000 rpm at 4 °C for 5 min, and resuspended in regular culture medium. PDL fibroblasts (PDLF) were cultured in DMEM containing 4500 mg/l glucose, 10% (v/v) FBS and 2% penicillin-streptomycin, whereas alveolar osteoblasts (AO) in Medium-199 containing 10% (v/v) FBS and 2% penicillin-streptomycin. Cells were replated in T-75 flasks (TPP, MO, USA) for expansion in 1:3 split ratio till passage 2 and cryopreserved for subsequent experiments.

For cryopreservation, trypsinized cells between 1 x 10⁶ to 2 x 10⁶ were pelleted and resuspended in 900 µl fresh culture medium containing 40% (v/v) FBS and mixed with 100 µl of dimethyl sulphoxide (DMSO; Sigma, MI, USA) to a final concentration of 10% (v/v) in each cryovial (Nalge Nunc Intl., NY, USA). Cryovials in Cryo 1 °C Freezing Container (Nalge Nunc Intl., NY, USA) containing isopropanol were placed into -80 °C freezer. Cryopreserved cells were transferred to a liquid nitrogen tank within 24 h for storage in the liquid phase. Cells were thawed in a 37 °C water bath with gentle agitation for about 2 min, and at least 10-fold volume of fresh culture medium was added, drop by drop initially, to thawed cell suspensions in a T-

75 flask (TPP, MO, USA), such that DMSO level was not more than 1% (v/v). Medium was changed after overnight incubation.

4.2.3. Osteogenic induction

Primary cultures of hPDLF and hAO between passage 3 to 5 were seeded at a density of 20,000 cells/cm² in six-well plates (TPP, MO, USA). hPDLF were cultured in DMEM (Gibco, Life Technologies, NY, USA) containing 10% FBS and 2% penicillin-streptomycin, whereas human alveolar osteoblasts (hAO) and human calvarial osteoblasts (hCO) were cultured in Medium 199 (Gibco, Life Technologies, NY, USA) containing the same. Osteogenic differentiation ($n=3$) was initiated one day after seeding on one half of randomly selected cultures by supplementation with 200 μ M L-ascorbic acid 2-phosphate magnesium (Asc; Sigma, WI, USA), 10mM β -glycerophosphate (β -GP; Sigma, WI, USA) and 100 nM dexamethasone (Dex; Sigma, WI, USA). Three ml of mineralizing culture medium was added per well, and medium change was performed every 2 to 3 days.

4.3. Results

4.3.1. Establishment of hPDLF and hAO cell lines

Representative images of explants showed that cellular outgrowth was observed after 7 days in culture (Fig. 4.1). Confluent cultures were obtained by day 21. The outgrowth varied between cell lines, depending upon the quantity and size of explants. Cells that migrated from hPDL explants, termed hPDL fibroblasts (hPDLF), appeared spindle-shaped and were uniformly orientated in subsequent passage. Cells that migrated from human alveolar bone chips, termed human alveolar osteoblasts (hAO), appeared more polygonal with varying cell orientations. hPDLF and hAO

demonstrated population doubling time between 2-3 days (not shown). Cells from different individuals were expanded as individual primary cell lines and numbered according to the sequence of tissue harvest. Cell morphology and viability were monitored at every passage.

4.3.2. hPDLF cell line demonstrated ALP induction

Dexamethasone, a member of the glucocorticoid class of hormones, promotes development of the osteoblast phenotype by selectively modulating expression of genes associated with cell growth and differentiation (Shalhoub *et al.*, 1992). A physiological concentration of Dex at 10 nM (Probst and Jungermann, 1983) is most commonly used in traditional bone (Wong *et al.*, 1990 and references within) and hAO cultures (Fernandes *et al.*, 1997; Costa and Fernandes, 2000; Perinpanayagam *et al.*, 2006). As for hPDLF, varying dosages of Dex – 10 nM (Lekic *et al.*, 2001; Ohno *et al.*, 2002), 100 nM (Arceo *et al.*, 1991; Liu *et al.*, 1997; Hou *et al.*, 2000), 500 nM (Matsuda *et al.*, 1993), 5 μ M (Ramakrishnan *et al.*, 1995) – have been supplemented for osteogenic differentiation. Yet, the effects of Dex dosage on ALP activities of hPDLF have not been reported.

In order to investigate the effects of dexamethasone on ALP activity, increasing levels of Dex at 1 nM, 10 nM and 100 nM were supplemented to hPDLF and hAO under mineralizing culture over 28 days. Representative data from ALP enzymatic assay showed that ALP activity increased significantly under Dex supplementation between day 7 to day 21 in hPDLF, followed by a decline to near starting levels at day 28 (Fig. 4.2A). ALP level peaked at day 14 under 100 nM Dex, and on day 21 for both 10 nM and 1 nM Dex. In hAO, ALP activity increased significantly under Dex supplementation at all time points, with the greatest

upregulation at day 28 (Fig. 4.2B). A dose-dependent effect was observed for hAO on day 14 and day 21, but not for hPDLF even upon repeated assays on two other cell lines (not shown).

Subsequently, 100 nM Dex was chosen on the basis of the greatest ALP upregulatory effect, and supplemented to hPDLF derived from ten individuals, four males and six females, aged 13-56 yr (25 ± 11 , mean \pm SD), under mineralizing culture. Corresponding hAO from three individuals within the sample pool were used for comparison. ALP level of each cell line was represented individually (Fig. 4.3A, B). In the absence of Dex, ALP activities of hPDLF ranged typically between 0.05 to 0.5 IU/mg protein. There was minimal induction at day 14 (Fig. 4.3A). In the presence of Dex however, ALP was characterized by a sharp rise in activity up to 2.5 IU/mg protein followed by a decline, indicative of matrix maturation between day 14 and day 21 (Owen *et al.*, 1990; Sodek and Cheifitz, 2000). Upregulation was observed at day 14 in half of the hPDLF cell lines. Among the remaining half, two cell lines showed a delayed increase at day 21, two did not demonstrate any increase, and one exhibited an anomalous pattern of ALP showing a steep decline (Fig. 4.3B). As for hAO, ALP activities ranged between 0.1 to 0.3 IU/mg protein, with no apparent upregulation (Fig. 4.3C). In the presence of Dex, ALP was induced at day 21, reaching an activity of 1.7 IU/mg protein (Fig. 4.3D).

To visualize ALP expression, hPDLF and hAO cell lines were stained for ALP enzymatic activity at day 14, corresponding to the time of upregulation (Appendix). Representative images showed that hPDLF was moderately stained for ALP under phase contrast light microscopy with occasional highly stained cells under normal culture (Fig. 4.4A). Under mineralizing culture, hPDLF demonstrated intense staining, localized at proliferating cell clusters (Fig. 4.4B), which were potential sites

of mineral-like nodule formation (Cho *et al.*, 1992). hAO was lightly stained for ALP, and appeared polygonal under normal culture condition (Fig. 4.4C). Under mineralizing condition, hAO exhibited intensely-stained cells of varying morphology (Fig. 4.4D).

4.3.3. hPDLF cell line demonstrated matrix maturation

To confirm the extent of matrix maturation, expression of ON, OPN and BSP was assayed at day 7, 14 and 21 as a measure of phenotypic differentiation (Knabe *et al.*, 2004). Western blot against whole cell lysates of paired hPDLF and hAO, derived from three individuals numbered 37, 40, 47 (Fig. 4.3), were performed in 12% gel. Each lane was normalized to total protein. ON was detected as a prominent ~38-kDa protein (Fig. 4.5A), as previously described in hPDLF (Ramakrishnan *et al.*, 1995). OPN, synthesized as 44-kDa and 55-kDa isoforms in osteoblasts (Kasugai *et al.*, 1991; Nagata *et al.*, 1991), was detected as a single ~44-kDa protein in whole cell lysates of hPDLF and hAO at day 7 in 12% gel (Fig. 4.5B), in accordance with results obtained with EDTA-extracts of ECM during osteogenic differentiation (Kasugai *et al.*, 1992). BSP, with an apparent M_r of 60-80 K on SDS-PAGE (Fisher *et al.*, 1987), was detected as ~60-kDa and ~80-kDa proteins in hPDLF and hAO from day 14 onwards (Fig. 4.5C).

Chemiluminescence signals of Western blot for three individuals were summarized in Table 4.1. Signals were graded as follows: -, negative signal; +/-, weak to undetectable signal; +, moderate signal; ++, intense signal. Synthesis of ON was increased in hAO and marginally in hPDLF under mineralizing culture at day 7 and day 14, with some degrees of downregulation at day 21. An increase followed by a decrease in expression of ON was in agreement to its role in directing extracellular

matrix remodeling (Kelm *et al.*, 1994) during the proliferative phase. OPN synthesis was increased in hAO and hPDLF under mineralizing culture at day 14 and day 21. The concomitant elevation of ALP and OPN levels at day 14 was indicative of matrix maturation under the influence of Dex (Owen *et al.*, 1990; Sodek and Cheifitz, 2000). An increase in BSP synthesis was observed in hAO under mineralizing culture at day 21, hypothetically leading to the mineralization phase of osteoblastic differentiation (Cowles *et al.*, 1998).

4.3.4. hPDLF cell line demonstrate mineral-like tissue formation

Multi-layered nodules were observed under mineralizing culture at day 21. Four distinct stages based on morphology under phase contrast light microscopy were identified during nodule formation (Fig. 4.6), as previously reported (Ramakrishnan *et al.*, 1995). hPDLF maintained its spindle-shaped morphology upon reaching confluency at day 7 (stage I; Fig. 4.6A), proliferated to form cell clusters (arrow) at day 14 (stage II; Fig. 4.6B), and generated multi-layered nodules (arrowhead) at day 21 (stage III; Fig. 4.6C). hAO demonstrated a similar progression, evidenced by confluency at stage I (Fig. 4.6D), cell clustering and production of ECM at stage II (Fig. 4.6E), and formation of nodules containing refringent material at cell clusters at stage III (Fig. 4.6F).

To assess the extent of mineral-like matrix formation, hPDLF and hAO cell lines from the ten individuals were cultured in the presence of 100 nM Dex up to day 28. In hPDLF, two patterns of mineral-like matrix formation were observed as previously reported (Liu *et al.*, 1997; Declercq *et al.*, 2005). The first was “diffuse” type, characterized by flat and randomly dispersed foci (Fig. 4.7A). The second was “nodular” type, characterized by three-dimensional nodule formation associated with

regions of cell and matrix condensation (Fig. 4.7B). In hAO, varying degrees of “nodular” mineral-like tissue were observed, with highly mineralized foci observed for hAO47 (Table 4.2, Fig. 4.7C). The presence of minerals was verified by von Kossa staining that distinguishes calcium as inorganic phosphate (Lillie and Fullmer, 1976). The morphology and extent of mineral-like tissue formation were documented for each cell line (Appendix). Amorphous brown-black precipitates overlying bright brown spots were detected under phase contrast light microscopy, indicative of mineral-like nodules and osteoids, respectively (Fig. 4.7D-F). Under no circumstance was positive von Kossa reaction obtained for control cultures (not shown).

Ten hPDLF and three corresponding hAO cell lines were categorized according to the extent and pattern of mineral-like nodule formation (Liu *et al.*, 1997; Declercq *et al.*, 2005). Von Kossa reaction was graded as follows: -, negative staining; -/+, weak to undetectable staining; +, moderate staining; ++, intense staining (Appendix, Table 4.2). In hPDLF, five out of 10 cell lines were moderately- and intensely-stained by von Kossa, consisting of “diffuse” and “nodular” types. Three cell lines were partially- or weakly-stained, demonstrating bright brown spots characteristic of osteoids. The remaining two cell lines did not show any signal. In hAO, two out of three cell lines exhibited positive von Kossa reaction in the form of “nodular” type foci, while the remaining one cell line demonstrated weak staining with osteoids stained bright brown.

To test whether there was a correlation between ALP activity and mineral-like nodule formation, ALP levels were plotted against von Kossa reaction (Fig. 4.8). Negative von Kossa staining was correlated with a low ALP activity of less than 0.5 IU/mg protein at day 21. Weak to partial staining was correlated with an intermediate ALP activity of up to 1.0 IU/mg protein. With the exception of hPDLF48 which

exhibited an early onset of mineralization (Fig. 4.3B, Table 4.2), the appearance of moderate to intense von Kossa staining was correlated with a high ALP activity of at least 1.0 IU/mg protein at day 21. When ALP activities at day 7 and 14 were plotted against von Kossa reaction, positive correlations were not seen (not shown).

4.5. Discussion

4.5.1. Characterization of hPDLF and hAO cell lines

hPDLF cell line was successfully established from approximately 80% of harvested tissue by explant culture. Similarly, hAO cell line was established by explantation culture, as cited (Fernandes *et al.*, 1997; Nefussi *et al.*, 1998; Costa and Fernandes, 2000; Perinpanayagam *et al.*, 2006). It has been shown previously that PDL explantation technique produced a mixture of fibroblast-like and epithelial cells derived from the epithelial rests of Malassez (ERM), whereas trypsinization of teeth yielded exclusively fibroblast-like cells (Brunette *et al.*, 1976; Blomlof and Otteskog, 1981). Initial experiments with trypsinization resulted in individual cells and tissue debris in suspension which did not attach (not shown). This was similar to earlier findings which reported very poor plating efficiency (0.024%) from trypsinized PDL cells (Brunette *et al.*, 1976). Moreover, fibroblast-like cells readily outgrow epithelial cells and dominate in primary culture (Ragnarsson *et al.*, 1985). With serial passaging, the eventual hPDL cell population was predominantly fibroblastic.

The osteogenic potential of hPDLF cell line obtained was evaluated in terms of ALP activity (Lomri *et al.*, 1988) after Dex (from 1 nM to 100 nM) supplementation. This was performed in comparison with hAO for two reasons. Firstly, patient-to-patient variation can be circumvented by obtaining hAO cell line from the same individual. Secondly, hAO is developmentally related to hPDLF as the

PDL and alveolar bone are both derived from the ectomesenchyme (Ten Cate, 1997; Cho and Garant, 2000), whereas skeletal bone, for example, is derived from the mesoderm (Reddi, 1981; Olsen *et al.*, 2000). When increasing levels of Dex between 1 nM to 100 nM were supplemented under mineralizing culture, Dex resulted in a dose-dependent response in hAO (Fig. 4.2B), in agreement with previous findings in osteoblast-like cells (Majeska *et al.*, 1985; Green *et al.*, 1990; Namkung-Matthai *et al.*, 1998). However, this was not observed for hPDLF (Fig. 4.2A). A recent publication at the time of writing reported a dose-dependent response under serum-free conditions in hPDLF (Hayami *et al.*, 2007). Hence, it was speculated that the above discrepancy was due to the compounding effects of serum factors such as cytokines (Hayami *et al.*, 2007) and the intrinsic heterogeneity (i.e. mixture of osteoprogenitors and fibroblasts) of hPDLF (Lekic *et al.*, 1997; Phipps *et al.*, 1997).

Protein synthesis of ON, OPN and BSP, representing proliferative, maturation and mineralization phases respectively, was studied by Western blot analysis for three pairs of hPDLF and hAO cell lines derived from the same individual (Fig. 4.5) and summarized in Table 4.1. High levels of ON mRNA and protein are associated with developing bones and teeth (Mundlos *et al.*, 1992), and with cementum and bone during periodontal healing and remodeling (Takano-Yamamoto *et al.*, 1994; Matsuura *et al.*, 1995). Expression of ON exhibits a specific induction by Dex in hAO obtained in this study (Fig. 4.5A, Table 4.1), but was less overt in hPDLF, paralleled by results obtained with bone marrow stromal cells which consist of heterogeneous mixture of cell lineages including osteoblastic cells (Cheng *et al.*, 1994). Synthesis of OPN was increased under mineralizing culture (Fig. 4.5B), as demonstrated for hAO (Xiao *et al.*, 2004) and hPDLF (Chien *et al.*, 1999). Whereas the 55-kDa form predominates in the conditioned medium, the 44-kDa form is associated with the mineralized matrix

(Kasugai *et al.*, 1992). The report of OPN as 61-kDa and 67-kDa forms in rat PDLF medium (Ramakrishnan *et al.*, 1995), is attributed to the anomalous migratory behaviour of OPN on SDS-PAGE of varying acrylamide content (Nagata *et al.*, 1991). Several phenotypes in fetal rat calvarial osteoblasts based on OPN expression were observed: OPN-negative cells enriched in osteogenic precursors, differentiating osteogenic cells that secrete OPN, and migrating stromal cells characterized by perimembranous OPN (Zohar *et al.*, 1997). The expression of OPN under normal culture of hPDLF, shown similarly by Ivanovski *et al.* (2001), could be explained by the fact that proliferating osteogenic cells, including periodontal ligament cells, express intracellular OPN associated with cell migration (Zohar *et al.*, 2000). The increase in BSP synthesis under mineralizing culture has been reported in hAO (Xiao *et al.*, 2004) and hPDLF (Chien *et al.*, 1999). The absence of such an increase in hPDLF in the given timeframe of 21 days could be indicative of a delayed upregulation, as BSP appeared to be produced primarily from day 21 onwards (Fig. 4.5). Whereas BSP was identified as a ~60-kDa protein in osteoblasts (Nagata *et al.*, 1991; Kasugai *et al.*, 1992), it was identified as a ~78-kDa protein in rat PDLF medium (Ramakrishnan *et al.*, 1995). The extensive glycosylation of BSP is the likely source of heterogeneity observed (Ganss *et al.*, 1999). BSP, unique to mineralized tissues, is expressed at high levels coincident with *de novo* formation of bone (Chen *et al.*, 1992) and cementum (MacNeil *et al.*, 1996), but supposedly absent from PDL proper (Matsuura *et al.*, 1995). However, BSP mRNA transcript, though reported absent in PDLF by Northern blot (Nohutcu *et al.*, 1996), was demonstrated by RT-PCR in PDLF under routine culture (Ivanovski *et al.*, 2001). The presence of BSP in Western blot could be attributable to a very low baseline expression of BSP in hPDLF *in vitro*.

Primary hPDLF established by explant culture in this thesis produced BSP as well as the 44-kDa form of OPN under both normal and mineralizing culture. This could be attributable to two sources. Firstly, osteo-progenitors reside perivascularly in the PDL (McCulloch, 1995; Lekic and McCulloch, 1996), and was postulated to be obtained during explant culture (Ragnarsson *et al.*, 1985). Secondly, osteoblast-like cells if present were thought to be derived from cementum. OPN and BSP are expressed by cementoblasts during the early stages of tooth root development, and also on mature fully erupted root surfaces (MacNeil *et al.*, 1995; D'Errico *et al.*, 1997; Sasano *et al.*, 2001).

4.5.2. Analysis of ALP activity and mineralization potential

The most important criterion for the characterization of the osteoblastic phenotype is the ability to form a mineralized collagenous matrix. The primary hPDLF and hAO cell lines established herein retained their ability to initiate mineral-like deposition upon osteogenic induction. Similar to those observed in other bone cell systems (Bellows *et al.*, 1992; Gundle *et al.*, 1995; Stein *et al.*, 1996), mineral-like nodule formation began to occur following maximal ALP activity (Fig. 4.6). This mineral-like formation was unlikely a result of biochemical precipitation of calcium phosphate, due to firstly, the presence of underlying osteoids observed as bright brown spots in the ECM (Fig. 4.7D-F) and secondly, the absence of von Kossa stain in control cultures.

ALP activity was identified in association with osteogenesis and cementogenesis (Groeneveld *et al.*, 1995), in which a localized increase in inorganic phosphate from ALP hydrolysis leads to an initiation of mineralization in the presence of physiological concentrations of Ca^{2+} (Stein *et al.*, 1996) (Fig. 4.9). In cloned

hPDLF populations, it has been found that a propensity to produce mineral-like tissue *in vitro* varied in direct proportion to the level of ALP expression, determined by the percentage of positively stained cells (Liu *et al.*, 1997). In this study, it was further demonstrated that a direct correlation between mineral-like tissue formation and ALP expression, in terms of enzymatic activity, exist in primary hPDLF and hAO cell lines (Fig. 4.8). This correlation was only obtained for ALP activity on day 21, as mineralization occurs in the stationary phase, i.e. day 14 to day 21, following maximal ALP induction in hAO (Fernandes *et al.*, 1997).

The occurrence of “diffuse” and “nodular” mineral-like tissue described in Fig. 4.7 was similarly reported in hPDLF clones (Liu *et al.*, 1997) and rat osteoblastic cells (Declercq *et al.*, 2005), the biological reason behind unknown. “Nodular” type was found in 15% of hPDLF clones (Liu *et al.*, 1997), and rat bone marrow, calvarial and early-passage periosteal derived cells (Declercq *et al.*, 2005). On the other hand, “diffuse” type was found in 85% of hPDLF clones (Liu *et al.*, 1997) and late-passage periosteal derived cells and UMR-106 cells (Declercq *et al.*, 2005). In this study, only five out of the ten hPDLF cell lines examined yielded adequate mineral-like tissues to be categorized; it is premature to arrive at a statistically significant representation of mineral-like tissue pattern in hPDLF. It is therefore worthwhile to expand the sample size in future studies, and to adopt a variety of biophysical techniques such as transmission electron microscopy and X-ray microanalysis to determine the ultrastructural morphology of the mineral-like tissue and the composition of calcium and phosphorus within.

4.5.3. Patient-to-patient variation

Thus far, it is evident that primary hPDLF cell line established in this study possessed osteogenic potential. However, a distinct cell line-to-cell line variation could be seen in terms of ALP activity (Fig 4.3), synthesis of bone-matrix proteins (Fig. 4.5), and mineral-like tissue formation (Table 4.2). This could be a result of extrinsic factors such as serial passaging as described by Fernandes *et al.* (1997), and/or intrinsic biological differences amongst patients as described by Arceo *et al.* (1991), Carnes *et al.* (1997) and Ivanovski *et al.* (2001).

It was reported that subcultured osteoblasts remained competent to express the developmental sequence during osteoblastic differentiation, but a lengthening of the time course was observed (Owen *et al.*, 1990). Specifically, the effect of Dex on ALP activity is dependent on the differentiation status of the cells (Stein *et al.*, 1996). For instance, hAO at passage 1 achieved maximal ALP level between day 14 to day 18, after which ALP activity dropped significantly (Costa and Fernandes, 2000; Fernandes *et al.*, 1997). At passage 4 onwards, hAO exhibited a delayed ALP induction at day 21, with a concomitant decrease in enzyme activity and mineralization potential (Fernandes *et al.*, 1997). Indeed, the basal ALP activity of hAO cell line between passage 3 to 5 in this study at 0.08 to 0.32 IU/mg protein (Fig. 4.3C) was lower than the reported level of 1.4 ± 0.2 IU/mg protein in early passages of mouse trabecular osteoblasts (Lomri *et al.*, 1988).

However, the same was not observed for hPDLF cell line. The basal ALP activity of hPDLF at 0.05 to 0.66 IU/mg protein (Fig. 4.3A) was within the reported range (Carnes *et al.*, 1997). Moreover, ALP upregulation for the majority of the hPDLF cell lines was not delayed (Fig. 4.3B). Furthermore, a strong correlation in osteogenic potential between paired hPDLF and AO cell lines from the same

individual was obtained. For example, hPDLF/hAO40 showed low, hPDLF/hAO37 moderate, and hPDLF/hAO47 high osteogenic potential as seen from the various criteria examined. Hence, while hAO cell line appeared to be sensitive to a loss of phenotypic differentiation from serial passaging, a delay and/or reduction in osteogenic potential in some hPDLF and hAO cell lines were not solely due to passaging effects, but also intrinsic biological differences.

In summary, this work demonstrated the feasibility of establishing hPDLF and hAO cell lines *in vitro*, and highlighted the importance of characterization in establishing the potential application of these cells in periodontal regeneration for successful clinical outcome. Following this initial establishment of primary hPDLF and hAO cell lines, characterization hAO was undertaken separately and in greater detail by another Ph.D. student in the laboratory (Zhou, 2006).

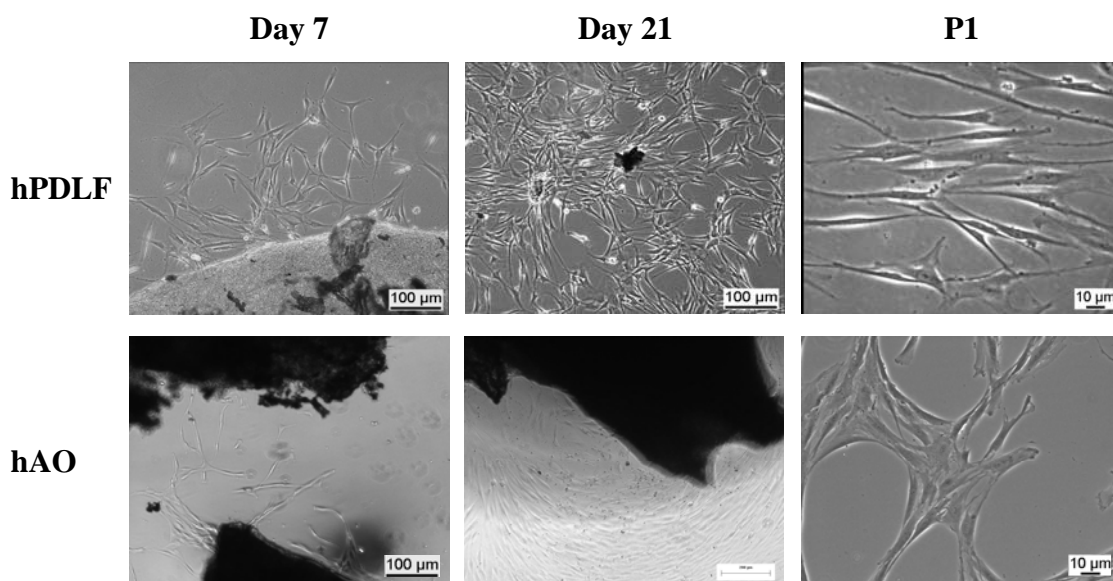


Figure 4.1. Representative images of cellular outgrowth and morphology of hPDLF and hAO. Cellular outgrowth was observed after 7 days in culture, and confluent cultures were obtained at day 21. hPDLF at passage 1 (P1) appeared spindle-shaped. hAO at P1 appeared more polygonal. Cells from different patients were expanded as individual cell lines, numbered according to sequence of tissue harvest.

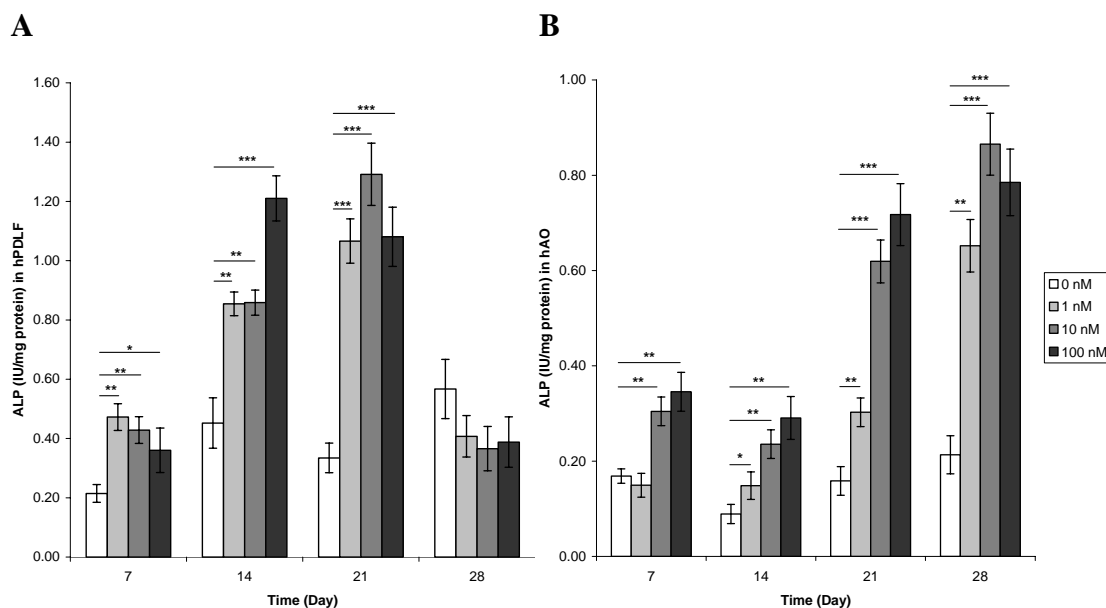


Figure 4.2. Effects of dexamethasone (Dex) on the alkaline phosphatase (ALP) activities of hPDLF and hAO. Representative data from ALP enzymatic assay ($n=3$) when increasing concentrations of Dex ranging from 1 nM to 100 nM were supplemented to (A) hPDLF and (B) hAO under mineralizing culture over 28 days. (A) ALP activity increased significantly under Dex supplementation between day 7 to day 21 in hPDLF, with the earliest peaked upregulation at day 14 by 100 nM Dex, followed by a decline at day 28. (B) ALP activity increased significantly under Dex supplementation in hAO at all time points, with the greatest upregulation at day 28. A dose-dependent effect was observed for hAO on day 14 and day 21. Values were expressed as means \pm SD. * $P < 0.05$; ** $P < 0.01$; *** $P < 0.001$.

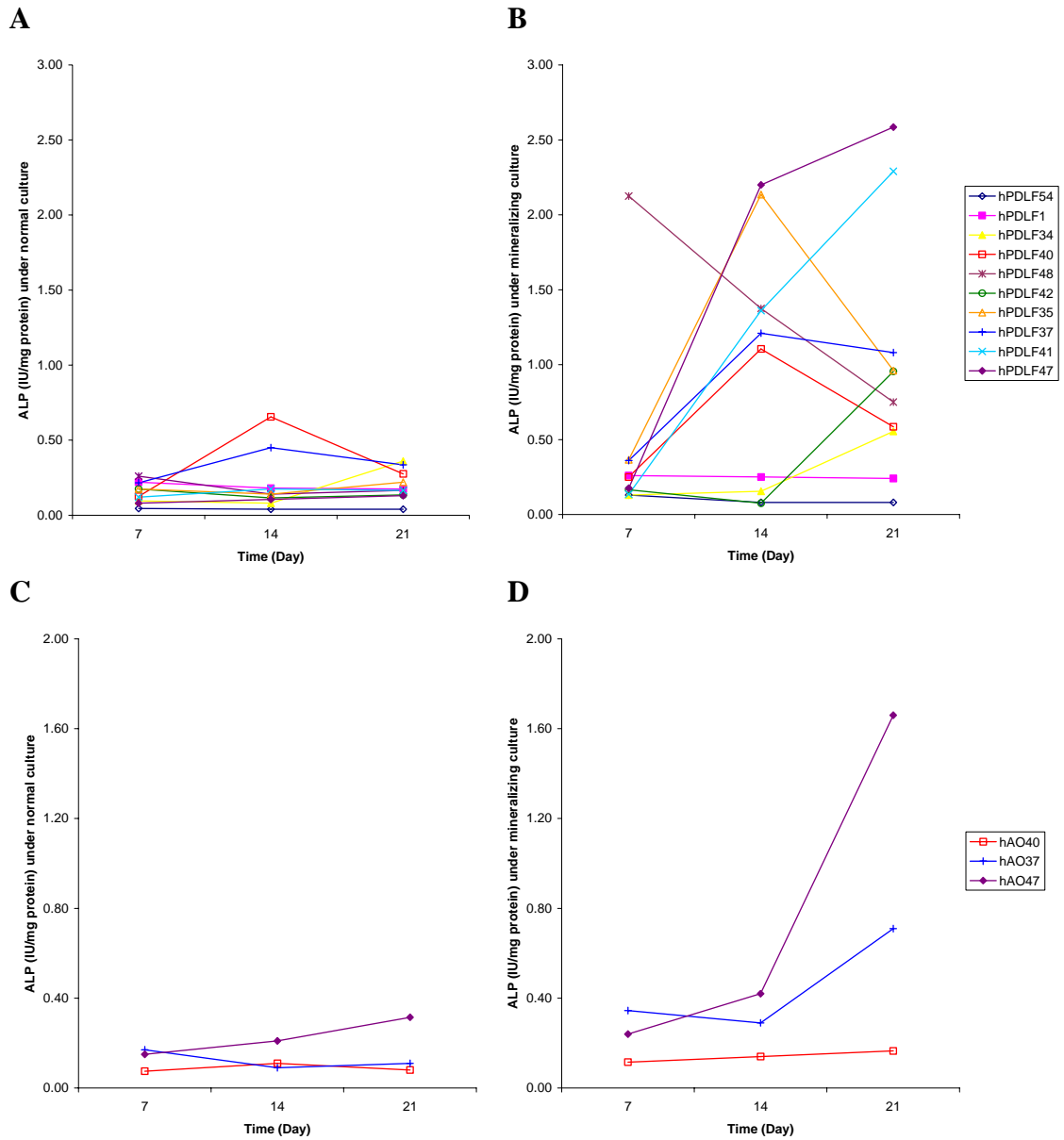


Figure 4.3. ALP activities of hPDLF and hAO cultured in the absence and presence of 100 nM Dex. Subsequently, 100 nM Dex was supplemented to hPDLF ($n=3$) derived from ten individuals, four males and six females, aged 13-56 yr (25 ± 11 , mean \pm SD) under mineralizing culture. Corresponding hAO ($n=3$) from three individuals were used for comparison. (A) In the absence of Dex, there was minimal ALP induction in hPDLF. (B) In the presence of Dex however, ALP was strongly upregulated at day 14 and day 21 in half and one-fifth of the hPDLF cell lines, respectively. As for hAO, (C) there was minimal induction in the absence of Dex, in contrast to a delayed increase at day 21 in two of the three hAO cell lines in the presence of Dex.

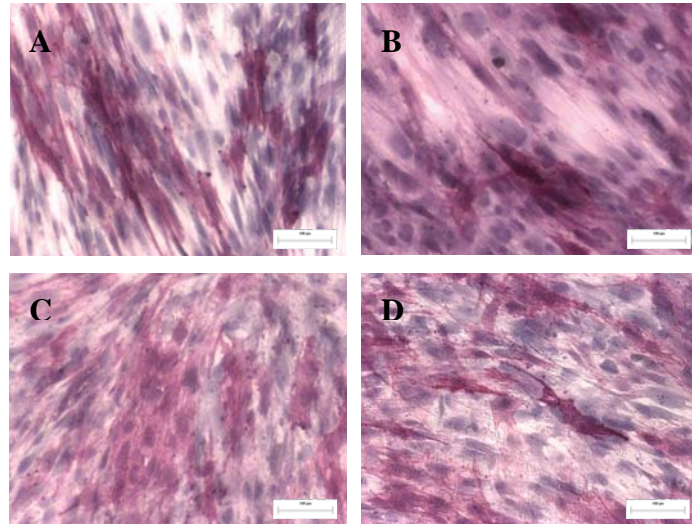


Figure 4.4. Representative images of (A-B) hPDLF and (C-D) hAO after staining for ALP under normal and mineralizing cultures, respectively. (A) hPDLF was moderately stained for ALP with occasional highly stained cells under normal culture. (B) Under mineralizing conditions, hPDLF demonstrated intense staining, localized at cell clusters. (C) hAO was lightly stained for ALP, and appeared polygonal under normal culture. (D) Under mineralizing culture, hAO exhibited intensely-stained cells of varying morphology.

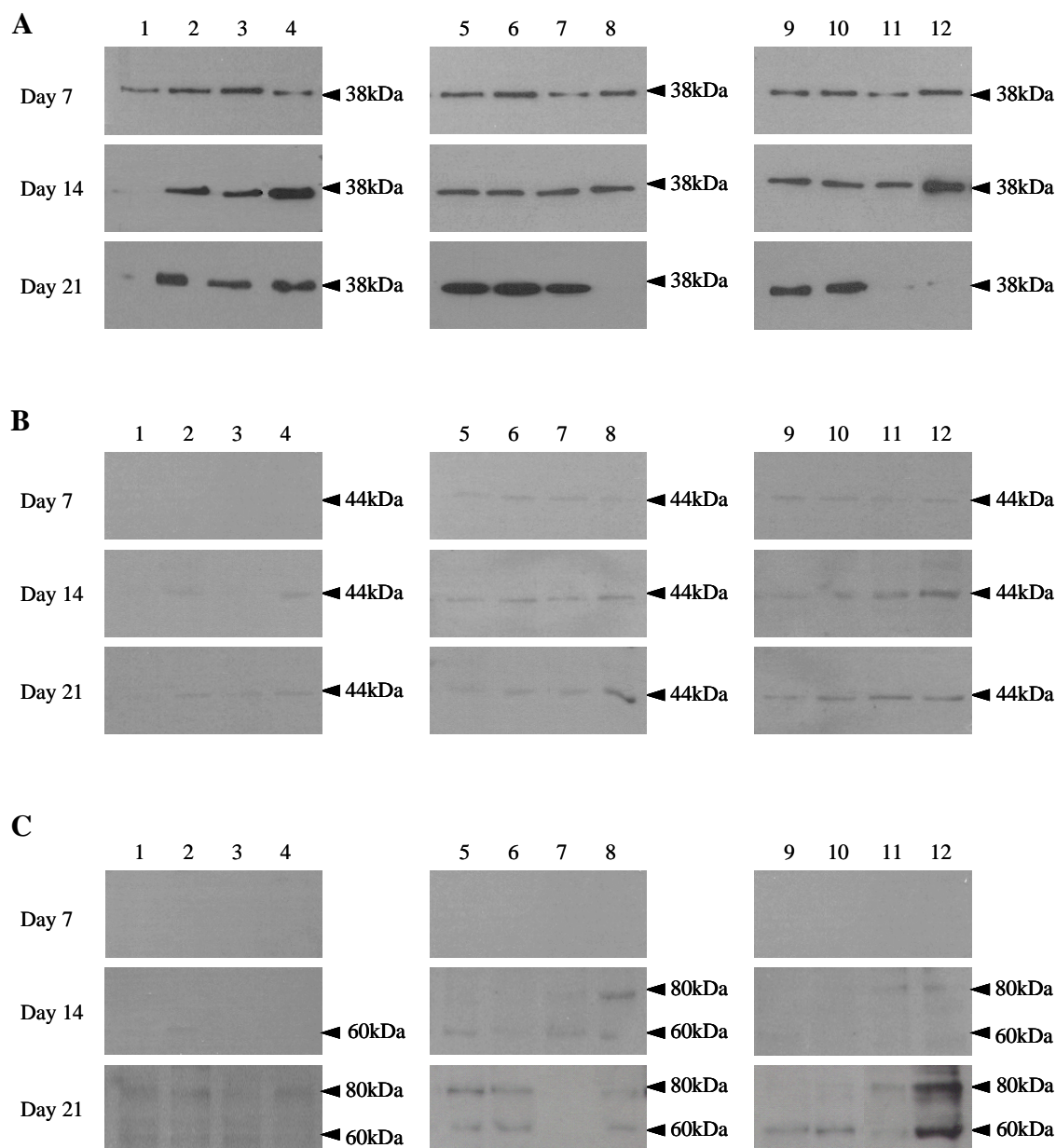


Figure 4.5. Western blot analysis of (A) osteonectin (ON), (B) osteopontin (OPN) and (C) bone sialoprotein (BSP) in whole cell lysates of paired hPDLF and hAO, derived from three individuals, under normal and mineralizing culture. Sample loading in each lane was normalized to total protein. ON was detected as a prominent ~38-kDa protein. OPN was detected as a single ~44-kDa protein at day 7. BSP was detected as ~60-kDa and ~80-kDa proteins in PDLF and hAO from day 14 onwards. Lane 1, hPDLF40 -Dex; lane 2, hPDLF40 +Dex; Lane 3, hAO40 -Dex; lane 4, hAO40 +Dex; Lane 5, hPDLF37 -Dex; lane 6, hPDLF37 +Dex; Lane 7, hAO37 -Dex; lane 8, hAO37 +Dex; Lane 9, hPDLF47 -Dex; lane 10, hPDLF47 +Dex; Lane 11, hAO47 -Dex; lane 12, hAO47 +Dex.

ON	hPDLF -Dex	hPDLF +Dex	hAO -Dex	hAO +Dex
Day 7	+	+	+	+
Day 14	-/+	+	+	+/>++
Day 21	-/>+++	+/>+++	-/+	-/>+++

OPN	hPDLF -Dex	hPDLF +Dex	hAO -Dex	hAO +Dex
Day 7	-/+	-/+	-/+	-/+
Day 14	-/+	+	-/+	+/>+++
Day 21	-/+	+	-/+	+/>+++

BSP	hPDLF -Dex	hPDLF +Dex	hAO -Dex	hAO +Dex
Day 7	-	-	-	-
Day 14	-/+	-/+	-/+	-/+
Day 21	+	+	-/+	+/>+++

Table 4.1. Summary of western blot results (Fig. 4.5) of osteonectin (ON), osteopontin (OPN) and bone sialoprotein (BSP) synthesis by paired hPDLF and hAO, derived from three individuals, under normal and mineralizing culture. Synthesis of ON was increased in hAO and marginally in hPDLF under mineralizing culture at day 7 and day 14. Levels of ON at day 21 was variable, with some degrees of downregulation. OPN synthesis was increased in hAO and hPDLF under mineralizing culture at day 14 and day 21. An increase in BSP synthesis was observed in hAO under mineralizing culture at day 21. Western blot signal was graded as follows: -, negative signal; -/+, weak to undetectable signal; +, moderate signal; +/+, intense signal.

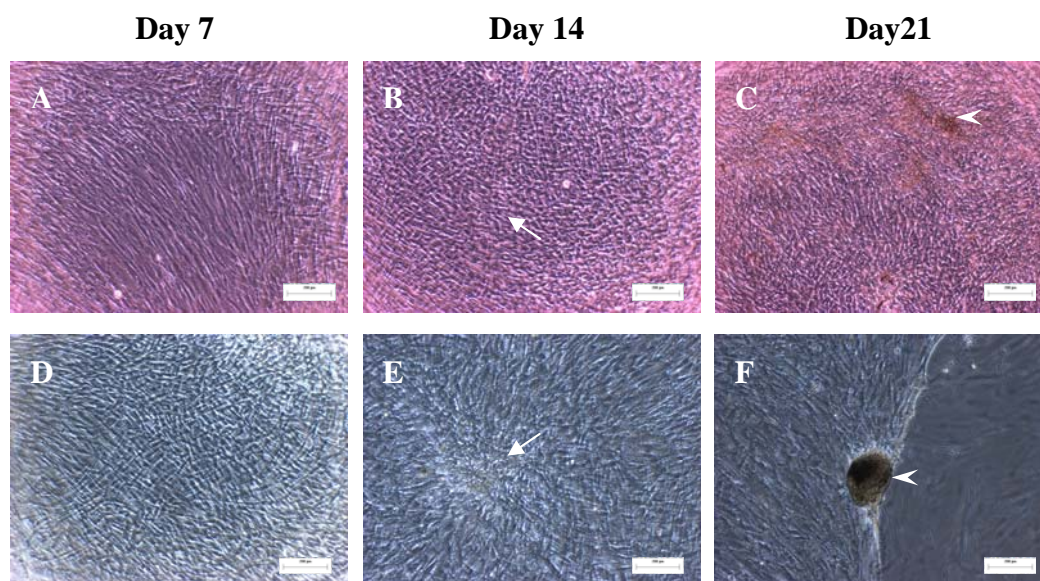


Figure 4.6. Representative morphology of hPDLF (A-C) and hAO (D-F) at stage I, II and III of nodule formation, respectively. hPDLF (A) appeared spindle-shaped at stage I, (B) proliferated to form cell clusters (arrow) at stage II, and (C) generated multi-layered nodules (arrowhead) at stage III. hAO (D) reached confluency at stage I, (E) produced ECM at cell clusters at stage II, and (F) formed nodules containing refringent material at cell clusters at stage III.

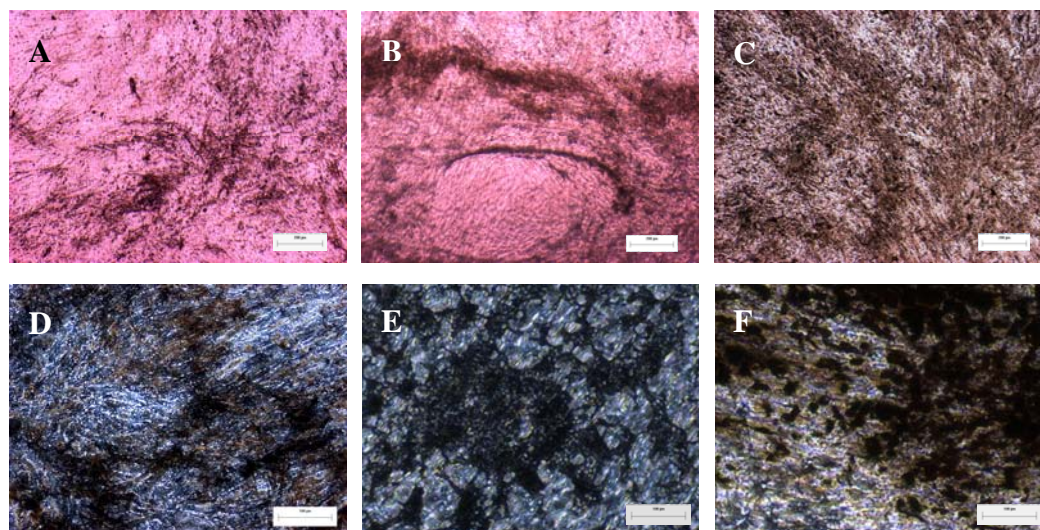


Figure 4.7. Mineral-like tissue formation in hPDLF and hAO under mineralizing culture, as observed (A-C) before and (D-F) after von Kossa staining at day 28. hPDLF gave rise to two patterns of mineral-like tissue formation, namely (A) diffuse type, characterized by flat and randomly dispersed foci, and (B) nodular type, characterized by three-dimensional nodule formation at regions of cell and matrix condensation, the latter of which was observed in (C) hAO. (D-F) Amorphous brown-black precipitates overlying bright brown spots were observed under von Kossa staining, indicative of mineral-like nodules and osteoids, respectively.

Source	Gender	Age	Tooth	Von Kossa stain	Type / Comments
hPDLF54	F	22	Third molar	-	NA
hPDLF1	F	56	Third molar	-	NA
hPDLF34	F	25	Third molar	-/+	NA, osteoid
hPDLF40	M	20	Third molar	-/+	NA, osteoid
hPDLF42	M	25	Third molar	-/+	NA, osteoid
hPDLF35	F	13	Premolar	+	Diffuse
hPDLF37	M	21	Third molar	+	Diffuse
hPDLF41	M	20	Third molar	+	Diffuse
hPDLF48	F	23	Third molar	++	Nodular, early mineralization
hPDLF47	F	23	Third molar	++	Nodular
hAO40	M	20	Third molar	-/+	NA, osteoid
hAO37	M	21	Third molar	+	Nodular
hAO47	F	23	Third molar	++	Nodular

Table 4.2. Biodata of donors, categorized by the pattern of mineral-like nodule formation at day 28 in hPDLF and hAO. In hPDLF, five out of 10 cell lines were moderately- and intensely-stained by von Kossa. Three were partially- or weakly-stained, demonstrating bright brown spots. The remaining two did not show any signal. In hAO, two out of three cell lines exhibited positive von Kossa reaction in the form of mineral-like foci, while the remaining one cell line demonstrated weak staining and bright brown spots. Von Kossa reaction was graded as follows: -, negative staining; -/+, weak to undetectable staining; +, moderate staining; ++, intense staining.

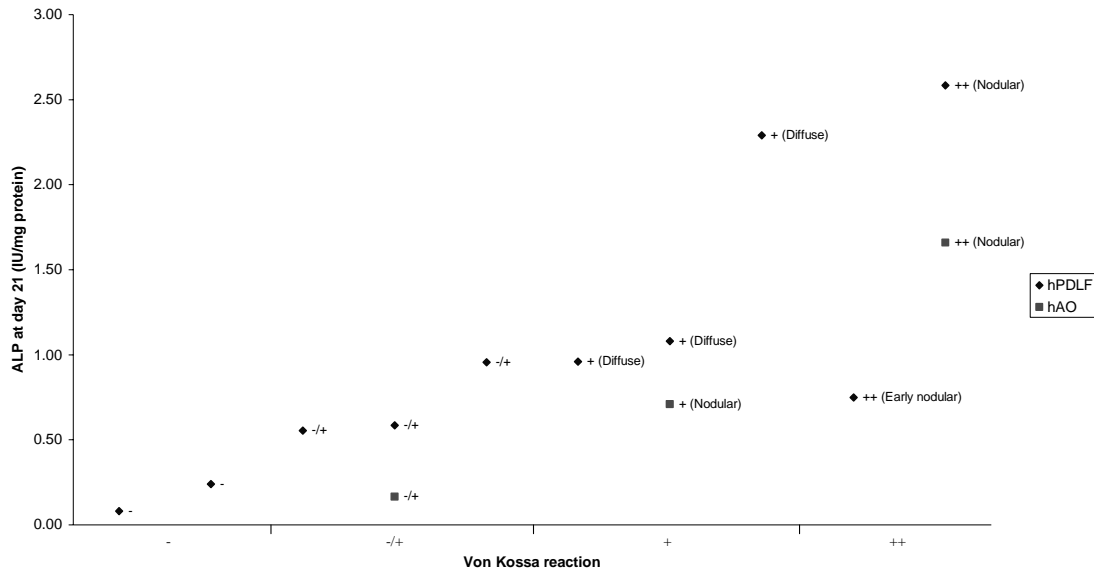


Figure 4.8. Correlation between ALP activity and mineral-like nodule formation in hPDLF and hAO. ALP activities at day 21 were plotted against von Kossa reaction (Table 4.2). Negative staining was correlated with a low ALP activity of less than 0.5 IU/mg protein. Weak to partial staining was correlated with an intermediate ALP activity of up to 1.0 IU/mg protein. With the exception of hPDLF48 which exhibited an early onset of mineralization (Fig. 4.3B, Table 4.2), the appearance of moderate to intense staining was correlated with a high ALP activity of at least 1.0 IU/mg protein.

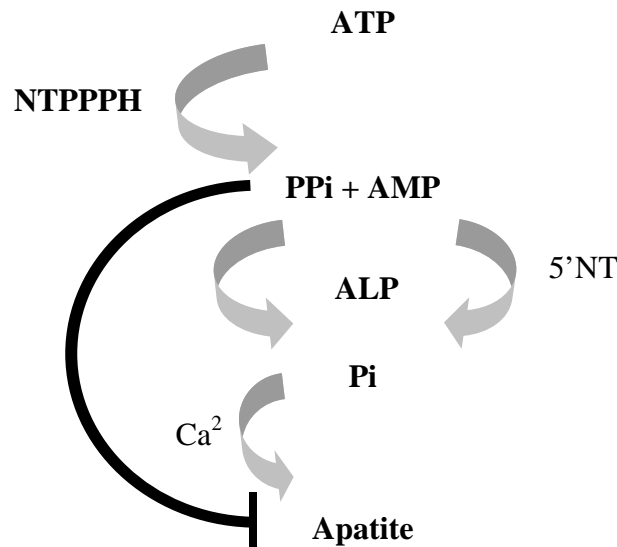


Figure 4.9. Schematic diagram showing the metabolism of ATP and AMP, and the role of ALP on mineralization. ATP is hydrolyzed by nucleoside triphosphate pyrophosphohydrolase (NTPPPH) to AMP and inorganic pyrophosphate (PPi), which are further degraded to yield inorganic phosphate (Pi) by ALP. The inorganic phosphate forms apatite in the presence of physiological concentrations of calcium (Ca^{2+}). An excess of PPi results in the inhibition of apatite deposition.

5. COLLAGEN SYNTHESIS DURING EXPANSION OF PRIMARY hPDLF *IN VITRO*

5.1. Background

The extracellular matrix (ECM) is composed of structural proteins, proteoglycans, growth factors and matricellular proteins. Whereas matricellular proteins serve as biological modulators by regulating cell-matrix interactions and cell function, structural proteins such as collagens contribute to the structural stability of the ECM (Bornstein and Sage, 2002).

In Chapter 4, we characterized the osteogenic potential of primary hPDLF cell lines established by explant culture in terms of the synthesis of bone-matrix proteins and mineral-like tissue formation. In this chapter, we seek to describe the collagen-synthetic capability of the cells, as collagens are the major constituent of the periodontal structures. The structural ECM, together with matricellular proteins and soluble factors, presumably act in concert to determine specific downstream effects on gene expression and cellular phenotype.

As described in Chapter 2, the PDL is characterized by fibrils of type I and III collagen, as well as minor collagens such as type V, VI, XII and XIV (Table 2.1). PDL cells *in vivo* exhibit a collagen-synthetic pattern resembling that of embryonic connective and wound-healing tissue, characterized by high collagen turnover, proportion of collagen III and dehydrodihydroxy-lysinonorleucine cross-link (Pearson *et al.*, 1975; Lekic and McCulloch, 1996; Beertsen *et al.*, 1997). However, a lack of phenotypic stability in subcultured monkey PDLF was previously reported *in vitro* (Limeback and Sodek, 1979).

Collagen metabolism, the combined process of synthesis and turnover, is dependent on intrinsic factors such as cell isolation (Weber *et al.*, 1986), cell cycle and cellular age (Mayne *et al.*, 1976), as well as extrinsic factors such as ascorbic acid (Asc) (Peterkofsky, 1972), serum (Narayanan and Page, 1977) and medium composition (Booth *et al.*, 1980). Attempts to correlate patterns of collagen synthesis *in vitro* and *in vivo* are hampered by such extrinsic factors. During culture expansion, cells were supplemented with fetal bovine serum (FBS) which has been shown to modulate collagen expression. In particular, type III collagen synthesis in human gingival fibroblasts peaked at 10% serum, but the proportion of collagens over total protein synthesis was correspondingly reduced (Narayanan and Page, 1977). Furthermore, platelet-derived growth factor present in serum was found to upregulate type V and concomitantly downregulate type III collagen in human gingival fibroblasts (Narayanan and Page, 1983).

For successful tissue engineering of the PDL, it is essential that hPDLF produce a collagenous matrix *in vitro*. Hence, it was hypothesized that hPDLF retained collagen-synthetic capability during 21-day culture expansion under 10% serum. Three cell lines established previously (Chapter 4) were studied under serum deprivation and culture expansion under the following conditions: i) 0.2% FBS, ii) 0.2% FBS + 200 μ M Asc, iii) 10% FBS, iv) 10% FBS + 200 μ M Asc. To ensure the consistency of serum factors such as growth factors, hormones and metabolites, serum from a single batch was used. Pepsin digestion of conditioned medium and whole cell extracts, in combination with quantitative ELISA for C-terminal propeptide of procollagen I (PICP) and immunofluorescence, were conducted to determine collagen synthesis and deposition *in vitro*.

5.2. Materials and methods

5.2.1. Collagen induction

Primary hPDLF cell lines between passage 3 to 5, derived from third molars of three females aged 21-23 yr (22 ± 1 , mean \pm SD), were seeded into tissue culture plates (TPP, MO, USA) at a density of 10,000 cells/cm², and incubated in DMEM (Gibco, Life Technologies, NY, USA) containing 10% FBS and 2% penicillin-streptomycin at 37 °C and 5% CO₂. After cell attachment was achieved, hPDLF were rinsed thrice with PBS and incubated with medium containing a descending series of serum concentrations, i.e. 2%, 0.5% and 0.2% FBS, 3 hr each. Cells were then starved in medium containing 0.2% FBS for 24 hours to achieve cell cycle arrest at the G0/G1 phase, as described (Lee and Piedrahita, 2002). Subsequently, hPDLF ($n=3$) were subjected to four culture conditions: i) 0.2% FBS, ii) 0.2% FBS + 200 μ M Asc, iii) 10% FBS, iv) 10% FBS + 200 μ M Asc.

0.2% FBS was the level commonly cited for growth factor supplementation studies in which the effects of serum factors were negligible (Matsuda *et al.*, 1992; Haase *et al.*, 1998; Ivanovski *et al.*, 2001). Two hundred μ M ascorbic acid 2-phosphate magnesium salt (Asc; Sigma, MI, USA), a thermo-stable phosphate derivative of L-ascorbic acid (Nomura *et al.*, 1969), was added to mimic the level present in gingival crevicular fluid (Meyle and Kapitza, 1990). In addition, 350 μ M of L-proline (Sigma), a precursor of collagen synthesis (Bornstein and Traub, 1979), was added to ensure that the incorporation of proline was not rate-limiting.

The day of collagen induction was designated as day 0. Fresh Asc aliquots (100X stock in DMEM at -20 °C) were added at medium change every 3 to 4 days, and approximately 500 μ l of medium was added per well in 24-well plates.

Experiments were performed at day 1, 7, 14 and 21. To ensure the consistency of serum factors, FBS from a single batch was used.

5.2.2. Reverse transcription polymerase chain reaction (RT-PCR)

Total cellular RNA from six-well-plate cultures ($n=3$) was extracted using Trizol reagent (Invitrogen, CA, USA) according to manufacturer's instructions. RNA was quantified with a NanoDrop spectrophotometer (NanoDrop, Delaware, USA). Optical density was read at 260 nm and 280 nm with ND-100 V3.1.0 software. Total yield in $\mu\text{g/ml}$ was obtained by multiplying the 260 nm reading $\times 10 \times 40$, whereas purity was determined from the ratio of 260 nm / 280 nm. RNA integrity was confirmed by denaturing agarose gel electrophoresis (Sigma). Agarose gels were cast by dissolving 1% (w/v) ultra-pure electrophoresis-grade agarose (Sigma) in Tris acetate EDTA (TAE) buffer (0.04M Tris acetate, 1 mM EDTA) supplemented with 0.5 $\mu\text{g/ml}$ ethidium bromide (Sigma). Samples were mixed with an appropriate amount of a 6X DNA gel loading dye (1X TAE, 30% (v/v) glycerol, 0.25% (w/v) bromophenol blue, 0.25% (w/v) xylene cyanol FF) and run at 80-100 voltage on electrophoresis machine (Bio-Rad Laboratories, CA, USA) alongside 1kb DNA ladder (Promega, WI, USA). Gels were viewed using a UV transilluminator (UVItec Limited, Cambridge, UK). Total RNA was temporarily stored at $-80\text{ }^{\circ}\text{C}$ until use.

Complementary DNA (cDNA) was synthesized from 1 μg of total RNA with moloney murine leukaemia virus reverse transcriptase (M-MLV RT, Promega) according to manufacturer's instructions. cDNA was temporarily stored at $-20\text{ }^{\circ}\text{C}$ before being used as templates for subsequent PCR amplification. PCR was performed using 2 μl of cDNA product with PCR kit (Promega), according to

manufacturer's instructions. Primer pairs used (1st BASE, Singapore) were presented in Table 5.1.

PCR samples were placed in a thermocycler (MiniCycler™, MJ Research, MA, USA) and subjected to one cycle of 95 °C for 2 min, then 25 cycles of denaturation at 95 °C for 30 sec, annealing at 60°C for 30 sec, and extension at 72°C for 1 min. A final single cycle of 10 min at 72°C was performed. Amplified products were separated by 1% agarose gel electrophoresis for verification of size and quality.

5.2.3. Collagen I assay

Type I collagen synthesis was determined from the amount of secreted C-terminal propeptide of procollagen I (PICP) in triplicate samples by ELISA (Metra Biosystems, CA, USA) (Melkko *et al.*, 1990). Briefly, 24-hr-conditioned medium was collected, supplemented with protease inhibitor cocktail (Section 3.6; Calbiochem, CA, USA) and stored at -80 °C. Samples were diluted 10-fold prior to use and assayed according to manufacturer's instructions. All steps were performed at room temperature. Fresh culture medium containing 0.2% and 10% FBS was tested to correct for the presence of background PICP levels.

5.2.4. SDS-PAGE

For the separation of collagens in pepsin-digested medium and cell layer fractions by SDS-PAGE, polyacrylamide gels (3% stacking and 5% resolving) were cast using 30% acrylamide/bis (37:5:1) solutions, TEMED (Bio-Rad Laboratories) and 10% (w/v) APS (Invitrogen). Equal proportions of medium fractions (60 µl out of a total 500 µl) and cell layer fractions (30 µl out of a total 250 µl) were denatured for 5 min at 90 °C in Laemmli's non-reducing sample buffer (156 mM Tris-HCl [pH 6.8],

5% (w/v) SDS, 50% (v/v) glycerol, 0.5% (w/v) bromophenol blue), and loaded alongside purified human type I collagen standard (Sigma) and Precision Plus protein pre-stained standards (Bio-Rad Laboratories). Fixed amounts of protein standard were loaded as internal controls for semi-quantitative densitometry. Gel electrophoresis was performed using the Hoefer SE 400 Electrophoresis System with heat exchanger (Hoefer, CA, USA) in Tris-glycine buffer (25 mM Tris, 192 mM glycine, 0.1% (w/v) SDS). Electrophoresis was run at a constant current of 30 mA and 60 mA for 3% stacking and 5% resolving gels respectively, until the dye front reached the bottom of the gel.

For the separation of pepsin-digested and intact collagens in 3-8% gradient NuPAGE® Tris-acetate gels (Invitrogen), please refer to section 3.8.1.

5.2.5. Immunofluorescence

Cells, seeded at a density of 10,000 cells/cm² on LabTek chamber slides (Nunc, Inc., IL, USA), were rinsed with sterile PBS, and fixed with absolute methanol at -20 °C for 10 min. After air-drying, blocking was performed with 5% bovine serum albumin (w/v) (Sigma) and 1% goat serum (v/v) (Invitrogen) in PBS for 2 h at room temperature. Cells were incubated with primary antibodies, namely anti-collagen I (1:5000; Sigma), anti-collagen III (1:500; Chemicon, CA, USA), anti-collagen XII and XIV (1:500) overnight in a humidified chamber at 4 °C. The antibodies against collagen XII and XIV were kind gifts from Dr Greg Lunstrum (Shriners Hospital for Children, OR, USA). For double labelling of collagens and viewing under Confocal laser scanning microscope, please see section 3.12 and 3.15 respectively. Singly-labelled samples were used as internal controls.

5.3. Results

5.3.1. Asc supplementation led to increased collagen synthesis

Cell proliferation, as reflected by the amount of total dsDNA, was approximately 4-fold higher under 10% serum ($p < 0.001$) (Fig. 5.1A). However, it was insignificantly different in the presence of Asc up to day 14. A spike in the quantity of dsDNA at day 21 under Asc supplementation could be attributed to the incomplete disaggregation of cells in post-confluent cultures, leading to an over-estimation of dsDNA. In contrast, total protein synthesis was significantly increased under 10% serum and Asc from as early as day 1 (< 0.05) (Fig. 5.12B). The fold increase in protein (mean \pm SD) in the presence of Asc over 21 days was 1.4 ± 0.3 and 1.3 ± 0.2 at 0.2% serum and 10% serum, respectively.

Gene expression of three representative collagens in the PDL, namely types I, III and XII, was verified by their respective $\alpha 1$ chains using RT-PCR (Fig. 5.2). Asc supplementation resulted in an increase in the expression of $\alpha 1$ (I) and $\alpha 1$ (III) from day 7 onwards, and of $\alpha 1$ (XII) from day 14 onwards. The coordinated increase in steady-state levels of both collagen $\alpha 1$ (I) and $\alpha 1$ (III) mRNA transcripts was similar to previous finding in human dermal fibroblasts (Phillips *et al.*, 1992). A lack of increase at day 1 showed that a lag of 24 h was required for the induction of collagen transcripts, as similarly reported for tendon cells and chondrocytes (Lyons and Schwarz, 1984; Sullivan *et al.*, 1994). Whereas collagen expression was similar over time under 10% FBS, there was a drastic decrease in overall mRNA synthesis by day 14 under 0.2% FBS, corresponding possibly to a state of cell quiescence as indicated by the low levels of dsDNA (Fig. 5.1A). Hence, only results at day 1 and day 7 were presented for 0.2% FBS.

C-terminal propeptide of procollagen I (PICP) was quantified in 24-h-conditioned medium to provide a stoichiometric representation of type I collagen synthesis *in vitro* (Melkko *et al.*, 1990). PICP values between 200-300 ng/ml were obtained from 2×10^4 primary hPDLF seeded in 24-well plates, similar to the values reported for primary hOB (Martinez *et al.*, 1998). Collagen I synthesis, as the level of PICP normalized to dsDNA, was significantly higher under 0.2% serum ($p < 0.001$) and under supplementation with Asc ($p < 0.05$) as early as day 1 (Fig. 5.3A). This early increase in collagen polypeptide synthesis was in agreement to the notion that the primary effects of Asc are post-transcriptional (Rowe and Schwarz, 1983; Sullivan *et al.*, 1994). Collagen synthesis decreased gradually under 0.2% serum, but drastically under 10% serum at day 7 when cell confluency was achieved (Appendix), reaching a steady state at day 14. This down-regulation was also described in human dermal fibroblasts within a pericellular (Jukkola *et al.*, 1991) or three-dimensional collagenous matrix (Mauch *et al.*, 1988). The fold increase in collagen synthesis due to Asc supplementation was 1.6 ± 0.3 and 1.6 ± 0.5 (mean \pm SD) at 0.2% serum and 10% serum, respectively.

ALP activity was significantly higher under 0.2% serum ($p < 0.001$) at all time points (Fig. 5.3B). ALP level peaked at day 14 under 0.2% FBS + Asc when cells were approaching confluency (Appendix), and thereafter declined. In contrast, ALP level under 0.2% FBS continued to rise. Under 10% serum, ALP activity was characterized by a drop at day 7 ($p < 0.01$), followed by an increase at day 14 ($p < 0.05$) in both the presence and absence of Asc. This was representative of ALP upregulation as previously described (Chapter 4). Unlike collagen I synthesis, ALP activity was not significantly higher in the presence of Asc.

5.3.2. Serum modulated type III and V collagen, as well as fibre morphology

Pepsin solubilises collagen by cleaving the intermolecular cross-links in the telopeptides, while leaving the triple-helical regions intact (Bailey *et al.*, 1970). Fibrillar collagens thus solubilized were identified through the characteristic mobility of the resultant α -chains on SDS-PAGE. Limited pepsin digests of conditioned medium depicting 3-day window of collagen synthesis (Fig. 5.4) and of cell layer depicting accumulative collagen deposition (Fig. 5.5) were run in non-reducing 5% Tris-glycine SDS-PAGE gels alongside purified type I collagen. Collagen I synthesis, evidenced by pepsin-resistant $\alpha 1(I)$ and $\alpha 2(I)$ chains, was observed to increase at day 7 and decrease slightly at day 21 (Fig. 5.4A, B). Collagen I deposition was observed to increase consistently up to day 14, with no further increase at day 21 (Fig. 5.5A, B).

The major fibrillar collagens in the PDL are types I, III and V. Under both 0.2% and 10% serum, types I and III collagen were detected in the medium (Fig. 5.4A, B), whereas types I, III and V collagen in the cell layer fraction (Fig. 5.5A, B). The predominant collagen is type I. Type III in the medium was verified by reducing SDS-PAGE, in which a disappearance of $\alpha 1(III)_3$ trimer and a corresponding increase in $\alpha 1(I)$ was noted (Appendix). Type V α -chains and type I β -chains were found exclusively in the cell layer under both 0.2% and 10% serum (Fig. 5.5A, B), in agreement with an association of secreted type V collagen with the matrix (Narayanan and Page, 1983). A band at the position of δ -chains was observed in the medium under 10% serum (Fig. 5.4B). This high molecular weight pepsin-resistant peptide is probably a supramolecular aggregate of a non-fibrillar collagen. In agreement, a faint band just below $\alpha 1(V)$ was observed in the cell layer (Fig. 5.5B), whose migratory pattern did not coincide with any of the fibrillar collagens reported in the PDL.

Multiple distinct γ - and δ -bands were present in the cell layer under 0.2% serum (Fig. 5.5A). Under 10% serum however, γ -components appeared indistinct and δ -chains were barely detectable (Fig. 5.5.B), suggestive of protein degradation. To accurately resolve these high molecular weight components, fresh aliquots of pepsin-digested cell layer at day 21 were run in non-reducing 3-8% gradient gels (Fig. 5.6). Similar to the 5% gel, two resolved bands were seen around 150 kDa, pointing to the presence of an additional pepsin-resistant peptide just below $\alpha 1(V)$. Unlike 5% gels which hindered the migration of high molecular weight peptides, 3-8% gradient gel allowed an improved resolution of these bands. Numerous γ - and δ -bands were demonstrated under 10% serum. Only minute differences in the migration of γ - and δ -chains were observed between 0.2% and 10% serum, unlike previously demonstrated (Fig. 5.5A, B). This provided further evidence for the presence of non-fibrillar collagens, as well as an accelerated degradation of δ -chains into γ -components under 10% serum.

The ratios of $\alpha 1(III)_3:\alpha 1(I)$ and $\alpha 1(V):\alpha 1(I)$ generated from pepsin-digests of medium and cell layer fractions (Fig. 5.4, 5.5) were analyzed using densitometry to examine the phenotypic expression of collagens over time (Fig. 5.7). Results showed that ratios of types III and V collagen relative to type I were modulated by serum level over time. Densitometric analysis of $\alpha 1(I)$ in pepsin-digested medium fractions after reduction at day 21 gave a fold increase of 1.3 and 1.2 under 0.2% and 10% serum respectively (Appendix), indicating that secreted type III collagen was approximately 20% of secreted type I collagen. In agreement, type III collagen in the medium was 14-15% of type I collagen as determined from $\alpha 1(III)_3:\alpha 1(I)$ ratio (Fig. 5.7A). Despite similar proportions of secreted type III collagen at both serum levels, the level in the cell layer under 10% serum was at most half of that under 0.2% serum (Fig. 5.7B), in

accordance to previous finding (Limeback and Sodek, 1979). Additionally, cultures under 10% serum possessed an increasing relative proportion of type V collagen over time as seen from $\alpha 1(V):\alpha 1(I)$ ratio, whereas the reverse was true for 0.2% serum (Fig. 5.7C), as observed for human gingival fibroblasts (Narayanan and Page, 1983). Moreover, an increase in $\alpha 1(I):\beta 11(I)$ ratio was obtained under both 0.2% and 10% serum over time (Fig. 5.7D), indicative of a reduction in collagen I cross-linking (Junker *et al.*, 1981).

Since the ratio of major fibrillar collagens with respect to type I and the degree of cross-linking were observed to differ (Fig. 5.7), we sought to investigate collagen deposition at the end of culture period. Collagen fibre morphology at day 21 differed in thickness, uniformity and alignment under the two serum levels. Thick, irregular fibres (arrowhead) in confluent group 0.2% FBS + Asc were seen under PCLM and fluorescence light microscopy, compared to densely-packed collagenous matrix obstructed by cells in post-confluent group 10% FBS + Asc (Fig. 5.8). Single and double immunolabeling for types I, III, XII and XIV was performed, counterstained with Hoechst 33258, and observed by Confocal laser microscopy (Fig. 5.9). Thick type I collagen fibres (green) formed from an aggregation of thin subunit fibrils at multiple branch points were demonstrated in the group 0.2% FBS + Asc. Collagen fibre alignment was randomized at extracellular vicinity of cells. Conversely, thin type I fibres aligned along the long axis of cells were demonstrated in the group 10% FBS + Asc. Some fibres were crisscrossed at post-confluent regions. Double-labeling established the presence of types XII and XIV of the sub-family of fibril associated collagens with interrupted triple helices (FACITs) (red), co-localized along the length of type I fibrils as previously described (Keene *et al.*, 1991). Signals of type III (red) were less distinct amidst perinuclear staining.

5.3.3. hPDLF produced the large isoforms of collagen XII and XIV

Type XII and XIV collagen are associated with the surface of banded type I collagen fibrils through a portion of the triple helix, whereas the N-terminal globular (NC-3) domain projects from the fibril surface, influencing additional interactions between fibrils, or between fibrils and the environment (Koch *et al.*, 1995). Furthermore, collagen XII is synthesized as large (320 kDa) and small (220 kDa) isoforms by alternative splicing within its non-collagenous (NC-3) domain (Koch *et al.*, 1995; Kania *et al.*, 1999). To see if serum modulated the synthesis of collagen XII and XIV, conditioned medium containing intact collagen XII and XIV were run on reducing 3-8% gradient gels and the proteins detected by Western blotting (Fig. 5.10A-C).

Type XIV collagen was detected as a prominent ~290-kDa protein under 10% serum with a faint band at ~220 kDa (Fig. 5.10A), in agreement with previous finding (Aubert-Foucher *et al.*, 1992). However, signals were undetectable under 0.2% serum. Type XII collagen was detected as a prominent ~320-kDa protein under both 0.2% and 10% serum (Fig. 5.10B). Several bands were seen under 10% serum, with at least one high molecular weight band. Western blot was repeated for hPDLF derived from three other individuals under 10% serum, along with purified type I collagen from human skin, under more stringent conditions. Two distinct bands were detected, one approximately 320 kDa, and the other a high molecular weight aggregate migrating above γ (I) (arrowhead) (Fig. 5.10C), in agreement to previous reports (Aubert-Foucher *et al.*, 1992; Lunstrum *et al.*, 1992). Analysis by densitometry of three independently-run SDS-PAGE gels determined that the ratio of type XII under 0.2% and 10% serum was equivalent to the ratio of total proteins loaded. No cross-reactivity of anti-collagen XII antibody to type I collagen was observed.

5.4. Discussion

5.4.1. Collagen synthesis and ALP activity

Ascorbic acid increases both the rate of procollagen gene transcription as well as the half-life of mRNA transcripts (Lyons and Schwarz, 1984). In addition, Asc plays an important role in the assembly of collagen-synthesizing polyribosomes, and as a cofactor in hydroxylation of proline (Sodek *et al.*, 1982). A stimulation of collagen I synthesis in the presence of Asc was in agreement with previous reports for hPDLF (Ishikawa *et al.*, 2004) and tooth organ culture (Bronckers, 1983). The extent of collagen induction was similar regardless of serum level. This indicated that serum level did not modulate the magnitude of Asc induction. The fold increase in collagen I synthesis was approximately 1.6 fold, lower than a previous report for hPDLF (Ishikawa *et al.*, 2004). This could be attributed to different cellular passage, patient-to-patient variation and conditions of experiment.

Collagen matrix accumulation precedes and is essential for sequential expression of differentiation-related proteins such as ALP by osteoblasts (Owen *et al.*, 1990; Franceschi, 1999). In this study, however, Asc was unable to increase ALP synthesis in hPDLF determined on a per cell basis (Fig. 5.2B) unlike previously reported (Ishikawa *et al.*, 2004). ALP activity of cells under 10% serum normalized to protein yielded values between 0.1-0.3 IU/mg, which was similar to values obtained under routine culture, i.e. in the absence of Asc (Chapter 4). These results were in line with recent reports, in which Asc failed to induce ALP upregulation at low and intermediate cell density cultures. This was attributed to the upregulation of collagenase-1 expression which led to an increase in collagen turnover (Shiga *et al.*, 2003; Hayami *et al.*, 2006).

5.4.2. Collagen deposition and fibre morphology

Despite a reduction in type III collagen deposition under 10% serum, the difference was reduced over culture time. The collagen III/collagen I ratio in pepsin-solubilized hPDLF at day 21 was 0.11 and 0.24 under 10% and 0.2% serum respectively (Fig. 5.7B), which fell into the lower and higher range of rat skin at 0.14-0.23 (Junker and Lorenzen, 1983; Levi and Werman, 1998). Moreover, collagen V/collagen I ratio, though increasing under 10% serum, was not significantly different at day 21 (Fig. 5.7C). In contrast to the earlier report of a lack of phenotypic stability in monkey PDLF in culture over 24 h (Limeback and Sodek, 1979), this study showed that hPDLF in 21-day expansion culture demonstrated a recovery of type III collagen and a slight but statistically insignificant increase in type V collagen in the cell layer fractions (Fig. 5.7).

In the human PDL, collagen fibril bundles, approximately 1 μm in thickness (Kuroiwa *et al.*, 1996), are consisted of a parallel arrangement of subunit fibrils between 50-80 nm (Schroeder, 1986). The diameter of collagen fibril bundles formed from an *in vitro* association of type III and type I collagens was reported to be smaller than that of type I alone, and correlated to the proportion of type III (Lapierre *et al.*, 1977). Despite the high proportion of type III collagen in 0.2% serum culture, thick collagen fibres were obtained in monolayer cultures under 0.2% serum (Fig. 5.9). Speculatively, complete procollagen processing via the cleavage of C-propeptide, which would otherwise be inhibited at conditions above 5% serum (Njieha *et al.*, 1982; Kessler *et al.*, 1986), enabled additional lateral growth of fibrils (reviewed in Silver *et al.*, 2003). Alternatively, the collagenous fibre morphology was dictated by fibronectin matrix, since fibronectin acts as a template for collagen deposition (reviewed in Embery *et al.*, 1995). Either way, the disuniformity in fibre thickness

under 0.2% serum and the thin collagenous fibre morphology under 10% serum pointed to other contributing factors responsible for fibrillogenesis in the PDL, such as small leucine-rich proteoglycans (Matheson *et al.*, 2005).

5.4.3. hPDLF exhibited a dedifferentiated phenotype during expansion *in vitro* that was partially reversed by serum deprivation

Collagen XII is highly expressed at locations bearing high tensile stress, such as tendons, ligaments, and in dense connective tissues of dermis, cornea, blood vessels, perichondria and periosteal (Sugrue *et al.*, 1989). Collagen XII was first purified from bovine PDL (Dublet *et al.*, 1988) and subsequently reported in the PDL of rat (Karimbux *et al.*, 1992) and mouse (MacNeil *et al.*, 1998), the expression of which increased with the alignment and organization of PDL fibril bundles during tooth eruption and attainment of occlusal contact. Whereas both the large and the small isoforms have been identified in mouse embryonic tissues (Oh *et al.*, 1993), the small isoform is the major product at later stages of development (Bohme *et al.*, 1995). Correspondingly, adult tendon, ligament and skin express mainly the small isoform (Kania *et al.*, 1999; Kato *et al.*, 2000).

hPDLF phenotype during culture expansion appeared to be dedifferentiated or embryonic-like, which was typical of that during morphogenesis and wound healing. These were demonstrated by the following observations. Firstly, hPDLF exhibited high proliferative rates and synthetic activities under culture expansion (Fig. 5.1). Coupled with a simultaneous reduction of both collagen I and ALP synthesis (Fig. 5.3), hPDLF matrix did not appear to achieve maturation (discussed in Chapter 4). Secondly, hPDLF possessed a collagenous matrix that was not highly cross-linked. The degree of cross-linking as estimated by alpha/beta chain ratio was not reported

for PDL. However, it is known that the ratio reported in pepsin-solubilized skin was between 2.1-2.9 (Junker and Lorenzen, 1983; Levi and Werman, 1998). Since the PDL is a dense connective tissue *in vivo*, an alpha/beta chain ratio of 6-7 under culture expansion (Fig. 5.7D) was suggestive of a low degree of collagen cross-linking. Thirdly, hPDLF matrix demonstrated high collagen turnover as seen from degradation of δ -chains (Fig. 5.5B), possibly by the action of matrix metalloproteinases (Shiga *et al.*, 2003; Hayami *et al.*, 2006).

On the other hand, serum deprivation appeared to result in a reversal of phenotype, as recently reported in human vascular smooth muscle cells (Han *et al.*, 2006), based on the following observations. Firstly, hPDLF become quiescent (Fig. 5.1), yet demonstrated a significantly higher level of collagen I and ALP synthesis (Fig. 5.3). The results corroborated with a previous finding that ALP induction was associated with mitogen deprivation, in which the upregulation of ALP expression required the cessation of proliferation (Abe *et al.*, 1998). The induction of ALP at day 14 coupled with the quiescent state of cells resembled the post-proliferative period of matrix maturation (Owen *et al.*, 1990; Sodek and Cheifitz, 2000). Secondly, hPDLF matrix appeared to achieve lateral growth of fibres and hence thick collagen fibre morphology (Fig. 5.8, 5.9). Serum deprivation hypothetically enabled more complete collagen processing regardless of cell density, resulting in an interconnected meshwork of collagen fibres. Thirdly, hPDLF retained high levels of collagen III synthesis and deposition, similar to PDL *in vivo* (Butler *et al.*, 1975).

However, this reversal was not complete. hPDLF under serum deprivation did not revert to a synthesis of the small type XII collagen isoform (Fig. 5.10). It had been suggested that collagen fibril arrangement during PDL development is related to the expression of collagen XII (Karimbux *et al.*, 1992), and that collagen XII expression

may be closely associated with the functional regeneration of the PDL (Karimbux and Nishimura, 1995). The small isoform, expressed within mature PDL, participates in fibril organization into functional parallel arrangement & insertion into cementum (Gordon *et al.*, 1989). However, transcription of collagen XII gene is switched from the short to the long splice variant under monolayer culture conditions (Oh *et al.*, 1993). The large isoform is the predominant product of fibroblasts *in vitro* from tendon (Trueb and Trueb, 1992) and skin (Oh *et al.*, 1993; Berthod *et al.*, 1997; Gerecke *et al.*, 1997; Dharmavaram *et al.*, 1998).

In summary, this work demonstrated the preservation of basic collagen synthetic capability in 21-day expansion cultures of hPDLF *in vitro*, and highlighted the possibility of dedifferentiation, which would be of importance for downstream clinical applications.

Product	Gene number	bp	Primer sequence
<i>AlphaI(I)</i>	NM-000088.2	501	sense 5'-CTGGCAAAGAAGGCGGCAAA-3' anti-sense 5'-CTCACCACGATCACCCTCT-3'
<i>AlphaI(III)</i>	NM0000902	559	Sense 5'-CAGTATTCTCCACTCTTGAGTTCAG-3' anti-sense 5'-GTGACAAAGGTGAAACAGGTGAAC-3'
<i>AlphaI(XII)</i>	NM_080645.1 NM_004370.4	237	sense 5'-CAAGAGGCGAGGTGCAAACCTGTTA-3' anti-sense 5'-CTCTGGATTTGGAATGCGGCTGAT-3'
<i>β-Actin</i>	BC013380.2	212	sense 5'-GAGACCTTCAACACCCAGCC-3' anti-sense 5'-GGCCATCTCTTGCTCGAAGTC-3'

Table 5.1. List of primer sequences and expected size of PCR products.

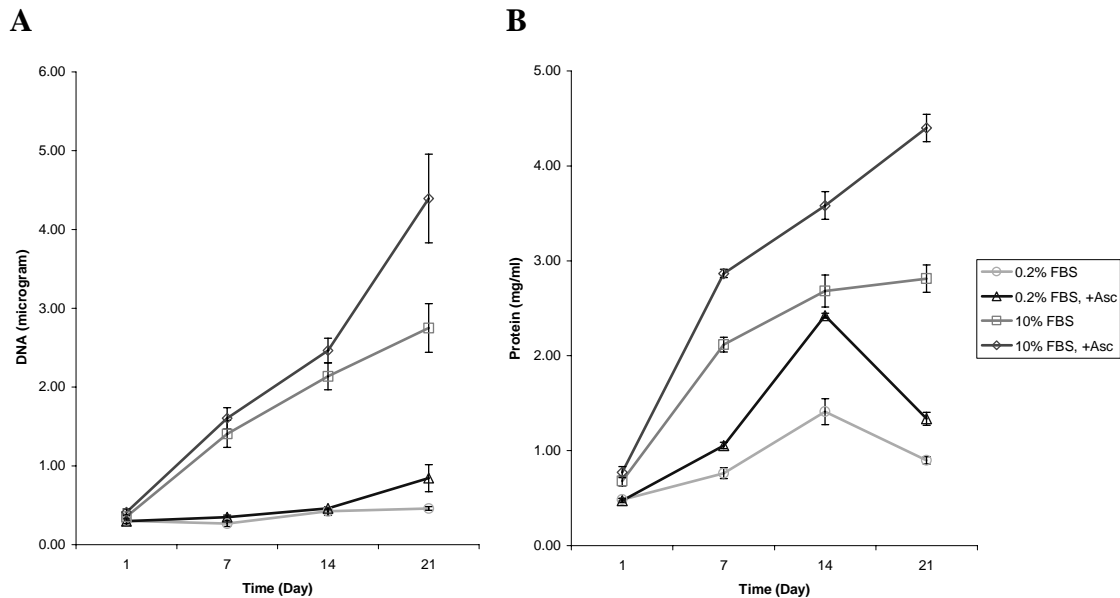


Figure 5.1. Synthesis of (A) DNA and (B) proteins over time. (A) Cell proliferation as reflected by the amount of total dsDNA was approximately 4-fold higher under 10% serum ($p < 0.001$), whereas it was not significantly different in the presence of Asc ($p > 0.05$) with the exception of day 21. (B) Total protein synthesis was significantly increased (< 0.05) under 10% serum and Asc from as early as day 1.

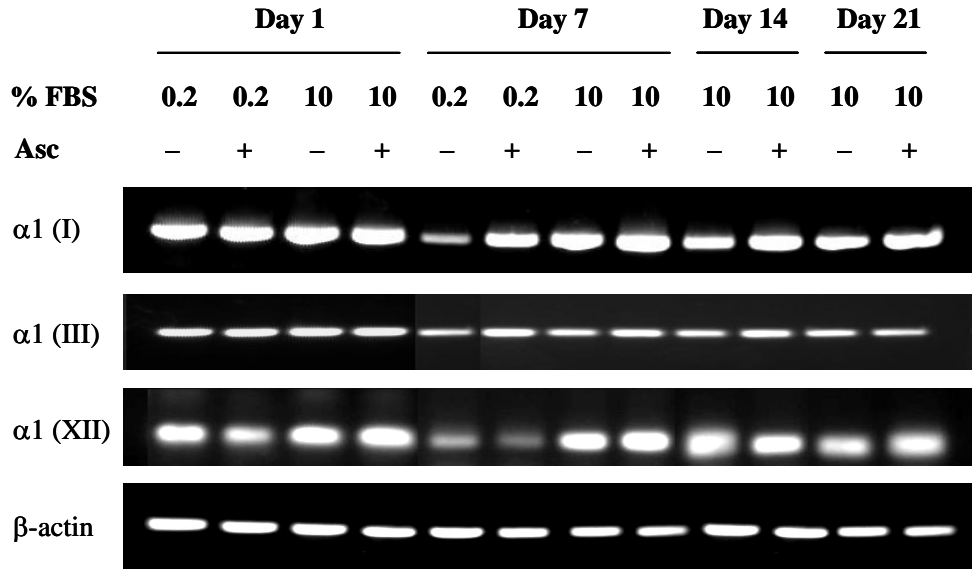


Figure 5.2. Gene expression of three representative collagens in the PDL, namely types I, III and XII, as represented by their respective $\alpha 1$ chains using RT-PCR. Asc supplementation resulted in an increase in the expression of $\alpha 1$ (I) and $\alpha 1$ (III) from day 7 onwards, and of $\alpha 1$ (XII) from day 14 onwards. No induction in collagen gene expression was observed at day 1. There was a drastic decrease in overall mRNA synthesis by day 14 under 0.2% FBS.

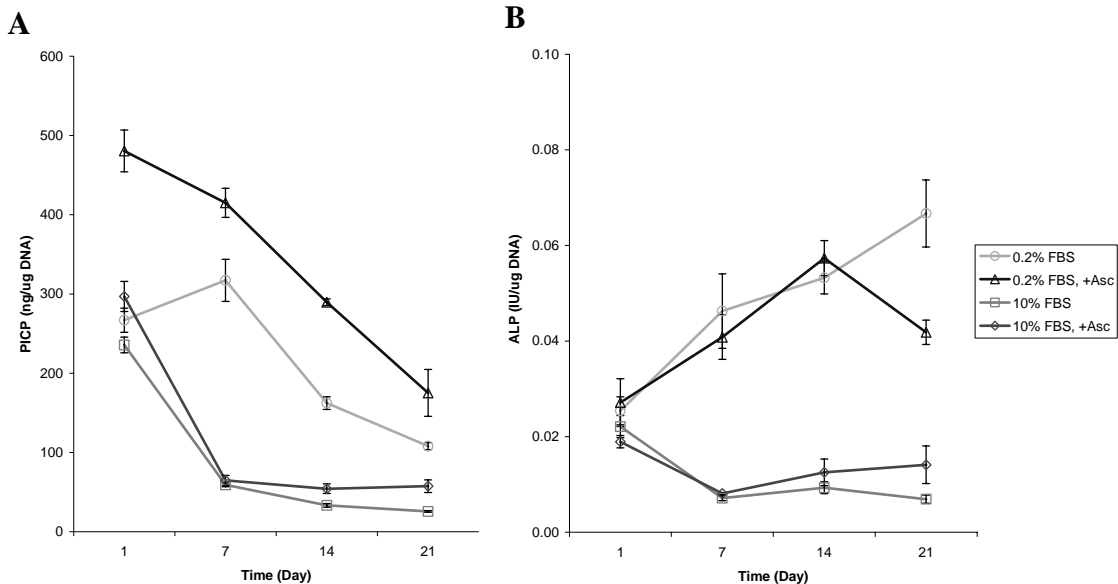


Figure 5.3. Synthesis of (A) collagen I and (B) alkaline phosphatase (ALP), normalized to dsDNA. (A) Collagen synthesis was significantly higher under 0.2% serum ($p < 0.001$) and under supplementation with Asc ($p < 0.05$). It decreased gradually over time under 0.2% serum, but drastically under 10% serum. (B) ALP activity was significantly higher under 0.2% serum ($p < 0.001$). ALP induction was observed on day 14 in the presence of Asc, after which it decreased and levelled off under 0.2% and 10% FBS, respectively.

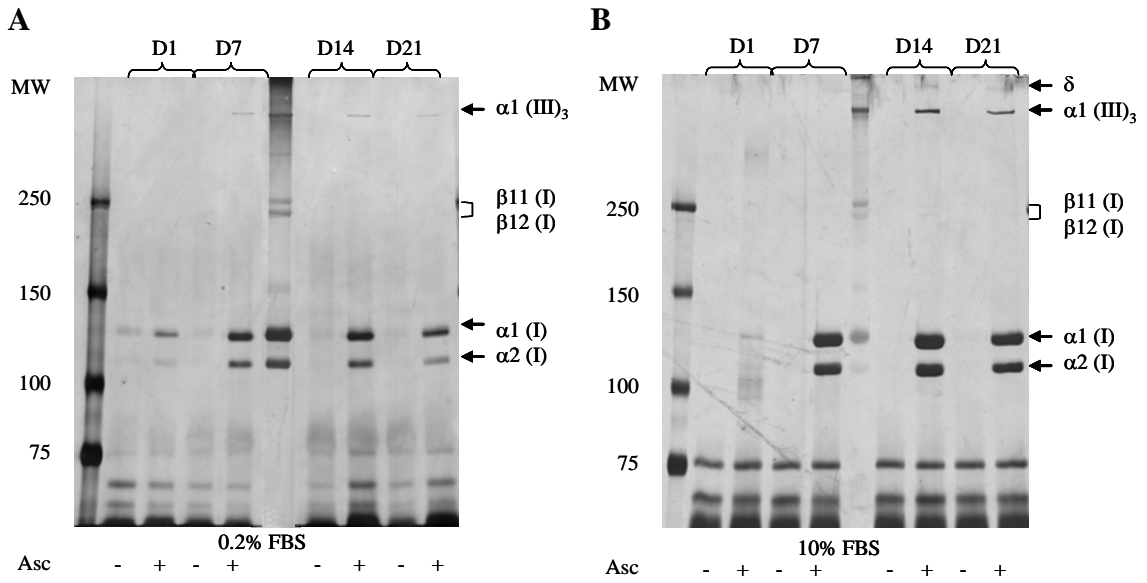


Figure 5.4. Three-day window of collagen synthesis. Representative images of silver-stained non-reducing SDS-PAGE in 5% Tris-glycine gel, showing pepsin digested 3-day conditioned medium under (A) 0.2% and (B) 10% FBS. Types I and III, and a non-fibrillar collagen were detected in the medium fraction.

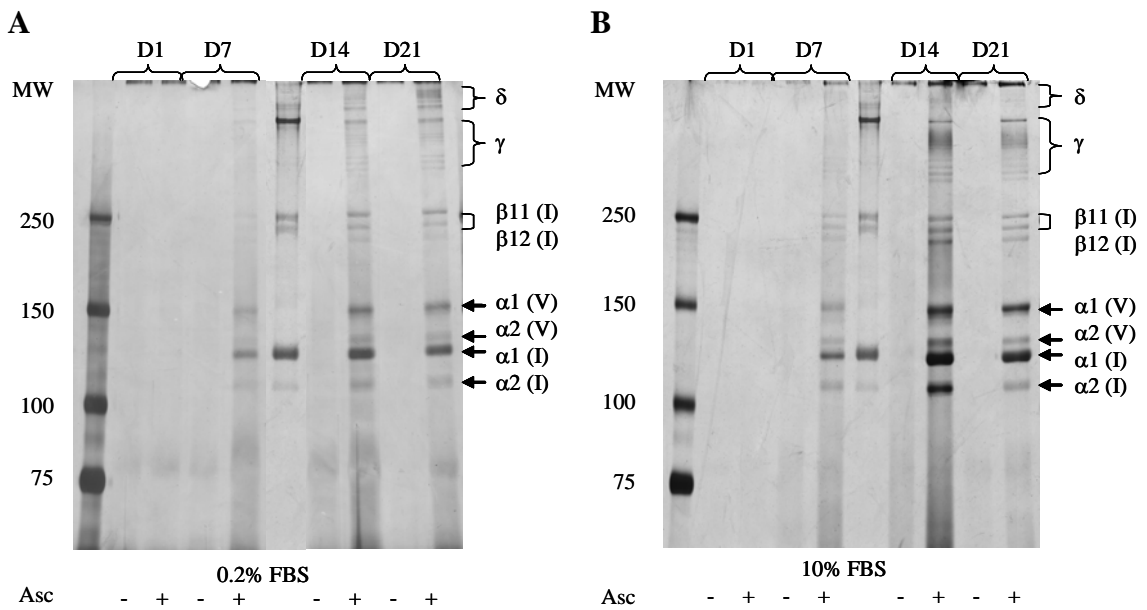


Figure 5.5. Accumulative collagen deposition. Representative images of silver-stained non-reducing SDS-PAGE in 5% Tris-glycine gel, showing pepsin digested cell layer under (A) 0.2% and (B) 10% FBS. Types I, III and V, and non-fibrillar collagen(s) were detected in the cell layer fraction. The predominant collagen is type I.

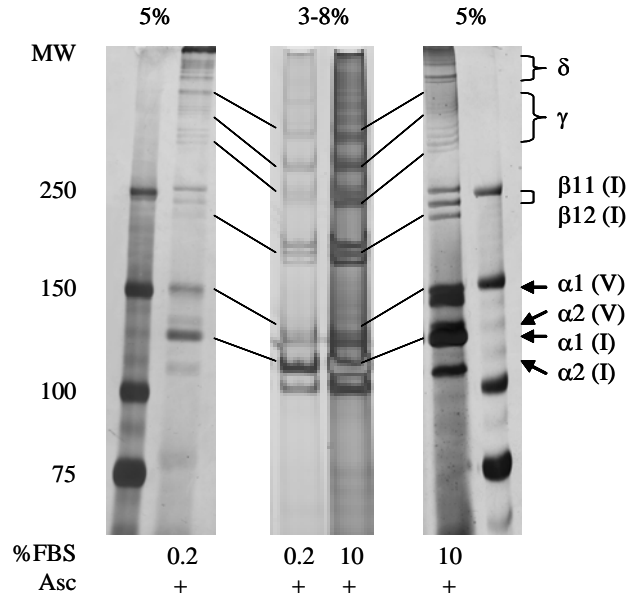


Figure 5.6. Silver-stained non-reducing SDS-PAGE of cell layer fractions in 3-8% Tris-acetate gel, as compared to that in 5% Tris-glycine gels. Two resolved bands were seen around 150 kD. In 3-8% gradient gels containing fresh digest, numerous γ - and δ -bands were demonstrated, with only minute differences in banding patterns under either 0.2% or 10% serum. This demonstrates the presence of non-fibrillar collagens, as well as the degradation of δ -chains into γ -components under 10% serum.

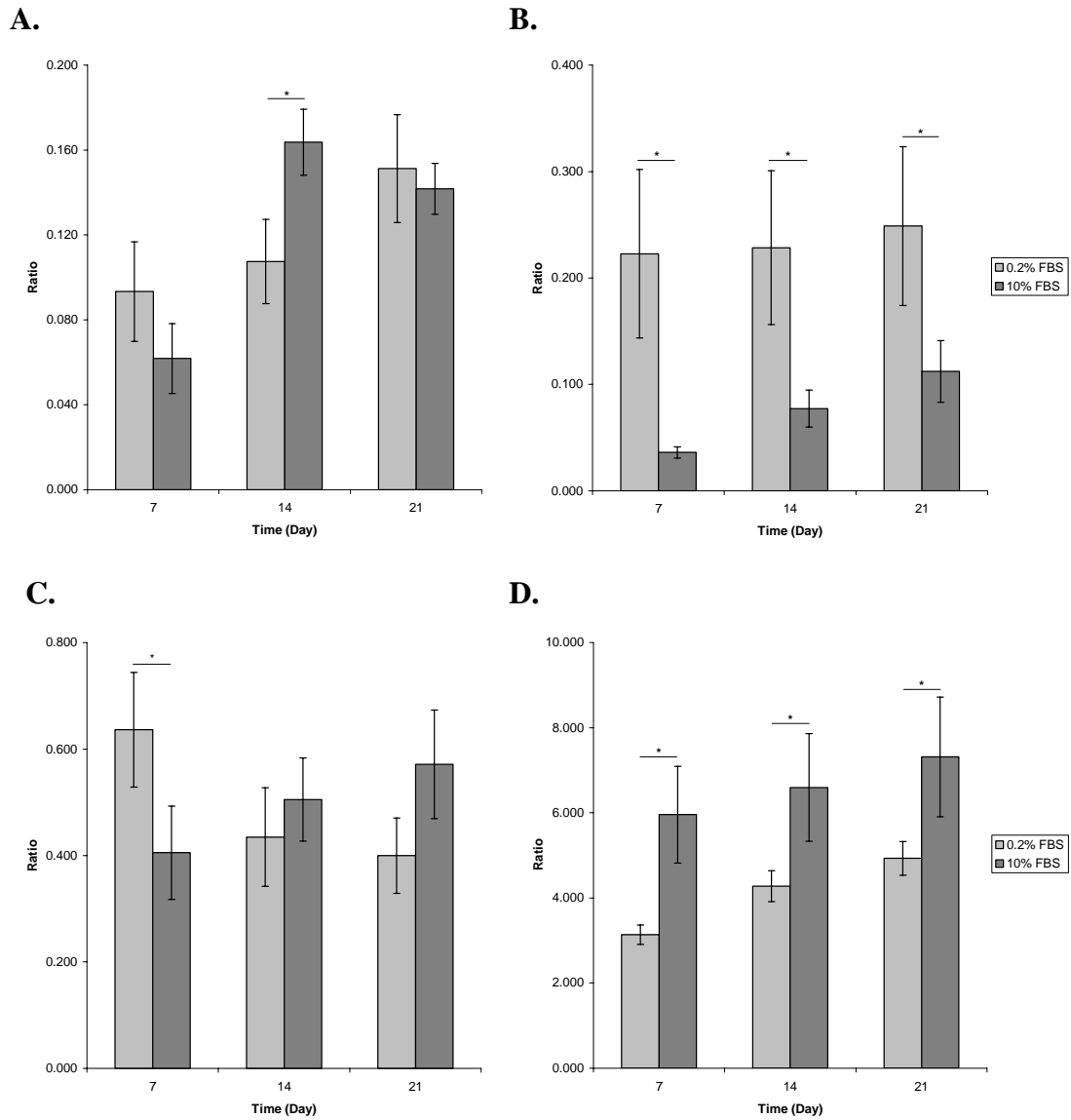


Figure 5.7. Ratio of collagenous peptides obtained by limited pepsin digestion of medium and cell layer fractions under 0.2% and 10% FBS over time, as determined by densitometry. $\alpha 1(\text{III})_3/\alpha 1(\text{I})$ in (A) medium and (B) cell layer fractions, (C) $\alpha 1(\text{V})/\alpha 1(\text{I})$ and (D) $\alpha 1(\text{I})/\beta 11(\text{I})$ in cell layer fractions. Values were expressed as means \pm SD of three independent experiments. * $P < 0.05$; ** $P < 0.01$.

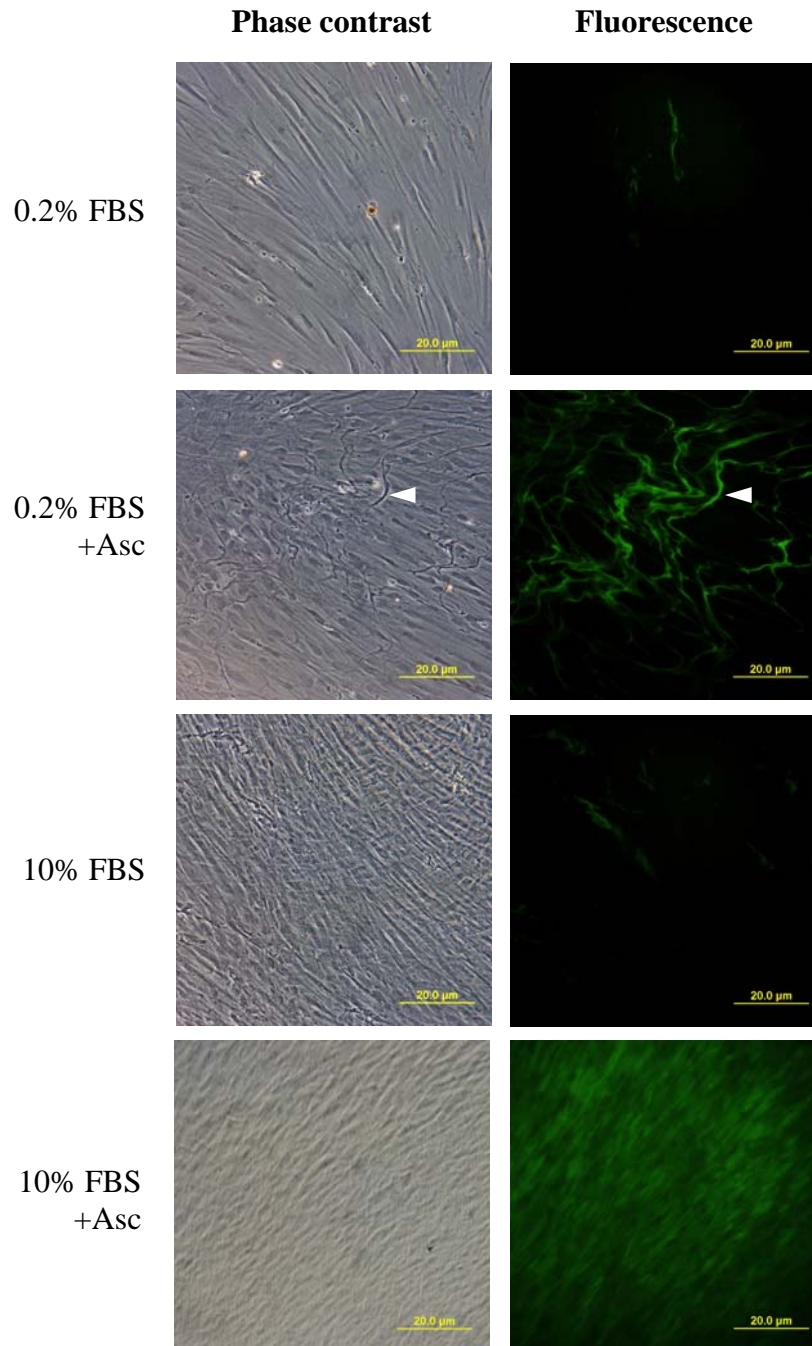


Figure 5.8. Phase contrast light (PCLM) and fluorescence light microscopy images of hPDLF cultures stained with anti-collagen I-FITC antibody at day 21 (200x magnification). Type I collagen fibres were observed in cultures supplemented with ascorbic acid. Thick, irregular fibres observable under light microscopy (arrowhead) were formed in group 0.2% FBS + Asc, whereas dense collagenous matrix, obstructed by post-confluent cells, were seen in group 10% FBS + Asc.

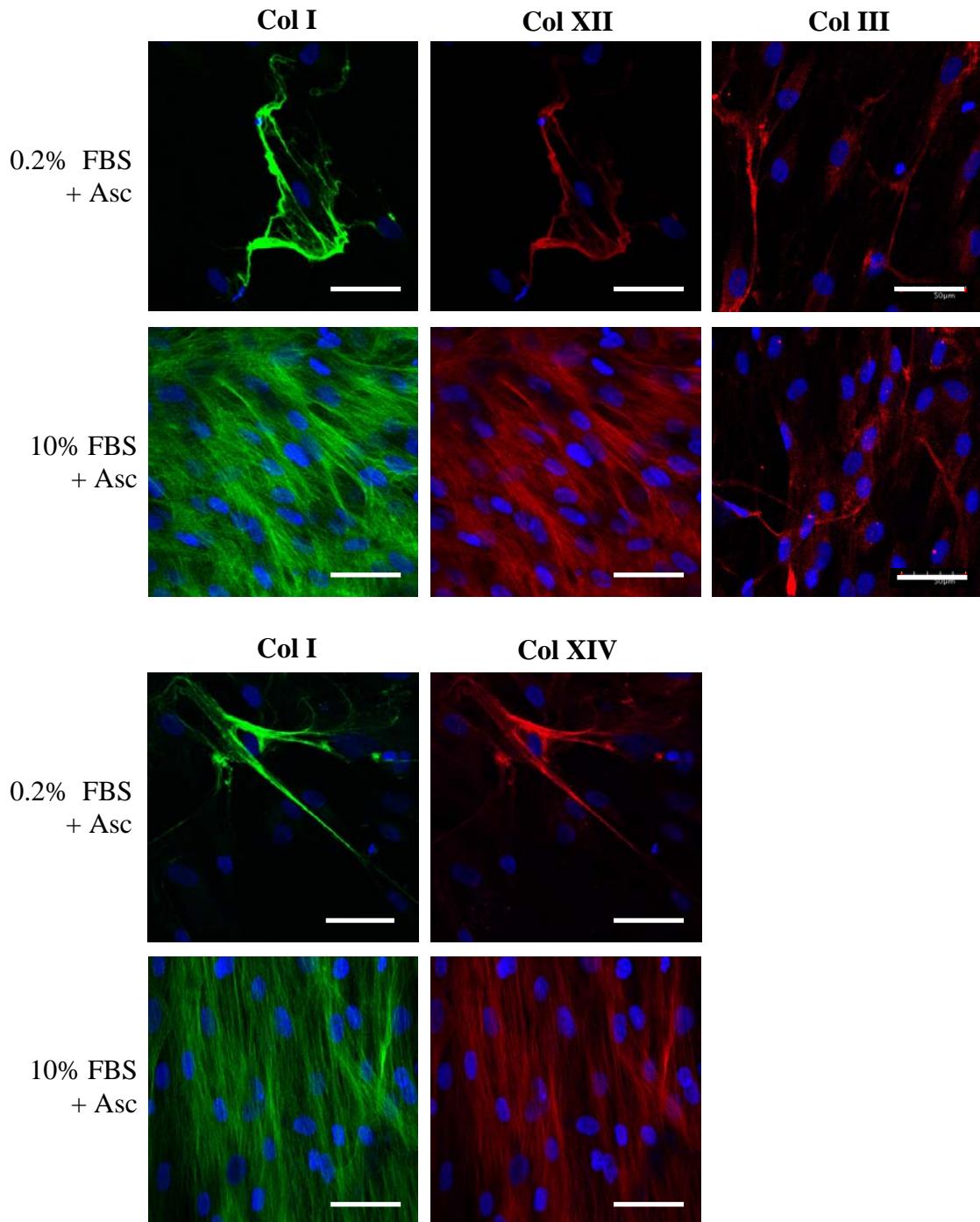


Figure 5.9. Confocal laser microscopy images of hPDLF cultures double immuno-labeled for collagen I/XII and I/XIV, and singly labeled for collagen III at day 21. Cells were counter-stained with Hoechst (scale bar = 50 μm). Thick, non-uniform and highly branched type I fibres (green) were formed in the group 0.2% FBS + Asc. Thin, uniform and parallel type I fibres were demonstrated in the group 10% FBS + Asc. Type XII and XIV (red) co-localized along the length of type I fibres. Type III fibres (red) were less distinct amidst perinuclear staining.

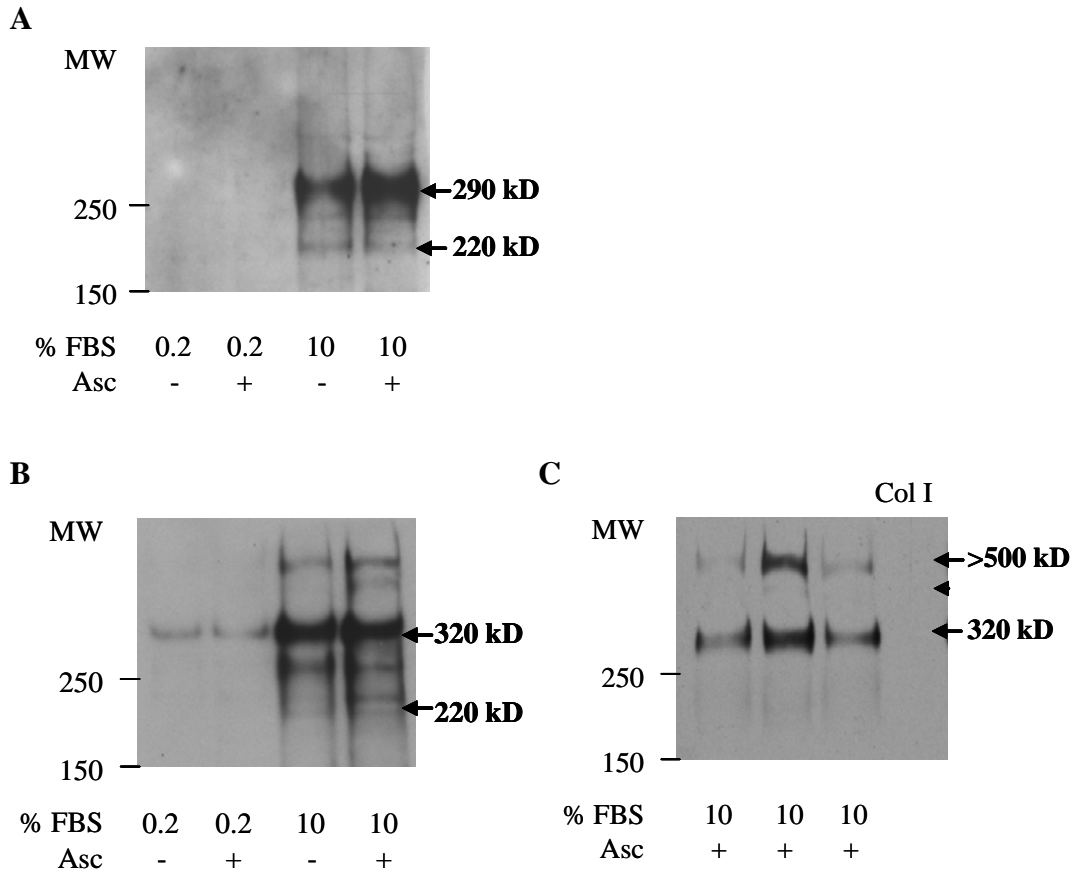


Figure 5.10. Western blot analysis of undigested medium. Conditioned medium were run in reducing 3-8% gradient Tris-acetate gel, transferred onto nitrocellulose membranes, and probed with antibodies against (A) collagen XIV and (B) collagen XII. Type XIV collagen was detected as a prominent ~290-kDa protein under 10% serum. (C) Western blot against collagen XII repeated for hPDLF derived from three other individuals. Type XII collagen was detected as the 320-kD isoform under both 0.2% and 10% serum, and as an additional high M.W. aggregate under 10% serum. No cross-reactivity of anti-collagen XII antibody to type I collagen was observed.

6. DEVELOPMENT OF hPDLF-MEMBRANE CONSTRUCTS

6.1. Background

Having established primary hPDLF cell line as reported in Chapter 4, and characterized the collagen synthetic capability of hPDLF in Chapter 5, this study aimed to evaluate the cytocompatibility of poly(ϵ -caprolactone) (PCL) as a candidate biomaterial for periodontal regeneration.

Cell adhesion to biomaterials, via the sequential events of protein adsorption, cell-substratum contact, cell attachment and spreading (Vogler, 1989; Horbett and Klumb, 1996), is considered to be one of the most important stages in cell-substratum interaction (Kirkpatrick and Dekker, 1992; Anselme *et al.*, 2000). This is because adhesive interactions control cell physiology by regulating cell shape (Folkman and Moscona, 1978), cytoskeleton arrangement (reviewed in Clark and Brugge, 1995; Giancotti and Ruoslahti, 1999) and matrix proteins deposition (reviewed in Schoenwaelder and Burrige, 1999). In turn, the organization of the cytoskeleton and the assembly of matrix proteins such as collagens or fibronectin (FN) determine cell function and proliferation (Sechler and Schwarzbauer, 1998).

The development of PDLF cell-scaffold constructs require the selection of an appropriate biomaterial and the characterization of PDLF on this substrate. PCL was short-listed as a potential biomaterial based on its biodegradability, tissue-compatibility and ease of processing (reviewed in Section 2.6). Biaxially-stretched, perforated PCL membranes, possessing excellent handling characteristics and enhanced gas permeability and fluid diffusability, were postulated to be applicable in tissue engineering (Htay *et al.*, 2004). *In vitro* biocompatibility testing of native PCL homopolymer demonstrated its ability to support the attachment and proliferation of

endothelial cells, fibroblasts, chondrocytes and osteoblasts (Ishaug-Riley *et al.*, 1999; Hutmacher *et al.*, 2001; Verderio *et al.*, 2001; Kweon *et al.*, 2003; Serrano *et al.*, 2004; Tang *et al.*, 2004), with further improvements upon alkali-treatment (Ng *et al.*, 2001; Schantz *et al.*, 2002a; Khor *et al.*, 2003; Thapa *et al.*, 2003; Serrano *et al.*, 2005; Ang *et al.*, 2006). However, the mechanism and the extent of improvement on cell adhesion have not been extensively reported.

FN is responsible for initial cell adhesion events (Yamada *et al.*, 1992), itself alone being sufficient in mediating cell attachment and phenotypic expression (Pierschbacher and Ruoslahti, 1984; Lewandowska *et al.*, 1989). The interaction between FN and $\alpha_5\beta_1$ integrin is highly specific, requiring both the Pro-His-Ser-Arg-Asn (PHSRN) synergy and the Arg-Gly-Asp (RGD) sequences at the 9th and 10th type III repeats (Pierschbacher *et al.*, 1981; Aota *et al.*, 1994). The interdomain tilt, as well as the RGD-PHSRN distance of 32 Å, are both important for $\alpha_5\beta_1$ integrin-mediated cell binding (Altroff *et al.*, 2004). Moreover, this interaction is highly dependent on surface chemistry, as the conformation of adsorbed FN is significantly different on varying substrates (Underwood *et al.*, 1993; Garcia *et al.*, 1999; Keselowsky *et al.*, 2003).

It was hypothesized that the alkali-treatment of PCL membranes facilitated hPDLF adhesion via an increase in the accessibility of the cell-binding domain on adsorbed FN, and that this early interaction would determine subsequent phenotypic expression (Fig. 6.1). As a first step in the development of hPDLF-membrane constructs, FN adsorption and cell adhesion assays reflective of the earliest stages of cell-substratum interactions were conducted, followed by an assessment of cell proliferation and matrix formation, to select a suitable PCL membrane substrate for tissue engineering of the PDL.

6.2. Material and methods

6.2.1. Preparation of PCL membranes

PCL membranes were fabricated as detailed in section 3.1, and classified into four groups as shown in Fig. 6.2. Membranes were cleaned in a sonication bath in 1% sodium dodecyl sulfate (SDS) for 15 min, washed extensively in deionized water and air-dried overnight before surface characterization.

6.2.2. Atomic force microscopy

Surface topography was obtained with a scanning probe microscope (Dimension 3100, Veeco Metrology Group, CA, USA). Membranes, 16 mm x 16 mm, were analyzed by Tapping ModeTM with a silicon cantilever in air. Scan sizes of 50 x 50 μm and 5 x 5 μm were imaged, at scan rates of 0.5 Hz and 1.0 Hz respectively for 256 scanning lines. Three representative atomic force microscopy (AFM) images of each scan size were obtained per membrane in triplicates. Images were subjected to flattening to the first order to remove vertical offset between scan lines, and standardized for the entire set of data. The root-mean-square (RMS) roughness (R_q), corresponding to the standard deviation of Z values within the area, and surface area were calculated from 5 x 5 μm areas and presented as mean value ($n=3$) \pm standard deviation.

6.2.3. Water contact angle measurements

Surface wettability of membranes measuring 8 mm x 8 mm was determined by sessile drop method at 25 °C with a VCA-Optima Surface Analysis System (AST, Singapore). A 1 μl droplet of deionised water was dispensed from the tip of a microlitre syringe. The sample stage was advanced towards the syringe until the

sample made contact with the droplet. The sample stage was then retracted, and the static advancing contact angle calculated from digital image capture. A series of values were obtained at every second up to 5 s, and a graph of contact angle kinetics were plotted to determine the optimal time point. Subsequent measurements were taken at 3 s-time point, and the contact angle was presented as mean value ($n=5$) \pm standard deviation.

6.2.4. Toluidine blue assay

The surface density of anionic carboxyl functional groups was determined by toluidine Blue O (TBO) via visible light spectrometry with slight modifications (Sano *et al.*, 1993). Membranes ($n=5$) before and after alkali-treatment, each 16 mm x 16 mm, were sandwiched between custom-made 316L stainless steel rings (Alson Engineering (S), Singapore) in 12-well plates. Carboxyl groups were complexed with 1 ml of 0.5 mM TBO (Sigma-Aldrich, WI, USA), pH 10, for 3 h under constant agitation at room temperature. Membranes were subsequently sandwiched between fresh rings and rinsed 6 times with an excess of distilled deionized water adjusted to pH 8, each 10 min, to remove non-complexed dye. Desorption of dye molecules bound to the carboxyl groups on membrane surface was conducted with 1 ml of 50% acetic acid solution for 10 min under vortexing, followed by quantification with a spectrophotometer (Unicam UV300, Thermo Spectronic, MA, USA) at 633 nm. Membranes were transferred to fresh wells at every step. The surface density of carboxyl groups was calculated from standard curve of known concentrations of TBO, based on the assumption that TBO was complexed to equivalent moles of carboxyl groups (Sano *et al.*, 1993) on both sides of membranes.

6.2.5. Fibronectin adsorption

Adsorption of FN in the competing presence or absence of a 100-fold excess of BSA was examined by a modified enzyme-linked immunosorbent assay (ELISA), as previously described (McClary *et al.*, 2000; Kowalczyńska *et al.*, 2002). Membrane discs of 4-mm diameter ($n=3$) were floated face down on 100 μl of 2 $\mu\text{g/ml}$ FN (Sigma) in PBS in the presence or absence of 200 $\mu\text{g/ml}$ of BSA (Sigma) for 2 h. Subsequently, membranes were rinsed thrice with 300 μl of PBS-T, blocked with 0.25% (w/v) BSA in PBS for 30 min, and incubated with 100 μl of either anti-human FN polyclonal antibody (Biodesign, ME, USA) or HFN7.1 monoclonal antibody (Developmental Studies Hybridoma Bank, IA, USA) diluted 1:250 in PBS containing 1% (w/v) BSA for 60 min. Membranes were rinsed thrice with PBS-T and blocked, as described above. Incubation with 100 μl of anti-rabbit or anti-mouse antibodies conjugated with alkaline phosphatase (Bethyl Laboratories, Inc., TX, USA) diluted 1:500 in PBS containing 1% (w/v) BSA was performed. After washing and transfer to fresh 96-well plates, the enzyme-substrate reaction was initiated with 200 μl of pNPP substrate (Sigma) per membrane. Negative controls, with primary and secondary antibodies alone, were also performed. To monitor the progression of enzyme-substrate reaction, absorbance at 410 nm was measured at every 5-min intervals with a microplate reader (Magellian, Tecan Group, Switzerland). All steps above were performed at room temperature.

6.2.6. Seeding of hPDLF onto PCL membranes

Primary hPDLF cell lines between passage 3 to 5, derived from third molars of three males aged 21-25 yr (24 ± 2 , mean \pm SD), were seeded at 10,000 cells/cm² in 50 μL aliquots containing DMEM (Gibco, Life Technologies, NY, USA), 10% FBS and

2% penicillin-streptomycin onto membranes, 16 mm x 16 mm, sandwiched between custom-made 316L stainless steel rings for the retention of cell suspensions. For cell adhesion and proliferation controls, cells were seeded in a similar manner onto 12-well tissue culture plates (TPP, MO, USA). Cell adhesion and morphology were monitored with PCLM (Olympus, IX70, Tokyo, Japan) after the removal of unattached cells with several rinse of PBS. Culture medium was added after incubation at 37 °C and 5 % CO₂ for 2-3 h when cell adhesion was achieved. Cell-seeded membranes were cultured in suspension in 12-well plates (TPP) for 3 weeks, and supplemented with 200 µM ascorbic acid 2-phosphate magnesium salt (Asc; Sigma) for induction of collagen synthesis, with medium change every 3 days.

6.2.7. Cell adhesion efficiency

Cell adhesion efficiency on membranes was determined at various time intervals after seeding (1, 2, 6 and 18 h) with PicoGreen® dsDNA quantitation assay (Section 3.3; Molecular Probes, Invitrogen, CA, USA), with slight modifications. Cell-seeded membranes ($n=3$) were disassembled from rings, washed thrice with PBS to remove unattached cells and freeze-stored at -80 °C overnight. Next, the cell-seeded membranes were thawed to room temperature and incubated in 100 µl of autoclaved distilled water in a sealed well at 37 °C for 1 hr, before being subjected to a second round of freeze-thaw. Samples and DNA standards in 100 µl aliquots were incubated with equal volumes of PicoGreen reagent, pre-diluted 200-fold in TE buffer, in triplicates in an opaque 96-well plate (TPP) for 5 min at room temperature in the dark. Fluorescence was measured at 485 nm excitation and 535 nm emission in a microplate reader (GENios, Tecan Group, Switzerland). Cell adhesion efficiency was

defined as the percentage of dsDNA harvested from attached cells on the membrane at the time of harvest / seeded (control).

6.2.8. Focal contact formation

Focal contact formation was determined *in situ* by localization of vinculin. Cells were seeded at 30% confluence onto substrates, simultaneously permeabilized and fixed in 3.7% paraformaldehyde containing 0.5% (v/v) Triton X-100 in cytoskeletal buffer for 5 min at room temperature, and subsequently post-fixed in 3.7% (w/v) paraformaldehyde for an additional 30 min at 4 °C (Kam *et al.*, 1995) to remove cell structures as well as vinculin not located in focal adhesions. Cells seeded similarly on LabTek chamber slides (Nunc, Inc., IL, USA) were used as positive controls. After rinsing thrice with cytoskeleton buffer, 3 min each time, cells were incubated in blocking buffer containing 2% (w/v) BSA and 7% (v/v) FBS in PBS for 30 min at room temperature. Cells were incubated with anti-vinculin monoclonal antibody, clone 3F393 (USBiological, MA, USA), diluted 1:100 in blocking buffer for 1 h at room temperature, and rinsed thrice with PBS-T, 5 min each time. For double-labelling of actin and vinculin, cells were incubated with Alexa Fluor 488-conjugated phalloidin (Section 3.12; Molecular Probes), and anti-mouse-tetramethylrhodamine isothiocyanate (TRITC)-conjugated secondary polyclonal antibody (DAKO, CA, USA), diluted 1:100, in 1% BSA in cytoskeleton buffer for 45 min at room temperature in the dark, followed by thrice rinsing with PBS-T, 5 min each time. Omission of primary antibodies and staining with secondary antibodies alone served as negative controls.

6.3. Results

6.3.1. Alkali-treatment and perforation increased surface roughness and area

Biaxially stretched membranes (mean thickness \pm SD, $10 \pm 2 \mu\text{m}$) with perforations (mean diameter \pm SD, $100 \pm 10 \mu\text{m}$) of $400/\text{cm}^2$ -density were fabricated. Representative surface morphologies of membranes obtained by SEM and AFM were shown (Fig. 6.3). UP/UT (native) membranes appeared smooth, with uniform distribution of uniaxially-oriented polymer fibrils (arrows) visible at 100x (inset) and 5000x magnification, as well as under AFM. The filamentous morphology of membranes is due to biaxial drawing of heat-pressed films, during which polymer fibrils were orientated along the lines of stress (Ng *et al.*, 2000). P/UT membranes possessed a textured but relatively smooth surface topography. Polymer fibrils (arrows) were less prominent than UP/UT membranes under AFM. Alkali-treated UP/T membranes showed a granulated morphology with a loss of surface fibril feature. P/T membranes possessed a similar granulated surface morphology with prominent macropores (inset), representing amorphous regions which were preferentially degraded in the presence of alkali (Ali *et al.*, 1993; Htay *et al.*, 2004).

Both UP/T and P/T membranes exhibited an increase in nano-scale surface roughness in the form of voids at sub-micron levels (arrowheads) to macropores (inserts), as reported elsewhere (Vance *et al.*, 2004), attributable to surface erosion during alkali-treatment (Htay *et al.*, 2004). Membrane perforation further augmented surface erosion at sites of perforation due to their high strain energy (Htay *et al.*, 2004). Image analysis of $5 \mu\text{m} \times 5 \mu\text{m}$ scan size showed that RMS surface roughness, corresponding to the standard deviation of Z values relative to the mean plane (Fig. 6.4A), was significantly increased on perforated (P vs. UP) as well as alkali-treated (T vs. UT) membranes ($p < 0.001$). Corresponding surface area (Fig. 6.4B) was more

significantly increased on alkali-treated membranes ($p < 0.001$) than it was on perforated membranes ($p < 0.05$).

6.3.2. Alkali-treatment increased surface wettability and accessibility of HFN7.1

Native membranes were hydrophobic, with an average static advancing contact angle of $81.0 \pm 4.8^\circ$. The contact angles on perforated membranes were not taken into consideration, as perforations were found to disturb the surface tension of the water droplet. During alkali-treatment, hydroxide anions hydrolyze ester bonds, breaking the polymer chain and exposing carboxyl and hydroxyl groups at the termini of two new chains (Gao *et al.*, 1998). To monitor the extent of hydrolysis, the surface density of anionic carboxyl functional groups was determined by toluidine Blue O (TBO), a cationic dye that binds to negatively charged groups (Kiernan, 2001). Alkali-treatment caused a two-fold increase in carboxyl functional group surface density. The values increased from 0.31 ± 0.05 nmol/cm² to 0.61 ± 0.05 nmol/cm² on unperforated membranes ($p < 0.001$), and from 0.34 ± 0.05 nmol/cm² to 0.62 ± 0.07 nmol/cm² on perforated membranes ($p < 0.001$). This was translated to an increase in the wettability of membranes, with a drop in static advancing contact angle to $69.0 \pm 4.1^\circ$ ($p < 0.001$).

HFN7.1 monoclonal antibody, whose epitope maps to a segment spanning the flexible link between the 9th and 10th type III repeats (Schoen *et al.*, 1982; Bowditch *et al.*, 1991), has been demonstrated to be an effective probe for the presentation of cell-binding domain in FN (Keselowsky *et al.*, 2003). Given that FN adsorption may lead to conformation change via domain rotation or extension (Baugh and Vogel, 2004), the binding of HFN7.1 to adsorbed FN on membranes was assayed using a modified ELISA (McClary *et al.*, 2000; Kowalczyńska *et al.*, 2002). In addition, a polyclonal

antibody targeting both native and denatured plasma FN (Yamada, 1983) was used to determine the extent of adsorption.

FN adsorbed from a concentration of 2 µg/ml in the presence and absence of a 100-fold excess (physiological ratio) of BSA (Grainger *et al.*, 2003), was assayed. Optical density as a function of enzyme-substrate reaction time at 5-min intervals revealed an approximately linear relationship up to 30 min, demonstrating the linear dependence of measured signals on the number of linked enzyme centres (results not shown). Optical density signals were lower in the presence of BSA, indicating competitive binding as reported previously (McClary *et al.*, 2000). An optical density signal at 30 min was chosen for statistical analysis. In the absence of BSA (Fig. 6.5A), optical density signal of anti-human FN polyclonal antibody was significantly higher on perforated (P vs. UP) ($p < 0.001$) and alkali-treated (T vs. UT) membranes ($p < 0.001$). In the presence of competing BSA, values were significantly higher on perforated membranes ($p < 0.05$) only. ELISA performed with HFN7.1 monoclonal antibody produced significantly higher values on perforated ($p < 0.01$) as well as alkali-treated membranes ($p < 0.01$) in both the absence and presence of BSA (Fig. 6.5 B). Therefore, the preferential binding of HFN7.1 indicated a greater accessibility of the synergy and RGD domains on FN adsorbed to alkali-treated membranes, regardless of the presence of competitive BSA.

6.3.3. Alkali-treatment increased cell adhesion and formation of focal contacts

In order to correlate the surface wettability of membranes and their capacity to support hPDLF adhesion, cell morphology was evaluated by direct observation with PCLM at 1 h, 2 h, 6 h and 18 h after seeding in serum-supplemented culture medium (magnification 600X) (Fig. 6.6). The above time points were chosen based upon a

previous characterization of cell adhesion kinetics on PCL, in which adhesion rates reached a plateau beyond 6 h (Ishaug-Riley *et al.*, 1999). hPDLF demonstrated filopodia (black arrows) on P/T and UP/T membranes by 1 h and 2 h, respectively. Cell flattening was observed on P/T membranes by 2 h, as seen from a decrease in phase contrast at cell boundary. In comparison, hPDLF remained spherical after 2 h on untreated membranes. At 6 h, pronounced cell clustering and formation of long cytoplasmic projections (black arrowheads) were observed on UP/UT membranes. By 18 h, cell spreading was complete, with increased cytoplasmic membrane density at the periphery of sheet-like lamellipodia (white arrows). A greater degree of hPDLF spreading was obtained on alkali-treated membranes.

The same samples used for cell morphology evaluation with PCLM were used to determine hPDLF adhesion efficiency, expressed as the percentage of dsDNA harvested from attached cells over that from the initial cell suspension, on the various membranes. Adhesion efficiency was significantly enhanced on alkali-treated (T vs. UT) membranes ($p < 0.001$) at 1 h, 2 h, 6 h and 18 h after seeding (Fig. 6.7). hPDLF demonstrated an initial burst in adhesion rate at 1 h, reaching a plateau of 51-55% at 6 h on alkali-treated membranes. On untreated membranes, cell adhesion rose gradually over time, reaching only 23-28% at 6 h, in agreement to a previous report of human articular chondrocytes on native spin-cast PCL films (Ishaug-Riley *et al.*, 1999). At 18 h, a slight increase attributable to DNA synthesis in cells having passed the restriction point in the cell cycle (reviewed in Skehan, 1988) was observed on alkali-treated membranes.

From PCLM observations, it was evident that cell adhesion was complete by 6 h, but cell spreading took place between 6 to 18 h (Fig. 6.6). Since cell spreading is controlled by cytoskeletal architecture (Cramer and Mitchison, 1995), the formation

of actin stress fibres and focal adhesions at later stages of cell adhesion were analyzed by confocal microscopy (Fig. 6.8). Immunolabelling of vinculin, a key component in focal adhesions (Zamir and Geiger, 2001), was performed. A pre-permeabilization technique was employed to facilitate the specific localization of vinculin to focal adhesions (Niederreiter *et al.*, 1994). At 6 h, *f*-actin organization and weak signals of vinculin (arrowheads) as focal complexes at cell periphery were observed on P/UT, UP/T and P/T membranes. At 12 h, *f*-actin remained disorganized in cells on UP/UT membrane, whereas it was incorporated into microfilament bundles (arrows) on alkali-treated membranes. Punctuated staining for vinculin, indicative of dot-like focal adhesions constituted of transmembrane and linker proteins (Bershadsky *et al.*, 1985), was seen on untreated membranes. Elongated staining for dash-like focal contacts of at least 2 μm in length from an association of transmembrane proteins with cytoskeletal actin (Bershadsky *et al.*, 1985) was obtained on alkali-treated membranes. By 24 h, stress fibres were observed on alkali-treated membranes, with concomitant formation of mature focal contacts approximately 5 μm in length, demonstrated by long spikes of vinculin at the terminating ends of stress fibres, indicative of FN assembly (Sechler and Schwarzbauer, 1997). On untreated membranes, stress fibres and focal contacts were sparse or poorly formed. Close-up images (numbered boxes) of vinculin at 24 h (Fig. 6.9) revealed centrally located focal adhesions (arrows) resembling “fibrillar” adhesions (Zamir *et al.*, 2000) on UP/T membranes, and elongated adhesions 10-20 μm in length (arrowhead) resembling “supermature” focal adhesions characteristics of myofibroblasts (Dugina *et al.*, 2001; Hinz *et al.*, 2003) on both UP/T and P/T membranes. These structures were absent from cells on untreated membranes.

6.3.4. hPDLF-membrane constructs demonstrated FN and collagenous matrix formation in the process of maturation

Thus far, an association between the conformation of adsorbed FN and the ability to support cell adhesion up to 24 h was established. To examine subsequent cell behaviour with the aim of developing hPDLF-membrane constructs, cells were cultured on membranes for up to 21 days in comparison with tissue culture plate (TCP) *in vitro*. Following initial attachment, hPDLF failed to maintain cell-substratum interactions; cytoplasmic retraction and significant cell clustering on untreated membranes were observed (Appendix). This precluded further characterization. Hence, UP/UT and P/UT membranes were excluded from subsequent experiments.

On UP/T and P/T membranes, hPDLF proliferated, migrated away from the site of seeding and reached cell confluency on hPDLF-membrane constructs as seen after Haematoxylin stain at day 21. Cell alignment on UP/T membranes was mostly unidirectional (Fig. 6.10A), whereas cells bridged between perforations on P/T membranes (Fig. 6.10B). hPDLF were found to migrate along membrane “flaps” (arrow) on P/T membranes (Fig. 6.10C) and adhere to the underneath side as seen under phalloidin staining (Fig. 6.10D), demonstrating contact guidance. Cells demonstrated strong staining for *f*-actin on both UP/T and P/T membranes (Fig. 6.10E, F) respectively at day 14. FDA/PI staining revealed high cell viability, as indicated by a high number of live cells (green) and a low number of dead cells (red) (Fig. 6.10G, H). Detachment of cell sheet (absence of staining) was observed on UP/T membranes at day 21 (Fig. 6.10G). Image analysis by Micro-Image® (Media Cybernetics, MD, USA), detailed in section 3.4, was used to quantify cell sheet coverage (Fig. 6.11). Results showed that hPDLF coverage was initially higher on UP/T membranes at day

7 ($p < 0.05$). However, coverage on P/T membranes caught up at day 14, and surpassed UP/T membranes at day 21 ($p < 0.01$).

In order to rule out cell proliferation as a contributing factor to differing cell retention over time, cell growth represented as dsDNA on the membranes and tissue culture plate (TCP) as a control were determined by PicoGreen® assay (Ng *et al.*, 2005), with slight modifications detailed in section 3.3. Results showed that there was a greater rate of cell proliferation on UP/T membranes up to day 14, but there was no statistically significant difference in the quantity of dsDNA harvested from UP/T and P/T membranes ($p > 0.05$) throughout 21 days (Fig. 6.12). The lower amount of dsDNA on membranes compared to TCP, approximately 55-67% at day 1, might be related to a reduced cell seeding efficiency (Fig. 6.7). Therefore, it could be inferred that cell numbers on UP/T and P/T were similar at the end of culture period, and cell sheet coverage was independent of cell number.

Given that cells on UP/T and P/T membranes displayed differences in focal adhesion morphology and distribution, it was speculated that substrate-induced differences in cell adhesion might influence downstream ECM synthesis and phenotypic expression. Western blot analysis of reducing SDS-PAGE containing whole cell lysates normalized by total protein quantity showed that the level of α -smooth muscle actin (~45 kDa), a mechano-sensitive protein that is constitutively expressed by hPDLF and recruited to stress fibres under high tension (Arora and McCulloch, 1994; Wang *et al.*, 2006), was similar in all samples at day 21. The level of FN (~240 kDa) produced by hPDLF-membrane constructs were also equivalent (approximately 1:1), but the amounts were approximately 30% of that on TCP (Fig. 6.13). Non-reducing SDS-PAGE of pepsin digests demonstrated the presence of collagens secreted into medium and deposited into cell layer (Fig. 6.14). Bands

corresponding to α -chains of major fibrillar collagens, type I, III and V, were detected. Type I collagen β -chains, indicative of cross-linking in the collagenous matrix (Rao *et al.*, 1982) were present. The relative proportions of collagen I, the predominant collagen in ECM of the PDL, was determined by densitometric analysis. The amount of secreted collagen I in the medium was similar in all samples, whereas the deposition of collagen I on membranes was approximately 60% of that on TCP.

Matrix organization on hPDLF-membrane constructs at day 21 were investigated by immunofluorescence for FN and type I collagen (Fig. 6.15). Confocal laser microscopy images confirmed the presence of fibrillar FN (red) and type I collagen (green). Fibrillar FN was randomly oriented and often seen lining the periphery of individual cells or cell clusters on both TCP and UP/T membranes. Collagenous matrix was in a similar orientation to fibrillar FN, the alignment of both was greater on P/T membranes. PCLM images depicting the corresponding surface morphology of hPDLF-membrane constructs demonstrated that cells on P/T membranes responded to contact guidance, aligning both cell and matrix to surface topography in the form of substrate grooves or folds (arrows), as shown previously (Teixeira *et al.*, 2003; Manwaring *et al.*, 2004). In particular, prominent collagen fibres were seen in highly aligned confluent cells traversing sites of perforation (arrowhead) on P/T membranes.

To investigate whether hPDLF-membrane constructs reached matrix maturation, ALP activity which peaks during the post-proliferative period of matrix maturation (Owen *et al.*, 1990; Sodek and Cheifitz, 2000) was assayed (Fig. 6.16). ALP activity normalized by total intracellular protein was upregulated in cells on TCP at day 14 up to a value of 0.29 IU/mg, after which it declined at day 21. This was in accordance to ALP induction patterns as previously described (Chapter 4). Cells on

UP/T and P/T membranes followed a pattern of delayed induction, reaching 0.29-0.35 IU/mg at day 21. ALP level on P/T membranes was significantly higher than UP/T membranes at day 14 ($p < 0.01$) and TCP at day 21 ($p < 0.01$). All ALP values were within the range reported for hPDLF under collagen induction (Appendix).

6.4. Discussion

6.4.1. Cytocompatibility of alkali-treated PCL membranes

In this study, alkali-treatment of biaxially stretched PCL membranes of $M_n = 10 \times 10^3$ and $M_w = 14 \times 10^3$ (Htay *et al.*, 2004) at 5 M NaOH and room temperature led to a two-fold increase in surface carboxyl functional group and an approximately 10-nm increase in RMS surface roughness (Fig. 6.4A). Alkali-treated membranes facilitated cell adhesion, increasing both rate and total adhesion efficiency by two-folds (Fig. 6.7), attributable to a greater accessibility of FN cell-binding domain (Fig. 6.5B).

A correlation between FN adsorption and cell adhesion, however, was not seen. Specifically, the amount of FN adsorption (Fig. 6.5A) was not significantly higher on UP/T membranes, unlike previous reports (Rouxhet *et al.*, 1998; McClary *et al.*, 2000). MicroBCA assay, as described previously (Ishihara *et al.*, 1999), showed that FN adsorption from a pure solution of 20 $\mu\text{g/ml}$, a 10-fold dilution of physiological plasma level (Hynes, 1990), resulted in $0.58 \pm 0.21 \mu\text{g/cm}^2$ and $0.30 \pm 0.10 \mu\text{g/cm}^2$ on UP/UT and UP/T membranes respectively (unpublished data). The surface densities of FN on native and alkali-treated PCL, within the range reported for tissue culture polystyrene at $0.4 \mu\text{g/cm}^2$ (Haas and Culp, 1982), were in agreement with a previous report that the saturation densities of FN on self-assembled monolayers (SAMs) were higher for CH_3 - than for COOH - and OH -presenting SAMs (Keselowsky *et al.*, 2003). Hence, the apparent contradiction could be attributed to the

method of detection, where higher FN densities were obtained on hydrophilic surfaces via radio-labelled-FN or -primary antibodies (Rouxhet *et al.*, 1998; McClary *et al.*, 2000), as compared to enzyme-tagged secondary antibodies for ELISA in this study and elsewhere (Kowalczyńska *et al.*, 2002).

In the case of perforated membranes, some peculiarities in the optical density ELISA readings were observed. Perforation alone resulted in increases in RMS surface roughness and area (Fig. 6.4), but not in surface density of carboxyl functional groups. In light of this, the significantly elevated FN adsorption and accessibility of cell-binding domain (Fig. 6.5) might be attributed to a leakage of FN solution through the perforations during adsorption and the resultant increased binding of antibodies to the top surface despite precautions. Nonetheless, a higher relative density of adsorbed FN and cell-binding domain on P/T membranes could be inferred from the earlier onset of cell flattening (Fig. 6.6) and focal complex formation (Fig. 6.8), given that cell adhesion and spreading increases with increasing RGD surface density (Berg *et al.*, 2004).

On native PCL, the reduction in cell-binding domain accessibility despite similar levels of FN adsorption to alkali-treated surfaces, was indicative of FN conformational change. Indeed, FN favours a compact conformation on hydrophobic surfaces accompanied by a greater perturbation of secondary structure (Culp and Sukenik, 1998), but an elongated one on hydrophilic surfaces via dimer arm extension (Bergkvist *et al.*, 2003; Baugh and Vogel, 2004). This was reflected in a retardation of cell spreading and a lack of well-developed stress fibres and focal contacts, suggestive of a disruption in $\alpha 5\beta 1$ integrin-mediated RhoA activation (Nobes and Hall, 1995), as reported for CH_3 -presenting SAMs (McClary *et al.*, 2000). Moreover, the

predominance of “classical” focal contacts restricted to cell periphery was indicative of $\alpha_v\beta_3$ integrin-mediated cell adhesion (reviewed in Zamir and Geiger, 2001).

6.4.2. Evaluation of hPDLF-membrane constructs

Further evaluation of 21-day cultures of constructs consisting of UP/T and P/T membranes revealed a prominent alignment of *f*-actin as well as a deposition of FN and collagen into the ECM. The loss of cell sheet observed on UP/T membranes (Fig. 6.10G) was speculated to result from a contractile phenotype, since the upregulation of actin bundle alignment in fibroblasts and collagen and FN matrix assembly have been found to coincide with tissue contraction (Welch *et al.*, 1990). However, hPDLF constitutively expressed similar levels of α -smooth muscle actin on UP/T and P/T membranes (Fig. 6.13).

Cell adhesion responses to topography and surface ligand density were cooperative (Ranucci and Moghe, 2001). Given that P/T membranes possessed surface texture in the form of perforations (Fig. 6.3) and supported the preferential development of “supermature” focal adhesions (Fig. 6.9) as compared to UP/T membranes, the higher cell coverage could be attributed to strengthened adhesion onto P/T membranes, attributed to cell anchorage at membrane “flaps” (Fig. 6.10C, 6.15). This affirmed the importance of surface topography in terms of organized roughness or texture, which was reported to play a greater role in adhesion than roughness amplitude (Anselme *et al.*, 2000; Ranucci and Moghe, 2001). Moreover, this also showed that biaxially stretched membranes, possessing a tensile strength of 42-55 MPa (Ng *et al.*, 2001; Ang *et al.*, 2006), are sufficiently rigid to withstand cell traction forces exerted by hPDLF.

Surface topography of P/T membranes led to a greater alignment of ECM matrix (Fig. 6.15). This would have implications in tissue engineering of the PDL, where collagen fibre alignment is essential in maintaining the tooth in a functional position and in resisting displacement forces during occlusal loading (reviewed in Kirkham and Robinson, 1995). Furthermore, the addition of appropriate surface topographies to guided tissue regeneration (GTR) membranes, by discouraging epithelial cell migration and promoting osteoblastic differentiation, is proposed to have the potential of improving clinical performance in periodontal tissue regeneration procedures (Owen *et al.*, 2005b).

In comparison to TCP, alkali-treated membranes did not facilitate as much ECM matrix formation (Fig. 6.13, 6.14), even though cell proliferation, viability and collagen synthetic ability of hPDLF on membranes were not perturbed (Fig. 6.10, 6.12). Collagen deposition was two-fold higher and FN production was three-fold higher on TCP. Given that FN acts as a template for collagen deposition (reviewed in Embery *et al.*, 1992), it therefore appeared that FN matrix assembly was the limiting factor for collagen deposition on PCL membranes. Even so, hPDLF on PCL membranes were able to undergo matrix maturation over time, as seen from the ALP upregulation at day 21 (Fig. 6.16), hypothetically due to substratum conditioning by cells during prolonged culture (Lim *et al.*, 2004).

In summary, cytocompatibility of alkali-treated PCL membranes was increased, attributable to a greater accessibility of fibronectin cell-binding domain. hPDLF-membrane constructs of perforated PCL membranes provided greater cell anchorage, and cell and matrix alignment than unperforated ones via contact guidance, while retaining its phenotypic expression of major collagen types and promoting matrix maturation.

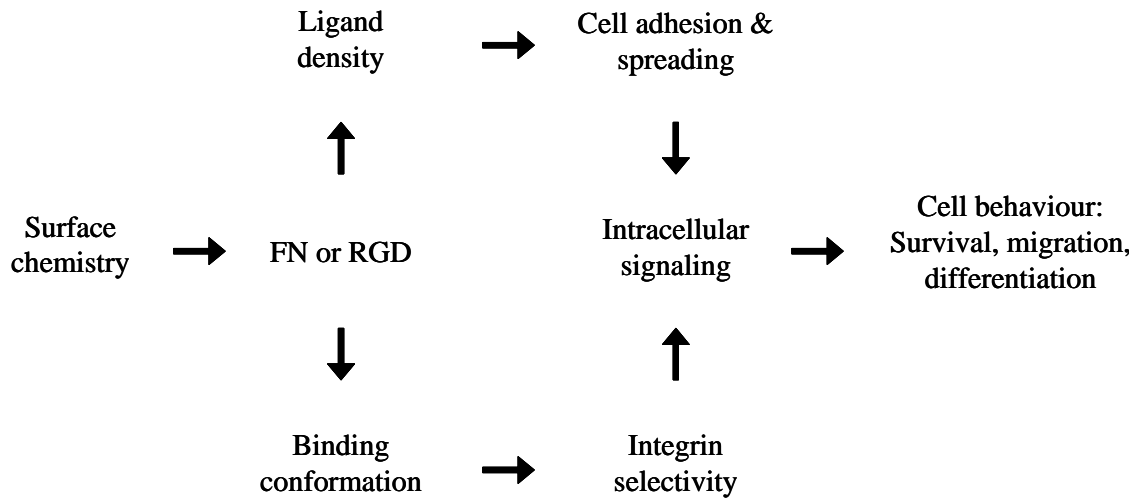


Figure 6.1. Modulation of cell behaviour through substrate-dependent changes in FN conformation (adapted from Garcia *et al.*, 1999).

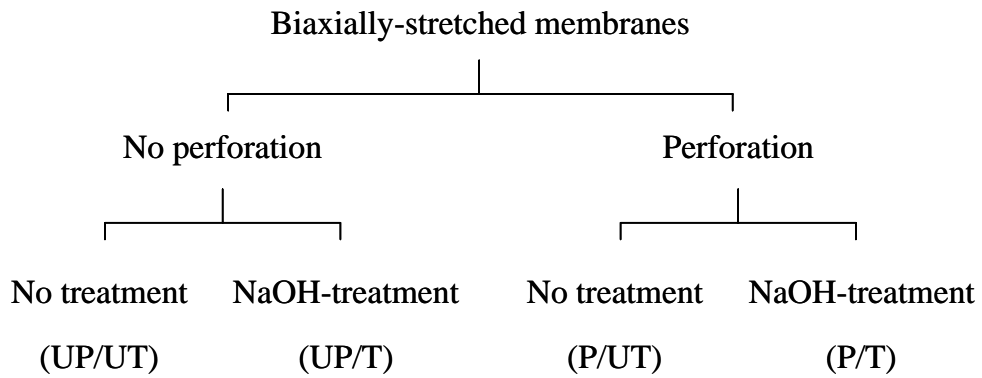


Figure 6.2. Manufacturing procedure and classification of PCL membranes.

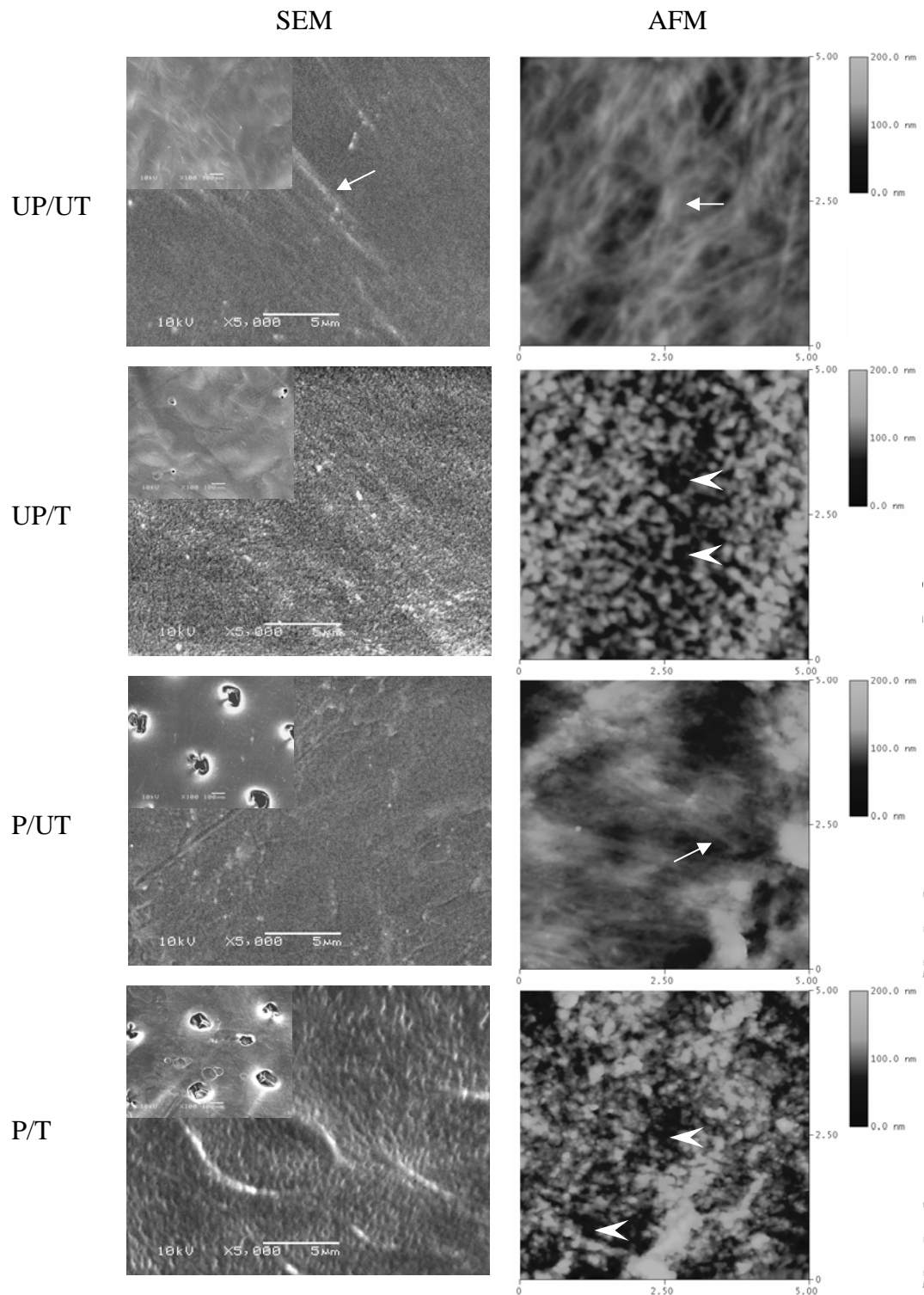


Figure 6.3. Representative surface morphologies of UP/UT, UP/T, P/UT, P/T membranes obtained by scanning electron (SEM) and atomic force (AFM) microscopy. UP/UT (native) membranes appeared smooth, with uniform distribution of uniaxially-oriented polymer fibrils (arrows). P/UT membranes possessed a textured but relatively smooth surface topography. UP/T membranes showed a granulated morphology with a loss of surface fibril feature. P/T membranes possessed a similar granulated surface morphology with prominent micropores (inset). Both UP/T and P/T membranes exhibited an increase in nano-scale surface roughness in the form of voids at sub-micron levels (arrowheads) to micropores (inserts).

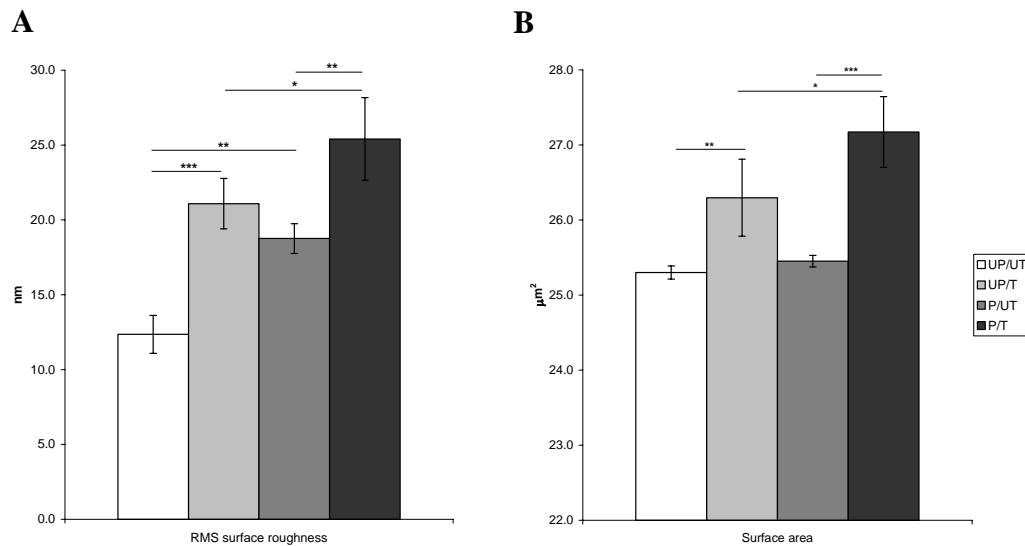


Figure 6.4. (A) Root-mean-square (RMS) surface roughness and (B) surface area of membranes obtained by AFM at a scan size of 5 µm x 5 µm. RMS surface roughness was significantly increased on perforated (P vs. UP) as well as alkali-treated (T vs. UT) membranes ($p < 0.001$). Image surface area was significantly increased on alkali-treated membranes ($p < 0.001$), but only slightly increased on perforated membranes ($p < 0.05$). Data are presented as mean \pm SD, $n = 3$. * $P < 0.05$; ** $P < 0.01$; *** $P < 0.001$.

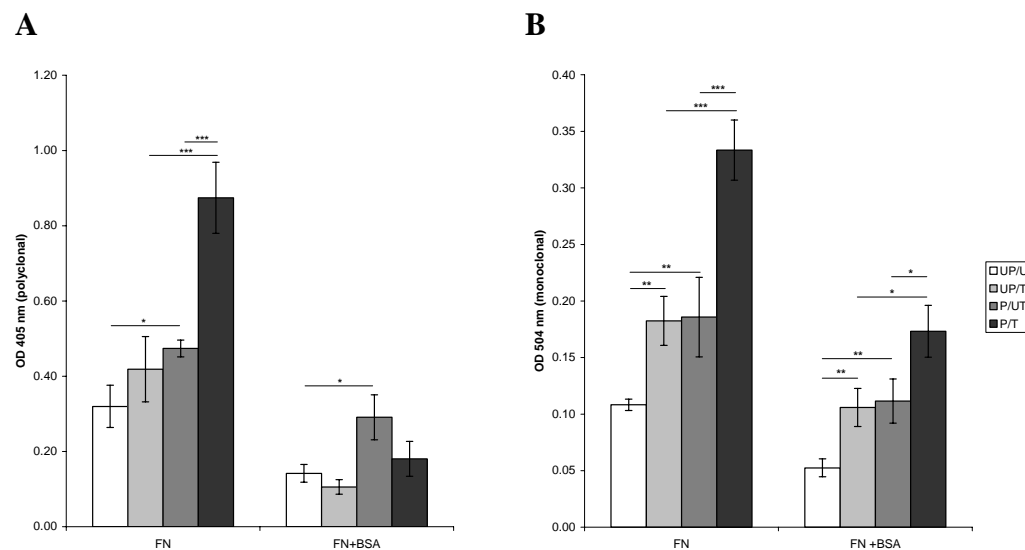


Figure 6.5. Optical density of ELISA of antibody binding to FN adsorbed from 2 µg/ml by (A) anti-FN polyclonal antibody and (B) HFN7.1 monoclonal antibody in the absence and presence of a 100-fold excess of BSA. (A) In the absence of BSA, binding of polyclonal antibody was significantly higher on perforated (P vs. UP) ($p < 0.001$) and alkali-treated (T vs. UT) membranes ($p < 0.001$). In the presence of competing BSA, binding of polyclonal antibody was significantly higher on perforated membranes ($p < 0.05$) only. (B) In contrast, binding of HFN7.1 was significantly higher on perforated ($p < 0.01$) as well as alkali-treated membranes ($p < 0.01$) in both the absence and presence of competing BSA. Data are presented as mean \pm SD, $n = 3$. * $P < 0.05$; ** $P < 0.01$; *** $P < 0.001$.

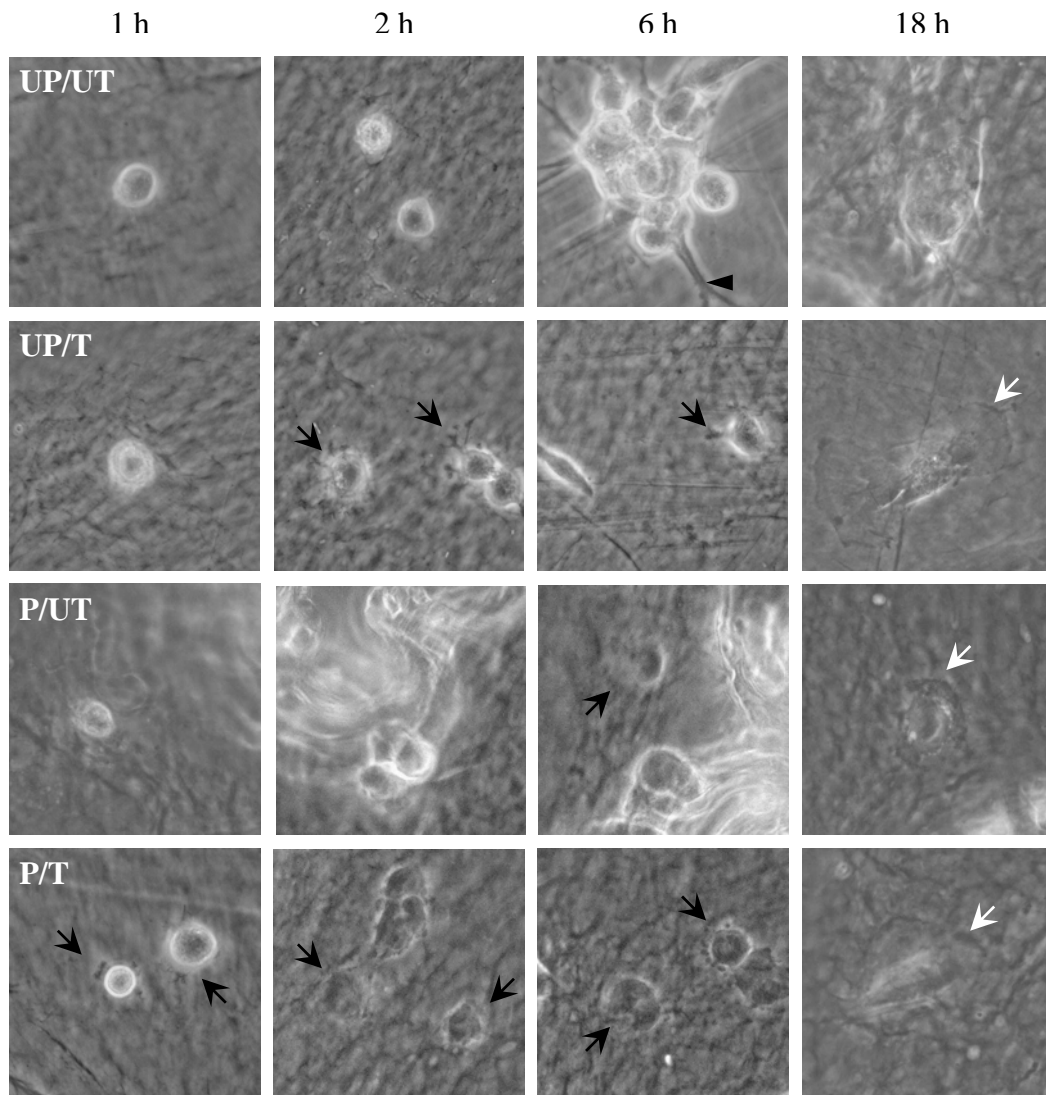


Figure 6.6. Representative PCLM images of hPDLF attached onto UP/UT, UP/T, P/UT, and P/T membranes at 1, 2, 6 and 18 h after seeding in culture medium containing 10% serum (magnification 600X). hPDLF demonstrated filopodia (black arrows) on P/T and UP/T membranes by 1 h and 2 h, respectively. Cell flattening was observed on P/T membranes by 2 h, as seen from a decrease in phase contrast at cell boundary. In comparison, hPDLF remained spherical after 2 h on untreated membranes. At 6 h, pronounced cell clustering and formation of long cytoplasmic projections (black arrowheads) were observed on UP/UT membranes. By 18 h, cell spreading was complete, with increased cytoplasmic membrane density at the periphery of sheet-like lamellipodia (white arrows). A greater degree of hPDLF spreading was obtained on alkali-treated membranes.

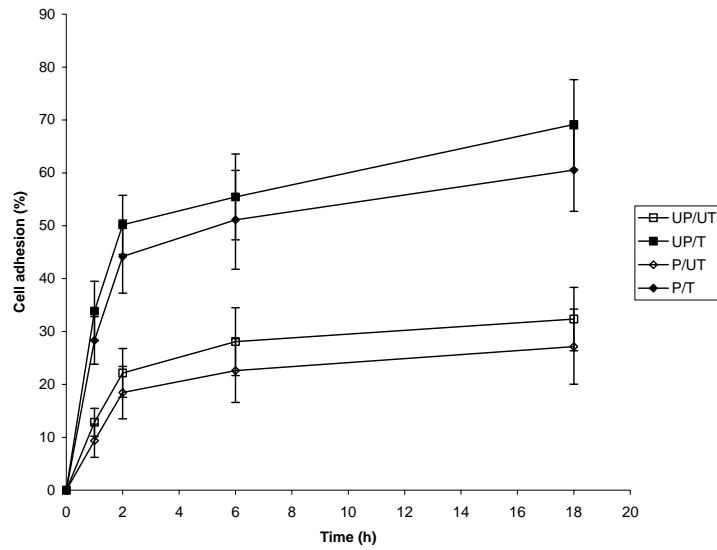


Figure 6.7. Adhesion efficiency of hPDLF, expressed as the percentage of double-stranded DNA (dsDNA) harvested from attached cells from initial cell suspension, at 1, 2, 6 and 18 h after seeding on membranes. Adhesion efficiency was significantly enhanced on alkali-treated (T vs. UT) membranes ($p < 0.001$) at all time points. hPDLF demonstrated an initial burst in adhesion efficiency at 1 h, reaching a plateau of $57 \pm 10\%$ by 6 h on alkali-treated membranes. Only about $27 \pm 7\%$ of hPDLF attached onto untreated membranes at 6 h. At 18 h, a slight increase attributable to DNA synthesis in cells having passed the restriction point in the cell cycle was observed on alkali-treated membranes. Data are presented as mean \pm SD, $n = 5$.

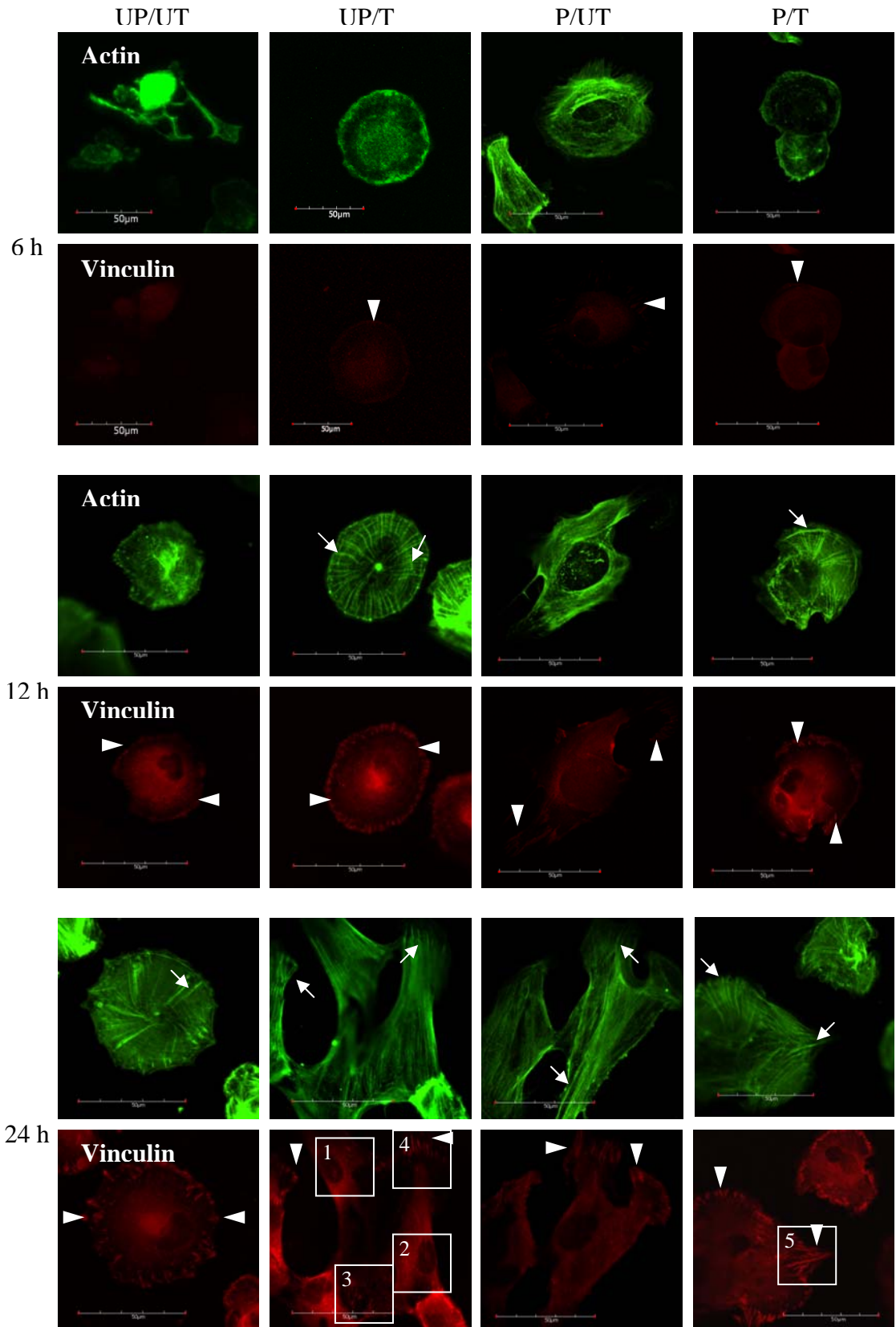


Figure 6.8. Immunofluorescence of *f*-actin (green) and vinculin (red) in hPDLF at 6, 12 and 24 h after seeding on membranes (scale bar = 50 μm). At 6 h, *f*-actin organization and weak signals of vinculin (arrowheads) as focal complexes at cell periphery were observed on P/UT, UP/T and P/T membranes. At 12 h, *f*-actin remained disorganized in cells on UP/UT membrane, whereas it was incorporated into microfilament bundles (arrows) on alkali-treated membranes. Immature dot-like focal adhesions were seen on untreated membranes, whereas dash-like focal contacts were obtained on alkali-treated membranes. By 24 h, stress fibres were observed on alkali-treated membranes, with concomitant formation of mature focal contacts approximately 5 μm in length, demonstrated by long spikes of vinculin. On untreated membranes, stress fibres and focal contacts were sparse or poorly formed.

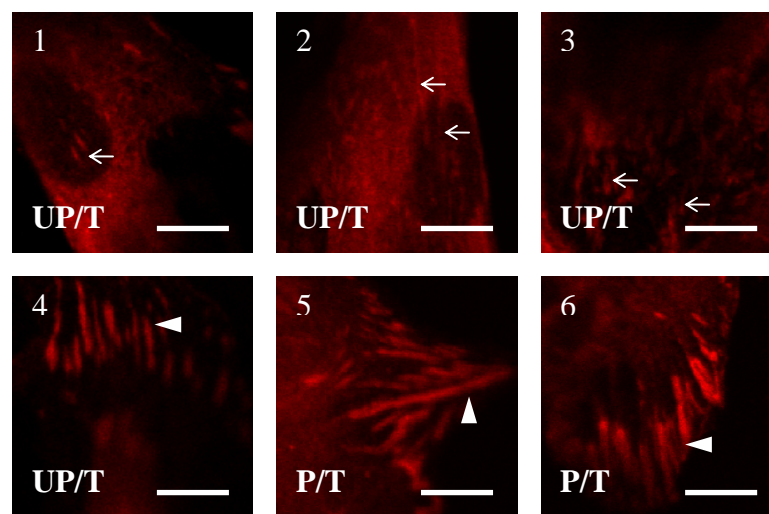


Figure 6.9. Close-up images of Fig. 6.8 (numbered boxes) of vinculin (red) at 24 h after seeding on membranes (scale bar = 10 μm). Centrally located focal adhesions (arrows) resembling “fibrillar” adhesions (Zamir et al., 2000) were observed on UP/T membranes, and 10-20 μm long adhesions (arrowhead) resembling “supermature” focal adhesions were observed on both UP/T and P/T membranes. These structures were absent from cells on untreated membranes.

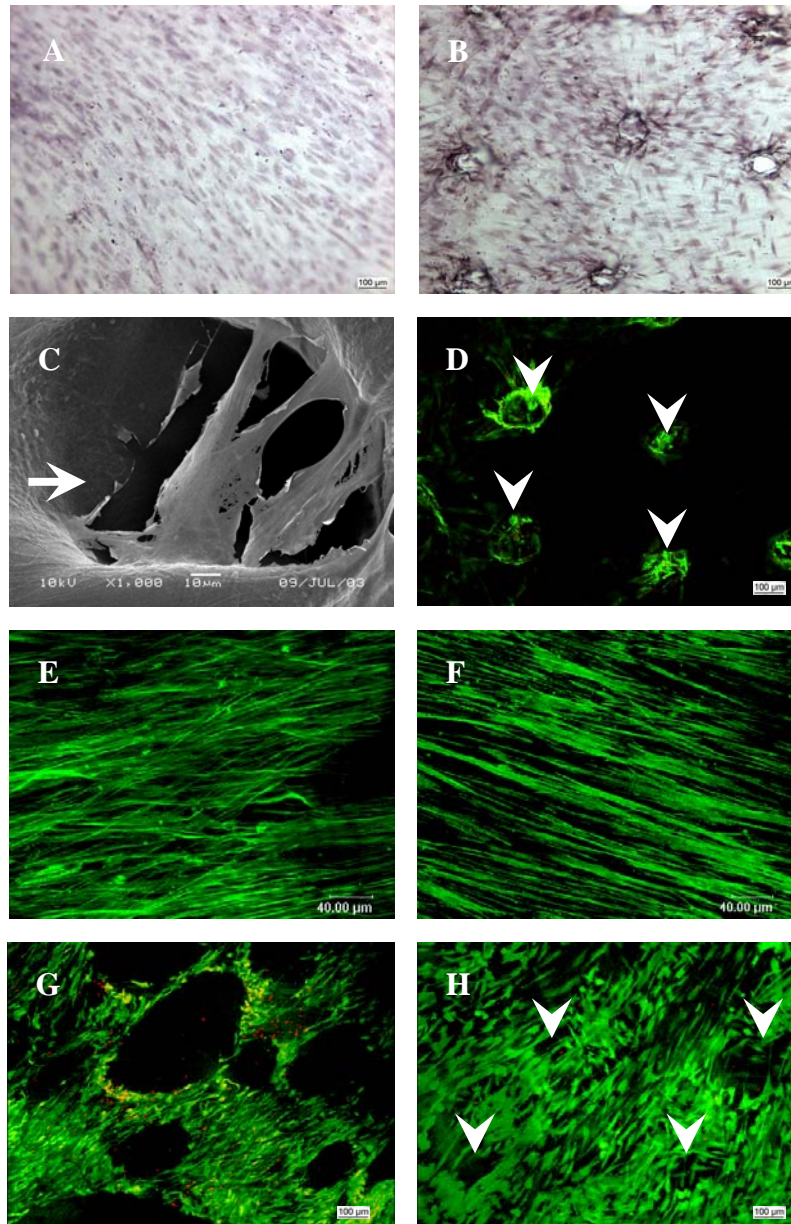


Figure 6.10. Representative images of hPDLF cell sheet on UP/T and P/T membranes (magnification 100X, unless stated otherwise). PCLM images of hPDLF showing (A) unidirectional alignment on UP/T membranes and (B) radial alignment on P/T membranes after Haematoxylin stain at day 21. (C) SEM image showing hPDLF bridging across and through perforations on membrane “flaps” (arrow). Confocal laser microscopy images of hPDLF (green) (D) migrating onto the underneath sides of membrane under phalloidin staining at day 14, demonstrating contact guidance. Cells demonstrated strong staining for f -actin (green) on both (E) UP/T and (F) P/T membranes at day 14. Comparison of cell viability at day 21 on (G) UP/T and (H) P/T membranes, showing detachment of cell sheet (absence of staining) on the former. Positions of perforations were indicated as arrowheads.

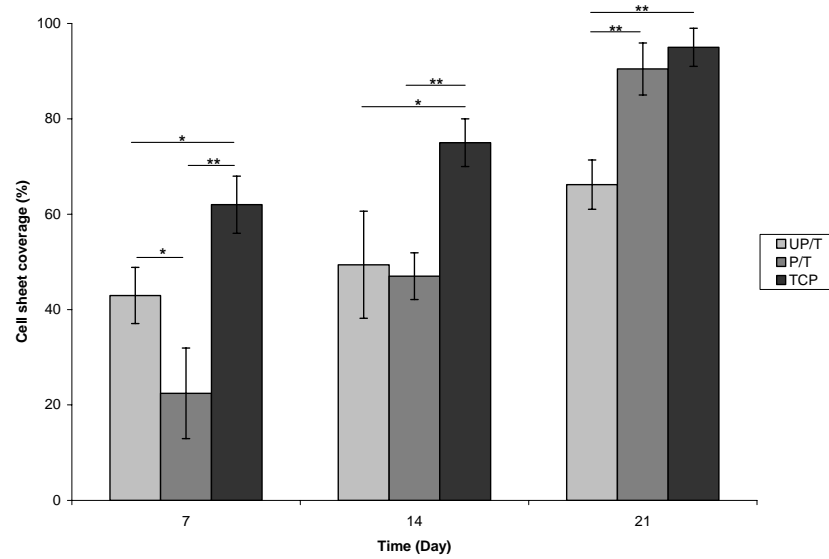


Figure 6.11. Cell sheet coverage on membranes as deduced from FDA/PI staining at 100X magnification after image analysis by Micro-Image[®] over 21 days. hPDLF coverage was initially higher on UP/T membranes at day 7 ($p < 0.05$). However, coverage on P/T membranes caught up at day 14, and surpassed UP/T membranes at day 21 ($p < 0.01$). Data are presented as mean \pm SD, $n = 3$. * $P < 0.05$; ** $P < 0.01$.

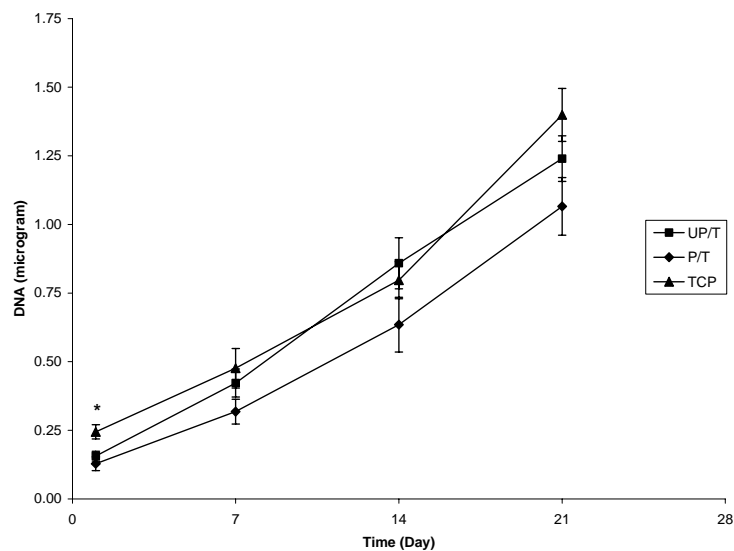


Figure 6.12. Cell proliferation in terms of dsDNA harvested from attached hPDLF over 21 days. Results showed that there was a greater rate of cell proliferation on UP/T membranes up to day 14, but no statistically significant difference in the quantity of dsDNA harvested from UP/T and P/T membranes ($p > 0.05$). The levels of dsDNA on membranes were approximately 55-67% of that on TCP at day 1. Data are presented as mean \pm SD, $n = 3$. * $P < 0.05$.

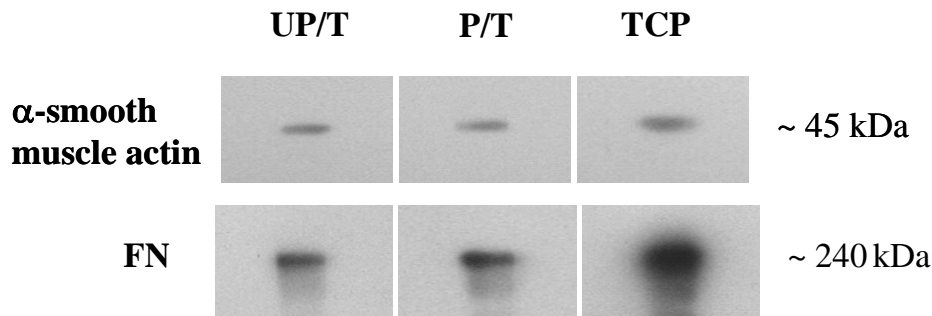


Figure 6.13. Western blot and densitometric analysis of reducing SDS-PAGE containing whole cell lysates of hPDLF cultured on UP/T, P/T membranes and TCP at day 21. hPDLF on UP/T and P/T membranes produced equivalent amounts of α -smooth muscle actin (~45 kDa) and FN (~240 kDa). However, the amount of FN on TCP was three-fold of that on membranes.

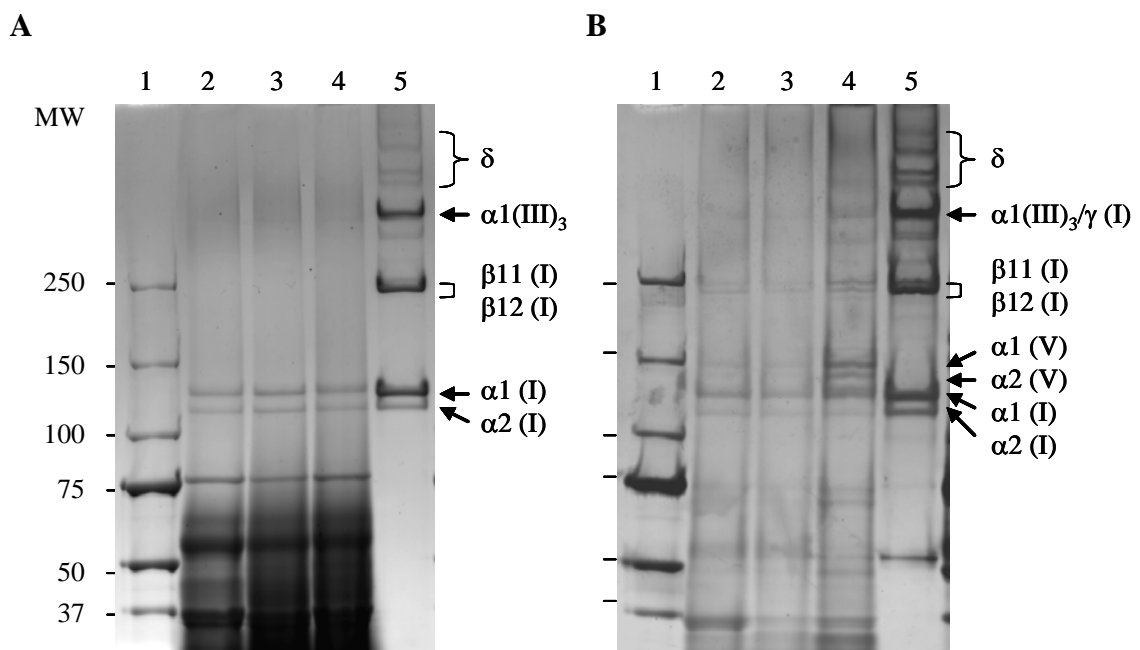


Figure 6.14. Representative images of non-reducing SDS-PAGE in 3-8% gradient Tris-acetate gel of (A) medium and (B) cell layer fractions after limited pepsin digestion at day 21. Bands corresponding to α -chains of major fibrillar collagens, type I, III and V, were detected. Type I collagen β -chains, indicative of cross-linking in the collagenous matrix (Rao *et al.*, 1982) were present. The relative proportions of collagen I, the predominant collagen in ECM of the PDL, was determined by densitometric analysis. The amount of secreted collagen I in the medium was similar in all samples, whereas the deposition of collagen I on membranes was approximately 60% of that on TCP. Lane 1: Protein ladder, 2: UP/T membrane, 3: P/T membrane, 4: TCP, 5: Col I standard.

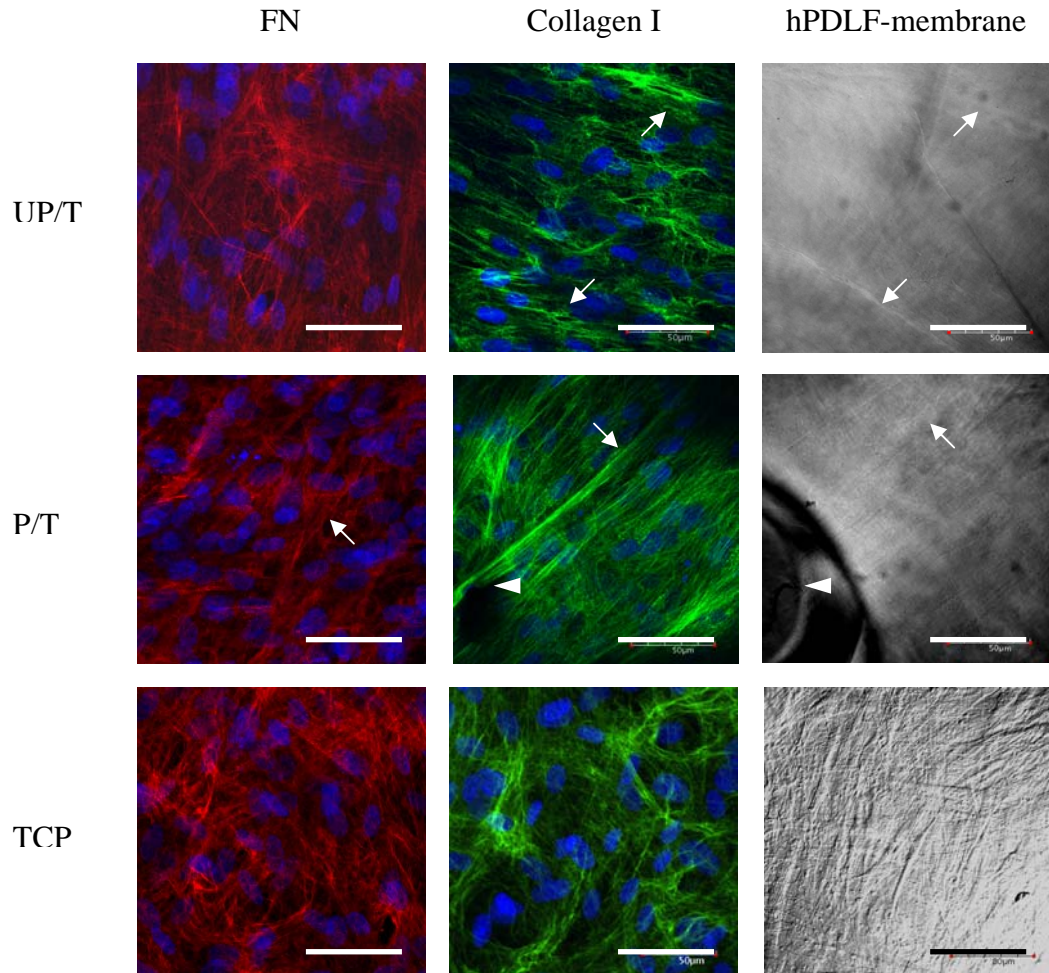


Figure 6.15. Representative confocal laser microscopy images of hPDLF immunolabeled for FN and type I collagen on UP/T membrane, P/T membrane and TCP at day 21 (scale bar = 50 μm). The presence of fibrillar FN (red) and type I collagen (green) was observed. Whereas fibrillar FN was randomized on TCP and often seen lining the periphery of discrete cells or cell clusters on both TCP and UP/T membranes, its organization on P/T membranes was directional. Collagenous matrix was in a similar orientation to fibrillar FN, the alignment of both was greater on P/T membranes. PCLM images depicting the corresponding surface morphology of hPDLF-membrane constructs demonstrated that cells on P/T membranes responded to contact guidance, aligning both cell and matrix to surface topography in the form of substrate grooves or folds (arrows). In particular, prominent collagen fibres were seen in highly aligned confluent cells traversing sites of perforation (arrowhead) on P/T membranes.

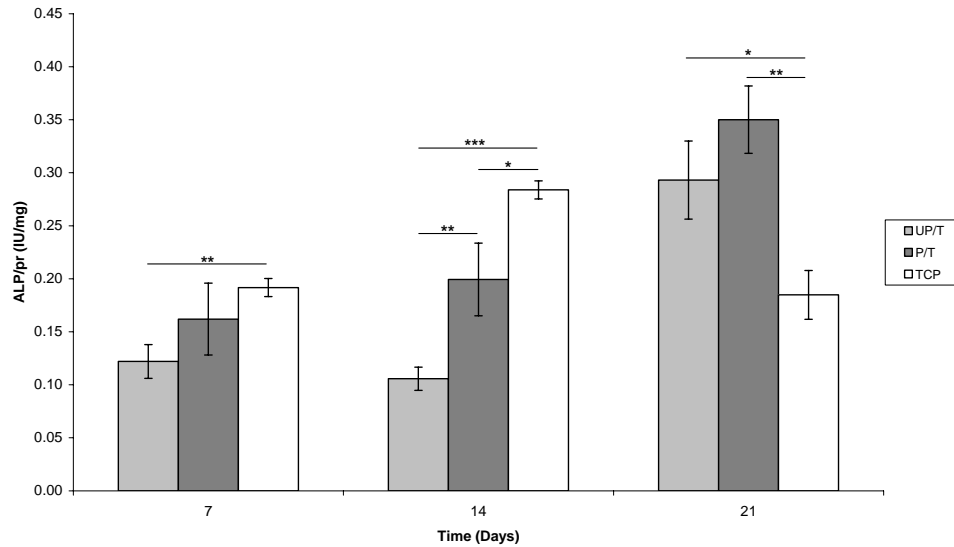


Figure 6.16. Level of alkaline phosphatase (ALP) of hPDLF at day 7, 14 and 21. ALP activity normalized by total intracellular protein was upregulated in cells on TCP at day 14 up to a value of 0.29 IU/mg, after which it declined at day 21. Cells on UP/T and P/T membranes followed a pattern of delayed induction, reaching 0.29-0.35 IU/mg at day 21. ALP level on P/T membranes was significantly higher than UP/T membranes at day 14 ($p < 0.01$) and TCP at day 21 ($p < 0.01$). All ALP values were within the range reported for hPDLF under collagen induction (Appendix). Data are presented as mean \pm SD, $n = 3$. * $P < 0.05$; ** $P < 0.01$; *** $P < 0.001$.

7. TISSUE ENGINEERING OF A hPDLF MEMBRANE-hAO SCAFFOLD DOUBLE CONSTRUCT

7.1. Background

To be applicable for tissue engineering and regeneration, the biomaterial surface has to be cytocompatible and to present chemical and physical cues to guide tissue morphogenesis and differentiation (reviewed in Griffith, 2002). Having demonstrated P/T membranes as suitable substrates for hPDLF-membrane constructs (Chapter 6), the objective of this chapter was to investigate the ability of hPDLF-membrane constructs consisting of alkali-treated and perforated PCL membranes to facilitate tissue regeneration in combination with hAO-scaffold constructs in an *in vivo* model.

The presence of an intact periodontium, consisting of gingiva, periodontal ligament, cementum and alveolar bone, is crucial for establishing a stable bone / tooth interface. Thus, the regeneration of periodontal tissues lost to inflammatory process related to either dental injuries (Sae-Lim *et al.*, 2004) or periodontal diseases (Amar, 1996) is considered the ultimate aim in tooth retention (Sae-Lim, 2001). Many therapeutic approaches, including the usage of guided tissue regeneration (GTR) membranes with or without bone grafts or substitute, failed to achieve predictable results (Bartold *et al.*, 2000) due to the complexity of the regenerative process at the soft-hard tissue interface (Amar, 1996). It was postulated that the provision of a prefabricated three-dimensional structure with the appropriate cells or inductive molecules would be a viable regenerative strategy (Bartold *et al.*, 2000).

Transplantation of periodontal scaffold-cell constructs had been previously reported. Investigations have included the implantation of human periodontal

ligament fibroblasts (hPDLF) on collagen scaffolds into Sprague-Dawley rats (Quteish *et al.*, 1991), of human cementum-derived cells on hydroxyapatite/tricalcium phosphate ceramic into immunodeficient mice (Grzesik *et al.*, 1998), and of human gingival autograft using hyaluronic acid scaffolds (Prato *et al.*, 2003). Recently, autologous PDL cells seeded onto a collagen sponge were used to regenerate cementum on the root surface in beagle dogs (Nakahara *et al.*, 2004). However, to the authors' knowledge, there have been no reports on scaffold-cell grafts harbouring hPDLF and human alveolar osteoblasts (hAO) forming the PDL-bone interface. Critical size defects involving multiple tissue types, such as the PDL and alveolar bone, require the application of scaffolds containing the appropriate cells for tissue development (Murphy and Mooney, 1999). Consequently, transplantation of tissue engineered grafts consisting of scaffold-cell constructs appears to be a promising technique in regenerating periodontium.

A double construct of hPDLF-seeded membrane and hAO-seeded scaffold was hypothesized to have potential application in tissue engineering periodontal structures. This chapter reports the two-phase study of a membrane-scaffold construct to investigate its ability in supporting hPDLF and hAO attachment and growth *in vitro*, and its feasibility for tissue engineering a PDL-alveolar bone interface *in vivo*.

7.2. MATERIALS AND METHODS

7.2.1. Preparation of membranes and scaffolds

Poly(ϵ -caprolactone) (PCL) membranes (mean thickness \pm SD, $10 \pm 2 \mu\text{m}$) with perforations (mean diameter \pm SD, $100 \pm 10 \mu\text{m}$) of $400/\text{cm}^2$ -density (Chapter 6) were fabricated, alkali-treated and sterilized as detailed in section 3.1. Thirty-four membranes, $16 \times 16 \text{ mm}^2$, were immersed in PDLF culture medium, i.e. DMEM

(Gibco, Life Technologies, NY, USA) containing 10% FBS, 4500 mg/mL glucose and 2% penicillin-streptomycin, at 37°C followed by overnight air drying. Subsequently, thirty membranes were sandwiched between custom-made 316L stainless steel rings (Alson Engineering (S), Singapore) for subsequent cell seeding. Four non-seeded membranes were set aside as negative controls.

PCL scaffolds, fabricated via fused deposition modelling (Hutmacher *et al.*, 2001) with a lay-down pattern of 0/60/120° and porosity approximately 65%, were kind gifts from Singapore Temasek Polytechnic. The fully interconnected pores had a size falling within the range of 360 x 430 x 620 µm (Hutmacher *et al.*, 2001). Scaffolds measuring 8 x 8 x 5 mm³ were treated with NaOH and sterilized as above for membranes. Thirty-four scaffolds were immersed overnight in alveolar osteoblast (AO) culture medium, i.e. Medium199 (Gibco) containing 10% FBS and 2% penicillin-streptomycin, at 37°C followed by overnight air drying. Four non-seeded scaffolds were set aside as negative controls.

7.2.2. Seeding and culture of hPDLF and hAO

hPDLF and hAO cell line from a periodontally sound molar of a healthy 23-year-old female, previously characterized to possess the highest osteogenic potential (Chapter 4) were used in this study. hPDLF between the fourth and fifth passages were seeded in 45 µL aliquots each onto thirty sandwiched membranes at 78,000 cells/cm² or 200,000 cells/membrane. Membrane-cell constructs were incubated at 37°C and 5% CO₂ for 2 h before DMEM was added. hAO were mixed with slow-setting fibrin glue in a 1:2 (v/v) ratio according to manufacturer's instructions (Tisseel® Kit, Baxter, Vienna, Austria). Fibrin glue was a kind gift from Dr. Katharina Bittner (Baxter, Hyland Immuno, Austria). Cell-fibrin mixtures in 55 µL

aliquots each were seeded at 625,000 cells/cm³ or 200,000 cells/scaffold onto thirty scaffolds. Scaffold-cell constructs, sparingly coated with 25 µL of fibrin glue, were incubated for 30 min before Medium199 was added. Medium change was performed every three days. Membrane-cell and scaffold-cell constructs were subjected to experiments every 7 days for a period of 21 days. All specimens were transferred to new wells before weekly experiments. Coating of the scaffold-cell constructs was repeated at day 7 to retain hAO in the scaffolds. Osteoinduction was carried out at day 14 using medium supplemented with 50 µg/mL ascorbic 2-phosphate, 10 mM β-glycerophosphate and 10⁻⁷ M dexamethasone (Sigma, MO, USA) as previously described (Schantz *et al.*, 2002b).

7.2.3. Cell metabolic assay

Cell metabolism was assayed separately ($n=3$) for cells retained on constructs and cells lost to the corresponding wells by CellTiter 96[®] AQueous One Solution Cell Proliferation Assay (Promega, WI, USA). The substrate, 3-(4,5-dimethylthiazol-2-yl)-5-(3-carboxymethoxyphenyl)-2-(4-sulfophenyl)-2H-tetrazolium (MTS), was bio-reduced into a brown formazan product by nicotinamide adenine dinucleotide phosphate (NADP) or its reduced form (NADPH) within living cells. Constructs were transferred to new wells prior to assay. Five-hundred µl of assay reagents (1:5 MTS to culture medium ratio) were added per well. After 3-h incubation at 37 °C and 5% CO₂, 100 µl aliquots of bio-reduced mixture from each test well were transferred to a 96-well plate. Absorbance at 490 nm was determined.

7.2.4. Implantation

At the fourth week of culture, scaffolds and membranes were paired for implantation (seeded experimental group, $n=9$; non-seeded control group, $n=4$). Scaffolds were trimmed at the edges and assembly of fibrin glue-coated membrane-scaffold constructs was performed 1 h prior to implantation to ensure adequate stability. Subcutaneous implantation was performed in accordance with the International Guiding Principles for Animal Research (Howard-Jones, 1985) and in a laminar flow hood under sterile conditions. Seven 12-week-old athymic Balb C mice (Animal Resources Centre, Murdoch, Australia) were anaesthetized intraperitoneally with 0.15 ml of Dormicum (Roche, Basel, Switzerland) and Hypnorm (Janssen, Beerse, Belgium) mixed at a ratio of 1:1 (v/v). After disinfection with iodine and 70% alcohol, approximately 10 mm-long incisions lateral to the dorsal spine were made to create bilateral subcutaneous pockets in accommodation of two randomly selected membrane-scaffold constructs, inserted with the membrane facing dorsally. The mice were euthanized after 4 weeks.

7.2.5. Histology

Excised tissue blocks were cut into two diagonal halves, fixed in 4% formaldehyde in PBS for 2 h at room temperature and immersed in 2 M sucrose (Sigma) at 4°C overnight. One half of tissue blocks were embedded in tissue freezing medium (H-TFM; Triangular Biomedical Science, NC, USA) and frozen by immersion in liquid nitrogen. Seven cryosections, 8 to 12 μm in thickness, were made in the vertical 'z' plane (Fig. 7.4A). One cryosection each was stained with haematoxylin and eosin (H&E) and Masson's Trichrome, while the remaining 5 were processed for immunostaining. The other diagonal half of tissue blocks were

embedded in poly(methyl methacrylate), and 3 sections each were processed for Hale Periodic Acid-Schiff (PAS) and Giemsa staining.

7.2.6. Immunohistochemical analysis

Cryosections were processed with affinity purified polyclonal antibodies against major ECM proteins present in PDLF and AO to verify tissue identify, i.e. type I collagen (1:200 dilution) (Biodesign, ME, USA), type III collagen (1:40 dilution) (Chemicon, CA, USA), fibronectin (1:200 dilution) (Biodesign), vitronectin (1:20 dilution) (Santa Cruz Biotechnology, CA, USA) and bone sialoprotein (BSP) (1:200 dilution) (Chemicon). Blocking was performed with 5% BSA (w/v) and 1% goat serum (v/v) in PBS for 30 min at room temperature. Sections were incubated with primary antibodies overnight at 4°C in a humidified chamber. Incubation with secondary antibodies, anti-rabbit IgG-horseradish peroxidase (HRP) (R&D Systems, MN, USA) and anti-goat IgG-HRP (Chemicon), was performed according to manufacturer's protocols (1:500 dilution). To distinguish between recipient and donor cells within the membrane-scaffold constructs, the former was identified by immunostaining with antibodies against mouse-IgG-specific antibody (1:250 dilution) (Santa Cruz Biotechnology). Immunostaining for each antibody was performed on 3 randomly selected cryosections, and counterstained with haematoxylin.

7.3. RESULTS

7.3.1. Adhesion and proliferation of hPDLF and hAO *in vitro*

hPDLF, previously characterized and found to possess the highest osteogenic potential (Chapter 4), attached uniformly on PCL membranes and appeared spindle-shaped at day 7 (Fig. 7.1A). Cells were seen to either bridge or migrate through

perforations (arrowheads) (Fig. 7.1B), leading to confluent cell layers on the membranes at day 14 (Fig. 7.1C). Under FDA/PI staining, cells appeared highly viable throughout the *in vitro* culture (Fig. 7.1C). However, the fluorescent signals on membranes disassembled from rings and rinsed during staining steps were frequently localized around perforations at day 21 (Fig. 7.1D).

hAO, derived from the same patient as hPDLF and found to possess adequate osteogenic potential (Chapter 4), were seen embedded in fibrin glue at day 7 (Fig. 7.2A, B). The initial onset of fibrinolysis was indicated by an increase in visibility of fibrin glue through the scaffold. At day 14, increased cell density and fibrin degradation within scaffold pores were observed (Fig. 7.2C, D). FDA/PI staining showed viable hAO cell layers over the scaffold bars (Fig. 7.2E). The attached hAO on the scaffold bars appeared elongated, while those within the pores bridged within the interconnected honey-comb-like scaffold pores, secreting ECM to replace the degrading fibrin network (Fig. 7.2F). At day 21, osteoinduced hAO in scaffolds demonstrated positive von Kossa staining at nodules (Fig. 7.2G).

Cell metabolic assay over 21 days (Fig. 7.3) showed a steep and steady increase in the metabolic rates of hPDLF on PCL membranes. hAO cultured on scaffolds showed a high metabolic rate in the first week, and a gentler increase at day 14 and day 21. There was a significant peak in the metabolic rates of hPDLF at the bottom of culture wells at week 2 ($p < 0.01$), whereas this was not as distinct for hAO.

7.3.2. Tissue formation of hPDLF-hAO double construct *in vivo*

At the fourth week of culture, scaffolds and membranes were paired for implantation (seeded experimental group, $n=9$; non-seeded control group, $n=4$). Membrane-scaffold constructs were assembled (Fig. 7.4A and Fig. 7.4B insert) and

implanted into the bilateral subcutaneous pockets of 12-week-old athymic Balb C mice (Fig. 7.4B) for 28 days. Both constructs and surrounding soft tissues were harvested for evaluation at the end of 28 days (Fig. 7.4C).

The mice tolerated the surgical procedures well. Displacement of membrane from construct was observed in 4 specimens (2 each from experimental and control groups), and these were excluded from analysis. The final sample consisted of seven from experimental group and two controls. Tissue ingrowth through membrane perforations at the membrane-scaffold interface (Fig. 7.5A) was observed in majority of specimens. There was a higher degree of vascular network infiltration and construct integration with recipient tissue in experimental group specimens. Hale-PAS and Giemsa staining gave uniform blue and pink coloration respectively, representing muscle-like tissue (Fig. 7.5A) and fibrous as well as adipose tissue (Fig. 7.5B). In contrast, non-seeded control group specimens were characterized by predominant adipose tissue (Fig. 7.5C) and the dissociation of tissue-scaffold entity. Under Masson's Trichrome staining, collagen was detected in dense fibrous tissue at the periphery of constructs (Fig. 7.5D) and as parallel fibers along scaffold bars in experimental group (Fig. 7.5E). Inflammatory cell infiltration and degradation of PCL were not observed (data not shown).

Immunostaining results for the major ECM proteins were summarized (Table 7.1). Sites of antigen localization were visualized by brown coloration, generated by the enzymatic conversion of 3,3'-diaminobenzidine (DAB) into brown precipitate by HRP. Negative controls in the absence of primary antibodies gave little or no staining. In accordance with the results of Masson's Trichrome staining (Fig. 7.5E), type I collagen was observed to be present along the scaffold bars (Fig. 7.6A), while the membrane-scaffold interface was positively stained for both collagen type I (Fig. 7.6C)

and III (Fig. 7.6B). Fibronectin was detected throughout the constructs – moderately at the tissue-scaffold interface and extensively at the periphery (Fig. 7.6D). Vitronectin expression was localized only around the vasculature (Fig. 7.6E). Staining for BSP gave negative results in all specimens examined. Immunostaining with anti-mouse IgG antibodies demonstrated the sites of recipient tissue within the constructs. The specificity of anti-mouse IgG antibody was verified by positive staining of nude mice dermal sections (Fig. 7.6F), and a lack of staining in human dermal fibroblasts (Fig. 7.6G) and alveolar osteoblasts *in vitro* (results not shown). Signals for anti-mouse IgG, detected mainly at the extracellular ECM, were localized throughout constructs in control groups (Fig. 7.6H), but mostly at the construct periphery and vasculature in experimental group (Fig. 7.6I, J). PDL tissue was largely indistinguishable from surrounding fibrous connective tissues, except at regions of membrane-scaffold interface, characterized by discrete cell layers and infiltration across perforated membranes (Fig. 7.6J).

7.4. DISCUSSION

7.4.1. Membranes and scaffolds supported cell adhesion and proliferation *in vitro*

This chapter describes a novel concept of a PDL-alveolar bone construct. Poly(ϵ -caprolactone) (PCL), a bioresorbable scaffold polymer investigated for soft and hard tissue engineering (Ng *et al.*, 2001; Schantz *et al.*, 2002b; Li *et al.*, 2003; Williamson and Coombes, 2004), was demonstrated in this study to support the attachment and growth of hPDLF (also described in Chapter 6) and hAO (Figs. 7.1, 7.2).

Fibrin glue was employed during hAO seeding as a carrier for the delivery of cells into scaffolds. Fibrin glue is biocompatible (Romanos and Strub, 1998) and can

be degraded by local fibrinolytic activity followed by the invasion of granulation tissue accompanied by macrophages (Warrer and Karring, 1992) at about 1 week post-injury (Amar, 1996). Components such as factor XIII and cross-linked fibrin were believed to stimulate cell proliferation, and facilitate the formation of a fibroblast network via the clot structure in wound healing (Redl *et al.*, 1985). In this study, hAO within PCL scaffolds demonstrated a high metabolic rate in the first 14 days of *in vitro* culture (Fig. 7.3). The lengthened process of fibrinolysis, initiated at day 7 and extended till day 14 as suggested by the increase in visibility through the scaffold (Fig. 7.2A-D), could be attributed to the action of aprotinin from fibrin glue. Aprotinin has been shown to negatively regulate plasmin (de Haan and van Oeveren, 1998) and hence slow down fibrin degradation. As cell proliferation and migration took place, hAO gradually emerged out of fibrin matrix and established contacts with PCL surface via focal adhesions (Schantz *et al.*, 2002b). hAO embedded in fibrin glue but unattached to PCL were lost with fibrinolysis onto the bottom of culture wells at day 14 (Fig. 7.3). Mineralized nodule formation, characterized by cell aggregates and positive von Kossa staining, was observed at day 21 (Fig. 7.2G), which were in accordance with previously reported *in vitro* studies on bone engineering (Schantz *et al.*, 2002b).

On the other hand, hPDLF seeded at a density of 78,000 cells/cm² or 200,000 cells/membrane did not achieve high cell densities on membranes at day 7 (Fig. 7.1A). hPDLF demonstrated a high rate of proliferation on membranes throughout the 21-day *in vitro* culture (Fig. 7.3), and reached cell confluency at day 14 (Fig. 7.1C). Coating with membranes with fibrin glue did not result in significant differences in either cell attachment or proliferation (unpublished data). Cell loss was observed during rinsing after disassembly of rings (Fig. 7.1D), possibly accounting for the peak

in hPDLF metabolic activity at the bottom of culture wells (Fig. 7.3). An intermediate seeding density of cells on scaffolds was found to be optimal for cell proliferation and ECM synthesis (Zhou *et al.*, 2006). In retrospect, hPDLF seeded at high cell densities did not achieve as much cell mass and matrix formation as when seeded at sub-confluence (Chapter 6). Nonetheless, a stable hPDLF-membrane interface from an integration of cell layers and membrane (Fig. 7.5A, 7.6D) was eventually obtained, attributed to cell migration through perforations (Fig. 7.1B, 7.7J).

7.4.2. Membrane-scaffold double construct facilitated tissue growth and vascularization *in vivo*

Histochemical examination of *in vivo* constructs in the experimental group after 28 days demonstrated highly vascularized tissue including ingrowth of muscle, fibrous and adipose tissues from the recipient (Fig. 7.5A-C). This incidentally also provided evidence for the advantages of a scaffold with high porosity with respect to nutrient supply which is a determining factor for the survival, proliferation, and differentiation of transplanted cells (Muschler *et al.*, 2004). Connective tissue invasion, identified by immunostaining with anti-mouse IgG antibodies, was detected mainly at the construct periphery and vasculature (Fig. 7.6I). Cells within constructs secreted ECM observed as collagen fibres aligning along scaffold bars (Fig. 7.5E), whereas cells at the membrane-scaffold interface secreted collagen, depositing between cell layers (Fig. 7.6C). Fibronectin and vitronectin, usually found to be present in newly-formed PDL and osteoid at 4 and 8 weeks post-injury (Matsuura *et al.*, 1995), were also detected in our constructs. Unlike the ubiquitous distribution of fibronectin, vitronectin was expressed only by cells near the vasculature (Fig. 7.6E), in accordance to its presence in the plasma, platelet α -granules and vessel wall (Jang

et al., 1998). On the other hand, cell penetration through the 100- μ m-diameter membrane perforations allowed for enhanced integration with the scaffolds (Fig. 7.5A, 7.6D, 7.6J). Despite this, membrane displacement was observed due to a lack of physical interlocking of the membrane and scaffold. However, the loss of construct integrity at the membrane-scaffold interface and the weakened bonding of tissue to scaffold bars were more pronounced in non-seeded controls, implicating the crucial role of seeded cells in scaffold-cell constructs.

The observation of increased ECM and mineralized nodule formation of hAO after 14 days *in vitro* (Fig. 7.2F, G) was in accordance with an earlier finding (Franceschi, 1999). Previous characterization of hAO derived from the same patient on tissue culture plastic demonstrated its ability to form mineral-like nodules *in vitro* (Chapter 4). A similar experiment involving the subcutaneous implantation of human periosteum-derived osteoprogenitor cells on PCL scaffold also reported bone formation (Schantz *et al.*, 2002b). Furthermore, studies from the same laboratory have demonstrated the ability of hAO to express osteogenic proteins such as osteopontin (OPN) and osteocalcin on PCL scaffolds (Zhou, 2006).

Given the observed intrinsic biological patient-to-patient variation among the ten primary hPDLF cell lines (Chapter 4), the selection of cells with the highest osteogenic potential *in vitro* was thought to facilitate tissue regeneration in hPDLF-hAO double constructs *in vivo*. However, no mineralization was found within the *in vivo* constructs in this study. Bone sialoprotein (BSP), a mineralized tissue-specific marker with an established role in bone calcification (Boskey, 1996), was not detected within the constructs, possibly suggestive of a loss of phenotypic differentiation. Taking into account the observation that hPDLF exhibited a dedifferentiated or embryonic-like phenotype during expansion culture in the presence of ascorbic acid

(Chapter 5), and that the PDL has been associated with root resorption due to prostaglandin E2 production (Ogiso *et al.*, 1992; Shiraishi *et al.*, 2001), it may be speculated that the interaction between hPDLF and hAO interfered with the osteogenesis of hAO at the interface of soft and mineralizing tissues. Future studies could encompass the separate evaluation of hPDLF and hAO cell-scaffold constructs in periodontal defects, and histological examination using ALU probes (Weisberg *et al.*, 1996) to assess the colonization of human-derived cells in recipient tissues.

In summary, alkali-treated PCL membranes and scaffolds supported hPDLF and hAO adhesion and proliferation *in vitro*, whereas membrane-scaffold double constructs facilitated tissue growth and vascularisation, but not mineralized tissue formation *in vivo*.

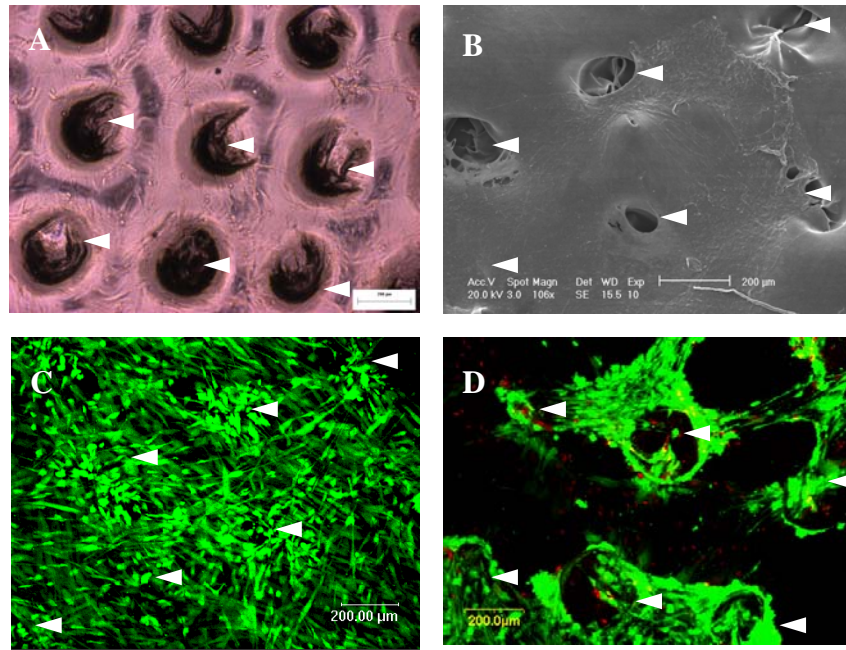


Figure 7.1. Attachment, growth and viability of hPDLF on PCL membranes. (A) Uniform distribution of hPDLF on membranes was observed under PCLM at day 7. (B) Bridging or migration of cells through perforations (arrowheads) was observed under SEM at day 14. Confocal laser microscopy images showing (C) highly viable cells at day 14, and (D) the localization of cells to sites of perforations at day 21 after FDA/PI staining.

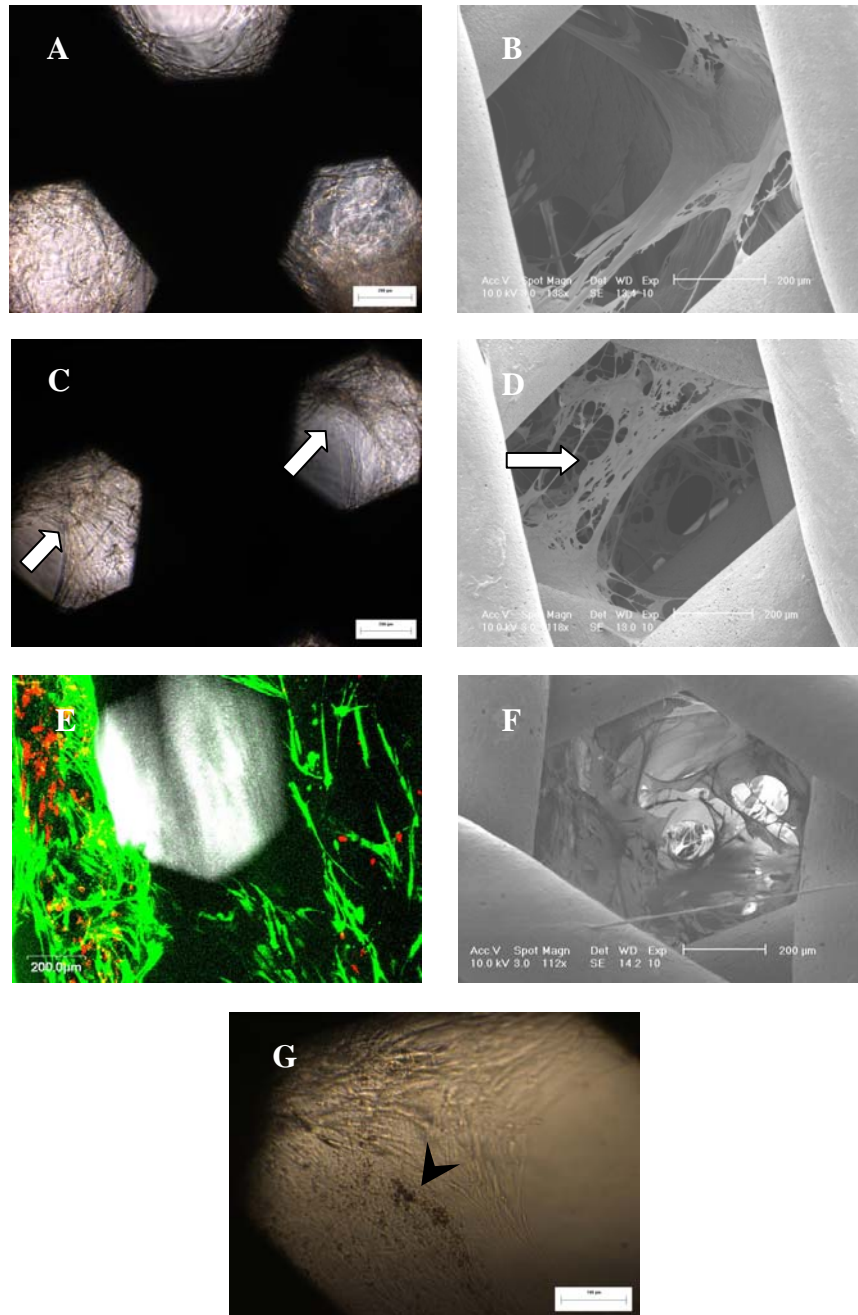


Figure 7.2. Attachment, morphology and viability of hAO on PCL scaffolds. hAO embedded in fibrin glue via (A) PCLM and (B) SEM at day 7. Prominent signs of fibrin degradation was observed via (C) PCLM and (D) SEM at day 14, as indicated by white arrow. (E) hAO proliferated and remained largely viable on scaffold bars under FDA/PI staining at day 14. (F) hAO were also observed to bridge within scaffold pores, secreting ECM to replace the degrading fibrin network. (G) Mineralized nodule formation (black arrowhead) was observed after von Kossa staining of osteoinduced hAO at day 21.

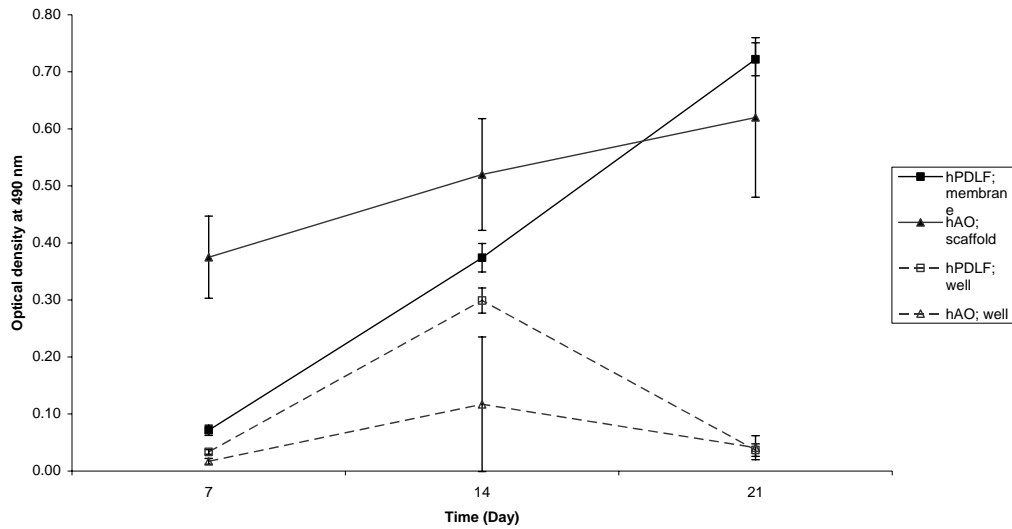


Figure 7.3. Metabolic activities of hPDLF on membranes and of hAO on scaffolds, with their respective wells at weekly intervals. Cell metabolic assay over 21 days showed a steep and steady increase in the metabolic rates of hPDLF on PCL membranes. hAO cultured on scaffolds showed a high metabolic rate in the first week, and a gentler increase at day 14 and day 21. There was a significant peak in the metabolic rates of hPDLF at the bottom of culture wells at week 2 ($p < 0.01$), whereas this was not distinct for hAO.

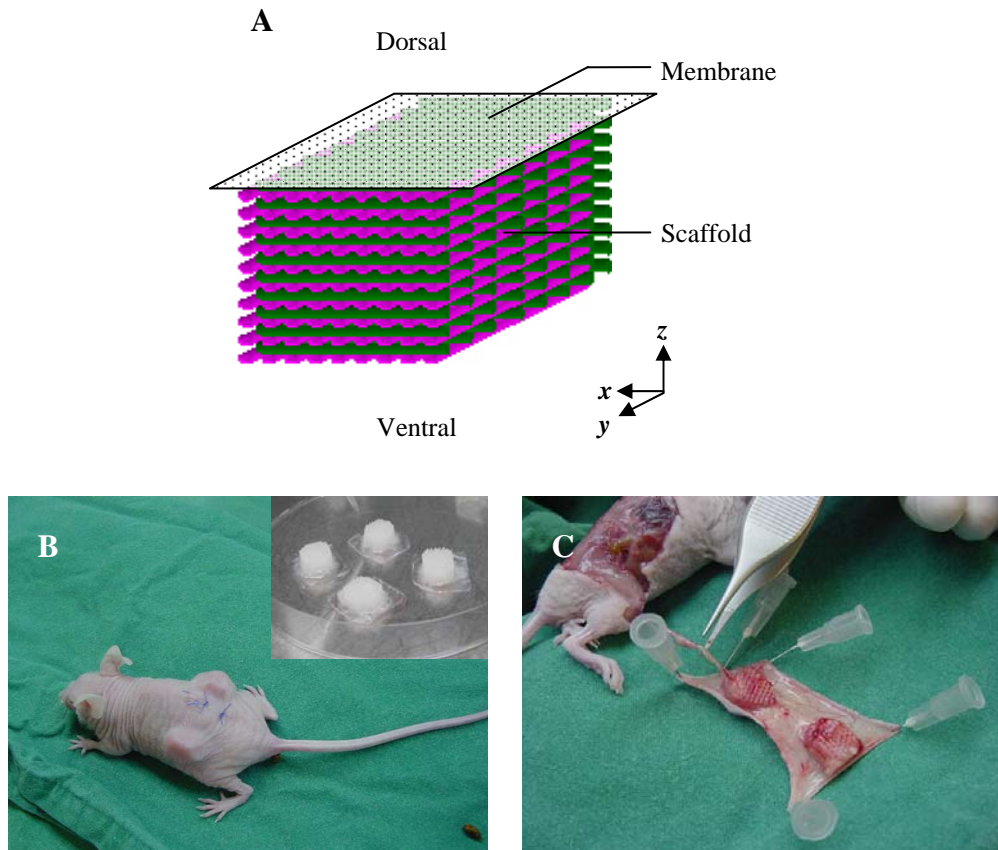


Figure 7.4. Implantation and excision of membrane-scaffold constructs. (A) Three-dimensional representation of a membrane-scaffold construct, with the implantation orientation indicated. (B) Twelve-week-old athymic Balb C mice carrying (insert) membrane-scaffold constructs assembled with fibrin glue in bilateral subcutaneous pockets with the membrane facing dorsally. (C) Both constructs and surrounding soft tissues were harvested for evaluation 28 days after implantation.

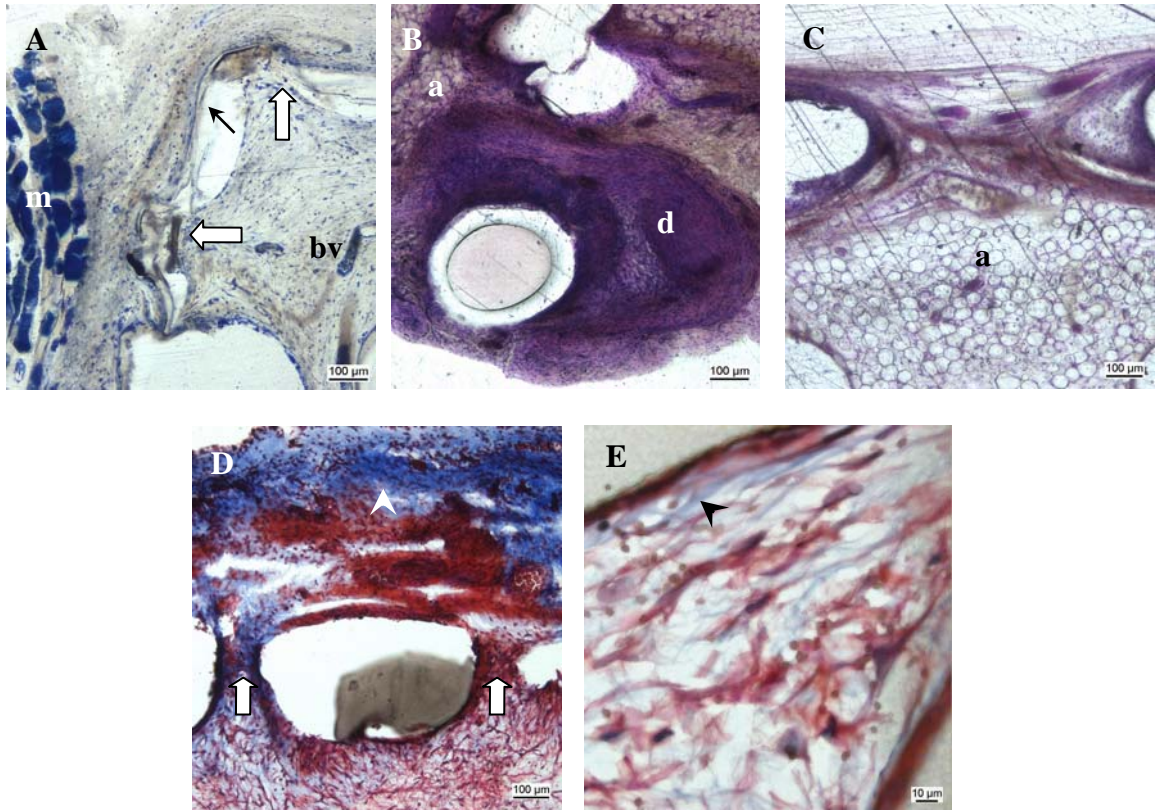


Figure 7.5. Histological analysis of constructs after 4-weeks *in vivo*. Representative morphology of constructs from experimental group after (A) Hale-PAS and (B) Giemsa staining. (C) Dislocation of PCL membrane and predominance of adipose tissue in non-seeded control. Presence of collagen at (D) periphery and (E) tissue-scaffold interface under Masson's Trichrome staining. Abbreviations: a, adipose tissue; bv, blood vessel; d, dense fibrous tissue; m, muscle-like; black arrow, PCL membrane; white arrow, tissue penetration across perforations; arrowhead, collagen fibers.

Protein	Group	Membrane	Central tissue	Tissue-scaffold interface
Collagen I	E	-/+	-/+	-/+
	C	-/+	-/+	-/+
Collagen III	E	-/+	-/+	-/+
	C	-/+	-/+	-
Fibronectin	E	+	+	+
	C	+	+	+
Vitronectin	E	-/+ ^a	-/+ ^a	-
	C	-/+ ^a	-/+ ^a	-
Bone sialoprotein	E	-	-	-
	C	-	-	-
Mouse IgG	E	+	-/+	-/+
	C	+	+	+

Table 7.1. Summary of immunostaining results. Abbreviations: E, experimental; C, non-seeded control; -, absent; +, present; ^a, staining localized at blood vessels.

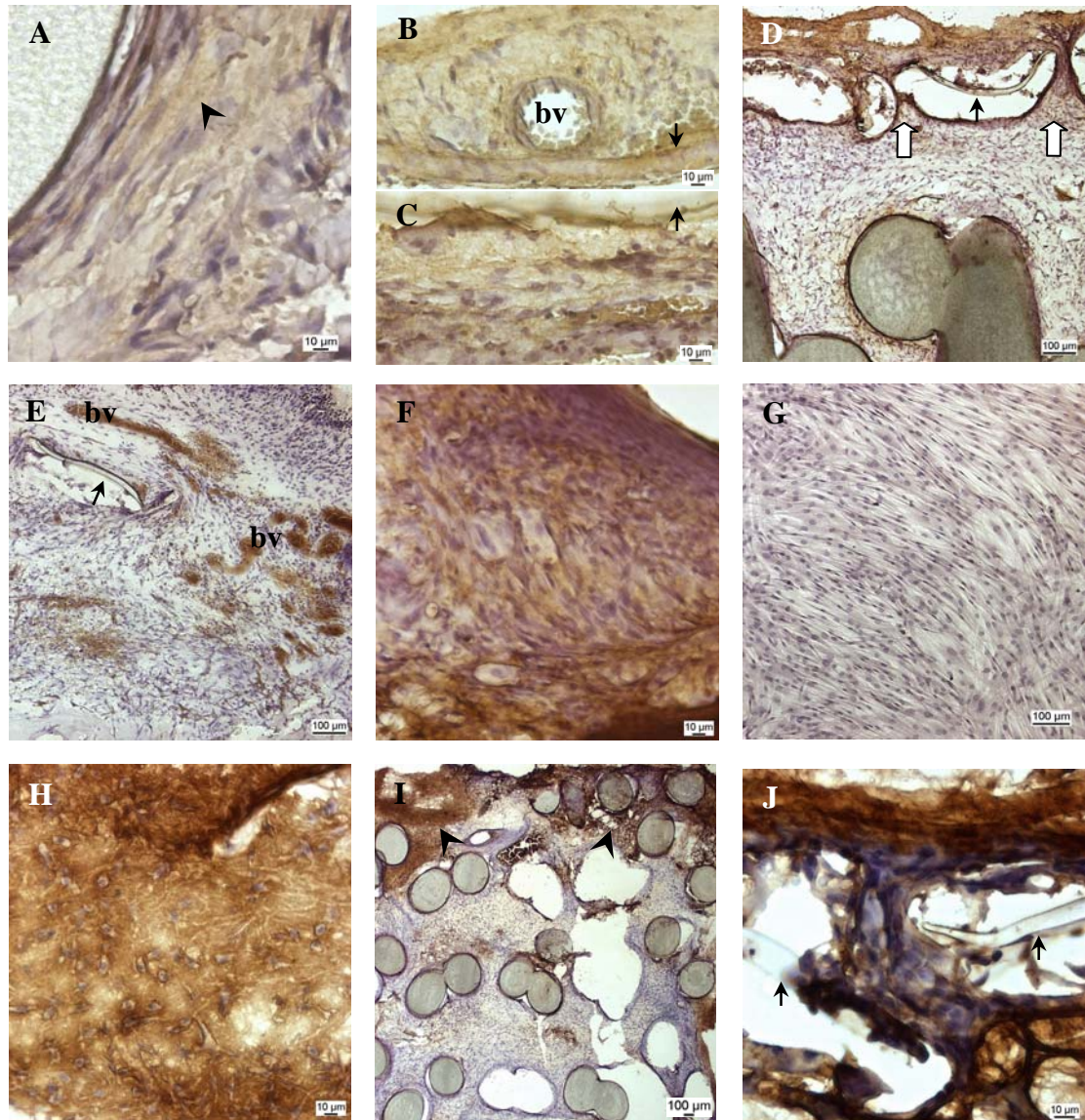


Figure 7.6. Immunohistochemical analysis of constructs after 4-weeks *in vivo*. (A) Expression of type I collagen at tissue-scaffold interface, as indicated by brown coloration. Expression of (B) type III and (C) type I collagen at membrane. Note the differing tissue morphology at (B) construct periphery and at (C) membrane-scaffold interface. (D) Expression of fibronectin, strong at periphery and moderate at tissue-scaffold interface. (E) Expression of vitronectin near vasculature. Immunostaining of anti-mouse IgG in (F) nude mice dermal sections (positive control) and (G) human dermal fibroblasts (negative control). Expression of anti-mouse IgG in (H) control and (I, J) experimental group. Cells of mouse origin (indicated by black arrowheads) were found mainly at the periphery and areas of vascularization. (J) Close up image at the membrane-scaffold interface, showing the infiltration of putative PDLF cell-sheet through the perforation. Abbreviations: bv, blood vessel; black arrow, PCL membrane; white arrow, tissue penetration across perforations.

8. GENERAL CONCLUSIONS AND FUTURE WORK

8.1. General conclusions

Ten hPDLF and three hAO primary cell lines from four males and six females, aged 13-56 yr (25 ± 11 , mean \pm SD), were established. hPDLF under osteogenic induction demonstrated an initial increase followed by a subsequent decrease in ALP and ON, an increased synthesis of bone-matrix protein OPN after day 14, and mineral-like tissue formation at day 28. Furthermore, hPDLF produced BSP as well as the 44-kDa form of OPN under both normal and mineralizing culture. Hence, hPDLF established by explant culture up to passage 3-5 retained osteo-progenitors and osteoblast-like cells capable of osteogenic differentiation *in vitro*.

Subsequent characterization under 21-day expansion culture with 10% serum supplemented with ascorbic acid showed that hPDLF preserved their collagen synthetic ability *in vitro*, as demonstrated by the synthesis of types I, III, V, XII and XIV. hPDLF matrix thus formed demonstrated a recovery of type III collagen deposition and an insignificant increase in type V collagen at the end of expansion.

Having established and characterized hPDLF, cell-substratum interactions of hPDLF on PCL membranes were examined as a first step in the development of hPDLF-membrane constructs. Cytocompatibility of alkali-treated PCL membranes was enhanced in terms of a two-fold increase in cell adhesion rate and total efficiency, attributable to a greater accessibility of fibronectin cell-binding domain. Constructs consisting of perforated PCL membranes provided greater cell anchorage, and cell and matrix alignment than unperforated ones via contact guidance, while retaining hPDLF phenotypic expression and promoting matrix maturation at day 21.

Based on the findings above, hPDLF and hAO, derived from the same individual and previously characterized to possess the highest osteogenic potential,

were cultured on alkali-treated, perforated membranes and alkali-treated scaffolds respectively. Vascularized, well-integrated hPDLF-hAO double construct was observed 28 days after subcutaneous implantation in athymic mice, but no further osteogenesis in the earlier-mineralized matrix was seen.

Given the intrinsic biological patient-to-patient variation among the ten primary hPDLF cell lines, the selection of cells with the highest osteogenic potential *in vitro* was thought to facilitate tissue regeneration in hPDLF-hAO double constructs *in vivo*. However, the outcome of ectopic implantation in athymic mice was unexpected. Taking into account the observation that hPDLF exhibited a dedifferentiated or embryonic-like phenotype during expansion culture in the presence of ascorbic acid, and that the PDL has been associated with root resorption due to prostaglandin E2 production (Ogiso *et al.*, 1992; Shiraishi *et al.*, 2001), the lack of mineralized tissue formation was probably due to an interaction between hPDLF and hAO.

8.2 Future work

The possibility of dedifferentiation, defined as a process in which a partially or terminally differentiated cell reverts to a more embryonic form, or an earlier developmental stage (reviewed in Liu *et al.*, 2006) is sometimes overlooked during culture expansion. This is of importance not only in the expression of genes and proteins specific to the stage of differentiation, but also the collagenous matrix which in turn determines downstream gene expression and cellular phenotype.

It has been reported that *in vitro* cultures of PDLF demonstrated a lack of phenotypic stability, and were selective for a more “fibroblast-like” phenotype (Limeback and Sodek, 1979; Nohutch *et al.*, 1996). However, according to the

author's knowledge, there has been no report on the redifferentiation of hPDLF *in vitro*. The preservation of the state of cell differentiation for downstream clinical applications such as tissue engineering have been recently studied in chondrocytes (Yang *et al.*, 2006), epithelial cells (Reuters *et al.*, 2006) and hepatocytes (Hansen *et al.*, 2006).

This study showed that serum deprivation appeared to result in a reversal of a dedifferentiated phenotype, as recently reported in human vascular smooth muscle cells (Han *et al.*, 2006). hPDLF, though quiescent, secreted significantly greater amounts of collagenous ECM and achieved matrix maturation as seen from ALP upregulation. Therefore, this study provides the foundation work for redifferentiation studies of PDLF. Yet, this reversal was not complete, as seen from the persistent synthesis of the large isoforms of type XII and XIV collagen. Future work could entail the analysis of type XII and XIV collagen transcripts over serial passages of hPDLF by RT-PCR using isoform-specific primers to pin-point the exact stage where a “switch” in isoform expression took place.

REFERENCE

- 52nd World Medical Association General Assembly. (2000). Ethical principles for medical research involving human subjects. World Medical Association Declaration of Helsinki. Edinburgh, Scotland.
- American Academy of Periodontology. (2005). Periodontal Regeneration. *J Periodontol.* 76: 1601-1622
- Abe T, Hara Y, Abe Y, Aida Y, Maeda K. (1998). Serum or growth factor deprivation induces the expression of alkaline phosphatase in human gingival fibroblasts. *J Dent Res.* 77(9): 1700-1707
- Abercrombie M, Heaysman JE, Pegrum SM. (1971). The locomotion of fibroblasts in culture. IV. Electron microscopy of the leading lamella. *Exp Cell Res.* 67(2): 359-367
- Akiyama SK, Yamada SS, Chen WT, Yamada KM. (1989). Analysis of fibronectin receptor function with monoclonal antibodies: roles in cell adhesion, migration, matrix assembly, and cytoskeletal organization. *J Cell Biol.* 109(2): 863-875
- Albelda SM and Buck CA. (1990). Integrins and other cell adhesion molecules. *FASEB.* 4: 2868-2880
- Ali SA, Zhong SP, Doherty PJ, Williams DF. (1993). Mechanisms of polymer degradation in implantable devices. I. Poly(caprolactone). *Biomaterials.* 14(9): 648-656
- Ali SA, Doherty PJ, Williams DF. (1994). Molecular biointeractions of biomedical polymers with extracellular exudate and inflammatory cells and their effects on the biocompatibility, in vivo. *Biomaterials.* 15(10): 779-785
- Altroff H, Schlinkert R, van der Walle CF, Bernini A, Campbell ID, Werner JM, Mardon HJ. (2004). Interdomain tilt angle determines integrin-dependent function of the ninth and tenth FIII domains of human fibronectin. *J Biol Chem.* 279(53): 55995-6003
- Amar S. (1996). Implications of cellular and molecular biology advances in periodontal regeneration. *Anat Rec.* 245: 361-373
- Ambrose EJ. (1961). The movements of fibrocytes. *Exp Cell Res. Suppl* 8: 54-73
- Anderegg CR, Martin SJ, Gray JL, Mellonig JT, Gher ME. (1991). Clinical evaluation of the use of decalcified freeze-dried bone allograft with guided tissue regeneration in the treatment of molar furcation invasions. *J Periodontol.* 62(4): 264-268
- Andrade JD. (1985). Principles of protein adsorption. In: Surface and interfacial aspects of biomedical polymers. Andrade JD. (eds). Vol 2. New York: Plenum Press. p. 1-80

- Ang LP, Cheng ZY, Beuerman RW, Teoh SH, Zhu X, Tan DT. (2006). The development of a serum-free derived bioengineered conjunctival epithelial equivalent using an ultrathin poly(epsilon-caprolactone) membrane substrate. *Invest Ophthalmol Vis Sci.* 47(1): 105-112
- Anselme K, Bigerelle M, Noel B, Dufresne E, Judas D, Iost A, Hardouin P. (2000). Qualitative and quantitative study of human osteoblast adhesion on materials with various surface roughnesses. *J Biomed Mater Res.* 49(2): 155-166
- Aota S, Nagai T, Yamada KM. (1991). Characterization of regions of fibronectin besides the arginine-glycine-aspartic acid sequence required for adhesive function of the cell-binding domain using site-directed mutagenesis. *J Biol Chem.* 266(24): 15938-15943
- Aota S, Nomizu M, Yamada KM. (1994). The short amino acid sequence Pro-His-Ser-Arg-Asn in human fibronectin enhances cell-adhesive function. *J Biol Chem.* 269(40): 24756-24761
- Arceo N, Sauk JJ, Moehring J, Foster RA, Somerman MJ. (1991). Human periodontal cells initiate mineral-like nodules in vitro. *J periodontol.* 62(8): 499-503
- Arora P, McCulloch CAG. (1994). Dependence of collagen remodelling on a α -smooth muscle actin expression by fibroblasts. *J Cell Physiol.* 159: 161-175
- Aubert-Foucher E, Font B, Eichenberger D, Goldschmidt D, Lethias C, van der Rest M. (1992). Purification and characterization of native type XIV collagen. *J Biol Chem.* 267(22): 15759-15764
- Bailey AJ, Peach CM, Fowler LJ. (1970). Chemistry of the collagen cross-links. Isolation and characterization of two intermediate intermolecular cross-links in collagen. *Biochem J.* 117(5): 819-831
- Bartold PM. (1995). Turnover in periodontal connective tissues: dynamic homeostasis of cells, collagen and ground substances. *Oral Dis.* (4): 238-253
- Bartold PM, Narayanan AS. (1998). Periodontal regeneration. In: *Biology of the periodontal connective tissues.* Bartold PM, Narayanan AS. (eds). Chicago: Quintessence Publishing Co. p. 241-267
- Bartold PM, McCulloch CAG, Narayanan AS, Pitaru S. (2000). Tissue engineering: a new paradigm for periodontal regeneration based on molecular and cell biology. *Periodontol 2000.* 24: 253-269
- Bartold PM, Narayanan AS. (2003). The Biochemistry and Physiology of Periodontal Connective Tissues. In: *Fundamentals of Periodontics.* Wilson TG Jr, Kornman KS. (eds). Chicago: Quintessence Publishing Co. p. 67-93
- Baugh L, Vogel V. (2004). Structural changes of fibronectin adsorbed to model surfaces probed by fluorescence resonance energy transfer. *J Biomed Mater Res A.* 69(3): 525-534

- Becker W, Becker BE, Berg L, Prichard J, Caffesse R, Rosenberg E. (1988). New attachment after treatment with root isolation procedures: report for treated Class III and Class II furcations and vertical osseous defects. *Int J Periodontics Restorative Dent.* 8(3): 8-23
- Beertsen W. (1975). Migration of fibroblasts in the periodontal ligament of the mouse incisor as revealed by autoradiography. *Arch Oral Biol.* 20(10): 659-666
- Beertsen W, McCulloch CA, Sodek J. (1997). The periodontal ligament: a unique, multifunctional connective tissue. *Periodontol 2000.* 13: 20-40
- Bellows CG, Heersche JN, Aubin JE. (1992). Inorganic phosphate added exogenously or released from beta-glycerophosphate initiates mineralization of osteoid nodules *in vitro*. *Bone Miner.* 17(1): 15-29
- Bentley KL, Klebe RJ. (1985). Fibronectin binding properties of bacteriologic petri plates and tissue culture dishes. *J Biomed Mater Res.* 19(7): 757-769
- Berg MC, Yang SY, Hammond PT, Rubner MF. (2004). Controlling mammalian cell interactions on patterned polyelectrolyte multilayer surfaces. *Langmuir.* 20(4): 1362-1368
- Bergkvist M, Carlsson J, Oscarsson S. (2003). Surface-dependent conformations of human plasma fibronectin adsorbed to silica, mica, and hydrophobic surfaces, studied with use of atomic force microscopy. *J Biomed Mater Res A.* 64(2): 349-356
- Berkovitz BKB, Shore RC. (1995). Cells of the Periodontal Ligament. In: *The Periodontal Ligament in Health and Disease*. Berkovitz BKB, Moxham BJ, Newman HN. (eds). London: Mosby-Wolfe. p. 9-34
- Bershady AD, Tint IS, Neyfakh AA Jr, Vasiliev JM. (1985). Focal contacts of normal and RSV-transformed quail cells. Hypothesis of the transformation-induced deficient maturation of focal contacts. *Exp Cell Res.* 158(2): 433-444
- Berthod F, Germain L, Guignard R, Lethias C, Garrone R, Damour O, van der Rest M, Auger FA. (1997). Differential expression of collagens XII and XIV in human skin and in reconstructed skin. *J Invest Dermatol.* 108(5): 737-742
- Birk DE, Trelstad RL. (1984). Extracellular compartments in matrix morphogenesis: collagen fibril, bundle, and lamellar formation by corneal fibroblasts. *J Cell Biol.* 99(6): 2024-2033
- Birk DE, Trelstad RL. (1986). Extracellular compartments in tendon morphogenesis: collagen fibril, bundle, and macroaggregate formation. *J Cell Biol.* 103(1): 231-240
- Blomlof L, Otteskog P. (1981). Composition of human periodontal ligament cells in tissue culture. *Scand J Dent Res.* 89(1): 43-47

- Bohme K, Li Y, Oh PS, Olsen BR. (1995). Primary structure of the long and short splice variants of mouse collagen XII and their tissue-specific expression during embryonic development. *Dev Dyn.* 204(4): 432-445
- Booth BA, Polak KL, Uitto J. (1980). Collagen biosynthesis by human skin fibroblasts. I. Optimization of the culture conditions for synthesis of type I and type III procollagens. *Biochim Biophys Acta.* 607(1): 145-160
- Bornstein P, Traub W. (1979). The biochemistry and biology of collagen. In: *Proteins.* Neurath H, Hill RL. (eds). New York: Academic Press Inc. p. 411-632
- Bornstein P, Sage EH. (2002). Matricellular proteins: extracellular modulators of cell function. *Curr Opin Cell Biol.* 14(5): 608-616
- Boskey A. (1996). Matrix proteins and mineralization: an overview. *Connect Tissue Res.* 35: 357-363
- Boudreau NJ, Jones PL. (1999). Extracellular matrix and integrin signalling: the shape of things to come. *Biochem J.* 339 (3): 481-488
- Bowditch RD, Halloran CE, Aota S, Obara M, Plow EF, Yamada KM, Ginsberg MH. (1991). Integrin alpha IIb beta 3 (platelet GPIIb-IIIa) recognizes multiple sites in fibronectin. *J Biol Chem.* 266(34): 23323-23328
- Boyan BD, Hummert TW, Dean DD, Schwartz Z. (1996). Role of material surfaces in regulating bone and cartilage cell response. *Biomaterials.* 17(2): 137-146
- Boyko GA, Melcher AH, Brunette DM. (1981). Formation of new periodontal ligament by periodontal ligament cells implanted *in vivo* after culture *in vitro*. A preliminary study of transplanted roots in the dog. *J Periodontal Res.* 16(1): 73-88
- Brekke JH, Toth JM. (1998). Principles of tissue engineering applied to programmable osteogenesis. *J Biomed Mater Res.* 43(4): 380-398
- Bronckers AL. (1983). A histological and biochemical study of the effect of vitamin C-deficiency on induction of amelogenesis in hamster molars *in vitro*. *Arch Oral Biol.* 28(8): 681-692
- Brunette DM, Melcher AH, Moe HK. (1976). Culture and origin of epithelium-like and fibroblast-like cells from porcine periodontal ligament explants and cell suspensions. *Arch Oral Biol.* 21(7): 393-400
- Brunette DM. (1986). Fibroblasts on micromachined substrata orient hierarchically to grooves of different dimensions. *Exp Cell Res.* 164(1): 11-26
- Brunette DM, Chehroudi B. (1999). The effects of the surface topography of micromachined titanium substrata on cell behavior *in vitro* and *in vivo*. *J Biomech Eng.* 121(1): 49-57

- Buckley MJ, Agarwal S, Gassner R. (1999). Tissue engineering and dentistry. *Clin Plast Surg.* 26(4): 657-662
- Burg KJL, Porter S, Kellam JF. (2000). Biomaterials development for bone tissue engineering. *Biomaterials.* 21: 2347-2359
- Burridge K, Fath K, Kelly T, Nuckolls G, Turner C. (1988). Focal adhesions: transmembrane junctions between the extracellular matrix and the cytoskeleton. *Annu Rev Cell Biol.* 4: 487-525
- Burridge K, Fath K. (1989). Focal contacts: transmembrane links between the extracellular matrix and the cytoskeleton. *Bioessays.* 10(4): 104-108
- Burridge K, Chrzanowska-Wodnicka M. (1996). Focal adhesions, contractility, and signaling. *Annu Rev Cell Dev Biol.* 12: 463-518
- Butler WT, Birkedal-Hansen H, Beegle WF, Taylor RE, Chung E. (1975). Proteins of the periodontium. Identification of collagens with the [alpha1(I)]2alpha2 and [alpha1(III)]3 structures in bovine periodontal ligament. *J Biol Chem.* 250(23): 8907-8912
- Carnes DL, Maeder CL, Graves DT. (1997). Cells with osteoblastic phenotypes can be explanted from human gingiva and periodontal ligament. *J Periodontol.* 68(7): 701-707
- Caton J, Nyman S. (1980). Histometric evaluation of periodontal surgery. I. The modified Widman flap procedure. *J Clin Periodontol.* 7(3): 212-223
- Caton J, Nyman S, Zander H. (1980). Histometric evaluation of periodontal surgery. II. Connective tissue attachment levels after four regenerative procedures. *J Clin Periodontol.* 7(3): 224-231
- Caton JG, DeFuria EL, Polson AM, Nyman S. (1987). Periodontal regeneration via selective cell repopulation. *J Periodontol.* 58(8): 546-552
- Chaignaud BE, Langer R, Vacanti JP. (1997). The history of tissue engineering using synthetic biodegradable polymer scaffolds and cells. In: *Synthetic biodegradable polymer scaffolds.* Atala A, Mooney D. (eds). Boston: Birkhäuser. p. 1-14
- Chen J, Shapiro HS, Sodek J. (1992). Development expression of bone sialoprotein mRNA in rat mineralized connective tissues. *J Bone Miner Res.* 7(8): 987-997
- Cheng SL, Yang JW, Rifas L, Zhang SF, Avioli LV. (1994). Differentiation of human bone marrow osteogenic stromal cells *in vitro*: induction of the osteoblast phenotype by dexamethasone. *Endocrinology.* 134(1): 277-286
- Cheng Z, Teoh SH. (2004). Surface modification of ultra thin poly (epsilon-caprolactone) films using acrylic acid and collagen. *Biomaterials.* 25(11): 1991-2001

- Chien HH, Lin WL, Cho MI. (1999). Expression of TGF-beta isoforms and their receptors during mineralized nodule formation by rat periodontal ligament cells *in vitro*. *J Periodontal Res.* 34(6): 301-309
- Cho MI, Matsuda N, Lin WL, Moshier A, Ramakrishnan PR. (1992). *In vitro* formation of mineralized nodules by periodontal ligament cells from the rat. *Calcif Tissue Int.* 50(5): 459-467
- Cho MI, Lin WL, Genco RJ. (1995). Platelet-derived growth factor-modulated guided tissue regenerative therapy. *J Periodontol.* 66(6): 522-530
- Cho MI, Garant PR. (2000). Development and general structure of the periodontium. *Periodontol 2000.* 24: 9-27
- Chou AM, Sae-Lim V, Lim TM, Schantz JT, Teoh SH, Chew CL, Hutmacher DW. (2002). Culturing and characterization of human periodontal ligament fibroblasts – A preliminary study. *Materials Science and Engineering C.* 20: 77-83
- Chou AM, Sae-Lim V, Hutmacher DW, Lim TM. (2006). Tissue engineering of a periodontal ligament-alveolar bone graft construct. *Int J Oral Maxillofac Implants.* 21(4): 526-534
- Clark EA, Brugge JS. (1995). Integrins and signal transduction pathways: the road taken. *Science.* 268(5208): 233-239
- Clark RAF. (1996). Wound repair: overview and general considerations. In: *The Molecular and Cellular Biology of Wound Repair.* Clark RAF. (eds). London: Plenum Press. p. 3-50
- Cohn SA. (1972). A re-examination of Sharpey's fibres in alveolar bone of the marmoset (*Saguinus fuscicollis*). *Arch Oral Biol.* 17(2): 261-269
- Coolidge ED. (1937). The thickness of the human periodontal membrane. *J Am Dent Assoc.* 24: 1260-1270
- Costa MA, Fernandes MH. (2000). Long-term effects of parathyroid hormone, 1,25-dihydroxyvitamin d(3), and dexamethasone on the cell growth and functional activity of human osteogenic alveolar bone cell cultures. *Pharmacol Res.* 42(4): 345-353
- Cowles EA, DeRome ME, Pastizzo G, Brailey LL, Gronowicz GA. (1998). Mineralization and the expression of matrix proteins during *in vivo* bone development. *Calcif Tissue Int.* 62(1): 74-82
- Cramer LP, Mitchison TJ. (1995). Myosin is involved in postmitotic cell spreading. *J Cell Biol.* 131(1): 179-189
- Crumley P. (1964). Collagen formation in the normal and stressed periodontium. *Periodontics.* 2: 53-61

- Culp LA, Sukenik CN. (1998). Cell type-specific modulation of fibronectin adhesion functions on chemically-derivatized self-assembled monolayers. *J Biomater Sci Polym Ed.* 9(11): 1161-1176
- Curtis ASG. (1964). The mechanism of adhesion of cells to glass. *J Cell Biol.* 20: 199-215
- Darney PD, Monroe SE, Klaisle CM, Alvarado A. (1989). Clinical evaluation of the Capronor contraceptive implant: preliminary report. *Am J Obstet Gynecol.* 160(5 Pt 2): 1292-1295
- de Haan J, van Oeveren W. (1998). Platelets and soluble fibrin promote plasminogen activation causing downregulation of platelet glycoprotein Ib/IX complexes: protection by aprotinin. *Thromb Res.* 92: 171-179
- Declercq HA, Verbeeck RM, De Ridder LI, Schacht EH, Cornelissen MJ. (2005). Calcification as an indicator of osteoinductive capacity of biomaterials in osteoblastic cell cultures. *Biomaterials.* 26(24): 4964-4974
- D'Errico JA, MacNeil RL, Takata T, Berry J, Strayhorn C, Somerman MJ. (1997). Expression of bone associated markers by tooth root lining cells, *in situ* and *in vitro*. *Bone.* 20(2): 117-126
- Dharmavaram RM, Huynh AI, Jimenez SA. (1998). Characterization of human chondrocyte and fibroblast type XII collagen cDNAs. *Matrix Biol.* 16(6): 343-348
- Dublet B, Dixon E, de Miguel E, van der Rest M. (1988). Bovine type XII collagen: amino acid sequence of a 10 kDa pepsin fragment from periodontal ligament reveals a high degree of homology with the chicken alpha 1(XII) sequence. *FEBS Lett.* 233(1): 177-180
- Dubreuil RR. (1991). Structure and evolution of the actin crosslinking proteins. *Bioessays.* 13(5): 219-226
- Dugina V, Fontao L, Chaponnier C, Vasiliev J, Gabbiani G. (2001). Focal adhesion features during myofibroblastic differentiation are controlled by intracellular and extracellular factors. *J Cell Sci.* 114(18): 3285-3296
- Elbert DL, Hubbell JA. (1996). Surface treatments of polymers for biocompatibility. *Annu Rev Mater Sci.* 26: 365-394
- Embery G, Waddington RJ, Hall RC. (1995). The ground substance of the periodontal ligament. In: *The Periodontal Ligament in Health and Disease*. Berkovitz BKB, Moxham BJ, Newman HN. (eds). London: Mosby-Wolfe. p. 83-101
- Engelberg I, Kohn J. (1991). Physico-mechanical properties of degradable polymers used in medical applications: a comparative study. *Biomaterials.* 12(3): 292-304
- Fernandes MH, Costa MA, Carvalho GS. (1997). Mineralization in serially passaged human alveolar bone cells. *J Mater Sci Mater Med.* 8(2): 61-65

- Fisher LW, Hawkins GR, Tuross N, Termine JD. (1987). Purification and partial characterization of small proteoglycans I and II, bone sialoproteins I and II, and osteonectin from the mineral compartment of developing human bone. *J Biol Chem.* 262(20): 9702-9708
- Folkman J, Moscona A. (1978). Role of cell shape in growth control. *Nature.* 273(5661): 345-349
- Franceschi RT. (1999). The developmental control of osteoblast-specific gene expression: role of specific transcription factors and the extracellular matrix environment. *Crit Rev Oral Biol Med.* 10: 40-57
- Freshney RI. (2000). Primary Culture. In: *Culture of Animal Cells.* Freshney RI. (ed). New York: Wiley-Liss. p. 149-175
- Gage JP, Francis MJO, Triffitt JT. (1989). The collagens. In: *Collagen and Dental Matrices.* Gage JP, Francis MJO, Triffitt JT. (eds). London: Wright. p. 8-24
- Ganss B, Kim RH, Sodek J. (1999). Bone sialoprotein. *Crit Rev Oral Biol Med.* 10(1): 79-98
- Gao J, Niklason L, Langer R. (1998). Surface hydrolysis of poly(glycolic acid) meshes increases the seeding density of vascular smooth muscle cells. *J Biomed Mater Res.* 42(3): 417-424
- Garcia AJ, Vega MD, Boettiger D. (1999). Modulation of cell proliferation and differentiation through substrate-dependent changes in fibronectin conformation. *Mol Biol Cell.* 10(3): 785-798
- Garrett S. (1996). Periodontal regeneration around natural teeth. *Ann Periodontol.* 1(1): 621-666
- Gerecke DR, Olson PF, Koch M, Knoll JH, Taylor R, Hudson DL, Champlaud MF, Olsen BR, Burgeson RE. (1997). Complete primary structure of two splice variants of collagen XII, and assignment of alpha 1(XII) collagen (COL12A1), alpha 1(IX) collagen (COL9A1), and alpha 1(XIX) collagen (COL19A1) to human chromosome 6q12-q13. *Genomics.* 41(2): 236-242
- Giancotti FG, Ruoslahti E. (1999). Integrin signaling. *Science.* 285(5430): 1028-1032
- Gordon MK, Gerecke DR, Dublet B, van der Rest M, Olsen BR. (1989). Type XII collagen. A large multidomain molecule with partial homology to type IX collagen. *J Biol Chem.* 264(33): 19772-19778
- Gottlow J, Nyman S, Karring T, Lindhe J. (1984). New attachment formation as the result of controlled tissue regeneration. *J Clin Periodontol.* 11(8): 494-503

- Gould TR, Melcher AH, Brunette DM. (1980). Migration and division of progenitor cell populations in periodontal ligament after wounding. *J Periodontal Res.* 15(1): 20-42
- Grainger DW, Pavon-Djavid G, Migonney V, Josefowicz M. (2003). Assessment of fibronectin conformation adsorbed to polytetrafluoroethylene surfaces from serum protein mixtures and correlation to support of cell attachment in culture. *J Biomater Sci Polym Ed.* 14(9): 973-988
- Green E, Todd B, Heath D. (1990). Mechanism of glucocorticoid regulation of alkaline phosphatase gene expression in osteoblast-like cells. *Eur J Biochem.* 188(1): 147-153
- Green AM, Jansen JA, van der Waerden JP, von Recum AF. (1994). Fibroblast response to microtextured silicone surfaces: texture orientation into or out of the surface. *J Biomed Mater Res.* 28(5): 647-653
- Griffith LG. (2000). Polymeric biomaterials. *Acta Mater.* 48: 263-277
- Griffith LG. (2002). Emerging design principles in biomaterials and scaffolds for tissue engineering. *Ann NY Acad Sci.* 961: 83-95
- Grinnell F, Feld MK. (1982). Fibronectin adsorption on hydrophilic and hydrophobic surfaces detected by antibody binding and analyzed during cell adhesion in serum-containing medium. *J Biol Chem.* 257(9): 4888-4893
- Groeneveld MC, Everts V, Beertsen W. (1995). Alkaline phosphatase activity in the periodontal ligament and gingiva of the rat molar: its relation to cementum formation. *J Dent Res.* 74(7): 1374-1381
- Grzesik WJ, Kuzentsov SA, Uzawa K, Mankani M, Robey PG, Yamauchi M. (1998). Normal human cementum-derived cells: isolation, clonal expansion, and *in vitro* and *in vivo* characterization. *J Bone Miner Res.* 13: 1547-1554
- Guan J, Sacks MS, Beckman EJ, Wagner WR. (2002). Synthesis, characterization, and cytocompatibility of elastomeric, biodegradable poly(ester-urethane)ureas based on poly(caprolactone) and putrescine. *J Biomed Mater Res.* 61(3): 493-503
- Gunatillake PA, Adhikari R. (2003). Biodegradable synthetic polymers for tissue engineering. *Eur Cell Mater.* 5: 1-16
- Gundle R, Joyner CJ, Triffitt JT. (1995). Human bone tissue formation in diffusion chamber culture *in vivo* by bone-derived cells and marrow stromal fibroblastic cells. *Bone.* 16(6): 597-601
- Haas R, Culp LA. (1982). Properties and fate of plasma fibronectin bound to the tissue culture substratum. *J Cell Physiol.* 113(2): 289-297

- Haase HR, Clarkson RW, Waters MJ, Bartold PM. (1998). Growth factor modulation of mitogenic responses and proteoglycan synthesis by human periodontal fibroblasts. *J Cell Physiol.* 174(3): 353-361
- Haisch A, Groger A, Radke C, Ebmeyer J, Sudhoff H, Grasnick G, Jahnke V, Burmester GR, Sittinger M. (2000). Macroencapsulation of human cartilage implants: pilot study with polyelectrolyte complex membrane encapsulation. *Biomaterials.* 21: 1561-1566
- Hammarstrom L, Alatli I, Fong CD. (1996). Origins of cementum. *Oral Dis.* 2(1): 63-69
- Han M, Wen JK, Zheng B, Cheng Y, Zhang C. (2006). Serum deprivation results in redifferentiation of human umbilical vascular smooth muscle cells. *Am J Physiol Cell Physiol.* 291(1): C50-58
- Hansen LK, Wilhelm J, Fassett JT. (2006). Regulation of hepatocyte cell cycle progression and differentiation by type I collagen structure. *Curr Top Dev Biol.* 72: 205-236
- Harrison JW, Roda RS. (1995). Intermediate cementum. Development, structure, composition, and potential functions. *Oral Surg Oral Med Oral Pathol Oral Radiol Endod.* 79(5): 624-633
- Hasegawa M, Yamato M, Kikuchi A, Okano T, Ishikawa I. (2005). Human periodontal ligament cell sheets can regenerate periodontal ligament tissue in an athymic rat model. *Tissue Eng.* 11(3-4): 469-478
- Hassell TM. (1993). Tissues and cells of the periodontium. *Periodontol 2000.* 3: 9-38
- Hauschka PV, Chen TL, Mavrakos AE. (1988). Polypeptide growth factors in bone matrix. *Ciba Found Symp.* 136: 207-225
- Hayami T, Zhang Q, Kapila Y, Kapila S. (2007). Dexamethasone's enhancement of osteoblastic markers in human periodontal ligament cells is associated with inhibition of collagenase expression. *Bone.* 40(1): 93-104
- Heath JP, Dunn GA. (1978). Cell to substratum contacts of chick fibroblasts and their relation to the microfilament system. A correlated interference-reflexion and high-voltage electron-microscope study. *J Cell Sci.* 29: 197-212
- Heineken FG, Skalak R. (1991). Tissue Engineering: A brief overview. *J Biomech Eng.* 113: 111
- Hill RW, Ramfjord SP, Morrison EC, Appleberry EA, Caffesse RG, Kerry GJ, Nissle RR. (1981). Four types of periodontal treatment compared over two years. *J Periodontol.* 52(11): 655-662

- Hinz B, Dugina V, Ballestrem C, Wehrle-Haller B, Chaponnier C. (2003). Alpha-smooth muscle actin is crucial for focal adhesion maturation in myofibroblasts. *Mol Biol Cell*. 14(6): 2508-2519
- Hoffman KR, Casey DJ. (1985). Effect of carboxyl end groups on hydrolysis of polyglycolic acid. *J Polym Sci Polym Ed*. 23: 1939-1954
- Holland SF, Tighe BJ. (1992). Biodegradable polymers. In: *Advances in Pharmaceutical Sciences*. Ganderton D, Jones T, McGinity J. (eds). London: Academic Press. p. 101-164
- Holmstrup P. (2003). Anatomy of the periodontium. In: *Fundamentals of periodontics*. Wilson TG Jr, Kornman KS. (eds). Chicago: Quintessence Publishing Co. p. 21-38
- Horbett TA. (1984). Mass action effects on competitive adsorption of fibrinogen from hemoglobin solutions and from plasma. *Thromb Haemost*. 51(2): 174-181
- Horbett TA, Klumb LA. (1996). Cell culturing: surface aspects and considerations. In: *Brash JL, Wojciechowski PW (ed.). Interfacial phenomena and bioproducts*. New York: Marcel Dekker. p 351-445
- Hou LT, Liu CM, Lei JY, Wong MY, Chen JK. (2000). Biological effects of cementum and bone extracts on human periodontal fibroblast. *J Periodontol*. 71(7): 1100-1109
- Howard-Jones N. (1985). A CIOMS ethical code for animal experimentation. *WHO Chronicle*. 39: 51-56
- Htay AS, Teoh SH, Hutmacher DW. (2004). Development of perforated microthin poly(ϵ -caprolactone) films as matrices for membrane tissue engineering. *J Biomater Sci Polym Ed*. 15: 683-700
- Hu WJ, Eaton JW, Ugarova TP, Tang L. (2001). Molecular basis of biomaterial-mediated foreign body reactions. *Blood*. 98(4): 1231-1238
- Hubbell J. (1995). Biomaterials in tissue engineering. *Biotechnology*. 13: 565-576
- Hutmacher DW. (2000). Scaffolds in tissue engineering bone and cartilage. *Biomaterials*. 21(24): 2529-2543
- Hutmacher DW, Schantz T, Zein I, Ng KW, Teoh SH, Tan KC. (2001). Mechanical properties and cell cultural response of polycaprolactone scaffolds designed and fabricated via fused deposition modelling. *J Biomed Mater Res*. 55: 203-216
- Hynes RO. (1987). Integrins: a family of cell surface receptors. *Cell*. 48(4): 549-554
- Hynes RO. (1990). *Fibronectins*. Hynes RO. (eds). New York: Springer-Verlag. p. 546

- Iglhaut J, Suggs C, Borjesson B, Aukhil I. (1987). Apical migration of oral epithelium in experimental dehiscence wounds. *J Clin Periodontol.* 14(9): 508-514
- Ishaug-Riley SL, Okun LE, Prado G, Applegate MA, Ratcliffe A. (1999). Human articular chondrocyte adhesion and proliferation on synthetic biodegradable polymer films. *Biomaterials.* 20(23-24): 2245-2256
- Ishihara K, Fukumoto K, Iwasaki Y, Nakabayashi N. (1999). Modification of polysulfone with phospholipid polymer for improvement of the blood compatibility. Part 1. Surface characterization. *Biomaterials.* 20: 1545–1551
- Ishikawa S, Iwasaki K, Komaki M, Ishikawa I. (2004). Role of ascorbic acid in periodontal ligament cell differentiation. *J Periodontol.* 75(5): 709-716
- Israelachvili J, Wennerstrom H. (1996). Role of hydration and water structure in biological and colloidal interactions. *Nature.* 379(6562): 219-225
- Iuliano DJ, Saavedra SS, Truskey GA. (1993). Effect of the conformation and orientation of adsorbed fibronectin on endothelial cell spreading and the strength of adhesion. *J Biomed Mater Res.* 27(8): 1103-1113
- Ivanovski S, Haase HR, Bartold PM. (2001). Isolation and characterization of fibroblasts derived from regenerating human periodontal defects. *Arch Oral Biol.* 46: 679-688
- Izzard CS, Lochner LR. (1976). Cell-to-substrate contacts in living fibroblasts: an interference reflexion study with an evaluation of the technique. *J Cell Sci.* 21(1): 129-159
- Jang YC, Arumugam S, Ferguson M, Gibran NS, Isik FF. (1998). Changes in matrix composition during the growth and regression of human hemangiomas. *J Surg Res.* 80: 9-15
- Jeong SI, Kim SH, Kim YH, Jung Y, Kwon JH, Kim BS, Lee YM. (2004). Manufacture of elastic biodegradable PLCL scaffolds for mechano-active vascular tissue engineering. *J Biomater Sci Polym Ed.* 15(5): 645-660
- Jukkola A, Risteli J, Risteli L. (1991). Effect of dextran on synthesis, secretion and deposition of type III procollagen in cultured human fibroblasts. *Biochem J.* 279: 49-54
- Junker P, Helin G, Lorenzen I. (1981). Effect of D-penicillamine on collagen, glycosaminoglycans, DNA and RNA of granulation tissue and connective tissue of skin, bone and aorta in rats. *Acta Pharmacol Toxicol (Copenh).* 48(4): 300-310
- Junker P, Lorenzen I. (1983). Reversibility of D-penicillamine induced collagen alterations in rat skin and granulation tissue. *Biochem Pharmacol.* 32(11): 1753-1757

- Kaldahl WB, Kalkwarf KL, Patil KD, Molvar MP, Dyer JK. (1996). Long-term evaluation of periodontal therapy: I. Response to 4 therapeutic modalities. *J Periodontol.* 67(2): 93-102
- Kam Z, Volberg T, Geiger B. (1995). Mapping of adherens junction components using microscopic resonance energy transfer imaging. *J Cell Sci.* 108(3): 1051-1062
- Kania AM, Reichenberger E, Baur ST, Karimbux NY, Taylor RW, Olsen BR, Nishimura I. (1999). Structural variation of type XII collagen at its carboxyl-terminal NC1 domain generated by tissue-specific alternative splicing. *J Biol Chem.* 274(31): 22053-22059
- Karimbux NY, Rosenblum ND, Nishimura I. (1992). Site-specific expression of collagen I and XII mRNAs in the rat periodontal ligament at two developmental stages. *J Dent Res.* 71(7): 1355-1362
- Karimbux NY, Nishimura I. (1995). Temporal and spatial expressions of type XII collagen in the remodeling periodontal ligament during experimental tooth movement. *J Dent Res.* 74(1): 313-318
- Kasemo B, Gold J. (1999). Implant surfaces and interface processes. *Adv Dent Res.* 13: 8-20
- Kasugai S, Todescan R Jr, Nagata T, Yao KL, Butler WT, Sodek J. (1991). Expression of bone matrix proteins associated with mineralized tissue formation by adult rat bone marrow cells *in vitro*: inductive effects of dexamethasone on the osteoblastic phenotype. *J Cell Physiol.* 147(1): 111-120
- Kasugai S, Nagata T, Sodek J. (1992). Temporal studies on the tissue compartmentalization of bone sialoprotein(BSP), Osteopontin(OPN) and SPARC protein during bone formation *in vitro*. *J Cell Physiol.* 152: 467-477
- Kato T, Nakayasu K, Kanai A, Nishiyama T, Imamura Y, Hayashi T. (2000). Distribution and isoform characterization of type XII collagen in bovine cornea. *Ophthalmic Res.* 32(5): 215-221
- Kawase T, Sato S, Miake K, Saito S. (1988). Alkaline phosphatase of human periodontal ligament fibroblast-like cells. *Adv Dent Res.* 2(2): 234-239
- Keene DR, Lunstrum GP, Morris NP, Stoddard DW, Burgeson RE. (1991). Two type XII-like collagens localize to the surface of banded collagen fibrils. *J Cell Biol.* 113(4): 971-978
- Kelm RJ Jr, Swords NA, Orfeo T, Mann KG. (1994). Osteonectin in matrix remodeling. A plasminogen-osteonectin-collagen complex. *J Biol Chem.* 269(48): 30147-30153
- Keselowsky BG, Collard DM, Garcia AJ. (2003). Surface chemistry modulates fibronectin conformation and directs integrin binding and specificity to control cell adhesion. *J Biomed Mater Res A.* 66(2): 247-259

- Kessler E, Adar R, Goldberg B, Niece R. (1986). Partial purification and characterization of a procollagen C-proteinase from the culture medium of mouse fibroblasts. *Coll Relat Res.* 6(3): 249-266
- Khor HL, Ng KW, Schantz JT, Phan T-T, Lim TC, Teoh SH, Hutmacher DW. (2002). Poly(ϵ -caprolactone) films as a potential substrate for tissue engineering an epidermal equivalent. *Mat Sci Eng C.* 20: 71-75
- Khor HL, Ng KW, Htay AS, Schantz JT, Teoh SH, Hutmacher DW. (2003). Preliminary study of a polycaprolactone membrane utilized as epidermal substrate. *J Mater Sci Mater Med.* 14(2): 113-120
- Kielty CM, Grant ME. (2002). The collagen family: Structure, assembly and organization in the extracellular matrix. In: *Connective Tissue and Its Heritable Disorders: Molecular, Genetic, and Medical Aspects.* Royce PM, Steinmann B. (eds). New York: Wiley-Liss. p. 159-221
- Kiernan JA. (2001). Classification and naming of dyes, stains and fluorochromes. *Biotech Histochem.* 76(5-6): 261-278
- Kimura Y. (1993). Biodegradable polymers. In: *Biomedical applications of polymeric materials.* Tsuruta T, Hayashi T, Kataoka K, Ishihara K, Kimura Y (eds). Boca Raton: CRC Press. p. 163-190
- Kirkham J, Robinson C. (1995). The biochemistry of the fibres of the periodontal ligament. In: *The periodontal ligament in health and diseases.* Berkovitz BKB, Moxham BJ, Newman HN. (eds). London: Mosby-Wolfe. p. 55-82
- Kirkpatrick CJ, Dekker A. (1992). Quantitative evaluation of cell interaction with biomaterials in vitro. *Adv Biomater.* 10: 31-41
- Kirkpatrick CJ, Bittinger F, Wagner M, Kohler H, van Kooten TG, Klein CL, Otto M. (1998). Current trends in biocompatibility testing. *Proc Inst Mech Eng [H].* 212(2): 75-84
- Knabe C, Berger G, Gildenhaar R, Howlett CR, Markovic B, Zreiqat H. (2004). The functional expression of human bone-derived cells grown on rapidly resorbable calcium phosphate ceramics. *Biomaterials.* 25(2): 335-344
- Koch M, Bohrmann B, Matthison M, Hagios C, Trueb B, Chiquet M. (1995). Large and small splice variants of collagen XII: differential expression and ligand binding. *J Cell Biol.* 130(4): 1005-1014
- Kohn J, Langer R. (1996). Bioresorbable and bioerodible materials. In: *Biomaterials science: an introduction to materials in medicine.* Ratner BD, Hoffman AS, Schoen FJ, Lemons JE. (eds). San Diego: Academic Press. p.64-73
- Kowalczyńska HM, Nowak-Wyrzykowska M, Dobkowski J, Kolos R, Kaminski J, Makowska-Cynka A, Marciniak E. (2002). Adsorption characteristics of human

- plasma fibronectin in relationship to cell adhesion. *J Biomed Mater Res.* 61(2): 260-269
- Kuroiwa M, Tachikawa T, Izumiya N, Takubo K, Yoshiki S, Higashi S. (1996). Ultrastructure of the rat periodontal ligament as observed with quick-freeze, deep-etch and replica methods: arrangement of collagen and related structures. *Acta Anat.* 157(4): 291-302
- Kweon H, Yoo MK, Park IK, Kim TH, Lee HC, Lee HS, Oh JS, Akaike T, Cho CS. (2003). A novel degradable polycaprolactone networks for tissue engineering. *Biomaterials.* 24(5): 801-808
- Lampugnani MG, Resnati M, Dejana E, Marchisio PC. (1991). The role of integrins in the maintenance of endothelial monolayer integrity. *J Cell Biol.* 112(3): 479-490
- Lang H, Schuler N, Arnhold S, Nolden R, Mertens T. (1995). Formation of differentiated tissues *in vivo* by periodontal cell populations cultured *in vitro*. *J Dent Res.* 74(5): 1219-1225
- Lang H, Schuler N, Nolden R. (1998). Attachment formation following replantation of cultured cells into periodontal defects - a study in minipigs. *J Dent Res.* 77(2): 393-405
- Langer R, Vacanti JP. (1993). Tissue engineering. *Science.* 260: 920-926
- Lapiere CM, Nusgens B, Pierard GE. (1977). Interaction between collagen type I and type III in conditioning bundles organization. *Connect Tissue Res.* 5(1): 21-29
- Larjava H, Hakkinen L, Rahemtulla F. (1992). A biochemical analysis of human periodontal tissue proteoglycans. *Biochem J.* 284 (1): 267-274
- Lee JH, Khang G, Lee JW, Lee HB. (1998). Interaction of different types of cells on polymer surfaces with wettability gradient. *J Colloid Interface Sci.* 205(2): 323-330
- Lee CK, Piedrahita JA. (2002). Inhibition of apoptosis in serum starved porcine embryonic fibroblasts. *Mol Reprod Dev.* 62(1): 106-112
- Lekic P, McCulloch CAG. (1996). Periodontal ligament cell populations: the central role of fibroblasts in creating a unique tissue. *Anat Rec.* 245: 327-341
- Lekic PC, Pender N, McCulloch CA. (1997). Is fibroblast heterogeneity relevant to the health, diseases, and treatments of periodontal tissues? *Crit Rev Oral Biol Med.* 8(3): 253-268
- Lekic P, Rojas J, Birek C, Tenenbaum H, McCulloch CA. (2001). Phenotypic comparison of periodontal ligament cells *in vivo* and *in vitro*. *J Periodontal Res.* 36(2): 71-79

- Lekovic V, Kenney EB, Kovacevic K, Carranza FA Jr. (1989). Evaluation of guided tissue regeneration in Class II furcation defects. A clinical re-entry study. *J Periodontol.* 60(12): 694-698
- Levi B, Werman MJ. (1998). Long-term fructose consumption accelerates glycation and several age-related variables in male rats. *J Nutr.* 128(9): 1442-1449
- Lewandowska K, Balachander N, Sukenik CN, Culp LA. (1989). Modulation of fibronectin adhesive functions for fibroblasts and neural cells by chemically derivatized substrata. *J Cell Physiol.* 141(2): 334-345
- Li WJ, Danielson KG, Alexander PG, Tuan RS. (2003). Biological response of chondrocytes cultured in three-dimensional nanofibrous poly(epsilon-caprolactone) scaffolds. *J Biomed Mater Res.* 67A: 1105-1114
- Lian JB, Stein GS. (1992). Concepts of osteoblast growth and differentiation: basis for modulation of bone cell development and tissue formation. *Crit Rev Oral Biol Med.* 3(3): 269-305
- Lillie RD, Fullmer HM. (1976). *Histopathologic technic and practical histochemistry.* Lillie RD, Fullmer HM. (eds). New York: McGraw-Hill
- Lim JY, Liu X, Vogler EA, Donahue HJ. (2004). Systematic variation in osteoblast adhesion and phenotype with substratum surface characteristics. *J Biomed Mater Res A.* 68(3): 504-512
- Limeback HF, Sodek J, Brunette DM. (1978). Nature of collagens synthesized by monkey periodontal-ligament fibroblasts *in vitro*. *Biochem J.* 170(1): 63-71
- Limeback HF, Sodek J. (1979). Procollagen synthesis and processing in periodontal ligament *in vivo* and *in vitro*. A comparative study using slab-gel fluorography. *Eur J Biochem.* 100(2): 541-550
- Limeback H, Sodek J, Aubin JE. (1983). Variation in collagen expression by cloned periodontal ligament cells. *J Periodontal Res.* 18(3): 242-248
- Lin WL, McCulloch CA, Cho MI. (1994). Differentiation of periodontal ligament fibroblasts into osteoblasts during socket healing after tooth extraction in the rat. *Anat Rec.* 240(4): 492-506
- Lincks J, Boyan BD, Blanchard CR, Lohmann CH, Liu Y, Cochran DL, Dean DD, Schwartz Z. (1998). Response of MG63 osteoblast-like cells to titanium and titanium alloy is dependent on surface roughness and composition. *Biomaterials.* 19(23): 2219-2232
- Lindhe J, Westfelt E, Nyman S, Socransky SS, Heijl L, Bratthall G. (1982). Healing following surgical/non-surgical treatment of periodontal disease. A clinical study. *J Clin Periodontol.* 9(2): 115-128

- Lindskog S. (1982). Formation of intermediate cementum. I: Early mineralization of aprismatic enamel and intermediate cementum in monkey. *J Craniofac Genet Dev Biol.* 2(2): 147-160
- Linsenmayer TF. (1991). Collagen. In: *Cell Biology of Extracellular Matrix.* Hay ED. (eds). New York: Plenum Press. p. 7-44
- Liu HW, Yacobi R, Savion N, Narayanan AS, Pitaru S. (1997). A collagenous cementum-derived attachment protein is a marker for progenitors of the mineralized tissue-forming cell lineage of the periodontal ligament. *J Bone Miner Res.* 12(10): 1691-1699
- Liu HX, Hu DH, Jia CY, Fu XB. (2006). Progress of cellular dedifferentiation research. *Chin J Traumatol.* 9(5): 308-315
- Lomri A, Marie PJ, Tran PV, Hott M. (1988). Characterization of endosteal osteoblastic cells isolated from mouse caudal vertebrae. *Bone.* 9(3): 165-175
- Lukinmaa PL, Mackie EJ, Thesleff I. (1991). Immunohistochemical localization of the matrix glycoproteins--tenascin and the ED-sequence-containing form of cellular fibronectin--in human permanent teeth and periodontal ligament. *J Dent Res.* 70(1): 19-26
- Lunstrum GP, McDonough AM, Marinkovich MP, Keene DR, Morris NP, Burgeson RE. (1992). Identification and partial purification of a large, variant form of type XII collagen. *J Biol Chem.* 267(28): 20087-20092
- Lyons BL, Schwarz RI. (1984). Ascorbate stimulation of PAT cells causes an increase in transcription rates and a decrease in degradation rates of procollagen mRNA. *Nucleic Acids Res.* 12(5): 2569-2579
- Mackie EJ, Halfter W, Liverani D. (1988). Induction of tenascin in healing wounds. *J Cell Biol.* 107(6): 2757-2767
- MacNeil RL, Somerman MJ. (1993). Molecular factors regulating development and regeneration of cementum. *J Periodontal Res.* 28: 550-559
- MacNeil RL, Berry J, D'Errico J, Strayhorn C, Piotrowski B, Somerman MJ. (1995). Role of two mineral-associated adhesion molecules, osteopontin and bone sialoprotein, during cementogenesis. *Connect Tissue Res.* 33(1-3): 1-7.
- MacNeil RL, Berry J, Strayhorn C, Somerman MJ. (1996). Expression of bone sialoprotein mRNA by cells lining the mouse tooth root during cementogenesis. *Arch Oral Biol.* 41(8-9): 827-835
- MacNeil RL, Berry JE, Strayhorn CL, Shigeyama Y, Somerman MJ. (1998). Expression of type I and XII collagen during development of the periodontal ligament in the mouse. *Arch Oral Biol.* 43(10): 779-787

- MacNeil RL, Somerman MJ. (1999). Development and regeneration of the periodontium: parallels and contrasts. *Periodontol* 2000. 19: 8-20
- Magnusson P, Larsson L, Magnusson M, Davie MW, Sharp CA. (1999). Isoforms of bone alkaline phosphatase: characterization and origin in human trabecular and cortical bone. *J Bone Miner Res.* 14(11): 1926-1933
- Majeska RJ, Nair BC, Rodan GA. (1985). Glucocorticoid regulation of alkaline phosphatase in the osteoblastic osteosarcoma cell line ROS 17/2.8. *Endocrinology.* 116(1): 170-179
- Malekzadeh R, Hollinger JO, Buck D, Adams DF, McAllister BS. (1998). Isolation of human osteoblast-like cells and *in vitro* amplification for tissue engineering. *J Periodontol.* 69(11): 1256-1262
- Maniatis T, Goodbourn S, Fischer JA. (1987). Regulation of inducible and tissue-specific gene expression. *Science.* 236(4806): 1237-1245
- Manwaring ME, Walsh JF, Tresco PA. (2004). Contact guidance induced organization of extracellular matrix. *Biomaterials.* 25(17): 3631-3638
- Mariotti A. (1993). The extracellular matrix of the periodontium: dynamic and interactive tissues. *Periodontol* 2000. 3: 39-63
- Martinez ME, Medina S, del Campo MT, Sanchez-Cabezudo MJ, Sanchez M, Munuera L. (1998). Effect of polyethylene on osteocalcin, alkaline phosphatase and procollagen secretion by human osteoblastic cells. *Calcif Tissue Int.* 62(5): 453-456
- Matheson S, Larjava H, Hakkinen L. (2005). Distinctive localization and function for lumican, fibromodulin and decorin to regulate collagen fibril organization in periodontal tissues. *J Periodontal Res.* 40(4): 312-324
- Matsuda N, Lin WL, Kumar NM, Cho MI, Genco RJ. (1992). Mitogenic, chemotactic, and synthetic responses of rat periodontal ligament fibroblastic cells to polypeptide growth factors *in vitro*. *J Periodontol.* 63(6): 515-525
- Matsuda N, Kumar N.M, Ramakrishnan PR, Lin WL, Genco RJ, Cho MI. (1993). Evidence for up-regulation of epidermal growth factor receptors on rat periodontal ligament fibroblastic cells associated with stabilization of phenotype *in vitro*. *Arch Oral Biol.* 38(7): 559-569
- Matsuura M, Herr Y, Han KY, Lin WL, Genco RJ, Cho MI. (1995). Immunohistochemical expression of extracellular matrix components of normal and healing periodontal tissues in the beagle dog. *J Periodontol.* 66(7): 579-593
- Mauch C, Hatamochi A, Scharffetter K, Krieg T. (1988). Regulation of collagen synthesis in fibroblasts within a three-dimensional collagen gel. *Exp Cell Res.* 178(2): 493-503

- Mayne R, Vail MS, Mayne PM, Miller EJ. (1976). Changes in type of collagen syntheses as clones of chick chondrocytes grow and eventually lose division capacity. *Proc Natl Acad Sci USA* 73: 1674-1678
- McClary KB, Ugarova T, Grainger DW. (2000). Modulating fibroblast adhesion, spreading, and proliferation using self-assembled monolayer films of alkylthiolates on gold. *J Biomed Mater Res.* 50(3): 428-439
- McCulloch CA, Melcher AH. (1983a). Continuous labelling of the periodontal ligament of mice. *J Periodontal Res.* 18(3): 231-241
- McCulloch CA, Melcher AH. (1983b). Cell migration in the periodontal ligament of mice. *J Periodontal Res.* 18(4): 339-352
- McCulloch CAG, Nemeth E, Lowenberg B, Melcher AH. (1987). Paravascular cells in endosteal spaces of alveolar bone contribute to periodontal ligament cell populations. *Anat Rec.* 219(3): 233-242
- McCulloch CA, Bordin S. (1991). Role of fibroblast subpopulations in periodontal physiology and pathology. *J Periodontal Res.* 26(3): 144-154
- McCulloch CA. (1995). Origins and functions of cells essential for periodontal repair: the role of fibroblasts in tissue homeostasis. *Oral Dis.* 1(4): 271-278
- Melcher AH. (1970). Repair of wounds in the periodontium of the rat. Influence of periodontal ligament on osteogenesis. *Arch Oral Biol.* 15(12): 1183-1204
- Melcher AH. (1976). On the repair potential of periodontal tissues. *J Periodontol.* 47: 256-260
- Melcher AH, Cheong T, Cox J, Nemeth E, Shiga A. (1986). Synthesis of cementum-like tissue *in vitro* by cells cultured from bone: a light and electron microscope study. *J Periodontal Res.* 21(6): 592-612
- Melkko J, Niemi S, Risteli L, Risteli J. (1990). Radioimmunoassay of the carboxyterminal propeptide of human type I procollagen. *Clin Chem.* 36(7): 1328-1332
- Meyle J, Kapitza K. (1990). Assay of ascorbic acid in human crevicular fluid from clinically healthy gingival sites by high-performance liquid chromatography. *Arch Oral Biol.* 35: 319-323
- Minabe M. (1991). A critical review of the biologic rationale for guided tissue regeneration. *J Periodontol.* 62(3): 171-179
- Minkoff R, Engstrom TG. (1979). A long-term comparison of protein turnover in subcrestal vs supracrestal fibre tracts in the mouse periodontium. *Arch Oral Biol.* 24(10-11): 817-824

- Mizuno N, Shiba H, Mouri Y, Xu W, Kudoh S, Kawaguchi H, Kurihara H. (2005). Characterization of epithelial cells derived from periodontal ligament by gene expression patterns of bone-related and enamel proteins. *Cell Biol Int.* 29(2): 111-117
- Mundlos S, Schwahn B, Reichert T, Zabel B. (1992). Distribution of osteonectin mRNA and protein during human embryonic and fetal development. *J Histochem Cytochem.* 40(2): 283-291
- Murphy WL, Mooney DJ. (1999). Controlled delivery of inductive proteins, plasmid DNA and cells from tissue engineering matrices. *J Periodontal Res.* 34(7): 413-419
- Muschler GF, Nakamoto C, Griffith LG. (2004). Engineering principles of clinical cell-based tissue engineering. *J Bone Joint Surg Am.* 86A: 1541-1558
- Nagata T, Bellows CG, Kasugai S, Butler WT, Sodek J. (1991). Biosynthesis of bone proteins [SPP-1 (secreted phosphoprotein-1, osteopontin), BSP (bone sialoprotein) and SPARC (osteonectin)] in association with mineralized-tissue formation by fetal-rat calvarial cells in culture. *Biochem J.* 274 (2): 513-520
- Nakae H, Narayanan AS, Raines E, Page RC. (1991). Isolation and partial characterization of mitogenic factors from cementum. *Biochemistry.* 30(29): 7047-7052
- Nakahara T, Nakamura T, Kobayashi E, Kuremoto K, Matsuno T, Tabata Y, Eto K, Shimizu Y. (2004). *In situ* tissue engineering of periodontal tissues by seeding with periodontal ligament-derived cells. *Tissue Eng.* 10: 537-544
- Namkung-Matthai H, Seale JP, Brown K, Mason RS. (1998). Comparative effects of anti-inflammatory corticosteroids in human bone-derived osteoblast-like cells. *Eur Respir J.* 12(6): 1327-1333
- Narayanan AS, Page RC. (1977). Serum modulates collagen types in human gingiva fibroblasts. *FEBS Lett.* 80(1): 221-224
- Narayanan AS, Page RC. (1983). Biosynthesis and regulation of type V collagen in diploid human fibroblasts. *J Biol Chem.* 258(19): 11694-11699
- Narayanan AS, Bartold PM. (1996). Biochemistry of periodontal connective tissues and their regeneration: a current perspective. *Connect Tissue Res.* 34(3): 191-201
- Nefussi JR, Baron R. (1985). PGE₂ stimulates both resorption and formation of bone *in vitro*: differential responses of the periosteum and the endosteum in fetal rat long bone cultures. *Anat Rec.* 211: 9-16
- Nefussi JR, Casamajor P, Serfaty R, Bolle M, Hugly C, Forest N. (1998). Activated adult human alveolar bone cells: a new model of matrix mineralization. *Eur J Oral Sci.* 106 (Suppl 1): 424-428
- Ng CS, Teoh SH, Chung TS, Hutmacher DW. (2000). Simultaneous biaxial drawing of poly(ϵ -caprolactone) films. *Polymer.* 41: 5855-5864

- Ng KW, Hutmacher DW, Schantz JT, Ng CS, Too HP, Lim TC, Phan TT, Teoh SH. (2001). Evaluation of ultra-thin poly(ϵ -caprolactone) films for tissue-engineered skin. *Tissue Eng.* 7(4): 441-455
- Ng KW, Leong DT, Hutmacher DW. (2005). The challenge to measure cell proliferation in two and three dimensions. *Tissue Eng.* 11(1-2): 182-191
- Niederreiter M, Gimona M, Streichsbier F, Celis JE, Small JV. (1994). Complex protein composition of isolated focal adhesions: a two-dimensional gel and database analysis. *Electrophoresis.* 15(3-4): 511-519
- Njieha FK, Morikawa T, Tuderman L, Prockop DJ. (1982). Partial purification of a procollagen C-proteinase. Inhibition by synthetic peptides and sequential cleavage of type I procollagen. *Biochemistry.* 21(4): 757-764
- Nobes CD, Hall A. (1995). Rho, rac, and cdc42 GTPases regulate the assembly of multimolecular focal complexes associated with actin stress fibers, lamellipodia, and filopodia. *Cell.* 81(1): 53-62
- Nohutcu RM, McCauley LK, Shigeyama Y, Somerman MJ. (1996). Expression of mineral-associated proteins by periodontal ligament cells: *in vitro* vs. *ex vivo*. *J Periodontal Res.* 31(5): 369-372
- Nomura H, Ishiguro T, Morimoto S. (1969). Studies on L-ascorbic acid derivatives. III. Bis(L-ascorbic acid-3,3') phosphate and L-ascorbic acid 2-phosphate. *Chem Pharm Bull.* 17: 387-393
- Nyman S, Lindhe J, Karring T, Rylander H. (1982). New attachment following surgical treatment of human periodontal disease. *J Clin Periodontol.* 9: 290-296
- Nyman S, Gottlow J, Lindhe J, Karring T, Wennstrom J. (1987). New attachment formation by guided tissue regeneration. *J Periodontal Res.* 22(3): 252-254
- Ogiso B, Hughes FJ, Melcher AH, McCulloch CA. (1991). Fibroblasts inhibit mineralised bone nodule formation by rat bone marrow stromal cells *in vitro*. *J Cell Physiol.* 146(3): 442-450
- Ogiso B, Hughes FJ, Davies JE, McCulloch CAG. (1992). Fibroblastic regulation of osteoblast function by prostaglandins. *Cell Signal.* 4(6): 627-639
- Oh SP, Griffith CM, Hay ED, Olsen BR. (1993). Tissue-specific expression of type XII collagen during mouse embryonic development. *Dev Dyn.* 196(1): 37-46
- Ohno S, Doi T, Fujimoto K, Ijuin C, Tanaka N, Tanimoto K, Honda K, Nakahara M, Kato Y, Tanne K. (2002). RGD-CAP (betaig-h3) exerts a negative regulatory function on mineralization in the human periodontal ligament. *J Dent Res.* 81(12): 822-825
- Okuda K, Momose M, Murata M, Saito Y, Inoie M, Shinohara C, Wolff LF, Yoshie H. (2004). Treatment of chronic desquamative gingivitis using tissue-engineered

- human cultured gingival epithelial sheets: a case report. *Int J Periodontics Restorative Dent.* 24(2): 119-125
- Olsen BR, Reginato AM, Wang W. (2000). Bone development. *Annu Rev Cell Dev Biol.* 16: 191-220
- Owen TA, Aronow M, Shalhoub V, Barone LM, Wilming L, Tassinari MS, Kennedy MB, Pockwinse S, Lian JB, Stein GS. (1990). Progressive development of the rat osteoblast phenotype *in vitro*: reciprocal relationships in expression of genes associated with osteoblast proliferation and differentiation during formation of the bone extracellular matrix. *J Cell Physiol.* 143(3): 420-430
- Owen GR, Meredith DO, ap Gwynn I, Richards RG. (2005). Focal adhesion quantification - a new assay of material biocompatibility? *Eur Cell Mater.* 9: 85-96
- Park JB. (2000). Biomaterials. In: *Biomedical Engineering Handbook*. Bronzino JD (eds). Boca Raton: CRC Press. p. 530-610
- Pearson CH, Wohllebe M, Carmichael DJ, Chovelon A. (1975). Bovine periodontal ligament. An investigation of the collagen, glycosaminoglycan and insoluble glycoprotein components at different stages of tissue development. *Connect Tissue Res.* 3(4): 195-206
- Pearson CH, Pringle GA. (1986). Chemical and immunochemical characteristics of proteoglycans in bovine gingival and dental pulp. *Arch Oral Biol.* 31(8): 541-548
- Perinpanayagam H, Martin T, Mithal V, Dahman M, Marzec N, Lampasso J, Dziak R. (2006). Alveolar bone osteoblast differentiation and Runx2/Cbfa1 expression. *Arch Oral Biol.* 51(5): 406-415
- Perrin DE, English JP. (1997). Polycaprolactone. In: *Handbook of biodegradable polymers*. Domb AJ, Kost J, Wiseman DM. (eds). Amsterdam: Harwood Academic Publishers. p. 63-77
- Peterkofsky B. (1972). The effect of ascorbic on collagen polypeptide synthesis and proline hydroxylation during the growth of cultured fibroblasts. *Arch Biochem Biophys.* 152: 318-328
- Pettit DK, Horbett TA, Hoffman AS. (1992). Influence of the substrate binding characteristics of fibronectin on corneal epithelial cell outgrowth. *J Biomed Mater Res.* 26(10): 1259-1275
- Phillips CL, Tajima S, Pinnell SR. (1992). Ascorbic acid and transforming growth factor-beta 1 increase collagen biosynthesis via different mechanisms: coordinate regulation of pro alpha 1(I) and Pro alpha 1(III) collagens. *Arch Biochem Biophys.* 295(2): 397-403
- Phipps RP, Borrello MA, Blieden TM. (1997). Fibroblast heterogeneity in the periodontium and other tissues. *J Periodontal Res.* 32(1): 159-165

- Pierschbacher MD, Hayman EG, Ruoslahti E. (1981). Location of the cell-attachment site in fibronectin with monoclonal antibodies and proteolytic fragments of the molecule. *Cell*. 26(2): 259-267
- Pierschbacher MD, Ruoslahti E. (1984). Variants of the cell recognition site of fibronectin that retain attachment-promoting activity. *Proc Natl Acad Sci USA*. 81(19): 5985-5988
- Piez KA. (1976). Primary structure. In: *Biochemistry of Collagen*. Ramachandran GN, Reddi AH. (eds). New York: Plenum. p. 1-44
- Pihlstrom BL, McHugh RB, Oliphant TH, Ortiz-Campos C. (1983). Comparison of surgical and nonsurgical treatment of periodontal disease. A review of current studies and additional results after 6 1/2 years. *J Clin Periodontol*. 10(5): 524-541
- Pitaru S, McCulloch CA, Narayanan SA. (1994). Cellular origins and differentiation control mechanisms during periodontal development and wound healing. *J Periodontal Res*. 29(2): 81-94
- Pitt CG, Marks TA, Schindler A. (1981). Biodegradable drug delivery systems based on aliphatic polyesters: application to contraceptives and narcotic antagonists. *NIDA Res Monogr*. 28: 232-253
- Pitt CG, Hendren RW, Schindler A, Woodward SC. (1984). The enzymatic surface erosion of aliphatic polyesters. *J Control Rel*. 1(1): 3-14
- Pitt CG. (1990). Poly-caprolactone and its copolymers. In: *Biodegradable polymers as drug delivery systems*. Chasin M, Langer R. (eds). New York: Marcel Dekker. p. 71
- Prato GP, Rotundo R, Magnani C, Soranzo C, Muzzi L, Cairo F. (2003). An autologous cell hyaluronic acid graft technique for gingival augmentation: a case series. *J Periodontol*. 74: 262-267
- Probst I, Jungermann K. (1983). The glucagon-insulin antagonism and glucagon-dexamethasone synergism in the induction of phosphoenolpyruvate carboxykinase in cultured rat hepatocytes. *Hoppe Seylers Z Physiol Chem*. 364(12): 1739-1746
- Purvis JA, Embery G, Oliver WM. (1984). Molecular size distribution of proteoglycans in human inflamed gingival tissue. *Arch Oral Biol*. 29(7): 513-519
- Quteish D, Singrao S, Dolby AE. (1991). Light and electron microscopic evaluation of biocompatibility, resorption and penetration characteristics of human collagen graft material. *J Clin Periodontol*. 18: 305-311
- Ragnarsson B, Carr G, Daniel JC. (1985). Isolation and growth of human periodontal ligament cells *in vitro*. *J Dent Res*. 64(8): 1026-1030
- Ramakrishnan PR, Lin WL, Sodek J, Cho MI. (1995). Synthesis of noncollagenous extracellular matrix proteins during development of mineralized nodules by rat periodontal ligament cells *in vitro*. *Calcif Tissue Int*. 57(1): 52-59

- Ramfjord SP, Caffesse RG, Morrison EC, Hill RW, Kerry GJ, Appleberry EA, Nissle RR, Stults DL. (1987). Four modalities of periodontal treatment compared over five years. *J Periodontal Res.* 22(3): 222-223
- Ranucci CS, Moghe PV. (2001). Substrate microtopography can enhance cell adhesive and migratory responsiveness to matrix ligand density. *J Biomed Mater Res.* 54(2): 149-161
- Rao JS, Rao VH, Bose SM. (1982). Effect of protein malnutrition on the crosslinking of dermal collagen in aging. *Exp Gerontol.* 17(3): 227-233
- Raspanti M, Cesari C, De Pasquale V, Ottani V, Strocchi R, Zucchelli G, Ruggeri A. (2000). A histological and electron-microscopic study of the architecture and ultrastructure of human periodontal tissues. *Arch Oral Biol.* 45(3): 185-192
- Reddi AH. (1981). Cell biology and biochemistry of endochondral bone development. *Coll Relat Res.* 1(2): 209-226
- Redl H, Schlag G, Dinges P. (1985). The use and biocompatibility of a human fibrin sealant for hemostasis and tissue sealing. In: *Biocompatibility of tissue analogs.* Vol 1. Williams DF. (eds). Boca Raton: CRC Press. p. 150-153
- Reuters I, Weber M, Schulze-Lohoff E. (2006). Rho/Rho kinase pathway regulates maintenance of the differentiated tubular epithelial cell phenotype on laminin-1. *Nephron Physiol.* 104(2): 95-106
- Rhodes N. (2004). Biocompatibility testing of tissue engineered products. *Vox Sang.* 87 (Suppl 2): 161-163
- Rihova B. (1996). Biocompatibility of biomaterials: hemocompatibility, immunocompatibility and biocompatibility of solid polymeric materials and soluble polymeric carriers. *Adv Drug Del Rev* 21: 157-176
- Rincon JC, Xiao Y, Young WG, Bartold PM. (2005). Production of osteopontin by cultured porcine epithelial cell rests of Malassez. *J Periodontal Res.* 40(5): 417-426
- Rincon JC, Young WG, Bartold PM. (2006). The epithelial cell rests of Malassez - a role in periodontal regeneration? *J Periodontal Res.* 41(4): 245-252
- Roberts WE, Wood HB, Chambers DW, Burk DT. (1987). Vascularly oriented differentiation gradient of osteoblast precursor cells in rat periodontal ligament: implications for osteoblast histogenesis and periodontal bone loss. *J Periodontal Res.* 22(6): 461-467
- Romanos GE, Strub JR, Bernimoulin JP. (1993). Immunohistochemical distribution of extracellular matrix proteins as a diagnostic parameter in healthy and diseased gingiva. *J Periodontol.* 64(2): 110-119

- Romanos GE, Strub JR. (1998). Effect of Tissucol on connective tissue matrix during wound healing: an immunohistochemical study in rat skin. *J Biomed Mater Res.* 39: 462-468
- Ross MH, Kaye GI, Pawlina W. (2002). *Histology: a text and atlas.* Baltimore: Lippincott Williams and Wilkins. p. 453
- Rouxhet L, Duhoux F, Borecky O, Legras R, Schneider YJ. (1998). Adsorption of albumin, collagen, and fibronectin on the surface of poly(hydroxybutyrate-hydroxyvalerate) (PHB/HV) and of poly (epsilon-caprolactone) (PCL) films modified by an alkaline hydrolysis and of poly(ethylene terephthalate) (PET) track-etched membranes. *J Biomater Sci Polym Ed.* 9(12): 1279-1304
- Rowe LB, Schwarz RI. (1983). Role of procollagen mRNA levels in controlling the rate of procollagen synthesis. *Mol Cell Biol.* 3(2): 241-249
- Ruardy TG, Schakenraad JM, van der Mei HC, Busscher HJ. (1995). Adhesion and spreading of human skin fibroblasts on physicochemically characterized gradient surfaces. *J Biomed Mater Res.* 29: 1415-1423
- Ruoslahti E, Pierschbacher MD. (1987). New perspectives in cell adhesion: RGD and integrins. *Science.* 238(4826): 491-497
- Sae-Lim V. (2001). Repair or regeneration of damaged dental structures - A dental trauma model. In: *Lifeline, National University Hospital, Singapore.* December. p. 7-8
- Sae-Lim V, Ong WY, Li Z, Neo J. (2004). The effect of basic fibroblast growth factor on delayed-replanted monkeys' teeth. *J Periodontol.* 75: 1570-1578
- Saito S, Rosol TJ, Saito M, Ngan PW, Shanfeld J, Davidovitch Z. (1990). Bone-resorbing activity and prostaglandin E produced by human periodontal ligament cells *in vitro.* *J Bone Miner Res.* 5(10): 1013-1018
- Saltzman WM, Parsons-Wingerter P, Leong KW, Lin S. (1991). Fibroblast and hepatocyte behavior on synthetic polymer surfaces. *J Biomed Mater Res.* 25(6): 741-759
- Sano S, Kato K, Ikada Y. (1993). Introduction of functional groups onto the surface of polyethylene for protein immobilization. *Biomaterials.* 14(11): 817-822
- Sasano Y, Maruya Y, Sato H, Zhu JX, Takahashi I, Mizoguchi I, Kagayama M. (2001). Distinctive expression of extracellular matrix molecules at mRNA and protein levels during formation of cellular and acellular cementum in the rat. *Histochem J.* 33(2): 91-99
- Sawada H, Konomi H. (1991). The alpha 1 chain of type VIII collagen is associated with many but not all microfibrils of elastic fiber system. *Cell Struct Funct.* 16(6): 455-466

- Scantlebury TV. (1993). 1982-1992: a decade of technology development for guided tissue regeneration. *J Periodontol.* 64(11 Suppl): 1129-1137
- Schakenraad JM, Busscher HJ, Wildevuur CR, Arends J. (1986). The influence of substratum surface free energy on growth and spreading of human fibroblasts in the presence and absence of serum proteins. *J Biomed Mater Res.* 20(6): 773-784
- Schakenraad JM, Busscher HJ, Wildevuur CR, Arends J. (1988). Thermodynamic aspects of cell spreading on solid substrata. *Cell Biophys.* 13(1): 75-91
- Schallhorn, R.G., McClain, P.K. (1988) Combined osseous composite grafting, root conditioning, and guided tissue regeneration. *Int. J. Periodontics Restorative Dent.* 8(4), 8-31
- Schantz JT, Hutmacher DW, Ng KW, Khor HL, Lim MT, Teoh SH. (2002a). Evaluation of a tissue-engineered membrane-cell construct for guided bone regeneration. *Int J Oral Maxillofac Implants.* 17(2): 161-174
- Schantz JT, Hutmacher DW, Chim H, Ng KW, Lim TC, Teoh SH. (2002b). Induction of ectopic bone formation by using human periosteal cells in combination with a novel scaffold technology. *Cell Transplant.* 11(2): 125-138
- Schoen RC, Bentley KL, Klebe RJ. (1982). Monoclonal antibody against human fibronectin which inhibits cell attachment. *Hybridoma.* 1(2): 99-108
- Schoenwaelder SM, Burridge K. (1999). Bidirectional signaling between the cytoskeleton and integrins. *Curr Opin Cell Biol.* 11(2): 274-286
- Schroeder HE. (1986). The Periodontium. In: *Handbook of Microscopic Anatomy.* Oksche A, Vollrath L. (eds). Berlin: Springer. p. 170-232
- Schroeder HE. (1992). Biological problems of regenerative cementogenesis: synthesis and attachment of collagenous matrices on growing and established root surfaces. *Int Rev Cytol.* 142: 1-59
- Sechler JL, Schwarzbauer JE. (1997). Coordinated regulation of fibronectin fibril assembly and actin stress fiber formation. *Cell Adhes Commun.* 4(6): 413-424
- Sechler JL, Schwarzbauer JE. (1998). Control of cell cycle progression by fibronectin matrix architecture. *J Biol Chem.* 273(40): 25533-25536
- Serrano MC, Pagani R, Vallet-Regi M, Pena J, Ramila A, Izquierdo I, Portoles MT. (2004). In vitro biocompatibility assessment of poly(epsilon-caprolactone) films using L929 mouse fibroblasts. *Biomaterials.* 25(25): 5603-5611
- Serrano MC, Portoles MT, Vallet-Regi M, Izquierdo I, Galletti L, Comas JV, Pagani R. (2005). Vascular endothelial and smooth muscle cell culture on NaOH-treated poly(epsilon-caprolactone) films: a preliminary study for vascular graft development. *Macromol Biosci.* 5(5): 415-423

- Sgouras D, Duncan R. (1990). Methods for the evaluation of biocompatibility of soluble synthetic polymers which have potential for biomedical use: 1-use of the tetrazolium-based colorimetric assay (MTT) as a preliminary screen for evaluation of *in vitro* cytotoxicity. *J Mater Sci Mater.Med.* 1: 61-68
- Shalhoub V, Conlon D, Tassinari M, Quinn C, Partridge N, Stein GS, Lian JB. (1992). Glucocorticoids promote development of the osteoblast phenotype by selectively modulating expression of cell growth and differentiation associated genes. *J Cell Biochem.* 50(4): 425-440
- Shiga M, Kapila YL, Zhang Q, Hayami T, Kapila S. (2003). Ascorbic acid induces collagenase-1 in human periodontal ligament cells but not in MC3T3-E1 osteoblast-like cells: potential association between collagenase expression and changes in alkaline phosphatase phenotype. *J Bone Miner Res.* 18(1): 67-77
- Shiraishi C, Hara Y, Abe Y, Ukai T, Kato I. (2001). A histopathological study of the role of periodontal ligament tissue in root resorption in the rat. *Arch Oral Biol.* 46: 99-107
- Silver FH, Freeman JW, Seehra GP. (2003). Collagen self-assembly and the development of tendon mechanical properties. *J Biomech.* 36(10): 1529-1553
- Simon CG Jr, Eidelman N, Kennedy SB, Sehgal A, Khatri CA, Washburn NR. (2005). Combinatorial screening of cell proliferation on poly(L-lactic acid)/poly(D,L-lactic acid) blends. *Biomaterials.* 26(34): 6906-6915
- Skehan P. (1988). Control models of cell cycle transit, exit, and arrest. *Biochem Cell Biol.* 66(6):467-477
- Slavkin HC, Bringas P Jr, Bessem C, Santos V, Nakamura M, Hsu MY, Snead ML, Zeichner-David M, Fincham AG. (1989). Hertwig's epithelial root sheath differentiation and initial cementum and bone formation during long-term organ culture of mouse mandibular first molars using serumless, chemically-defined medium. *J Periodontal Res.* 24(1): 28-40
- Sodek J, Feng J, Yen EH, Melcher AH. (1982). Effect of ascorbic acid on protein synthesis and collagen hydroxylation in continuous flow organ cultures of adult mouse periodontal tissues. *Calcif Tissue Int.* 34(4): 408-415
- Sodek J, Cheifitz S. (2000). Molecular regulation of osteogenesis. In: *Bone engineering.* Davies JE. (eds). Toronto: Em Squared Inc. p. 31-43
- Somerman MJ, Archer SY, Imm GR, Foster RA. (1988). A comparative study of human periodontal ligament cells and gingival fibroblasts *in vitro*. *J Dent Res* 67(1): 66-70
- Somerman MJ, Young MF, Foster RA, Moehring JM, Imm G, Sauk JJ. (1990). Characteristics of human periodontal ligament cells *in vitro*. *Arch Oral Biol.* 35(3): 241-247

- Steffensen B, Duong AH, Milam SB, Potempa CL, Winborn WB, Magnuson VL, Chen D, Zardeneta G, Klebe RJ. (1992). Immunohistological localization of cell adhesion proteins and integrins in the periodontium. *J Periodontol.* 63(7): 584-592
- Stein GS, Lian JB. (1993). Molecular mechanisms mediating proliferation / differentiation interrelationships during progressive development of the osteoblast phenotype. *Endocr Rev.* 14(4): 424-442
- Stein GS, Lian JB, Stein JL, van Wijnen AJ, Frenkel B, Montecino M. (1996). Mechanisms regulating osteoblast proliferation and differentiation. In: *Principles of Bone Biology.* Bilizikian JP, Raisz LG, Rodan GA. (eds). New York: Academic Press Inc. p. 69
- Stieglitz T. (2004). Considerations on surface and structural biocompatibility as prerequisite for long-term stability of neural prostheses. *J Nanosci Nanotechnol.* 4(5): 496-503
- Straus AH, Carter WG, Wayner EA, Hakomori S. (1989). Mechanism of fibronectin-mediated cell migration: dependence or independence of cell migration susceptibility on RGDS-directed receptor (integrin). *Exp Cell Res.* 183(1): 126-139
- Suggs LJ, Mikos AG. (1996). Synthetic biodegradable polymers for medical applications. In: *Physical properties of polymers handbook.* Mark JE (eds). New York: AIP Press. p. 615-624
- Sugrue SP, Gordon MK, Seyer J, Dublet B, van der Rest M, Olsen BR. (1989). Immunoidentification of type XII collagen in embryonic tissues. *J Cell Biol.* 109(2): 939-945
- Sullivan TA, Uschmann B, Hough R, Leboy PS. (1994). Ascorbate modulation of chondrocyte gene expression is independent of its role in collagen secretion. *J Biol Chem.* 269(36):22500-22506
- Takano-Yamamoto T, Takemura T, Kitamura Y, Nomura S. (1994). Site-specific expression of mRNAs for osteonectin, osteocalcin, and osteopontin revealed by *in situ* hybridization in rat periodontal ligament during physiological tooth movement. *J Histochem Cytochem.* 42(7): 885-896
- Tang ZG, Black RA, Curran JM, Hunt JA, Rhodes NP, Williams DF. (2004). Surface properties and biocompatibility of solvent-cast poly[ε-caprolactone] films. *Biomaterials.* 25(19): 4741-4748
- Tang L, Hu W. (2005). Molecular determinants of biocompatibility. *Expert Rev Med Devices.* 2(4): 493-500
- Teixeira AI, Abrams GA, Bertics PJ, Murphy CJ, Nealey PF. (2003). Epithelial contact guidance on well-defined micro- and nanostructured substrates. *J Cell Sci.* 116(10): 1881-1892

- Ten Cate AR. (1996). The role of epithelium in the development, structure and function of the tissues of tooth support. *Oral Dis.* 2(1): 55-62
- Ten Cate AR. (1997). The development of the periodontium--a largely ectomesenchymally derived unit. *Periodontol* 2000. 13: 9-19
- Nanci A, Ten Cate AR. (2003). Development of the tooth and its supporting tissues. In: *Oral histology: development, structure, and function.* Nanci A. (eds). St. Louis: Mosby. p. 81-102
- Thapa A, Webster TJ, Haberstroh KM. (2003). Polymers with nano-dimensional surface features enhance bladder smooth muscle cell adhesion. *J Biomed Mater Res A.* 67(4): 1374-1383
- Thomson RC, Yaszemski MJ, Mikos AG. (1997). Polymer scaffold processing. In: *Principles of Tissue Engineering.* Lanza RP, Langer R, Chick WL. (eds). Texas: Academic Press Inc. p. 263-272
- Trueb J, Trueb B. (1992). The two splice variants of collagen XII share a common 5' end. *Biochim Biophys Acta.* 1171(1): 97-98
- Turner CE, Glenney JR Jr, Burridge K. (1990). Paxillin: a new vinculin-binding protein present in focal adhesions. *J Cell Biol.* 111(3): 1059-1068
- Underwood PA, Steele JG, Dalton BA. (1993). Effects of polystyrene surface chemistry on the biological activity of solid phase fibronectin and vitronectin, analysed with monoclonal antibodies. *J Cell Sci.* 104 (3): 793-803
- van Dijk LJ, Schakenraad JM, van der Voort HM, Herkströter FM, Busscher HJ. (1991). Cell-seeding of periodontal ligament fibroblasts. A novel technique to create new attachment. A pilot study. *J Clin Periodontol.* 18(3): 196-199
- van Wachem PB, Beugeling T, Feijen J, Bantjes A, Detmers JP, van Aken WG. (1985). Interaction of cultured human endothelial cells with polymeric surfaces of different wettabilities. *Biomaterials.* 6(6): 403-408
- Van Wachem PB, Vreriks CM, Beugeling T, Feijen J, Bantjes A, Detmers JP, van Aken WG. (1987a) The influence of protein adsorption on interactions of cultured human endothelial cells with polymers. *J. Biomed. Mater. Res.* 21(6): 701-718
- van Wachem PB, Hogt AH, Beugeling T, Feijen J, Bantjes A, Detmers JP, van Aken WG. (1987b). Adhesion of cultured human endothelial cells onto methacrylate polymers with varying surface wettability and charge. *Biomaterials.* 8(5): 323-328
- Vance RJ, Miller DC, Thapa A, Haberstroh KM, Webster TJ. (2004) Decreased fibroblast cell density on chemically degraded poly-lactic-co-glycolic acid, polyurethane, and polycaprolactone. *Biomaterials.* 25(11): 2095-2103
- Vellanoweth RL, Suprakar PC, Roy AK. (1994). Transcription factors in development, growth, and aging. *Lab Invest.* 70(6): 784-799

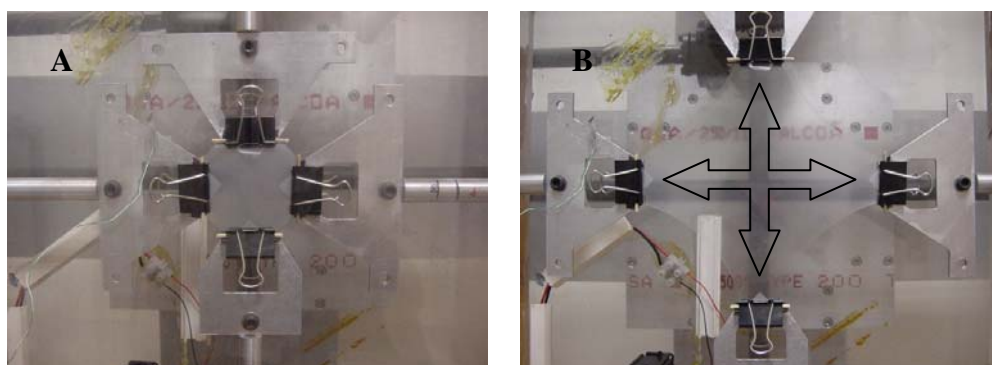
- Verderio E, Coombes A, Jones RA, Li X, Heath D, Downes S, Griffin M. (2001). Role of the cross-linking enzyme tissue transglutaminase in the biological recognition of synthetic biodegradable polymers. *J Biomed Mater Res.* 54(2): 294-304
- Vert M, Li SM. (1992). Bioresorbability and biocompatibility of aliphatic polyesters. *J Mater Sci Mater Med.* 3: 432-446
- Vidal S, Horvath E, Kovacs K, Lloyd RV, Scheithauer BW. (2003). Microvascular structural entropy: a novel approach to assess angiogenesis in pituitary tumors. *Endocr Pathol.* 14: 239-247
- Vogler EA. (1989). A compartmentalized device for the culture of animal cells. *Biomater Artif Cells Artif Organs.* 17(5): 597-610
- von Recum AF, van Kooten TG. (1995). The influence of micro-topography on cellular response and the implications for silicone implants. *J Biomater Sci Polym Ed.* 7(2): 181-198
- Vroman L, Adams AL. (1969). Identification of rapid changes at plasma-solid interfaces. *J Biomed Mater Res.* 3(1): 43-67
- Wan Y, Wang Y, Liu Z, Qu X, Han B, Bei J, Wang S. (2005). Adhesion and proliferation of OCT-1 osteoblast-like cells on micro- and nano-scale topography structured poly(L-lactide). *Biomaterials.* 26(21): 4453-4459
- Wang YX, Robertson JL, Spillman WB Jr, Claus RO. (2004). Effects of the chemical structure and the surface properties of polymeric biomaterials on their biocompatibility. *Pharm Res.* 21(8): 1362-1373
- Warrer K, Karring T. (1992). Effect of Tisseel on healing after periodontal flap surgery. *J Clin Periodontol.* 19: 449-454
- Washburn NR, Yamada KM, Simon CG Jr, Kennedy SB, Amis EJ. (2004). High-throughput investigation of osteoblast response to polymer crystallinity: influence of nanometer-scale roughness on proliferation. *Biomaterials.* 25(7-8): 1215-1224
- Weber L, Mauch C, Kirsch E, Müller PK, Krieg T. (1986). Modulation of collagen type synthesis in organ and cell cultures of fibroblasts. *J Invest Dermatol.* 87: 217-220
- Weisberg TF, Cahill BK, Vary CP. (1996). Non-radioisotopic detection of human xenogeneic DNA in a mouse transplantation model. *Mol Cell Probes.* 10(2): 139-146
- Welch MP, Odland GF, Clark RA. (1990). Temporal relationships of F-actin bundle formation, collagen and fibronectin matrix assembly, and fibronectin receptor expression to wound contraction. *J Cell Biol.* 110(1): 133-145
- Whang K, Healy KE, Elenz DR, Nam EK, Tsai DC, Thomas CH, Nuber GW, Glorieux FH, Travers R, Sprague SM. (1999). Engineering bone regeneration with bioabsorbable scaffolds with novel microarchitecture. *Tissue Eng.* 5(1): 35-51

- Wikesjo UM, Nilveus RE, Selvig KA. (1992). Significance of early healing events on periodontal repair: a review. *J Periodontol.* 63(3): 158-165
- Williamson MR, Coombes AG. (2004). Gravity spinning of polycaprolactone fibres for applications in tissue engineering. *Biomaterials.* 25: 459-465
- Wong MM, Rao LG, Ly H, Hamilton L, Tong J, Sturtridge W, McBroom R, Aubin JE, Murray TM. (1990). Long-term effects of physiologic concentrations of dexamethasone on human bone-derived cells. *J Bone Miner Res.* 5(8): 803-813
- Wong WH, Mooney DJ. (1997). Synthesis and properties of biodegradable polymers as synthetic matrices for tissue engineering. In: *Synthetic biodegradable polymer scaffolds.* Atala A, Mooney D. (eds). Boston: Burkhäuser. p. 51-84
- Woodward SC, Brewer PS, Moatamed F, Schindler A, Pitt CG. (1985). The intracellular degradation of poly(epsilon-caprolactone). *J Biomed Mater Res.* 19(4): 437-444
- Worapamorn W, Li H, Haase HR, Pujic Z, Girjes AA, Bartold PM. (2000). Cell surface proteoglycan expression by human periodontal cells. *Connect Tissue Res.* 41(1): 57-68
- Xiao Y, Haase H, Young WG, Bartold PM. (2004). Development and transplantation of a mineralized matrix formed by osteoblasts *in vitro* for bone regeneration. *Cell Transplant.* 13(1): 15-25
- Yamada KM, Olden K. (1978). Fibronectins - adhesive glycoproteins of cell surface and blood. *Nature.* 275(5677): 179-184
- Yamada KM. (1983). Cell surface interactions with extracellular materials. *Annu Rev Biochem.* 52: 761-799
- Yamada KM, Aota S, Akiyama SK, LaFlamme SE. (1992). Mechanisms of fibronectin and integrin function during cell adhesion and migration. *Cold Spring Harb Symp Quant Biol.* 57: 203-212
- Yamada S, Murakami S, Matoba R, Ozawa Y, Yokokoji T, Nakahira Y, Ikezawa K, Takayama S, Matsubara K, Okada H. (2001). Expression profile of active genes in human periodontal ligament and isolation of PLAP-1, a novel SLRP family gene. *Gene.* 275(2): 279-286
- Yanagisawa I, Sakuma H, Shimura M, Wakamatsu Y, Yanagisawa S, Sairenji E. (1989). Effects of "wettability" of biomaterials on culture cells. *J Oral Implantol.* 15(3): 168-177
- Yang AQ. (2002). Preliminary evaluation of poly-(caprolactone) and poly-(caprolactone)-tricalcium phosphate composite polymer membrane as potential

- scaffold for tissue engineering of periodontal ligament and effects of cell seeding density on PDLF activity. BSc Dissertation. National University of Singapore.
- Yang KG, Saris DB, Geuze RE, Helm YJ, Rijen MH, Verbout AJ, Dhert WJ, Creemers LB. (2006). Impact of expansion and redifferentiation conditions on chondrogenic capacity of cultured chondrocytes. *Tissue Eng.* 12(9): 2435-2447
- Young DS. (1977). Classification of enzymes and current status of enzyme nomenclature and units. *Ann Clin Lab Sci.* 7(2): 93-98
- Zamir E, Katz M, Posen Y, Erez N, Yamada KM, Katz BZ, Lin S, Lin DC, Bershadsky A, Kam Z, Geiger B. (2000). Dynamics and segregation of cell-matrix adhesions in cultured fibroblasts. *Nat Cell Biol.* 2(4): 191-196
- Zamir E, Geiger B. (2001). Molecular complexity and dynamics of cell-matrix adhesions. *J Cell Sci.* 114(20): 3583-3590
- Zein I, Hutmacher DW, Tan KC, Teoh SH. (2002). Fused deposition modeling of novel scaffold architectures for tissue engineering applications. *Biomaterials.* 23(4): 1169-1185
- Zhang X, Schuppan D, Becker J, Reichart P, Gelderblom HR. (1993). Distribution of undulin, tenascin, and fibronectin in the human periodontal ligament and cementum: comparative immunoelectron microscopy with ultra-thin cryosections. *J Histochem Cytochem.* 41(2): 245-251
- Zhou YF. (2006). Characterization of human alveolar osteoblasts on 2-D and 3-D substrates. PhD Dissertation. National University of Singapore.
- Zhou YF, Sae-Lim V, Chou AM, Hutmacher DW, Lim TM. (2006). Does seeding density affect in vitro mineral nodules formation in novel composite scaffolds? *J Biomed Mater Res A.* 78(1): 183-193
- Zhu Y, Gao C, Shen J. (2002). Surface modification of polycaprolactone with poly(methacrylic acid) and gelatin covalent immobilization for promoting its cytocompatibility. *Biomaterials.* 23(24):4889-4895
- Zohar R, Lee W, Arora P, Cheifetz S, McCulloch C, Sodek J. (1997). Single cell analysis of intracellular osteopontin in osteogenic cultures of fetal rat calvarial cells. *J Cell Physiol.* 170(1): 88-100
- Zohar R, Suzuki N, Suzuki K, Arora P, Glogauer M, McCulloch CA, Sodek J. (2000). Intracellular osteopontin is an integral component of the CD44-ERM complex involved in cell migration. *J Cell Physiol.* 184(1): 118-130

APPENDIX

Chapter 3: Fabrication of PCL membranes



Biaxial stretching of (A) heat pressed PCL films into (B) 10 μm -thin membranes.

The directions of stretch are indicated with arrows.

Chapter 3: Whole cell lysis and total protein quantification

Cells cultured in six-well plates were rinsed with sterile PBS and lysed in chilled Wally Langdons lysis buffer containing 20 mM Tris (pH 8.0), 150 mM NaCl, 1 mM EDTA, 1% (v/v) Triton X-100 and protease inhibitor cocktail (Calbiochem) for 5 min on ice. Cells were removed from the wells with cell scrappers (Iwaki, Japan) and whole cell lysates were centrifuged at 14,000 rpm for 10 min at 4°C.

Total proteins were quantitated in triplicates at each time point by Bradford assay (Bio-Rad Laboratories, CA, USA), in which the Coomassie[®] Brilliant Blue G-250 dye exhibits an absorbance maximum shift from 465nm to 595nm upon protein binding. Protein supernatants were diluted 100-fold in autoclaved deionized water. Six dilutions of the protein standard, bovine serum albumin (BSA) (Sigma), were prepared in the following concentrations : 0 µg/ml, 5 µg/ml, 10 µg/ml, 15 µg/ml, 20 µg/ml and 25 µg/ml. Twenty-five µl of Coomassie dye was added to 100 µl of each standard or diluted sample, mixed and incubated for 5 min at room temperature in a 96-well plate. Absorbance was measured at 595nm using a microplate reader (GENios, Tecan Group, Switzerland), and protein concentrations (mg/ml) were determined from standard curve.

Chapter 3: Primary and secondary antibodies used for Western blotting.

Primary antibodies	Dilution	Type	Source
Anti-osteonectin (ON)	1:1000	Monoclonal	Developmental Studies Hybridoma Bank (DSHB), IA, USA
Anti-osteopontin (OPN)	1:1000	Monoclonal	
Anti-bone sialoprotein (BSP)	1:1000	Monoclonal	
Anti-collagen XII	1:5000	Polyclonal	Gift from Dr Greg Lunstrum, Shriners Hospital for Children, OR, USA
Anti-collagen XIV	1:5000	Polyclonal	
Fibronectin	1:5000	Polyclonal	Biodesign, ME, USA
α -smooth muscle actin	1:1000	Monoclonal	DAKO, CA, USA

Secondary antibodies	Dilution	Type	Source
Rabbit anti-mouse-HRP	1:5000	Polyclonal	Santa Cruz Biotechnology, CA, USA
Goat anti-rabbit-HRP	1:5000	Polyclonal	

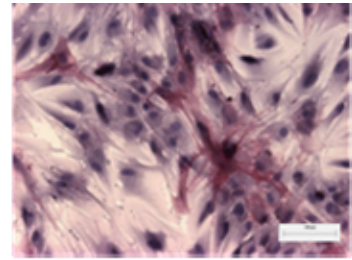
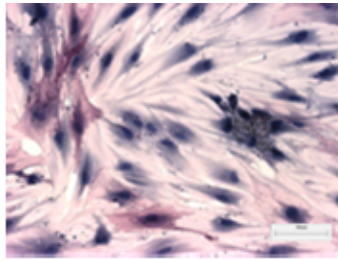
Chapter 4: Alkaline phosphatase (ALP) stain

Cell line

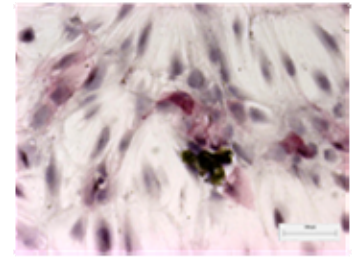
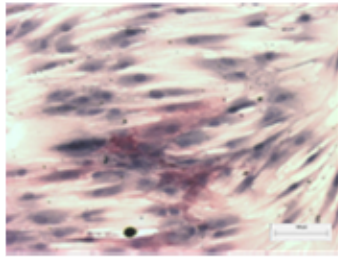
- Dex

+ Dex

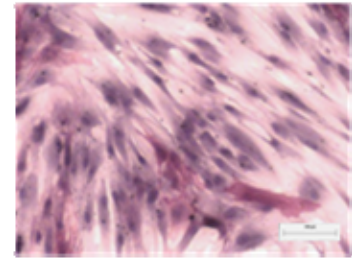
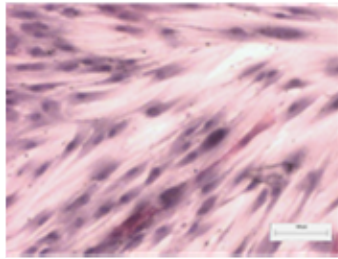
hPDLF1



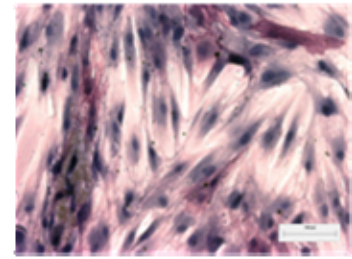
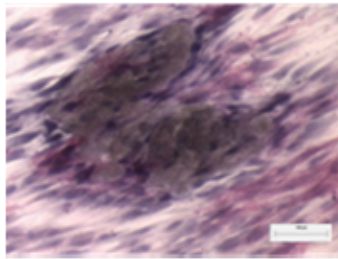
hPDLF54



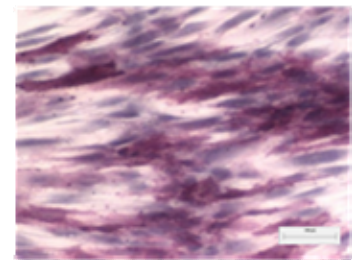
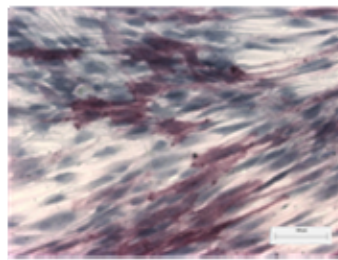
hPDLF42



hPDLF34



hPDLF40

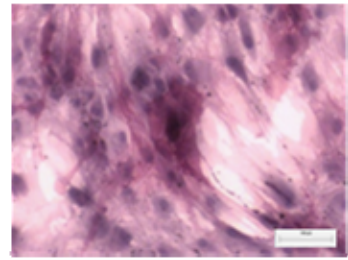
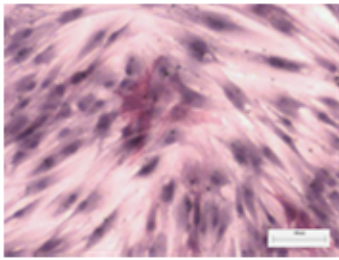


Cell line

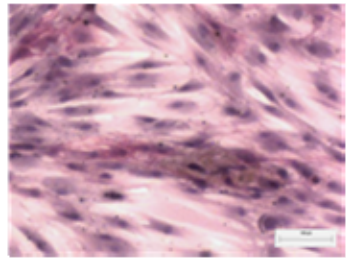
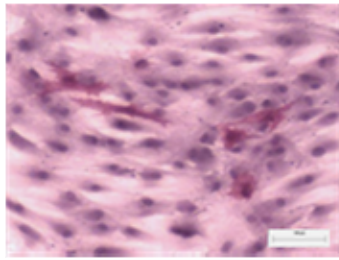
- Dex

+ Dex

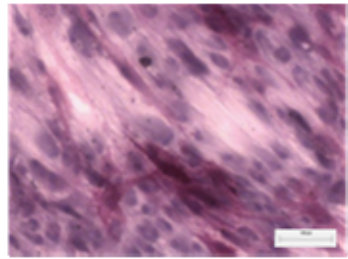
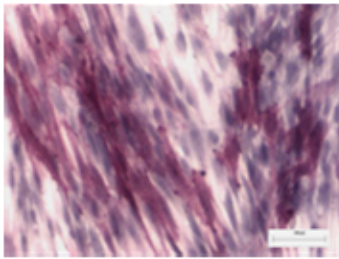
hPDLF35



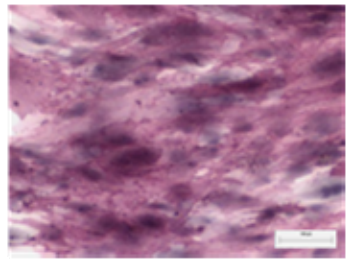
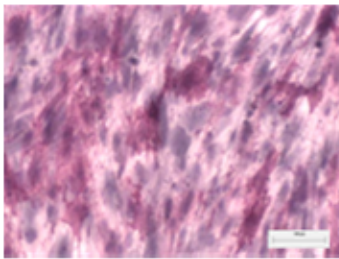
hPDLF41



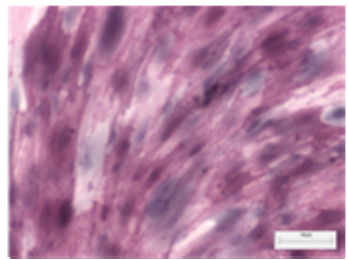
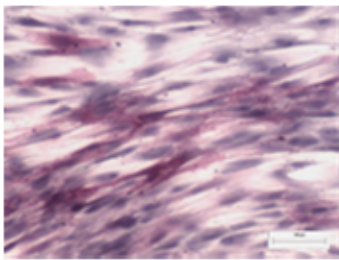
hPDLF37



hPDLF48



hPDLF47

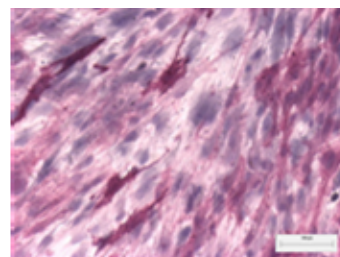
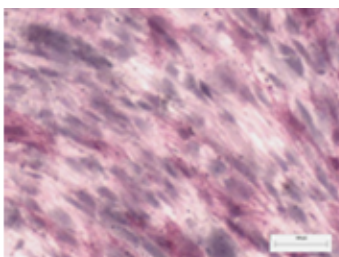


Cell line

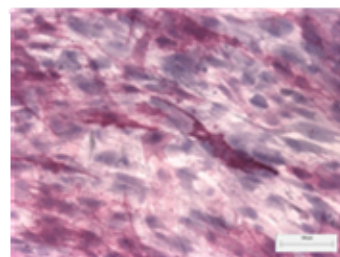
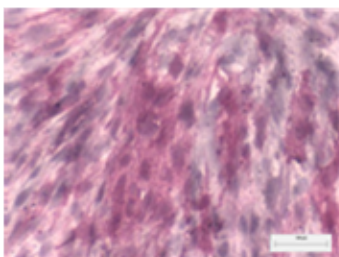
- Dex

+ Dex

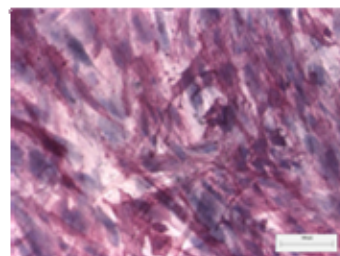
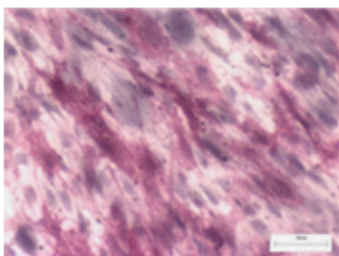
hAO40



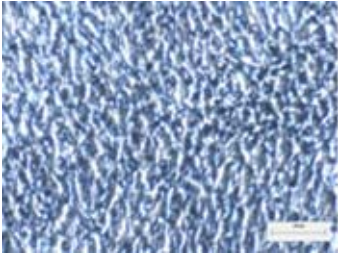
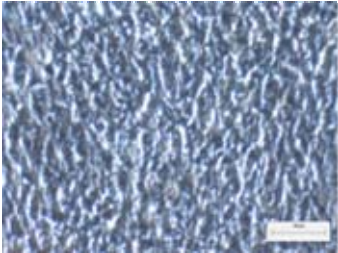
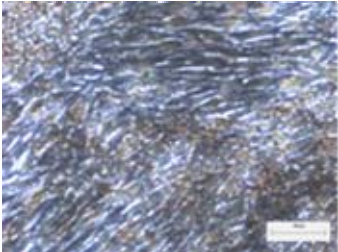
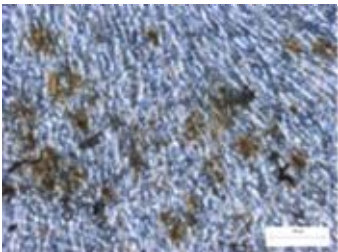
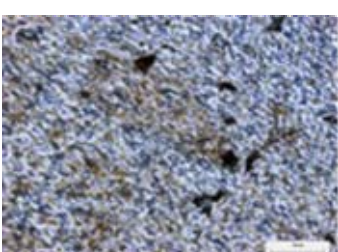
hAO37

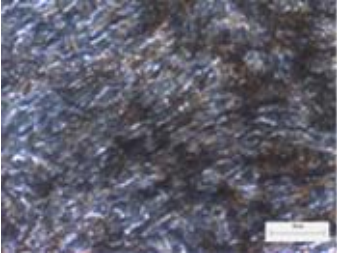
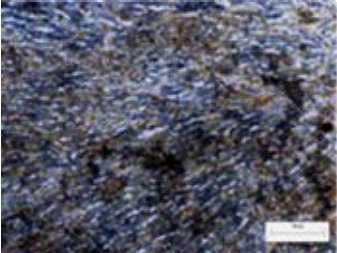
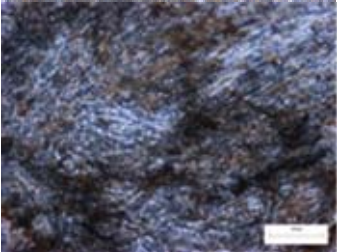
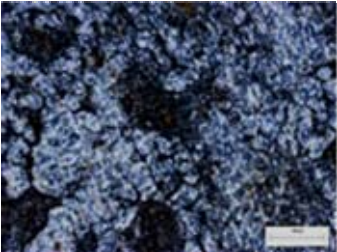
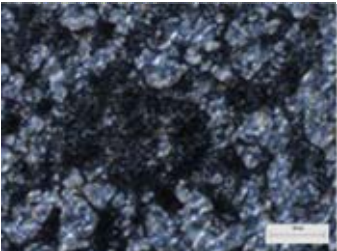


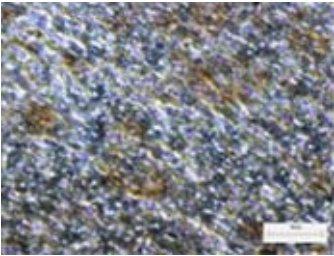
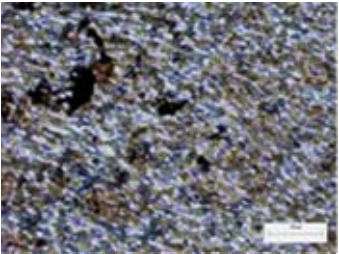
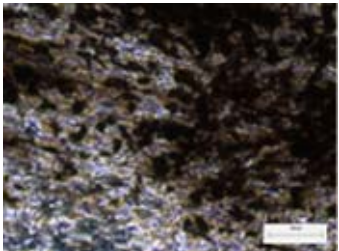
hAO47



Chapter 4: Von Kossa stain

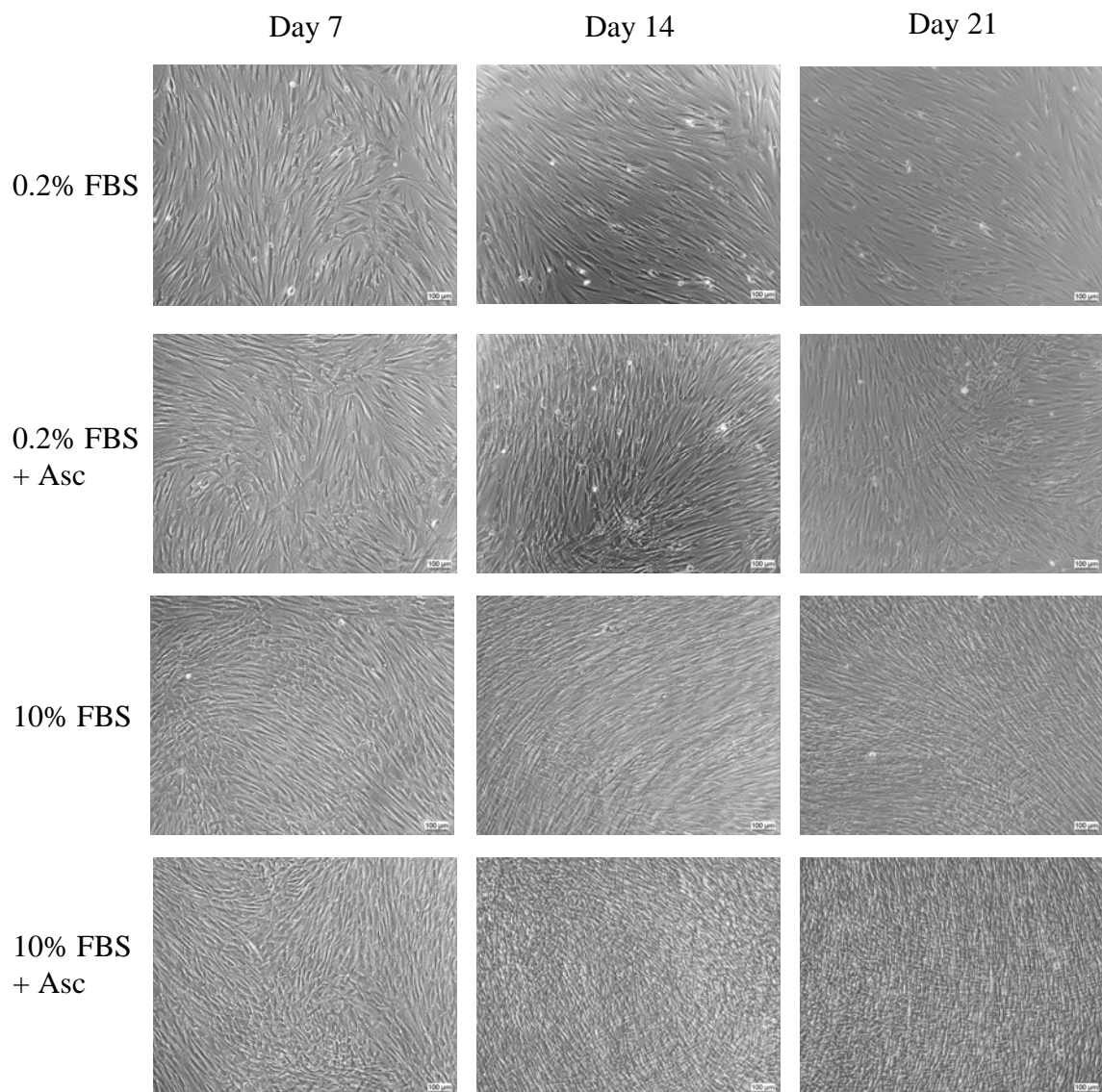
Cell line	Image	Type / Comments	Score
hPDLF1		NA	-
hPDLF54		NA	-
hPDLF42		NA, osteoid	-/+
hPDLF34		NA, osteoid	-/+
hPDLF40		NA, osteoid	-/+

Cell line	Image	Type / Comments	Score
hPDLF35		Diffuse	+
hPDLF41		Diffuse	+
hPDLF37		Diffuse	+
hPDLF48		Nodular, early	++
hPDLF47		Nodular	++

Cell line	Image	Type / Comments	Score
hAO40		NA, osteoid	-/+
hAO37		Nodular	+
hAO47		Nodular	++

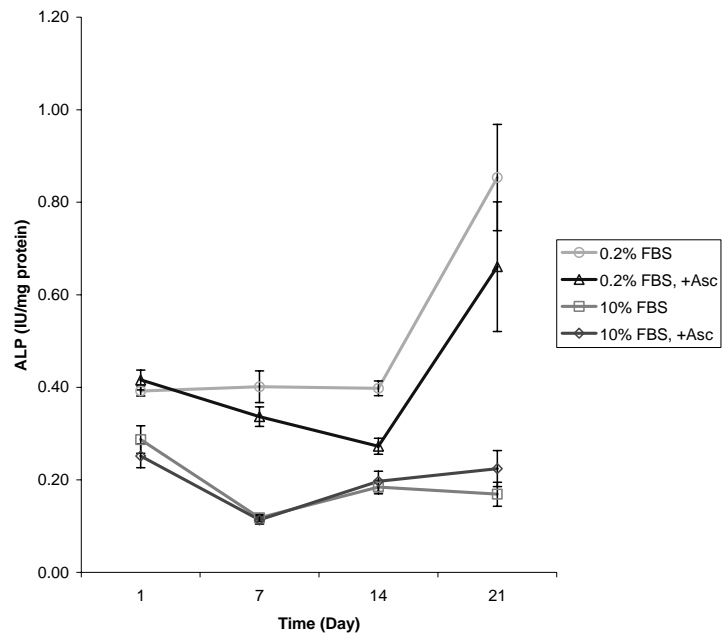
Type of mineralization was categorized as according to Liu *et al.* (1997) and Declercq *et al.* (2005). “Diffuse” type was characterized by the appearance of flat and randomly dispersed foci. “Nodular” type was characterized by three-dimensional nodule formation, associated with regions of cell and matrix condensation. Von Kossa reaction was graded as follows: -, negative staining; -/+, undetectable to weak staining, +, moderate staining; ++, intense staining.

Chapter 5: Cell morphology



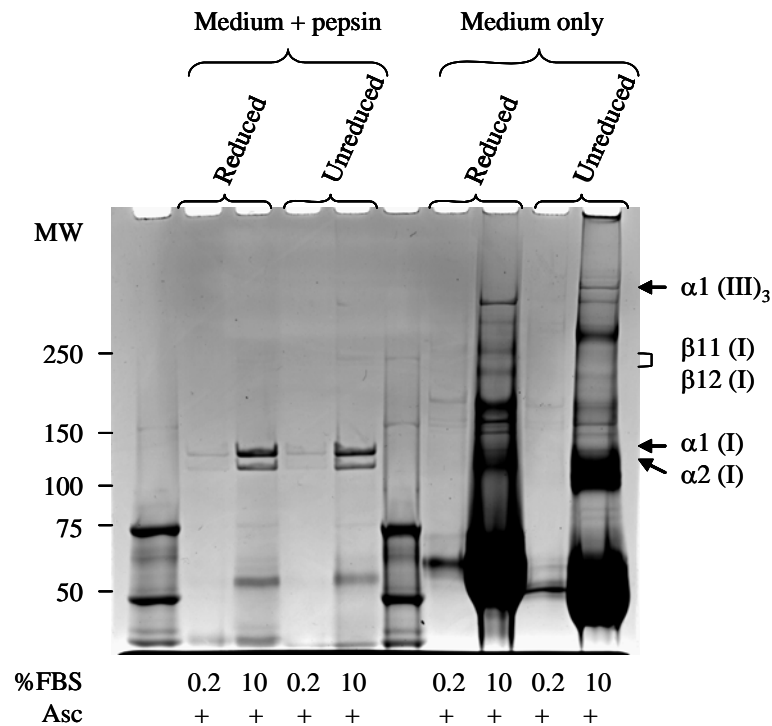
Morphology of hPDLF demonstrating cell quiescence and proliferation under 0.2% and 10% serum respectively over time.

Chapter 5: ALP activity as IU/protein



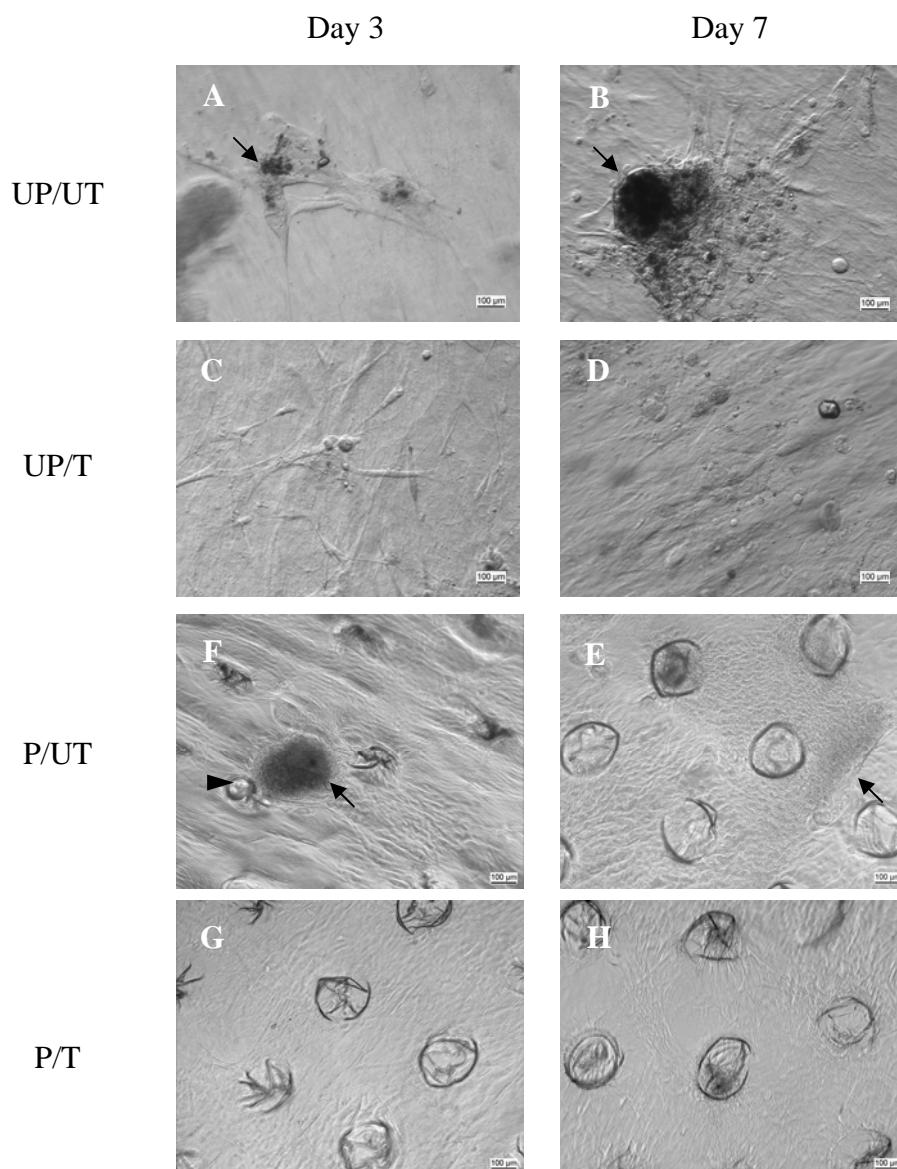
Levels of alkaline phosphatase (ALP) normalized to total protein.

Chapter 5: SDS-PAGE



SDS-PAGE of pepsin-digested and undigested medium fractions at day 21 in 3-8% gradient Tris-acetate gel before and after reduction. Type III collagen was verified by a disappearance of $\alpha 1(\text{III})_3$ trimer and a corresponding increase in $\alpha 1(\text{I})$. Densitometric analysis of $\alpha 1(\text{I})$ in pepsin-digested medium fraction after reduction revealed a fold increase of 1.3 and 1.2 under 0.2% and 10% serum respectively, indicating that secreted type III collagen was approximately 20% of secreted type I collagen.

Chapter 6: Cell seeding onto membranes



Cell morphology and growth of hPDLF on PCL membranes. At day 3, cell-cell association (arrows) was evident on untreated membranes, whereas uniform attachment showing spindle-shaped morphology was obtained on alkali-treated membranes. hPDLF migrated out from cell clusters onto untreated membranes at day 7, whereas those on alkali-treated membranes proliferated to form a well-attached layer.